SEGREGATION VESICLES IN

MID-OCEAN RIDGE BASALTS: IMPLICATIONS

FOR STRUCTURAL AND PALEOMAGNETIC STUDIES

OF OCEANIC CRUST

Submitted in partial fulfillment of the require-
ments for the Degree of Doctor of Philosophy at
Dalhousie University, September 24, 1981.

by

Nancy Anne Van Wagoner

DALHOUSIE UNIVERSITY

FACULTY OF GRADUATE STUDIES

The undersigned hereby certify that they have read and
recommended to the Faculty of Graduate Studies for acceptance
a thesis entitled " Segregation Vesicles in Mid-Ocean
 Ridge Basalts: Implications For Structural and
 Paleomagnetic Studies of Oceanic Crust
                                                        ."

by   Nancy Anne Van Wagoner
in partial fulfillment of the requirements for the degree of
Doctor of Philosophy.

                              Dated   September 23, 1981

External examiner   _   _____

Research Supervisor   _   _____

Examining Committee   ___

                       ___   ___

                       _____

                       _____

DALHOUSIE UNIVERSITY

Date September 24, 1981

Author___ Nancy Anne Van Wagoner

Title___ Segregation Vesicles in Mid-Ocean Ridge Basalts: Implications

for Structural and Paleomagnetic Studies of Oceanic Crust

Department or School___ Department of Geology, Dalhousie University

Degree__ Ph.D.___   Convocation__ October___   Year__ 1981___

Permission is herewith granted to Dalhousie University to circulate and to have copied for non-commercial purposes, at its discretion, the above title upon the request of individuals or institutions.

Signature of Author

THE AUTHOR RESERVES OTHER PUBLICATION RIGHTS, AND NEITHER THE THESIS NOR EXTENSIVE EXTRACTS FROM IT MAY BE PRINTED OR OTHERWISE REPRODUCED WITHOUT THE AUTHOR'S WRITTEN PERMISSION.

CONTENTS

LIST OF ILLUSTRATIONS

LIST OF TABLES

Table

LIST OF APPENDICES

ABSTRACT

Segregation vesicles commonly occur in sea-floor basalts. They generally are spherical in shape, 0.1 - 0.3 mm in diameter, and partially filled with a dark, crescent-shaped lining of aphanitic residue. This residue is a chilled residual melt which entered the vesicle sometime after crystallization had proceeded sufficiently to maintain the integrity of the vesicle but before final crystallization, and flowed to the bottom of the vesicle before solidifying. The crescent-shaped lining can, therefore, be used as an indicator of the cooling orientation of the rock.

By measuring the segregation vesicle inclinations in a pair of thin sections cut along two mutually perpendicular planes, a plane defining the horizontal orientation of the rock can be determined. Results of testing this technique on 17 sea-floor basalt samples, previously oriented by megascopic features, show that segregation vesicle and megascopic orientations agree. The technique can be used to determine the dip of basalt samples recovered in drill cores and to orient basalts in order to determine the paleomagnetic inclination acquired upon cooling. Analyses of the scatter of segregation vesicle inclinations of 34 rock samples indicate that the error associated with dip and magnetic inclination determinations generally are less than $\pm 36^{\circ}$ and $\pm 44^{\circ}$, respectively.

Application of the technique to rocks recovered by dredge and submersible from the Mid-Atlantic Ridge around 35.6° N during the AMAR expedition increased the number of samples available for a paleomagnetic polarity study by almost 50 percent. The results of this study show that about 85 percent of the rocks collected are normally magnetized.

Results of application of the technique for structural and magnetic polarity studies of DSDP cores 332A, 332B, 334, 395 and 395A, and 396B, which penetrated 117 to 583 m into North Atlantic oceanic basement crust, suggest that this crust is structurally heterogeneous. Although rocks dipping 4° to 40° occur in Holes 334, 395 and 395A, and 396B, dips in Holes 332A and

332B range from 20° upright to 14° overturned. As a consequence of tilting, the true thickness of rock units in Holes 332A and 332B may be 50 percent less than the vertical thickness. Tilting may also result in reorientation of the original direction of magnetization acquired by the rocks upon cooling. This suggests that, at least some of the time, the source of marine magnetic surface anomalies may not be in the upper 500 m of oceanic crust. The tilting may result from a number of deformation processes including subsidence, normal block faulting, and mass wasting.

INTRODUCTION

PROBLEM AND PURPOSE

According to the theory of plate tectonics, new oceanic crust is continuously generated at mid-ocean ridges. This crust acquires a magnetic signature at the ridge determined by the earth's ambient magnetic field, and then spreads laterally away from the ridge maintaining this signature. Reversals in the earth's magnetic field with time then lead to the formation of sea floor magnetic lineations (Vine and Matthews, 1963; and Dietz and Holden, 1970).

This theory has gained wide acceptance over the past 20 years. It is a paradigm that has helped to explain and unify much of geologic process and history. Still unknown, however, are the geologic structures inflicted upon oceanic crust as it spreads. Also unknown, therefore, is how any such structural complexities might affect the nature and thickness of rocks responsible for sea floor magnetic lineations.

In order to try to resolve these problems, dredge surveys, deep submersible dives and photographic surveys at mid-ocean ridges and fracture zones, and ocean crustal drilling projects have been carried out (e.g. Fox, 1973; ARCYANA, 1975; Heirtzler, 1975; Dmitriev, Heirtzler and others, 1978a; Donnelly, Francheteau and others, 1979a; Johnson, 1979a; and Crane and Ballard, 1981). These studies however, are limited in the type and scale of information they can contribute to the understanding of ocean crustal structure and magnetism.

Rocks recovered during dredging surveys are poorly located and commonly consist primarily of talus fragments. These rocks can, therefore, only be used to give a general idea about the surface distribution of rock types. They also usually lack the orientation features necessary for magnetic polarity studies.

Although useful information about the geologic structure at mid-ocean ridges is obtained by diving and by photographic surveys, this information is limited to structural features which are observable in surface exposures. It is even difficult to obtain information about the structure of the vertical section by observing fault scarp exposures because these scarps may parallel the strike direction of dipping units, thus exposing apparently flat-lying beds. The rocks recovered during dive surveys, however, are well located and, along with diver observations and photographs, give good information about the surficial distribution of rock types and flow morphologies, but usually lack orientation features and are, therefore, useless for magnetic polarity studies.

Rocks recovered during ocean drilling by the Deep Sea Drilling Project (DSDP) give more information about the distribution of rock types in the vertical section, but represent only a narrow window into oceanic crust. Because the in-place orientation of some of the section is preserved during rock recovery, these rocks can be used to obtain information about the magnetic polarity profile of the section of crust that was drilled. It has been impossible, however, to unambiguously determine the geologic structure of the rocks re-

covered in these drill cores. Thus, it is impossible to be sure that the measured paleomagnetic inclinations of the recovered rocks are not affected by tilting and that the observed lithologic units are representative of a depositional stratigraphic sequence and not the result of deformation.

Several lines of evidence suggest structural disturbances of the upper 500 m of North Atlantic oceanic crust. For example, breccia of possible tectonic origin was recovered at DSDP Site 333 (Aumento, Melson and others, 1977b). It also occurs at the base of Holes 395A and 396B (Dmitriev, Heirtzler and others, 1978b; and Melson, Rabinowitz and others, 1978b), in minor amounts in Holes 417 and 418 (Robinson and others, 1979), and may have caused the drilling problems at site 319 (Dmitriev, Heirtzler and others, 1978a). Partially tectonized plutonic complexes with brecciated zones were recovered at shallow depths in Holes 334 (Aumento, Melson and others, 1977c) and 395 (Melson, Rabinowitz and others, 1978b) and plutonic breccia of possible talus origin overlies basaltic basement at sites 395 and 395A (Melson, Rabinowitz and others, 1978b). There is a lack of lateral continuity between the rocks recovered in holes drilled only 500 m (396 and 396B), 100 m (332A and 332B), and less than 50 m (417A and 417D) apart suggesting structural offsets between these holes (Aumento, Melson and others, 1977a, Natland, 1978; and Donnelly, Francheteau and others, 1979b). The steep dips of pillow margins recovered in Hole 417D and the occurrence of apparently thicker pillows in this hole compared with those in Hole 417A suggests tilting

of the rocks at site 417D (Donnelly, Francheteau and others, 1979b; and Robinson and others, 1979), and the dip of layering in limestone units which are intercalated with basalt also suggests tilting of rocks recovered in Holes 417D (Donnelly, Francheteau and others, 1979b) and 332A (this study). Slick-ensided fracture surfaces along which small scale displacements occurred, indicating both reverse and normal faulting, were observed in Holes 417D and 418A (Choukroune, 1979). Finally, the measurement of non-dipolar magnetic inclinations and the occurrence of magnetic polarity changes in the vertical section of rocks recovered at sites 332A, 332B, 396B, 417D, and 418 (Hall and Ryall, 1977; Peterson, 1978; Bleil and Smith, 1979; and Hall and Robinson, 1979) may be a result of structural rotation of the rocks.

Attempts have been made to use such features as the dip of pillow margins, sedimentary layering, other megascopic geopetal features, and non-dipolar magnetic inclinations to estimate the amount of tilt of rocks recovered in some of these cores (Hall and Ryall, 1977; Johnson, 1978; Bleil and Smith, 1979; Donnelly, Francheteau and others, 1979b and c; Hall and Robinson, 1979; and Robinson and others, 1979). Based on these features alone, however, the amount of tilt cannot be accurately determined.

Original dips of pillow margins may vary from horizontal to nearly vertical and these dips cannot be distinguished from structural dips in drill core samples.

Although depositional dips of sedimentary stratification may commonly be shallow, semi-consolidated limestone with sedimentary dips of 30° to 50° was observed during submersible dives in the rift proximal to the Oceanographer Transform (P.J. Fox, per. com., 1981). Furthermore, sedimentary layers are rarely recovered in ocean basement cores.

Megascopic features such as cooling levels, which are sub-horizontal ledges that mark the position of temporary stands of lava within a cooling pillow, are more clearly indicative of the horizontal cooling position of sea floor basalts (Ballard and others, 1975; and Prevot and others, 1976) and have been used to orient dredge haul basalt samples for paleomagnetic studies (Johnson and Atwater, 1977; and Clark and others, 1978). Such features are also rare, however, in drill core samples and when present may be ambiguous in interpretation.

Structural interpretations based on deviations of magnetic inclinations from the expected dipole value are especially speculative. These interpretations first require the assumption of an original magnetic polarity, either normal or reversed. Secondly, it must be assumed that deviations from dipolar inclinations result from tilting, and are not the result of initial magnetization during magnetic excursions, anomalous inclination due to secular variation, or for older rocks, a north-south component of motion of the sea floor since formation. Even accepting these assumptions, the magnetic inclination which results from tilting depends upon the angle between the axis of structural rotation and magnetic

declination which is unknown.

Determining the geologic structure of oceanic crust is critical to understanding structural processes at spreading centers and the nature of sea floor magnetism. A method of orienting sea floor basalt samples for both structural and paleomagnetic studies, which is independant of the problems mentioned above, has been wanting. The segregation vesicle technique of sea floor basalt orientation is such a method.

Segregation vesicles are vesicles that are entirely or partly filled with interstitial material. They were first recognized by Teall (1889) for an occurrence of these vesicles in the Tynemouth Dyke of northeast England and have been described by several other workers (Table 1). Bideau and others (1977) recognized that there is a preferred orientation to these linings in segregation vesicles in sea floor basalts. They proposed that gravity controls the orientation of the lining and suggested that these vesicles may be used to orient dredge haul basalt samples for paleomagnetic studies.

The main purpose of this thesis is to present evidence that the segregation vesicle technique is, in fact, a reliable method of sea floor basalt orientation which can be used in determining the magnetic polarity of rocks collected during dredge and dive surveys and the dip and paleomagnetism of rocks recovered by drill cores. A simple method of applying the technique to these sorts of studies is proposed. The technique is then applied to a study of the paleomagnetism of rocks recovered during a dredge and dive survey of the Mid-

Table 1. Previously recognized occurrences and geologic settings of segregation vesicles.

Reference	Location	Geologic setting
Teall, J. J. H., 1889	Tynemooth Dyke, North Sea coast of NE England.	Locally porphyric and/or amygdaloidal anorthite-augite and olivine tholeiitic dike.
Osann[1], 1889	?	?
Judd, J. W., 1890	Mt. Ben Hiant, Western Isles of Scotland.	Newer Tertiary aphyric pyroxene andesite lava flow[2].
Sollas[3], 1893	Barnesmore in Donegal.	Augite-andesite dike.
Teall, J. J. H., 1899	Ballantrae and Sanguhar areas, Southern Uplands of Scotland.	Lower Silurian basic pillow lavas.
Harker, A., 1904	Skye.	Three occurrences in Tertiary dikes.
	Isle of Scalpay.	Finely crystalline, basic porphyritic dike.
	Isle of Soay.	Along the doleritic base of a sill.
	Sleat and Isle of Ornsay.	Augite-andesite dikes.
Bailey, E. B., and others, 1924	Island of Mull.	Three occurrences in a Tertiary igneous complex: 1) pillow lavas of "central type" basalts; 2) craignurite (dark-gray augite-andesite sills; 3) dolerite ring dikes.
Nicholls, G. D., 1958	Builth Wells.	Ordovician spilitic pillow lavas of the Lower Spillitic Formation of the Builth Volcanic Series.
Smith, R. E., 1967	New South Wales, Australia.	Ordovician basaltic pillow lavas of the Walli Andesite.
Upton, B. G. J., and Wadsworth, W. J., 1971	Cratère Bory, Piton de la Fournaise, Réunion.	Recent basaltic pahoehoe lavas which floor the crater.
Donnelly, T. W., 1972	St. Thomas and St. John, Virgin Islands.	Spilite flows of the mid-Cretaceous Water Island Formation (the basal unit of an island-arc volcanic sequence).
Thompson, G., and others, 1976	Eastern Pacific Ocean, about 15° S., Nazca Plate, Bauer Deep, DSDP site 319A.	Early Miocene microdoleritic flow.

Table 1.   Continued.

Reference	Location	Geologic setting
Baragar, W. R. A., and others, 1977	West of Mid-Atlantic Ridge, 37° N., DSDP site 332B.	Base of a 4 m thick medial Pliocene picrite flow.
	DSDP site 332B.	Near the upper and lower margins of a Middle Miocene Pillow basalt.
Bideau, D., and others, 1977	Mid-Atlantic Ridge, 37° N., Famous area.	Quaternary pillow basalts.
Sato, H., 1978	150 km east of Mid-Atlantic Ridge, 23° N., DSDP site 396B.	Microcrystalline and intersertal parts of Middle Miocene pillow and massive flows.
Bernoulli, D., and others, 1978	Tyrrhenian Basin, east Mediterranean Sea, DSDP site 373A.	Basaltic clast of an Early Pliocene carbonate cemented basaltic breccia (segregation vesicles photographed but not described).
Shibata, T., and others, 1979	Oceanographer Fracture Zone, North Atlantic Ocean, 35° N., 35° W.	Abyssal tholeiitic basalts.
Donnelly, T. W., and others, 1979b	Western Atlantic Ocean, Bermuda Rise, 25° N., DSDP site 417A.	Late Cretaceous porphyritic-subophitic massive basalt flow.
Juteau, T., and others, 1979	Western Atlantic Ocean, Bermuda Rise, 25° N., DSDP site 417A and D.	Late Cretaceous pillow basalts.
Robinson, P., 1980	Gulf of California, East Pacific Rise, DSDP sites 483B and 484A.	Mid-oceanic ridge basalts.

[1]Journal not available. This occurrence is referred to in Judd (1890).

[2]This unit was later identified as an intrusive sill by Sir A. Geikie (in Harker, 1904, p. 400).

[3]Journal not available. This occurrence is referred to in Harker (1904).

Atlantic Ridge, and the geologic structure and paleomagnetism of rocks recovered in DSDP cores from the North Atlantic Ocean. Based on these studies, interpretations are made about the structural and magnetic characteristics of portions of the crust beneath slowly spreading ocean basins.

STUDY AREAS, SAMPLE COLLECTION,AND FIELD WORK

Rocks used for this study were collected during the AMAR 1978 Expedition to the Mid-Atlantic Ridge, during DSDP Legs 37, 45, and 46, and during the Iceland Research Drilling Project (IRDP), 1978.

The AMAR cruise took place during July and August, 1978. The study area included portions of both the Famous and Amar Rift Valleys of the Mid-Atlantic Ridge (Figure 1). These rift valleys are located SW of the Azores Islands, between 36° and 37° N and are separated by Fracture Zone B. The study areas are referred to as Narrowgate and Amar. Two areas located on the east and west mountain tops of the Famous Rift Valley were also investigated.

The three vessels used for the survey were the deep water submersible, Alvin, along with its support ship, Lulu, both operated by Woods Hole Oceanographic Institute, and the University of Miami Research Vessel, Gilliss.

Two methods of sampling were used. The mechanical arms of the submersible, Alvin, were used to collect well positioned samples from the study area. To increase areal coverage, dredge haul samples were also collected. Pingers placed
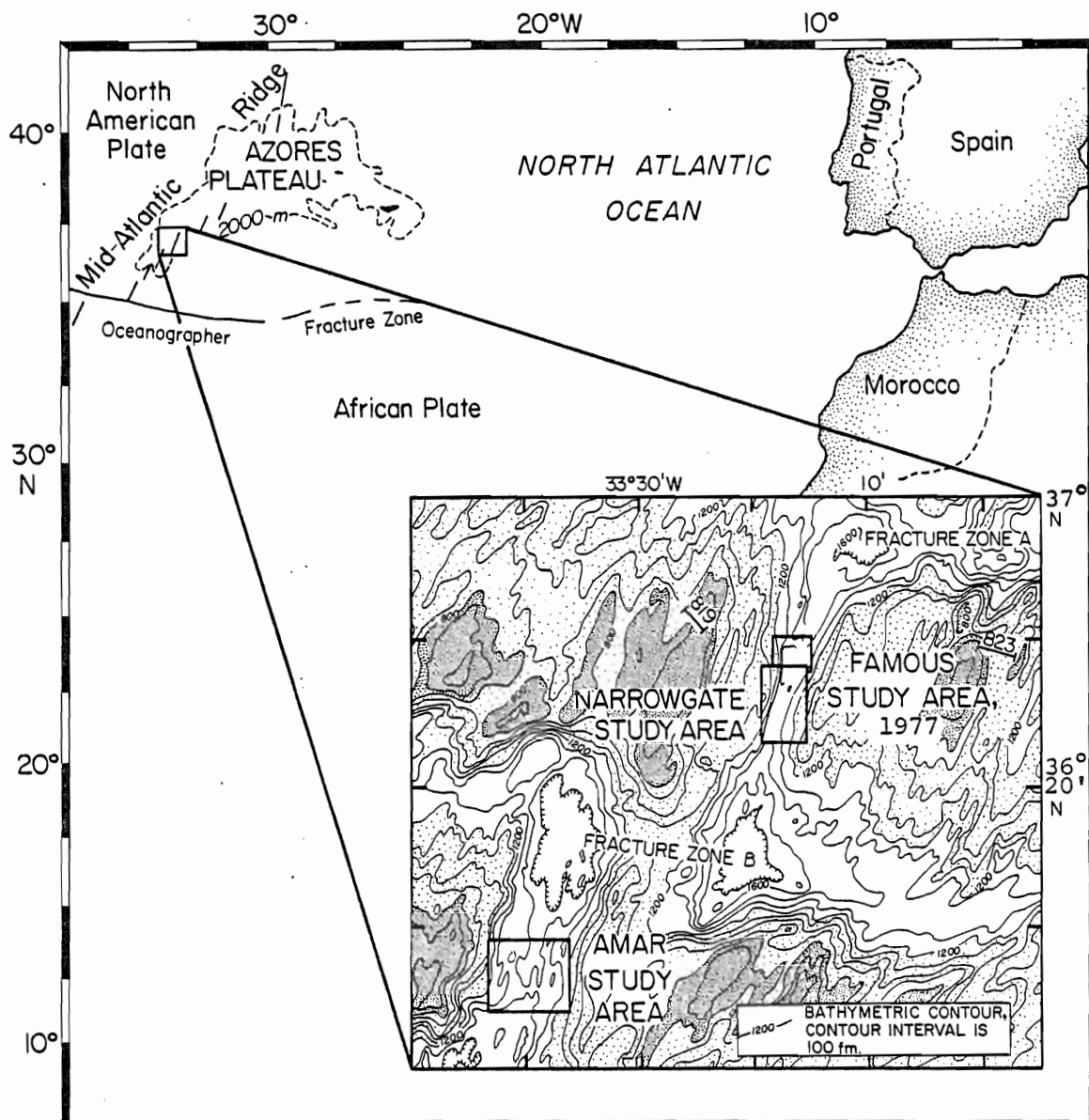
Figure 1. Study areas of the AMAR 1978 Expedition. 819 and 823 are dive track lines. Also shown is the study area of the FAMOUS 1977 Expedition.

on the Alvin and dredge allowed their position to be monitored within a transponder net by the Woods Hole ACNAV navigation system. Using this system, the accuracy of relative position- ing, with respect to the transponder net, can be within 10 to 20 m (Ballard and Van Andel, 1977; and Atwater and others, 1978).

The rocks collected were catalogued and described according to their location, physical, petrological, and orientation characteristics, and photographed and sampled aboard ship. The samples used for this study were taken with a drill press equipped with a 2.5 cm diameter diamond drill bit. A more de- tailed description of shipboard operations is in Atwater and others (1978).

Following the cruise any rocks with ambiguous descriptions of orientation features were re-examined, photographed and sampled, at Woods Hole Oceanographic Institute (April, 1980).

Legs 37, 45 and 46, of the DSDP took place during June-July, 1974, December and January, 1976, and February and March, 1976 respectively. The rocks recovered in DSDP Holes 332A, 322B, and 334, drilled during Leg 37, 395 and 395A, drilled during Leg 45, and 396B drilled during Leg 46 were studied for this project (Figure 2). These rocks were recovered prior to ini- tiation of this project and were catalogued, described, and sampled according to DSDP procedures (Dmitriev, Heirtzler and others, 1978a).

The Leg 37 samples studied were donated by Drs. James Hall and Patrick Ryall at Dalhousie University. They contributed

407 408 IRDP

• 409

Ridge

Charlie Gibbs F.Z.

Atlantic

333 332A,B
335
334 Azores

Oceanographer F.Z.

Bermuda

Atlantis F.Z.

Madeira

Canaries

417A 417D
418A 418B

Kane F.Z.

395 396,
395A 396A,B

Mid

Vema F.Z.
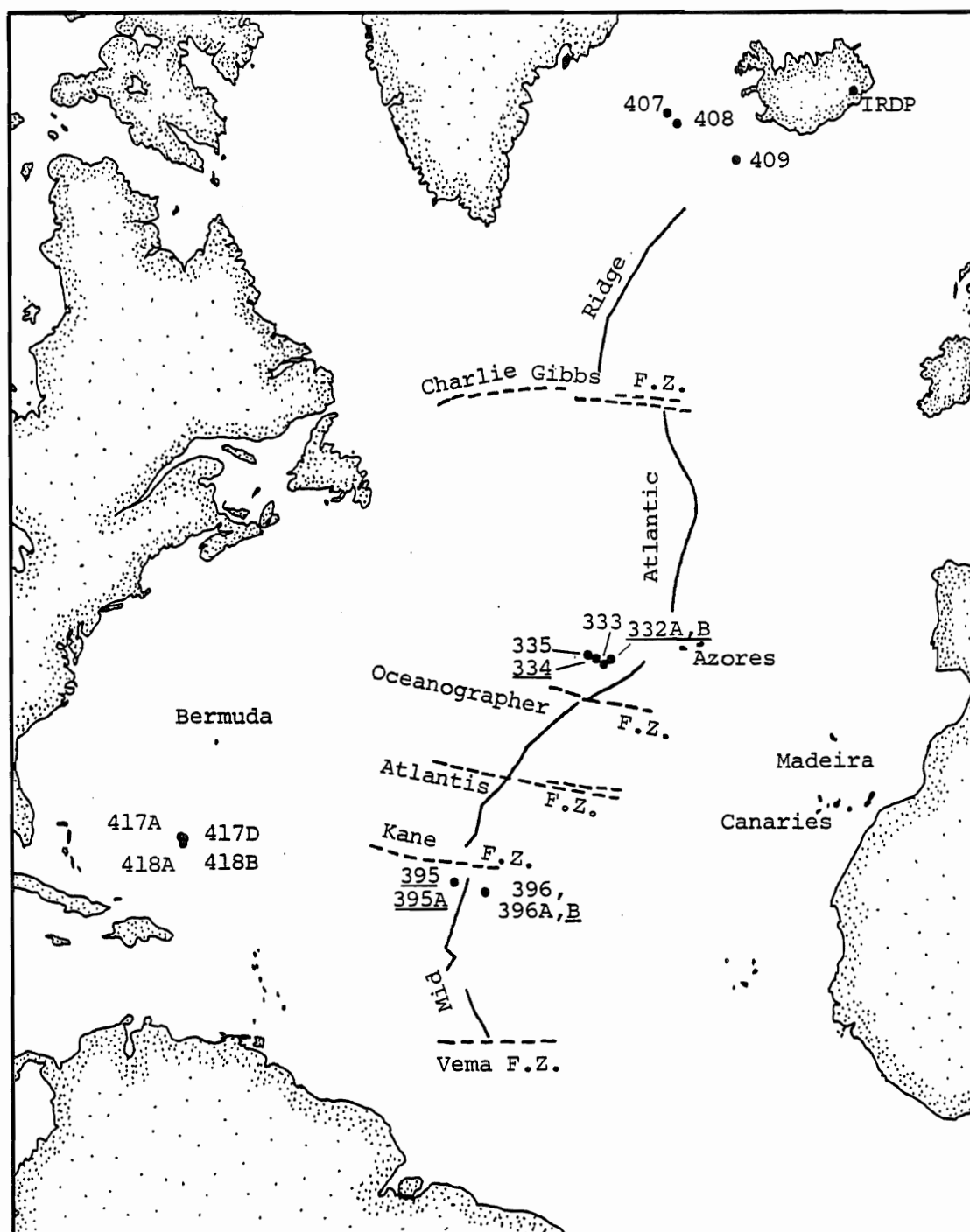
Figure 2. Index map to DSDP holes studied (underlined) or referred to in text.

samples used for their paleomagnetic study which had been demagnetized to 500 to 1000 oe in order to determine the stable NRM inclinations. The Leg 45 and 46 rocks were sampled at the Lamont-Doherty Geological Observatory DSDP Core Repository during September, 1979.

During October, 1980, a final visit was made to the Lamont-Doherty Repository to recheck the location and orientation of all DSDP rock samples. Selective portions of the cores containing megascopic structural features such as contacts, sedimentary layering, vug fillings, breccia, slickensides, and fracturing were also described.

The IRDP took place during June-August, 1978 at Reydarfjordur, Iceland (Figure 2). During this project a 1900 m hole was drilled into the Tertiary lava pile and the surrounding subaerial section was mapped. Samples were collected from both the drill core and the subaerial section.

The remaining samples used in this study are from Recent shallow marine lava flows which originated subaerially on the Island of Hawaii. These rocks were examined in thin sections donated by Dr. Peter Weigand at California State University, Northridge.

SEGREGATION VESICLES

TERMINOLOGY

The term, segregation vesicles, was formally proposed by Smith (1967) for any vesicles bearing features similar to those which occur in the Ordovician basaltic pillow lavas of the Walli Andesite of New South Wales, Australia. These vesicles are 3 to 4 mm in diameter and are filled or partly filled with glassy to fine-grained material which is texturally similar to the mesostasis and interpreted to be residual melt (Figure 3). He proposed the term because he believed segregation vesicles to be genetically similar to segregation veins described by Kuno and others (1957) and Kuno (1965).

Segregation vesicles occur in several environments but most commonly occur in submarine lavas (Table 1). Because their exact mode or modes of formation is unknown, a descriptive rather than genetic term would be more appropriate to refer to these features. The term, segregation vesicles, however, is well established, having been used since 1967 (Smith, 1967) (Table 1) and is adopted here.

The terminology used to describe such vesicles in this study is similar to the terminology proposed by Smith (1967) (Figure 3). Smith, however used the term "lining" to refer to the mesostasis in segregation vesicles. This term is confusing because other secondary material may also occur as a "lining" in these vesicles. The term "lining" is, therefore, replaced by "aphanitic residue".

principal
surface

central
zone

subsidiary
surface

aphanitic
residue

0.1 mm
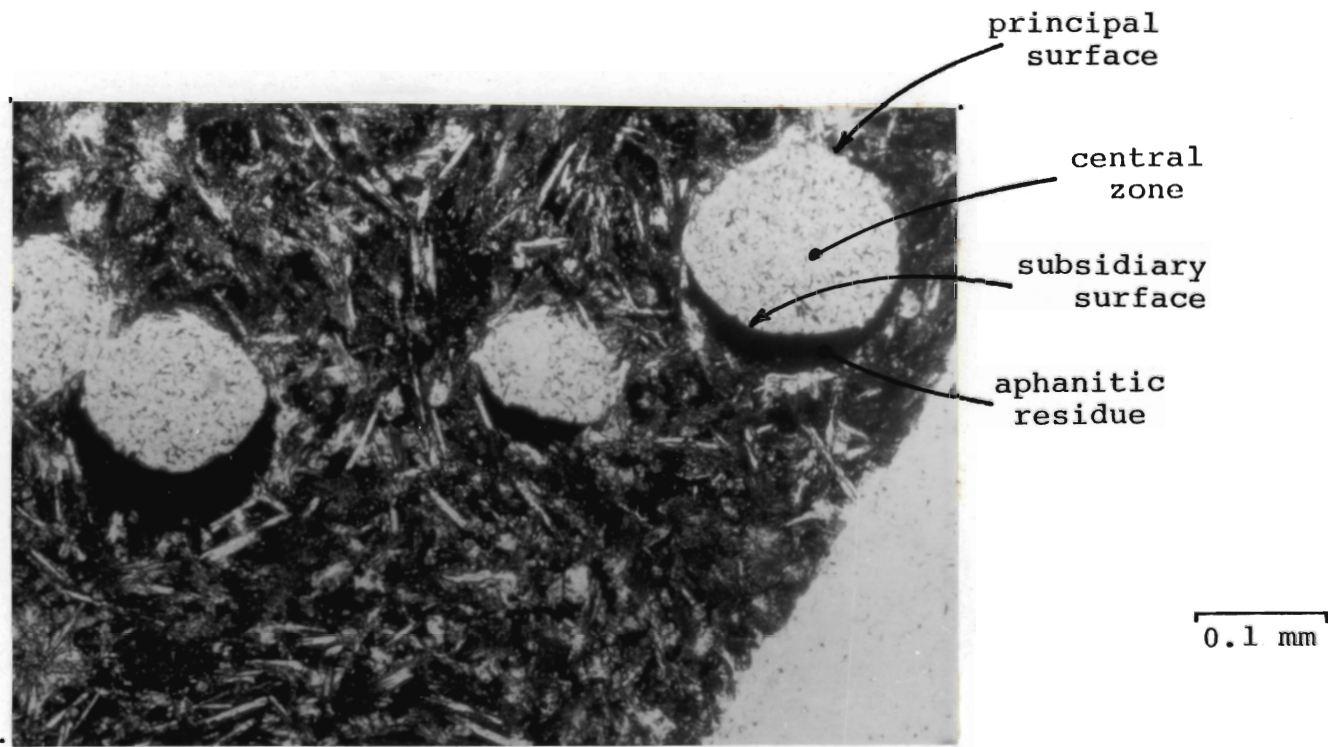
Figure 3. Photograph of segregation vesicles showing
terminology used to describe them.

GEOCHEMICAL STUDIES

Textural evidence suggests that the aphanitic residue in segregation vesicles can be described as a residual melt formed as a late fractionation product of the host rock (Teall, 1889; Harker, 1904; and Smith, 1967). This relationship has been confirmed by three geochemical studies.

Upton and Wadsworth (1971) showed that the glass contained in segregation vesicles in the basalts of Cratère Bory, Réunion is rhyodacitic in composition (Table 2). Although the difference in composition between the glass in the segregation vesicles and the composition of the host rock is extreme (Figure 4) such evolved glasses occur in the interstices of tholeiitic dikes (Vincent, 1950; Walker, Vincent and Mitchell, 1952; and Elliott, 1956, in Upton and Wadsworth, 1971). Upton and Wadsworth (1971) suggested that the rhyodacitic glass developed by fractionation of the host rock during unusually oxidizing conditions.

Comparison of the composition of aphanitic residue in segregation vesicles in DSDP basalts with the bulk chemical composition of the host rock by Baragar and others (1977) confirmed that the residue is a late fractionation product of the host rock. The major chemical changes are an enrichment of iron relative to magnesium and a decrease in alumina due to pyroxene and plagioclase fractionation, respectively (Table 2, Figure 4). This fractionation trend is further emphasized by a comparison of the glass composition of these

Table 2. Major element analyses of magma residue in segregation vesicles (SV), Mesostasis, basaltic rocks (bulk), and glasses.

| | 396B 20-1* | | | | | | | 332B 33-2* | | 332B 35-3* | | 335 6-1* | | | | | | Réunion* | | 332B* | 332B* | 6.1 | 335* | |
| | 53-55 | 83-84 | 113-122 | | | 93-102 | | 85-88 | | 81-84 | | 52-55 | | 61-64 | | 129-131 | | Cratère Bory | | 33.3 30 | 35.3 81 | | 47-49 | |
	-bulk	glass	SV	mesostasis	SV	SV	mesostasis	bulk	SV	bulk	SV	bulk	SV	bulk	SV	bulk	SV	bulk	SV	glass	glass	glass	glass	glass
SiO_2	49.92	50.60	51.30	50.60	52.60	49.10	51.90	42.83	46.40	44.53	49.43	46.86	45.18	48.25	46.56	47.86	45.82	49.15	64.94	50.95	50.41	49.56	50.30	50.03
TiO_2	1.04	1.35	2.36	2.79	2.69	2.37	2.78	1.00	2.79	0.68	1.09	1.19	1.74	1.17	1.63	1.27	2.01	2.99	1.12	1.13	0.71	1.28	1.18	1.14
Al_2O_3	17.64	15.30	11.68	10.10	11.10	10.28	9.98	15.00	13.16	17.56	13.03	15.70	10.09	15.29	11.43	15.83	9.39	14.79	13.92	15.04	16.20	15.21	14.30	15.94
Fe_2O_3								4.31		5.68		4.25		5.63		5.51		1.59	2.92					
FeO	7.93	9.39	11.57	12.33	12.59	11.94	12.58	4.84	20.08	4.62	11.07	4.88	14.16	4.38	12.19	4.52	14.01	9.96	0.84	10.13	9.14	9.66	9.95	9.10
MnO	0.16	0.16	0.23	0.28	0.22	0.27	0.26	0.16	0.23	0.15	0.17	0.15	0.17	0.15	0.20	0.14	0.20	0.18	0.12			0.21	0.21	0.17
MgO	7.39	7.89	5.76	4.75	6.71	6.99	5.91	7.66	3.24	4.65	5.85	7.32	8.93	7.47	6.79	6.81	8.44	6.03	1.88	7.39	8.84	8.29	7.80	8.25
CaO	12.79	14.11	14.11	13.89	13.58	14.57	12.29	14.12	7.88	13.27	13.19	13.00	11.54	11.66	13.75	11.64	13.44	10.99	3.76	12.41	12.59	11.83	12.20	11.51
Na_2O	2.42	2.75	2.75	2.41	2.73	2.72	2.56	2.05	3.81	2.35	2.70	2.37	2.13	2.42	2.70	2.45	2.07	2.87	3.87	2.08	2.07	2.34	2.30	2.70
K_2O	0.21	0.25	0.25	0.28	0.38	0.38	0.45	0.22	0.73	0.21	0.25	0.20	0.26	0.39	0.37	0.29	0.30	0.81	3.66	0.17	0.08	0.24	0.22	0.14
P_2O_5	0.11							0.12		0.12		0.11		0.11		0.13		0.31	1.04	0.10	0.08			
H_2O^+	0.88							1.20		1.38		1.28		1.18		1.89		0.14	0.38					
H_2O^-								0.32		1.06		1.16		1.36		1.08								
CO_2								6.03		3.80		1.05		0.09		0.20			1.26					
S								0.02	0.00	0.02	0.00	0.05	0.00	0.01	0.00	0.03	.0.00							
TOTAL	100.49	99.1	100.0	97.40	102.60	98.90	98.70	100.11	98.32	100.26	96.78	100.02	94.20	99.56	95.62	99.65	95.68	99.81	99.71	99.40	100.12	98.62	98.96	98.98

*Analyses for 396B are microprobe determinations from Sato (1978). Bulk and SV compositions for 332B and 335 are from Baragar and others (1977). Bulk analyses are by gravimeter, colorimetric, atomic absorption, Pratt method titration, acid evolution, and Penfield tube determinations. SV analyses are averages of multiple microprobe determinations. Analyses for Réunion are X-ray flourescence determinations from Upton and Wadsworth (1971). Microprobe glass analyses of 332B and 335 are from Aumento and others (1977a).
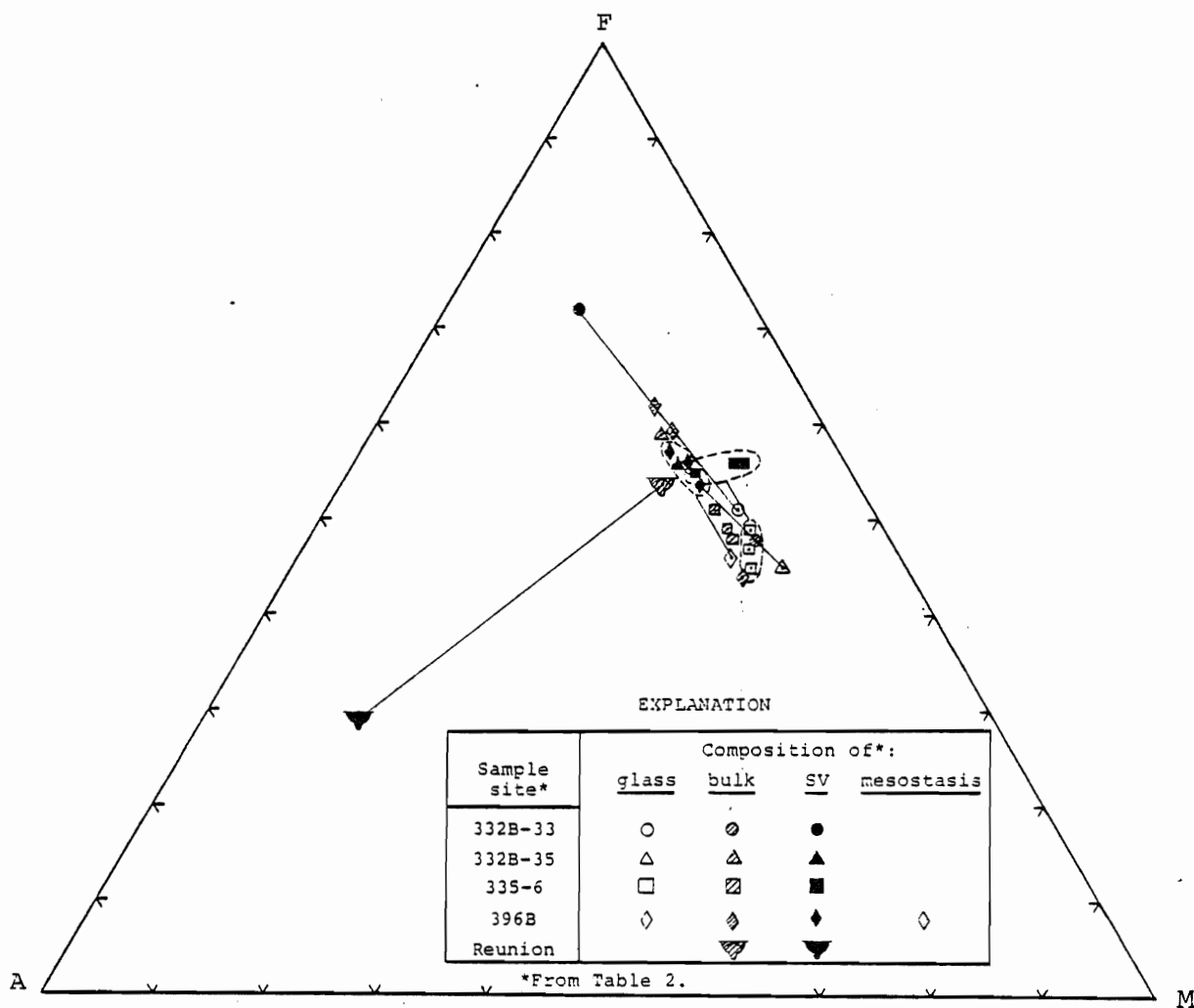
Figure 4. AFM diagram showing the composition of aphanitic residue in segregation vesicles in relation to the composition of the host rock and mesostasis of some seafloor basalts. The diagram illustrates that the residue in segregation vesicles is a fractionation product of the host rock. Data are from Table 2. $F = FeO + Fe_2O_3$.

rocks to that of the magma residue in vesicles (Table 2, Figure 4).

There is an apparent Mg enrichment of the magma residue in vesicles of DSDP Hole 335. Baragar and others (1977) attributed this apparent trend to alkali depletion due to plagioclase fractionation, but it may also simply reflect analytical error. Mg-chlorophaeite and dolomite occur as secondary minerals in some of these vesicles and may have altered some of the residual melt material. The defocussed microprobe beam used to analyze the residual melt may either have been placed over an altered portion of this material or may have overlapped onto secondary minerals. This possibility is suggested by the low totals of some residual glasses from these holes (Table 2).

Sato (1978) compared the composition of aphanitic residues in segregation vesicles to that of the host rock (whole rock and glass chemistry), and to the composition of the mesostasis of basalts from DSDP Hole 396B (Table 2). His data show that the FeO to MgO ratio of the mesostasis is higher than that of the material in segregation vesicles (Figure 4) suggesting that the fillings have retained an earlier composition of a continually evolving melt.

These geochemical studies support the interpretation that the aphanitic residue in segregation vesicles is a fractionate of the host rock. The final composition of the filling magma residue depends upon the initial bulk composition of the rock, its cooling environment and history, and the amount of fractionation before chilling. These complications result in a

wide variation of composition of magma residues in segregation vesicles even from similar rocks with a similar bulk composition (Figure 2).

The residue must enter the vesicle sometime after crystallization is sufficient to maintain the integrity of the vesicle but before final solidification of the rock. Magma remaining in the interstices of the rock continues to fractionate, resulting in a more evolved chemistry (Figure 4). The solidus temperature of the residue in segregation vesicles must be slightly higher than that of the mesostasis. The rock may, therefore, still be slightly plastic at the time the melt in the segregation vesicles chills.

DESCRIPTION OF SEGREGATION VESICLES IN SEA FLOOR BASALTS

Introduction

During this investigation over 700 segregation vesicles occurring in 37 different sea floor basalt samples were studied for descriptive purposes. Twenty-one of the samples were recovered from the Famous and Amar Rift Valleys during the AMAR 1978 Expedition and 16 of the samples were recovered from an area west of the Famous Rift Valley during Leg 37 of the DSDP. Observations were made using a standard petrographic microscope and thin sections ground to .03 mm. These observations are synthesized along with information on the characteristics and distribution of segregation vesicles in sea floor pillows and flows described by previous workers

(Baragar and others, 1977; Bideau and others, 1977; Sato, 1978; Donnelly, Francheteau and others, 1979b; and Juteau and others, 1979).

Distribution of Segregation Vesicles in Pillows and Flows

Segregation vesicles generally are absent in the glassy, quenched or spherulitic outer chilled margin of pillows and flows. Their first occurrence is just inside the glassy rind where true glassy matrix disappears and the spherulitic texture of the rock grades into an aborescent or sheaf-like texture of intergrowths of hollow plagioclase microlites and plumose pyroxene crystals (Juteau and others, 1979; Bideau and others, 1977; and Bryan, 1972). The vesicles are most abundant in the microcrystalline and intersertal parts of the rock, near the upper and lower margins of pillows and flows, where they commonly are associated with plagioclase $\pm$ pyroxene and olivine microlites in an irregular or pilotaxitic arrangement (Bideau and others, 1977; and Sato, 1978). They are rare to absent in the most crystalline intergranular to subophitic portions of the rock (Bideau and others, 1977; and Sato, 1978).

Shape, Size, and Microcrysts Surrounding Segregation Vesicles

The apparent shape of a vesicle depends in part upon the direction of observation. To estimate the frequency of occurrence of different vesicle shapes, the vesicles observed in thin section were divided into 3 categories: 1) circular; 2) slightly irregular with minor protrusion voids; and 3) very

irregular with protrusion voids. An overwhelming number of vesicles appear circular in thin section, indicating that the dominant shape of segregation vesicles is spherical (Figure 5). The significance of protrusion voids is uncertain. Bideau and others (1977) believed they formed by gas escape during cooling. Some irregularities in the circular shape probably are the result of destruction during thin sectioning.

The size of a vesicle measured in thin section is controlled in part by the orientation of the thin section plane through the vesicle. Unless this plane intersects the center of a spherical vesicle, the measured diameter will be less than the true diameter.

The segregation vesicles measured range in size from 0.05 to 2.09 mm in diameter, a range which is consistent with the observations of other workers (Sato, 1978; and Bideau and others, 1977). A majority are between 0.1 and 0.3 mm diameter (Figure 6).

Plagioclase microlites surrounding the vesicles may be arranged tangentially, radially, obliquely or randomly around the vesicles. A tangential arrangement of these microcrysts tends to be most common in parts of pillows of flows which have an intersertal texture. Whereas, in microcrystalline or pilo-taxitic portions of the rock segregation vesicles may be de-lineated by oblique or randomly arranged microlites (Sato, 1978).
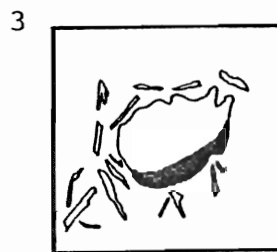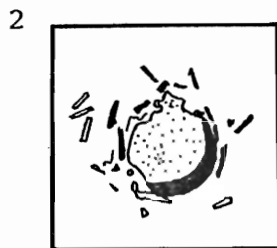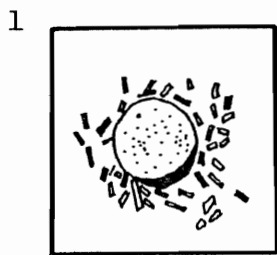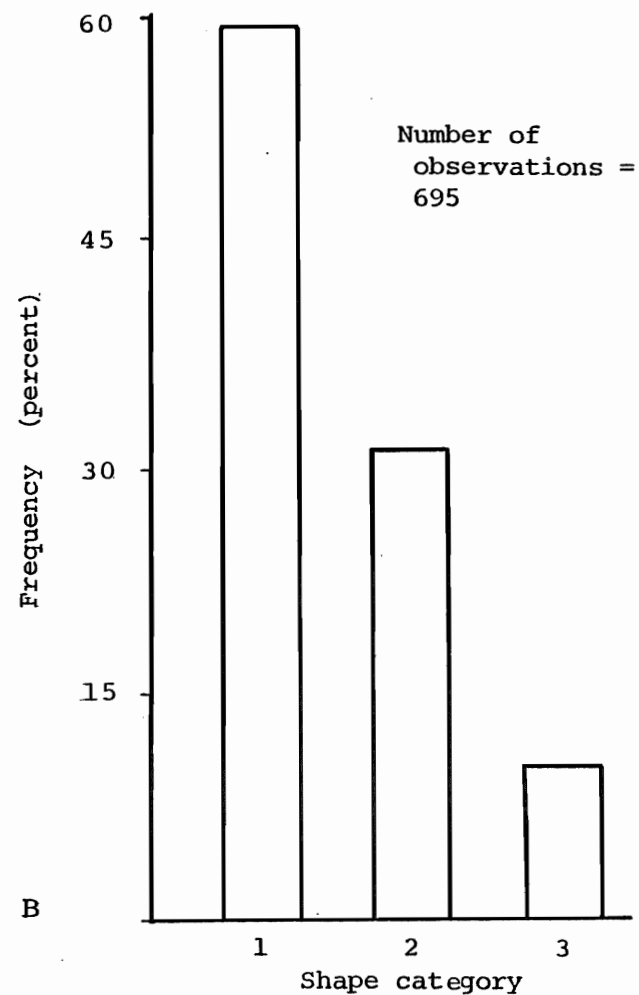
Figure 5. A) Sketches illustrating the shape categories into which segregation vesicles were divided. 1 is circular; 2 is slightly irregular with minor protrusion voids; 3 is very irregular with protrusion voids. B) Graph illustrating the frequency of occurrence of each shape.
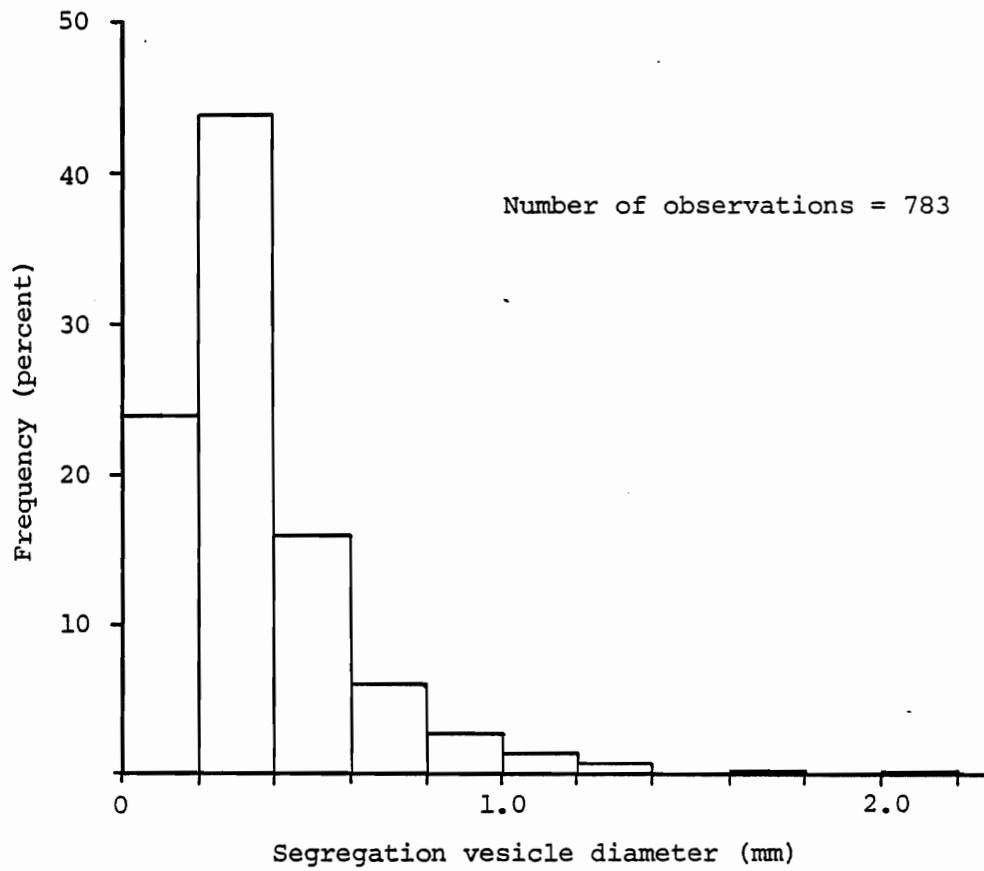
Figure 6. Graph showing the size range and frequency of occurrence of segregation vesicle diameters.
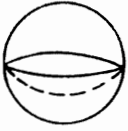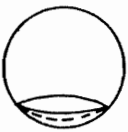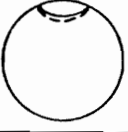
Shape, Crystallinity, and Amount of Residue in Segregation
Vesicles

Bideau and others (1977) recognized that the segregated
material forms a concave upward, crescent-shaped meniscus in
segregation vesicles. The apparent variability of this shape
depends upon the amount of fill and direction of observation
(Figure 7). Over 64 percent of the vesicles observed have
symmetrical linings (Figure 8).

The crystallinity of residual melt in segregation vesicles
is always similar to that of the residual melt in interstices
of the groundmass. It varies from being a devitrified glass
to a semi-crystalline, generally dark material, containing a-
bundant opaque oxides. Rarely it consists of plagioclase,
pyroxene or olivine microlites that are readily recognizable
by standard petrographic techniques.

Bideau and others (1977) recognized that the amount of fill
in segregation vesicles is related to the actual volume of
residual melt available to enter the vesicle and space avail-
able for the melt. The observed amount of fill depends upon
the actual volume of residual melt in segregation vesicles and
the direction of observation (Figure 7). Donnelly, Francheteau
and others (1979b) estimated about 50 percent fill in the se-
gregation vesicles they observed.

The amount of fill of 606 segregation vesicles observed in
23 different rock samples was estimated in thin section and the
diameter of the principal surface was measured. From these
measurements the volume of each vesicle contained within the

Figure 7. Schematic diagram of the theoretical shape of segregation vesicles, segregated material, and their expected appearance in cross section. In addition to expected theoretical shapes, irregular shapes are rarely observed. Modified after Bideau and others (1977).
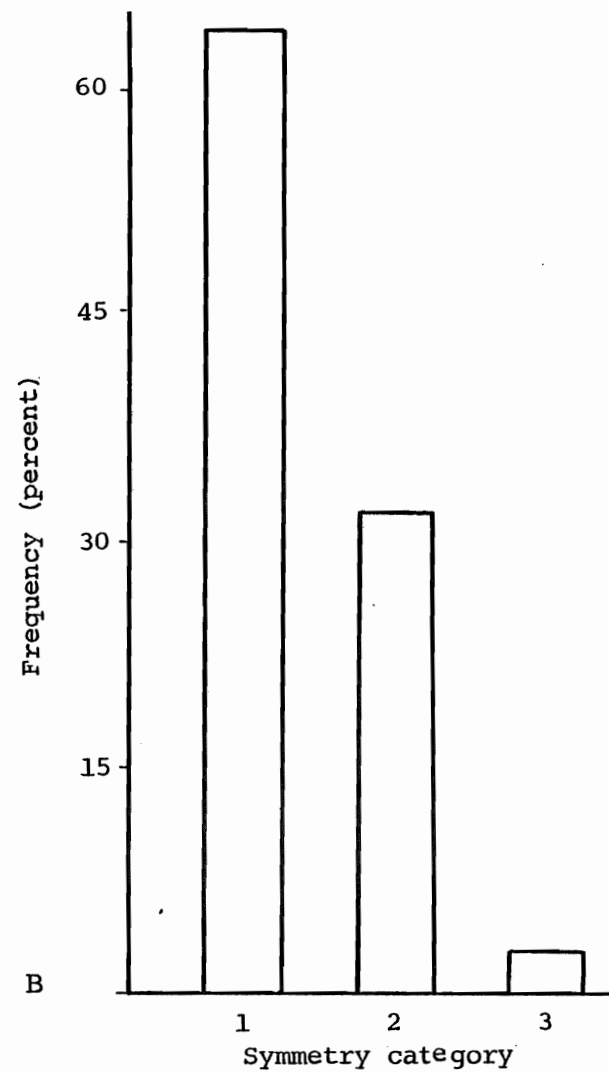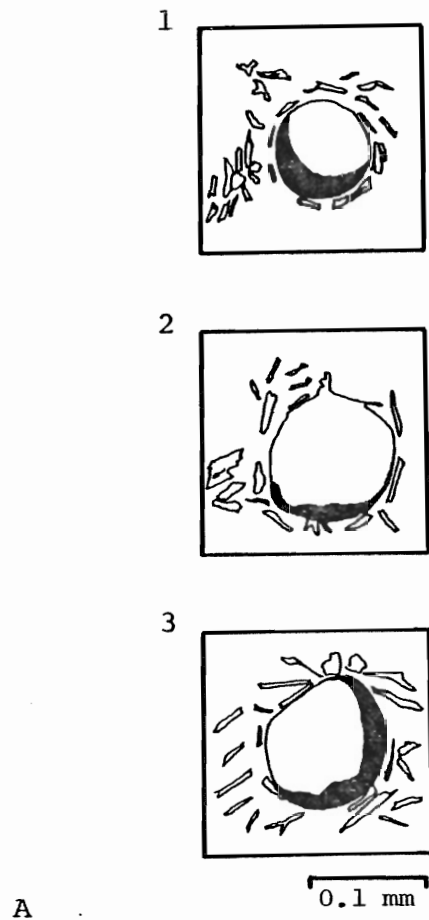
Figure 8. A) Sketches illustrating the symmetry categories into which the linings of residual melt were divided. 1 is symmetrical; 2 is slightly asymmetrical; 3 is asymmetrical. B) Graph illustrating the frequency of occurrence of each symmetry category.

principal and subsidiary surface was determined, assuming

spherical vesicles. The percent volume difference between

the two spheres was then determined as the ratio between the

two volumes (Appendix I). This ratio gives the apparent vol-

ume percent of segregated material in the vesicle.

In 59 percent of the observed vesicles the residue oc-

cupies less than 20 percent of the volume (Figure 9). These

data also suggest that the gas volume change required to make

room for the residue is usually less than 20 percent.

RECOGNITION OF THE POTENTIAL OF SEGREGATION VESICLES AS A ROCK ORIENTATION TOOL

Although Upton and Wadsworth (1971) recognized that the

residual glass in the Réunion Island basalt was concentrated

in the lower part of the vesicle, Bideau and others (1977)

first proposed the segregation vesicle technique of sea

floor basalt orientation. Their technique was based upon

the recognition that there is a preferential orientation to

the crescent-shaped linings of segregated material along the

bottom of vesicles with their concavity pointing upward. They

suggested that once the residual melt enters the vesicle it

flows, under the force of gravity, to the bottom of the vesicle

before solidifying while the volatile phase occupies the space

near the top. A line connecting the points of the crescent can,

therefore, be used as an indicator of original horizontality.

A test of the technique on two pillow basalts of known orienta-

tion indicated agreement within 15° between the known orien-
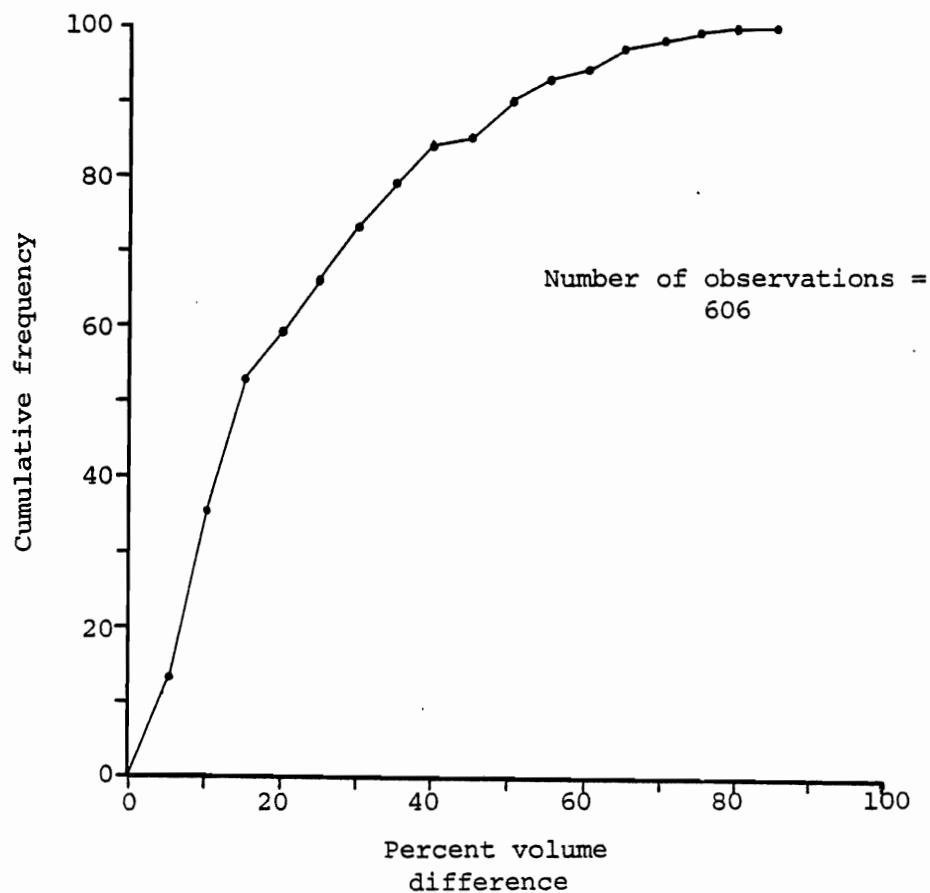
Figure 9. Cumulative frequency curve of the percent volume difference between the segregation vesicle volumes given by the principal and subsidiary surfaces. There apparently is less than 20 percent volume difference between most of these samples. This suggests that less than 20 percent volume reduction of the gas occupying the vesicle is required to make room for the residual melt.

tation of the rock and that given by segregation vesicles.

Bideau and others (1977) suggested that the technique would mainly be applicable to orienting dredge haul basalt samples for magnetic polarity studies. The segregation vesicles probably form at about $1000^{\circ}C$ so that the vertical axis of the rock given by segregation vesicles is acquired before the rock passes through the Curie temperature (about $150^{\circ}C$). As a caution, they suggested segregation vesicles from the interior of the rock should be used because this portion of the rock is the last to cool and has the least chance of being affected by deformation after cooling. Based on the 15° angular difference between the known and segregation vesicle orientation of their test samples, they suggested that the technique would be applicable for magnetic polarity studies outside a band of 20° latitude of the paleoequator. They did not recognize the applicability of the technique as a tool for interpreting the structural profile of sea floor basalts recovered in drill cores.

Although they showed their technique to be potentially useful, additional testing, along with a more rigorous statistical treatment of the data, is required to establish its reliability.

FORMATION OF SEGREGATION VESICLES

Introduction

Although the main purpose of this thesis is to evaluate
the validity of, and once evaluated to use the segregation
vesicle technique of sea floor basalt orientation, it is de-
sirable to understand the physical and chemical properties of
the crystal-liquid-vapor system and environment of extrusion
that allowed these features to form. It is stressed, however,
that the validity of the technique probably is independent of
the mode of formation of segregation vesicles (Bideau and
others, 1977).

Any mechanism for the formation of segregation vesicles
must explain three processes: 1) the formation of a vesicle;
2) the volume decrease of the gas which occupies the vesicle,
in order to make room for the residual melt, without destroying
the vesicle shape, requiring that this decrease occurs after
the rock is sufficiently crystallized to maintain the inte-
grity of the vesicle; and 3) the movement of residual melt
from the interstices of the rock to the vesicle interior with-
out disruption of the vesicle shape. This movement must occur
sometime after the rock is 50 (Sato, 1978) to 70 (Bideau and
others, 1977) percent crystallized.

Previous Explanations

Teall (1889) suggested that segregation vesicles in tho-
leiitic dikes grew by displacement of the porphyritic con-

stituents around them, resulting in a tangential arrangement of crystals around the growing bubbles. Sometime after most of the porphyritic constituents were formed, but before final crystallization of the rock, residual melt entered some vesicles owing to absorption, escape, or condensation of the gas. He did not, however, speculate upon which of these mechanisms of gas evacuation most likely occurred.

Smith (1967) considered four possible mechanisms for partial evacuation of vesicle gas, to explain the formation of segregation vesicles in the Walli Andesite (Table 1). These mechanisms are; 1) shrinkage of gas during cooling at constant pressure according to Charles' Law; 2) escape of gas during cooling; 3) solution of vesicle gas in residual melt due to its increased solubility in the melt with cooling; and 4) shrinkage of gas during cooling with increasing pressure according to the General Gas Law.

He discounted the first three mechanisms. Calculations according to Charles' Law indicated that the reduction in temperatures during cooling was insufficient to account for the estimated change in volume of the vesicle gas. There was no evidence, such as ruptured vesicles, to indicate that the gas escaped during cooling. It also seemed unlikely that the gas was dissolved in the melt. Although solubility of the gas may increase with decreasing temperatures (Hamilton and others, 1964; and Moore, 1965), crystallization also continues leaving less melt to redissolve the gas (Smith, 1967).

Preferring the last mechanism, Smith (1967) suggested that a change in external pressure was created as the Walli Andesite lava flowed from a subaerial, near shore position of extrusion, down a sloping shoreline to a submarine position of deposition. This depositional environment is consistent with other geologic observations. His calculations according to the General Gas Law indicated that a change of pressure with cooling could create the necessary volume contraction of the gas, which he believed to be 50 percent.

This mechanism may account for the special set of circumstances associated with the formation of segregation vesicles in the Walli Andesite, but cannot provide a general explanation. Smith (1967) ignored previously reported occurrences of segregation vesicles in dikes and other pillow basalts (Table 1) which were not deposited on a sloping shoreline.

The Recent Cratère Bory lavas form a congealed lava lake in the Piton de la Fournaise (Upton and Wadsworth, 1971) (Table 1). Segregation vesicles rarely occur in these rocks, but there is no indication that the ambient pressure changed significantly as the rocks cooled. Upton and Wadsworth (1971) preferred the solubility mechanism to explain the formation of these segregation vesicles. They suggested that ground water became locally involved with the lava, vaporizing rapidly to form bubbles in the basalt while normal vesiculation proceeded due to the exsolution of CO_2 gas. Because the melt was undersaturated with respect to water, the water vapor in the bubbles was dissolved by the melt, leading to oxidation

of the melt and development of the rhyodacite fractionation trend (Figure 4). The residual melt then entered the vesicles by a process of suction toward the low pressure sites in vesicles caused by water vapor evacuation (Upton and Wadsworth, 1971).

Baragar and others (1977) proposed a similar mechanism for the formation of segregation vesicles in mid-ocean ridge basalts (Table 1). They suggested that because these basalts are undersaturated with respect to water, water vapor in vesicles would be dissolved during crystallization by residual melt. Such resolution along with contraction of the gas due to cooling would create low pressure sites at the vesicles as well as sufficient space for the residual melt in vesicles. The residual melt would then be forced into the vesicles under high external pressure.

Bideau and others (1977) noted the occurrence of protrusion voids around vesicle margins and, therefore, suggested that vesicle gas escaped during intrusion of the residual melt into the vesicles.

Evaluation

Introduction

In order to evaluate proposed mechanisms for the formation of segregation vesicles in sea floor basalts, the physical and chemical properties of the liquid, gas, and solid phases throughout the cooling history of the mid-ocean ridge basalt system must be understood. Unfortunately, little is known about these pro-

perties. Also crucial to the problem but poorly understood
is how exsolution of different volatile phases during cooling
will affect the physical properties of the remaining melt.
The following evaluation is based upon what is known from
experimental data about the physico-chemical properties of
basic silicate melts as well as what can be deduced about
segregation vesicle formation from their shape and textural
characteristics.

Bubble Formation

Presuming the gas is of internal origin, bubbles begin to
form when the melt is supersaturated with respect to a vapor
phase (Sparks, 1978). In submarine basalts the dominant vola-
tile constituent that produces vesicles is CO_2 (Moore and others,
1977; and Delaney and others, 1978). These rocks are under-
saturated with respect to water (Moore, 1965) such that water
alone will never enter into a volatile phase at depths greater
than 500 m (Moore, 1970).

If a melt becomes even slightly supersaturated with res-
pect to a volatile phase a bubble will result (Sparks, 1978).
Ease of bubble nucleation is aided by the electrostatic energy
density at the bubble embryo surface due to the presence of
absorbed ions such as oxygen, sulfur, and phosphorus (Levine,
1972 and 1973), which act as surfactants. In sea floor basalts
the surfactant may be sulfur or sulfur radicals. This is sug-
gested by the occurrence of vesicles lined with iron, nickel,
and copper sulfide spherules in the outer glassy rind of

pillow basalts (Moore and Calk, 1971; Yeats and Mathez, 1976; and Moore and others, 1977). The presence of these sulfides suggests that during early stages of formation, the vesicles contained a substantial content of gaseous sulfur which later reacted to form sulfide spherules (Moore and others, 1977). Bubble nucleation is further enhanced by the presence of solid boundaries where super saturation pressures are reduced (Fischer, 1948; Wilcox and Kuo, 1973; and Sparks, 1978). Microcrysts and phenocrysts probably act as bubble nucleation sites. Vesicles in the well-quenched portion of glassy rims of pillow basalts commonly are attached to crystals (Delaney and others, 1978) and segregation vesicles usually are surrounded by a web-like network of these crystals.

The degree of vesiculation is controlled by the volatile content of the lava at the time of eruption and the confining pressure induced by the water column (Moore, 1970; and Duffield, 1978). Bubble growth occurs by both the diffusion of gas dissolved in the magma to bubble sites and decompression of the gas inside the bubble as the hydrostatic pressure is decreased. Diffusional growth rate is a function of the composition, solubility, and degree of supersaturation of the volatile phase (Sparks, 1978).

CO_2 solubility primarily depends upon pressure and temperature, increasing significantly at pressures in excess of about 20 Kbars (Khitarov and Kadik, 1973). Experimental evidence indicates that acidic and basic silicate melts can only dissolve 0.1 to 0.6 weight percent CO_2 at pressures up to 3 to 5

Kbars. At any given pressure and temperature conditions CO_2 solubility also is markedly dependent upon bulk composition, increasing as the ratio of network modifiers (e.g. Na_2O, K_2O, CaO, MgO, etc.) to network builders (SiO_2, Al_2O_3, P_2O_5) increases. CO_2 is, therefore, more soluble in basic than acidic melts.

Solubility curves for CO_2 in basic melts at pressures less than 30 Kbars and temperatures less than 1850° have been determined (Khitarov and Kadik, 1973; and Spera and Bergman, 1980).

The estimated CO_2 concentration in some sea floor basalt melts prior to crystallization is about 0.2 to 0.4 weight percent (based on analysis of glass-vapor inclusions in phenocrysts). Although some of this gas ends up trapped as inclusions in phenocrysts, CO_2 contents of matrix glasses are still close to the saturation curve (about 0.08 to 0.16 weight percent) at pressures (about 0.2 to 0.5 Kbars) and temperatures (about 1000 to 1200^OC) of quenching (Delaney and others, 1978; and Spera and Bergman, 1980). If magma chambers beneath mid-ocean ridges are located at shallow depths it is possible that CO_2 degassing occurs prior to extrusion. Several authors have suggested that such magma chambers are located at depths of 2 to 5 km (Kusznir and Bott, 1976; Rosendahl, 1976; and Rosendahl and others, 1976). Assuming a lithostatic pressure gradient of 0.3 Kbars/ km (Carmichael and others, 1974), and a pressure due to the overlying water column of 200 to 500 bars, this depth corresponds to a pressure of about 1 to 2 Kbars. Even at these pressures, and temperatures of about 1200^OC, a basic melt with as

little as .08 weight percent CO_2 could become vapor saturated (Delaney and others, 1978; and Spera and Bergman, 1980).

The insoluble nature of CO_2 at low pressures implies that early bubble growth probably is the result of diffusion of CO_2 to bubble nuclei within the magma chamber. Outgassing probably occurs rapidly once the magma rises to a level at which the supersaturation pressure of the CO_2 content is reached. Decompressional bubble growth then follows as the volatile saturated magma rises from the magma chamber to the eruptive site. Assuming that CO_2 begins to evolve from a melt in a shallow magma chamber experiencing a lithostatic pressure of 1 Kbar, the melt is then extruded at a depth of 5000 m (0.5 Kbars), the evolving volatiles exhibit ideal gas behavior, and there is no resistance to bubble growth, calculations according to Charles' Law indicate that the rising bubble may double in volume.

The pressure of the gas inside a growing bubble in a sea-floor basalt must equal or exceed the surrounding hydrostatic pressure, plus the excess pressure (viscous pressure, surface tension pressure, and inertial pressure) (Rosner and Epstein, 1972). Magnitudes of excess pressures determined for subaerial basalts are small, ranging from .001 to .1 bars (Sparks, 1978), and hence are ignored here. The CO_2 pressure must, however equal the confining pressure of the overlying water column. This pressure may range from 260 to 280 bars assuming a pressure gradient of 1 bar per 10 m of water depth (Gross, 1972) and rift valley depths similar to Famous Rift Valley depths of

2600 to 2800 meters (Phillips and Flemming, 1978).

At some point the vesicle will stop growing. This occurs when the melt is no longer saturated with respect to a volatile phase or there is a balance between the internal pressure of the bubble and the dissolved vapor pressure of the gas (Sparks, 1978). For Leg 37, and Amar and Famous Rift Valley basalts, occurrence of spherical vesicles, undeformed by flow stresses or the weight of the overlying rock indicates that cessation of growth occurs after the melt has solidified sufficiently to maintain the shape of the vesicle. This temperature is referred to as the rigid temperature (Moore and others, 1977).

Process of Gas Evacuation and Flow of Residual Melt into the Vesicles

Once a vesicle is established there is potential for a segregation vesicle to form if a variety of conditions are met. One of the most controversial problems of segregation vesicle formation on the sea floor is what process causes the gas to partially evacuate the vesicle, making room for the residual melt.

With cooling, the gas in the vesicle will shrink. Smith (1967) suggested that the gas in Walli Andesite segregation vesicles shrank to half of its maximum volume prior to intrusion of the residual melt. A similar estimate was made for segregation vesicles of some DSDP basalts (Donnelly, Francheteau and others, 1979b). Observations of segregation vesicles

in basalts from the Famous and Amar Rift Valleys and Leg 37 basalts during this study indicate that volume shrinkage usually is less than 20 percent (Figure 9).

The temperature decrease that occurs between the rigid temperature and the time the last melt enters the vesicles probably is around 150°C (Smith, 1967; based on cooling temperatures of tholeiitic basalt in Alae lava lake, Hawaii from Peck and others, 1965 and 1966). Smith (1967) used Charles' Law to show that such a temperature decrease can decrease the absolute volume of the gas (assuming ideal behavior) by 17 percent. This volume change is consistent with observations of this study (Figure 9).

Although the gas shrinks, below the rigid temperature the container (vesicle) is fixed in volume. The pressure of the gas on the vesicle walls, however, will decrease to some value less than the confining pressure of the overlying water column. By application of the General Gas Law (keeping volume constant, and assuming a 250°C temperature decrease), the pressure of the gas inside the vesicle may decrease by approximately 20 percent. For rocks erupted on some parts of the Famous Rift Valley this means a pressure decrease from about 260 bars to 208 bars. As soon as the gas starts to shrink, therefore, a pressure gradient is established. The width of this gradient is unknown, but it probably is narrow.

This pressure gradient may then initiate flow of nearby residual melt into the vesicle. Flow may continue until the pressure inside the vesicle equals that outside the vesicle

or the melt becomes too viscous or crystalline to flow.

This explanation conflicts with that of Bideau and others (1977) who suggested that the gas leaves the vesicles through protrusion voids. Observations of vesicle shapes during this study, however, indicate that segregation vesicles generally are spherical and without protrusion voids (Figure 5). Where there are protrusion voids it is difficult to determine when in the cooling history they formed, if they actually resulted in escape of the volatile or only formed as a result of local variations in pressure in the neighborhood of the growing bubble, or if they were caused by destruction of the vesicle wall during thin sectioning. Furthermore, volatile escape by vesicle disruption requires that the pressure inside the bubble exceed the confining pressure. Under these conditions there is no way to explain the flow of residual melt to the vesicle site, except by forceful injection.

The suggestion of Baragar and others (1977) that the vapor in segregation vesicles is resorbed by the residual melt is equally unlikely. CO_2 gas is not very soluable in silicate melts and its solubility decreases with decreasing temperature and pressure (Spera and Bergman, 1980). Furthermore, bubbles form because the melt is saturated with respect to a vapor phase (Sparks, 1978) and it is unlikely that a melt will resorb a phase with which it is already saturated.

Physico-Chemical Properties of Residual Melt

Once the residual melt enters the vesicle it presumably flows to the bottom before solidifying (Bideau and others, 1977). The shape of the subsidiary surface is controlled by an interaction of the rate of viscous flow of the cooling melt and the rate of cooling (Smith, 1967). The symmetrical, crescent-shaped aphanitic meniscus in sea floor basalt vesicles and its preferential orientation suggests a rapid flow rate. The quenched or fine-grained nature of the residual melt also indicates a rapid cooling rate. The cooling rate must be slow enough, however, to allow the fluid to flow and develop a symmetrical form in equilibrium with the earth's gravitational field.

The fact that residual melt can enter some vesicles and flow rapidly to the bottom of the vesicle before chilling implies it probably is not very viscous and is dense enough to flow rapidly. It also must have a low surface tension in order to penetrate the crystalline web around the vesicle and form a symmetrical, concave-upward-shaped meniscus inside the vesicle. These physical properties probably are largely accommodated by changes in the volatile concentration and composition, and changes in the Fe to Mg ratio of the residual melt during cooling.

For a given composition, melt viscosity largely is dependent upon temperature and volatile concentration (Murase and McBirney, 1973; and Scarfe, 1973). When vesiculation occurs sea floor basalts are saturated with respect to CO_2 (Moore

and others, 1977; Delaney and others, 1978). Dissolution of CO_2 in silicate melts increases polymerization and results in a measurable increase in the viscosity of the melt (Spera and Bergman, 1980). As the melt exsolves CO_2 and crystallizes, the ratio of H_2O to CO_2 in the remaining melt may increase drastically (Khitarov and Kadik, 1973). Although viscosity generally increases with decreasing temperature (Murase and McBirney, 1973), the effect of an increased weight percent of dissolved water in the residual melt may act to depolymerize the melt and minimize the viscosity (Shaw, 1972; and Scarfe, 1973).

Disassociation of silicate polymers with increased water content probably also helps reduce the surface tension. Experimental evidence also indicates that surface tension decreases with decreasing temperature (Murase and McBirney, 1973).

Density variations during magmatic evolution depend upon the composition of the evolving melt. During fractionation sea floor basalt magmas follow a Skaergaard trend with the residual melt having a higher Fe to Mg ratio than the initial melt (Figure 4). An increase in this ratio leads to an increase in density. Although H_2O acts to decrease melt density this effect seems to be offset by the increase in Fe (Bottinga and Weill, 1970; and Sparks and others, 1980).

Conclusion

Segregation vesicles in sea floor basalts form sometime after the melt cools sufficiently to maintain the integrity of the vesicle. During vesicle formation the pressure of the gas inside the vesicle equals the ambient pressure, but with cooling the gas pressure decreases to a value less than the ambient pressure. This pressure decrease establishes a pressure gradient along which residual melt may flow to low pressure sites inside vesicles.

Segregation vesicles generally are restricted to microcrystalline and intersertal portions of pillows and flows where crystallization proceeds sufficiently to maintain the form of the vesicle but not to restrict flow of residual melt within the framework of the crystallizing rock (Baragar and others, 1977). Once the residual melt enters the vesicle it flows to the bottom before solidifying.

In order to enter and form a concave-upward crescent-shaped meniscus inside a vesicle the residual melt must be dense, of low viscosity, and have a low surface tension. These physical characteristics probably are primarily accommodated by changes in the volatile composition and Fe content of the evolving melt.

The explanation presented here is only applicable to the formation of segregation vesicles in sea floor basalts. The exact process of formation probably is different for the various environments in which they form (dikes, lava lakes, and shallow water basalts).

<center>THE SEGREGATION VESICLE TECHNIQUE OF
SEA FLOOR BASALT ORIENTATION: TESTING, METHODS, AND PROCEDURES</center>

INTRODUCTION TO TESTS OF THE TECHNIQUE

Several tests are necessary to establish the reliability
of the segregation vesicle technique as an orientation tool
with possible applications for paleomagnetic and structural
studies.

Observations of segregation vesicles indicate that cres-
cent-shaped linings of aphanitic residue in vesicles of the
same rock have slightly different orientations. A test of uni-
formity is, therefore, necessary to establish that the residue
in segregation vesicles is preferentially oriented. It is then
important to show that for rocks which can be oriented by an
acceptable megascopic criterion, there is a significant compo-
nent of the preferred orientation of the segregation vesicles
in the known orientation of the rock. Finally, the orientation
of the rock given by segregation vesicles must agree with the
orientation given by an acceptable megascopic criterion, within
the limits of reliability of those criteria. If these tests
are successful, then it is necessary to establish the limits
of the reliability of the orientation of the rock given by
segregation vesicles, considering the scatter of the data.

The technique has the potential to be used to determine
structural dips of submarine basalts which are sampled in place
(that is, by drill core). This application of the technique,
however, is only useful if the scatter of the data is small
enough to give a reliable estimate of the dip within a reasonably

small error. For this application of the technique two criteria must be satisfied. It must be shown that, in test cases, the segregation vesicle orientation of the rock has an error margin that is less than 45° and that this orientation agrees with the known orientation of the rock.

The technique may also be used to determine the magnetic polarity of dredge haul basalt samples (Bideau and others, 1977). A test of the reliability of this application of the technique is how well the magnetic inclinations of rocks oriented by segregation vesicles agree with the inclinations of rocks of the same age and location oriented by an acceptable megascopic criterion. If there is good agreement, then the geographical regions within which the technique may be used for magnetic polarity studies depends upon the reliability of the determined magnetic inclination. As will be shown, to establish these limits it is necessary to determine the error associated with this magnetic inclination based upon the error in the orientation of the rock due to scatter of segregation vesicle data.

SAMPLING AND PROCEDURES FOR MAKING MEASUREMENTS

The Sample Set

Ideally, the segregation vesicle technique of sea-floor basalt orientation should be tested on subaerial samples that can be well oriented in the field. This test was attempted. Over 300 thin sections of subaerial basalts from eastern Ice-

land (Figure 2) and 40 thin sections of shallow-water basalts originating from subaerial Hawaiian volcanoes were examined. Spherical vesicles with crescentic-shaped linings of aphanitic residue were not observed in the Hawaiian samples and were only very rarely observed in the Iceland sections.

Rocks successfully used to test the technique were collected during the AMAR cruise to the Mid-Atlantic Ridge (Figure 1). Submarine samples can be used as test rocks because megascopic subhorizontal features, which are indicative of their cooling position, can be used to orient these rocks with some degree of reliability (Ballard and others, 1975; Prevot and others, 1976; Bideau and others, 1977; and Wells and others, 1979). Thirty eight samples which can be oriented by such megascopic features, were collected during the AMAR cruise.

Well oriented minicore samples were taken from these rocks by setting the rocks in a gravel-filled wash basin such that the horizontal orientation feature was situated either perpendicular or parallel to the long axis of the drill bit. The drilled sample was then labeled with a scribe line and arrow to indicate the vertical axis and "up" direction of the minicore. Three mutually perpendicular axes were ascribed to this orientation with the +x axis pointing toward the "up" direction and the y and z axes forming the reference horizontal plane (Figure 10). Arbitrarily oriented minicore samples were taken from rocks lacking megascopic geopetal features. One to 3 cores were taken from each rock.

Of the 38 samples with megascopic geopetal features col-

Sample 821-6

A

5 cm

2.5 cm

Cooling cavity

Drips
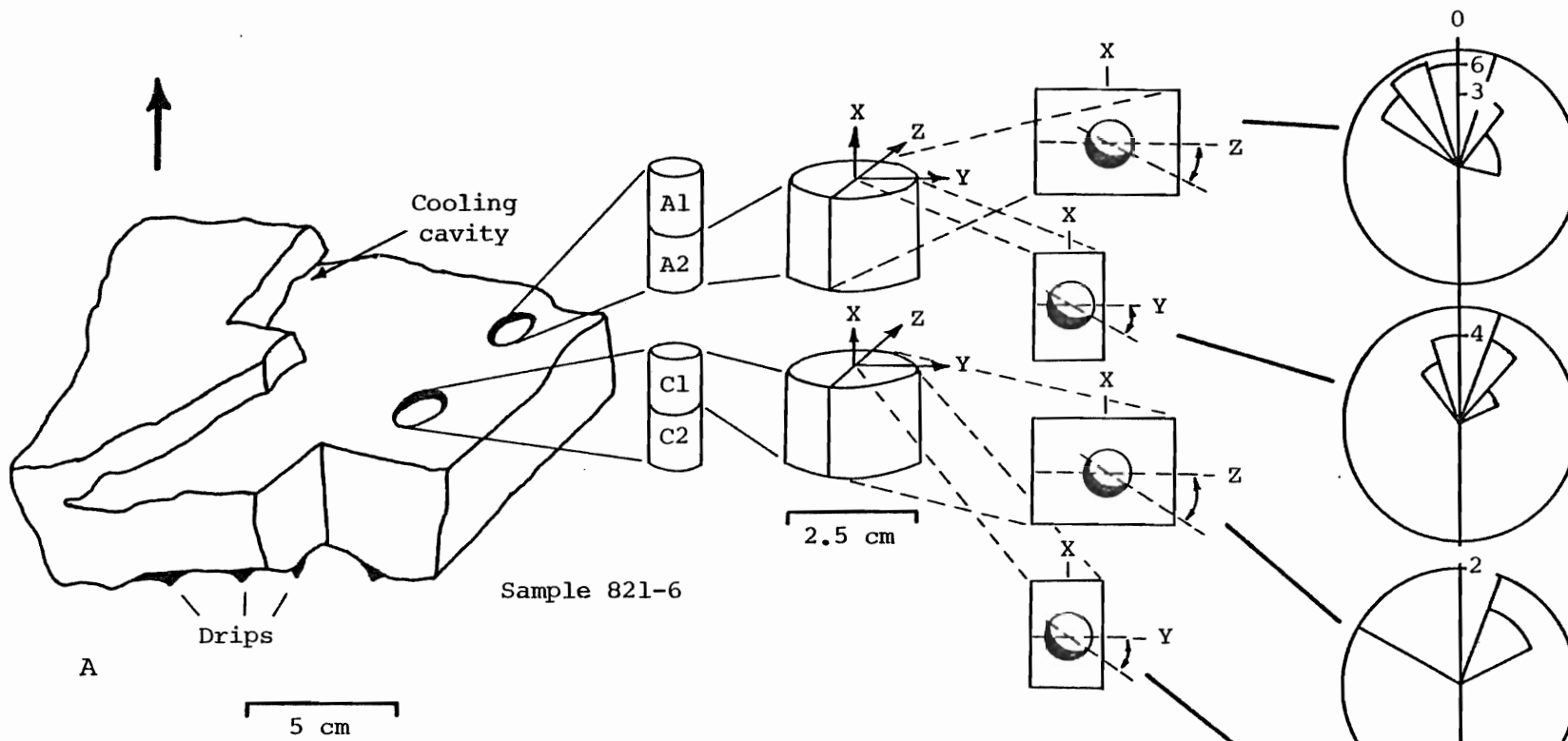
Figure 10A. Sketch of a rock used to test the segregation vesicle technique showing location and orientation of minicore samples. Arrow indicates up direction based on megascopic criterion. Schematically shown is the orientation of thin section planes and the manner in which segregation vesicle inclinations are measured. Equal area histograms show distribution of segregation vesicle inclinations actually measured in each thin section. Numbers on the ordinate indicate the number of measurements. $0°$ is the up direction from megascopic criterion. The mean value of segregation vesicle inclinations falls within $20°$ of this up direction for all thin sections. Statistical data are from Table 3.

Figure 10B-F (following pages). Sketches of some of the rocks used to test the segregation vesicle technique showing minicores and histograms as above.
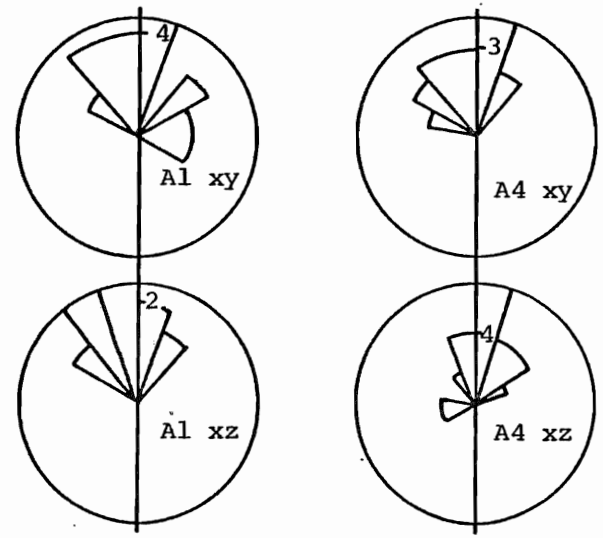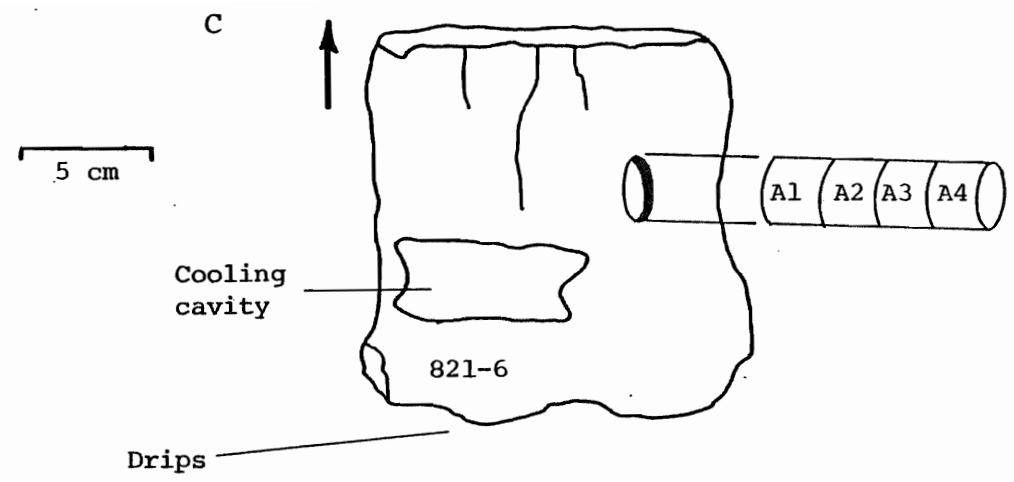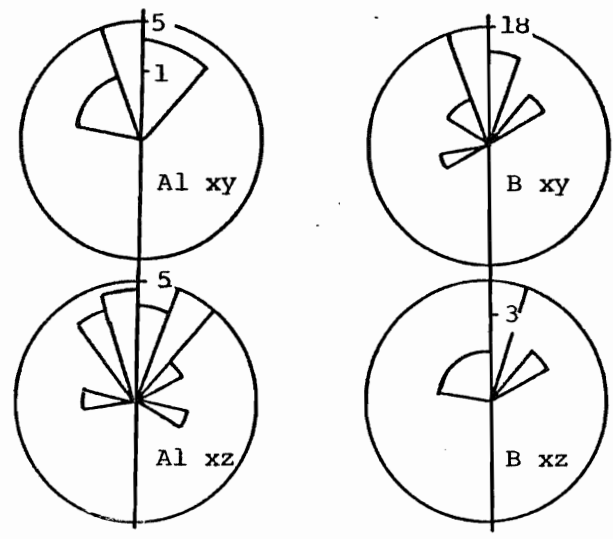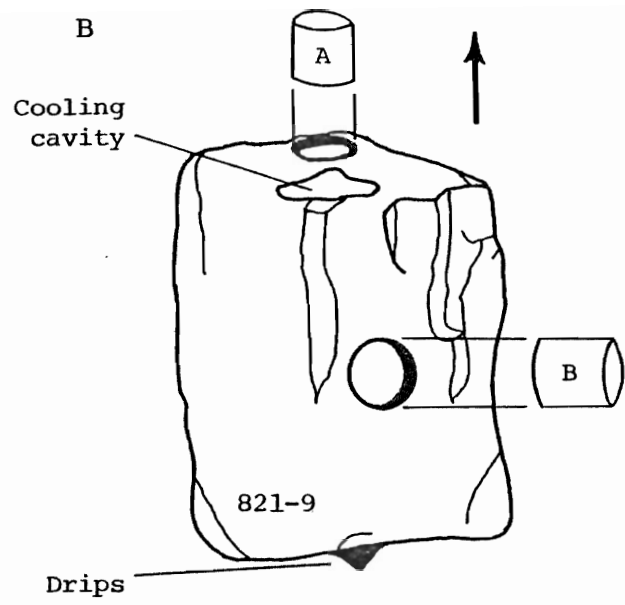
Figure 10. Continued.
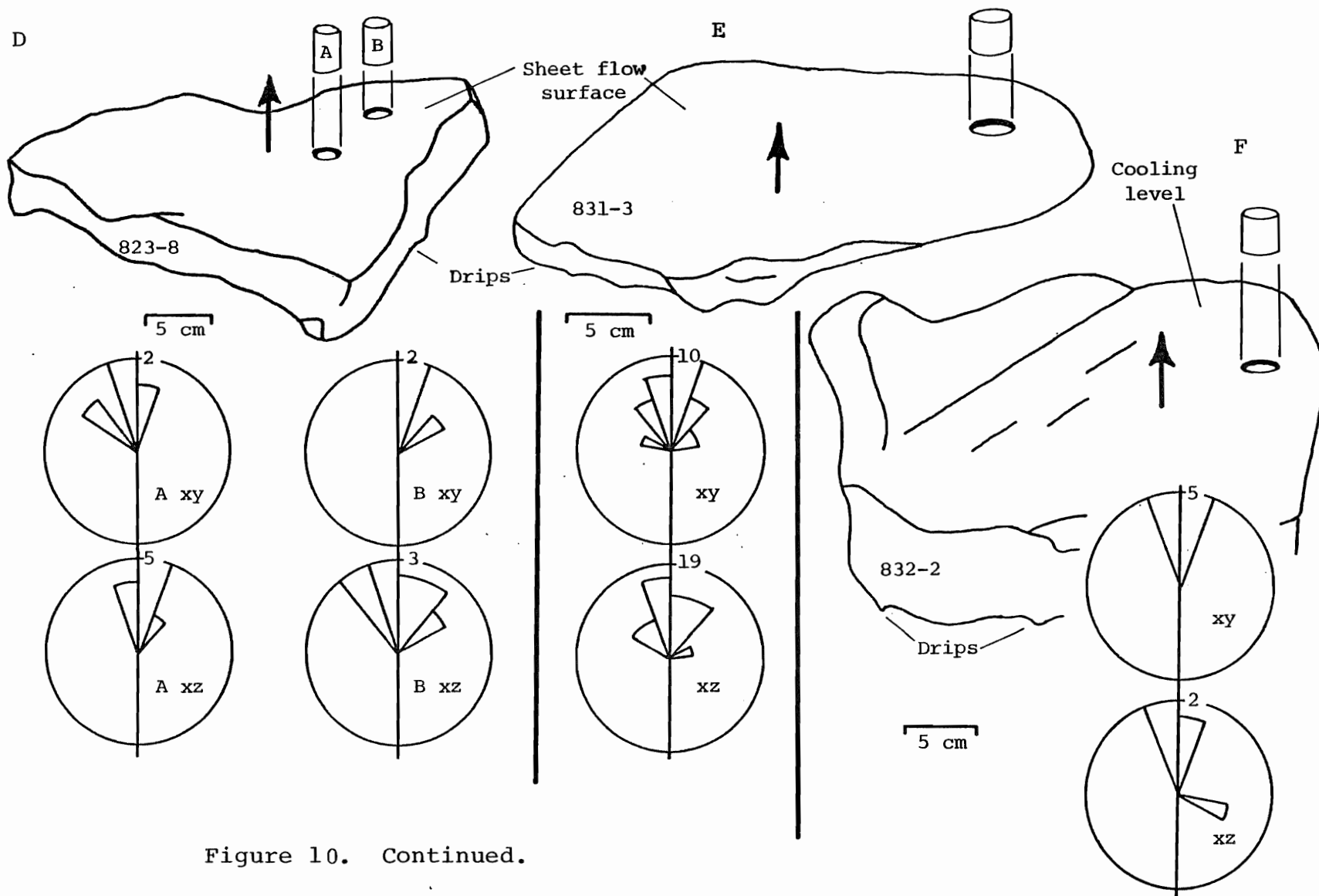
Figure 10. Continued.

lected, 17 also have segregation vesicles. These samples were used to test for agreement between the segregation vesicle and megascopic orientation of the rock. An additional 17 of the samples collected have no megascopic orientation features but have segregation vesicles. These samples were used for other tests of the technique.

Megascopic Orientation of Sea Floor Basalts

Introduction

A sea floor basalt orientation scheme, based on megascopic geopetal features was established in order to classify rocks according to the reliability of these features as indicators of the cooling position of the rock. This scheme consists of four categories ranging from "MC-1" (megascopic criterion-1) which is the most reliable, to "MC-4" which is the least reliable (Figure 11). Only rocks with "MC-3" or better were used to test for agreement between the segregation vesicle orientation and megascopic orientation of the rock.

MC-1: Hollow Layered Pillow Fragments With Well Developed Stalactites

Morphologically, rocks of this category are characterized by a broken pillow shell and one or more flat shelves. These shelves may be drain-away ledges or flattened gas cavities (Figure 11A).

Drain-away ledges mark temporary stands of lava within the pillow. Because lava is fluid, these ledges generally are sub-
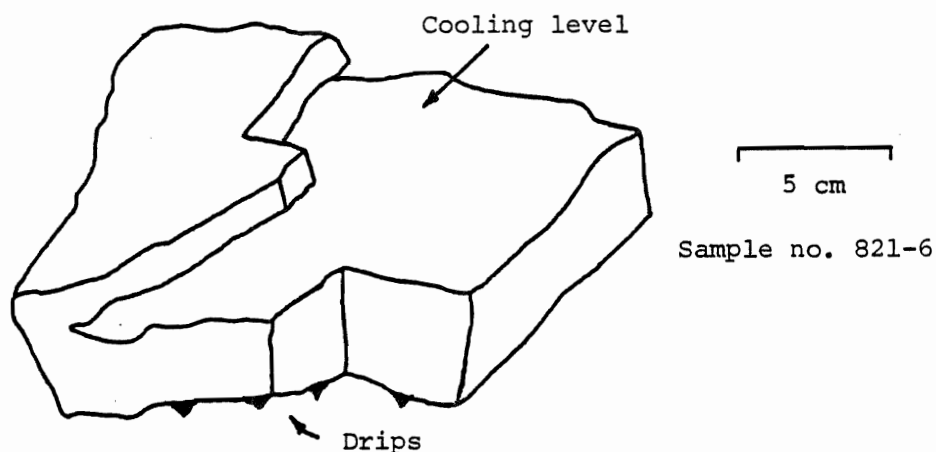
Figure 11A. Sketch of an "MC-1" rock. Rocks of this cat-category are hollow layered pillow fragments with well developed drips. Reliability of orientation features is ±15°.
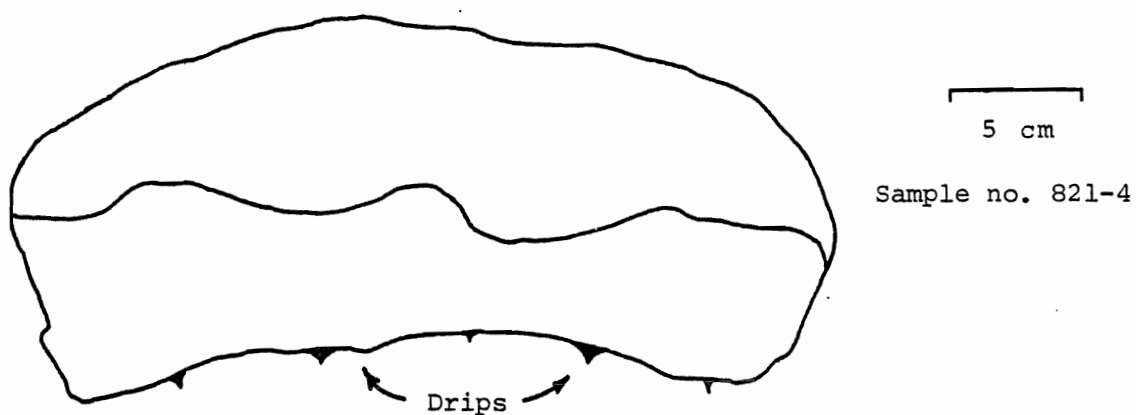
Figure 11B. Sketch of an "MC-2" rock. Rocks of this category are hollow pillow fragments, sheet flows, or ledges with moderately well developed drips. Reliability is ±45°.

Smooth upper surface

5 cm

Sample no. 831-1

Scoriaceous inner
surface
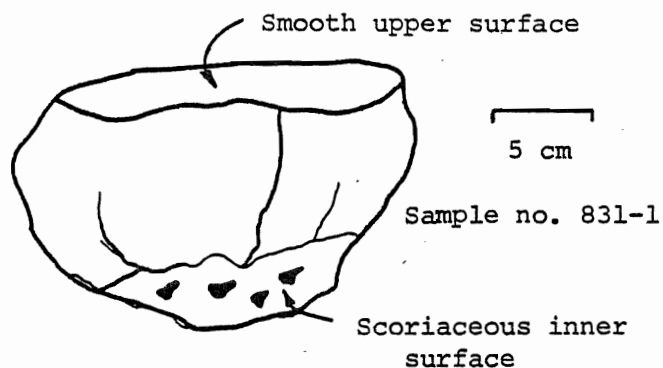
Figure 11C. Sketch of an "MC-3" rock. Rocks of this cat-
egory are pillow or massive flow fragments. They have a
smooth outer surface and scoriaceous inner surface. Relia-
bility is ±70°.

Flat surface

5 cm
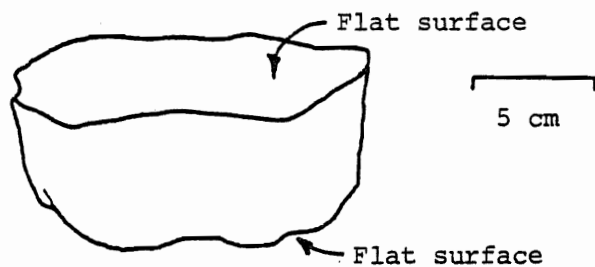
Flat surface

Figure 11D. Sketch of an "MC-4" rock. Rocks in this cat-
egory are layered pillow fragments or flat sheet flow frag-
ments without drips. Reliability is ±180°.

horizontal with a very flat and smooth upper surface. The sub-
horizontal orientation of these ledges was observed in the
field during submersible studies of spreading centers (Ballard
and Moore, 1977; and Wells and others, 1979) and in exposures
of subglacial pillow basalts in Iceland (Wells and others,
1979).

If the pillow breaks, the lava below the chilled ledge may
drain away forming curtain-like or drip-like septa or stalac-
tites on the bottom of the ledge. Such septa generally are
about 1 cm in length. These septa allow for determination of
the upward facing surface of the ledge, while the flat ledge
allows for determination of the horizontal position of the
rock during cooling (Prevot and others, 1976; and Ballard and
Moore, 1977).

Flattened gas cavities may also indicate the horizontal
cooling position of a sea floor basalt. These are discrete
cavities, distinguished from drain-away shelves by the occur-
rence of vertical internal walls separating them from other
cavities. They presumably formed as large gas cavities which
were flattened during cooling by the weight of the portion of
flow overlying the cavity as the gas pressure inside the cav-
ity decreased. Field observations confirmed that the flatten-
ed surface of these cavities indicates the subhorizontal
cooling position of the rock on the sea floor (Prevot and
others, 1976; Bideau and others, 1977; and Wells and others,
1979). The upward facing surface of the cavity may be dis-
tinguished from the downward facing surface by its smoother

appearance (Bideau and others, 1977). If such a determination is not possible, septa or drips on other rock surfaces may be used to determine the upright position of the rock.

These flattened cavities must not be confused with scoria-ceous zones or cavities which occur at the center of a pillow. Such features have no preferred orientation with respect to the cooling position of the rock.

Several factors complicate the use of these features as indicators of original horizontality. Stalagmites or driplets of basalt from the septa at the bottom of a drain away ledge or pillow crust may accumulate on the upper surface of the ledge below (Wells and others, 1979). These may be confused with stalactites but usually are worm-like in appearance and lack the relief of stalactites. Furthermore, the presence of a chilled glassy crust can not be used to indicate the upper surface of a ledge or cavity. The occurrence or thickness of a glassy crust does not depend upon which wall of the cavity faced up during cooling but rather upon how rapidly the lava was quenched and how much glass has spalled off since quenching. In fact, drain-away ledges will commonly have a thicker layer of glass on the downward facing than on the upward facing sur-face (W.B. Bryan, per. com., 1980).

Although ledges in pillow basalts generally are flat, they may be broadly bowed upward (Ballard and Moore, 1977, photo no. 54). If the curvature is broad enough, a fragment of the ledge sampled from the sea floor may still seem flat. An es-timated error of about 15° must, therefore, be associated with

any orientation based on these criteria.

MC-2: Arcuate Hollow Pillow Fragments, Sheet Flows, or Ledges With Moderately Well Developed Stalactites

Rocks of this category are arcuate forms with moderately well-developed stalactites. The arcuate fragment may be a drain-away ledge, pillow crust, or sheet flow fragment (Figure 11B).

Drain-away ledges with stalactites on the underside of the ledge, have been described. If the ledge is arcuate, such that the ambiguity of cooling position of the rock is greater than 15 degrees, then the rock is classified here.

Pillow basalts may break open during cooling, spilling their molten contents but maintaining their pillow form (Bellaiche and others, 1974; and Ballard and Moore, 1977). As the lava inside the pillow drains out, stalactites may form, extending downward from the underside of the upper pillow crust. These stalactites are similar to those which form on the bottom of drain-away ledges, but may be more poorly defined. Curtain-like septa may also develop an arcuate, concave upward form along the sub-vertical walls of the pillow crust.

During sheet flow deposition the thin outer, ropy and commonly undulating surface of the flow may chill and remain at a fixed level while the lava below this level drains away. Again, stalactites may form on the underside of the sheet flow, which can give a rough estimate of the vertical position of the rock during cooling.

Because rock fragments of this category have an arcuate

outer surface it is not possible to make a precise determina-
tion of their horizontal cooling position. However, they also
have stalactites which give a rough indication of the vertical
orientation and "up" axis during cooling. This combination of
features can be used to determine the orientation of the rock
to within about 45° of its cooling position.

Caution must be used in interpreting the cooling position
of rocks using these morphologic features. Stalactites which
develop on these arcuate fragments may not be well defined.
While the relatively smooth outer surface of the rock compared
to the rough interior surface is usually sufficient to dis-
tinguish the outer from the inner portion of the pillow or
sheet flow, stalactites may be of insufficient quality to de-
fine a vertical. If the rock is highly phyric, glass covered
phenocrysts may protrude into the rough interior surface,
adding to the roughness, and may even appear to be stalactites.
It may also be possible to mistake pillow buds (Ballard and
Moore, 1977) for stalactites.

MC-3: Pillow Or Massive Flow Fragments Without Stalactites

Rocks of this category are fragments of pillows or massive
flows, with radial fractures or jointing, a glassy outer margin
and a rough or scoriaceous interior. The outside surface may be
flat or slightly arcuate. This surface is distinguished from
the inner surface by its smooth glassy appearance, compared to
the irregular, scoriaceous inner surface (Figure 11C).

These criteria are sufficient to distinguish the outer

from the inner surface of the rock. The actual cooling position of the rock, however, can only be determined to within 70° at best.

MC-4: Layered Pillow Fragments Or Sheet Flows Without Stalactites

These rock fragments are slab shaped or have very flat features such as a drain-away ledge, flattened gas cavity, or sheet flow crust (Figure 11D). Such features are good indicators of the horizontal position of the rock at the time it cooled (as previously described), but due to the absence of stalactites, it is impossible to distinguish the upward- from the downward-facing surface of the rock. True orientation of a rock based only on a flat feature is purely speculative. It is possible to be in error by 180°.

Magnetic Measurements

As previously described, minicores, either oriented with respect to the megascopic orientation of the rock or arbitrarily oriented, were drilled from rocks collected during the AMAR cruise (Figure 10). Prior to cutting the rocks for thin sectioning, magnetic measurements were made using a Schonstedt DSM-1 Digital Spinner Magnetometer. Figure 12 shows the conventions used for measuring magnetic direction with respect to the orientation axes of minicore samples. The magnetic declination is arbitrary with respect to the geographic position of oriented samples, and the magnetic direction is only relative to the orientation axes
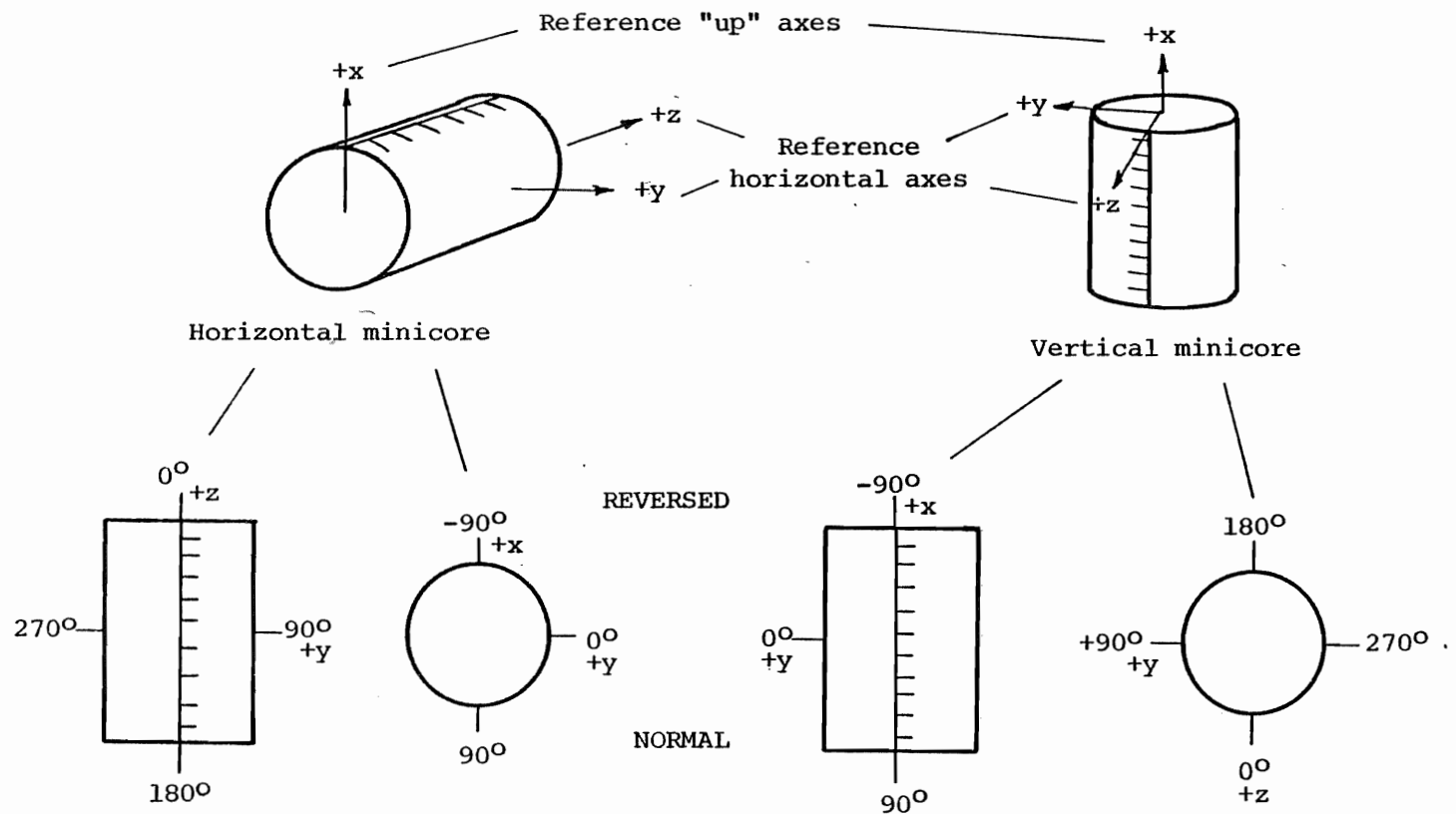
Figure 12. Diagram showing the conventions used for measureing the magnetic direction with respect to the orientation axes of horizontally and vertically drilled minicore samples. Magnetic declination varies from 0° to 360° from the +z toward the +y direction. Magnetic inclination varies from −90° to +90° with reversed inclinations pointing toward the +x and normal inclinations pointing toward the −x axis in the northern hemisphere.

of the minicore for samples lacking megascopic geopetal features.

Twenty samples were demagnetized at steps of 50 to 100 oe, following each remanence measurement, to 500 oe using an alternating field demagnetization unit. This unit is designed with a two-axis tumbler, which prevents acquisition of rotational remanent magnetization by reversing its sense of rotation after every complete rotation about the vertical axis. The magnetic inclination and declination of these samples changed less than 5° throughout the demagnetization process (Figure 13). Although the median demagnetizing field (MDF) varies greatly between samples (Figure 13) it does not seem to be a measure of directional stability. Samples with both low and high MDFs remained directionally stable through 500 oe demagnetization.

Wide ranges in MDF were previously recognized in median valley basalts although there appears to be a general increase in the MDF of these basalts with age (Johnson and Atwater, 1977). This variation may occur because MDF is partly controlled by magnetic grain size. The decrease in MDF with age may be due to a decrease in effective grain size caused by the formation of cracks in titanomagnetite grains as they alter to titanomaghemite (Ade-Hall and others, 1976; and Johnson and Atwater, 1977).

Regardless of MDF value, directional stability of these samples with alternating field demagnetization indicates that the direction of original cooling thermal remanent magnetization (TRM) is similar to the direction of the natural remanent magnetization (NRM). Soft components of chemical or viscous
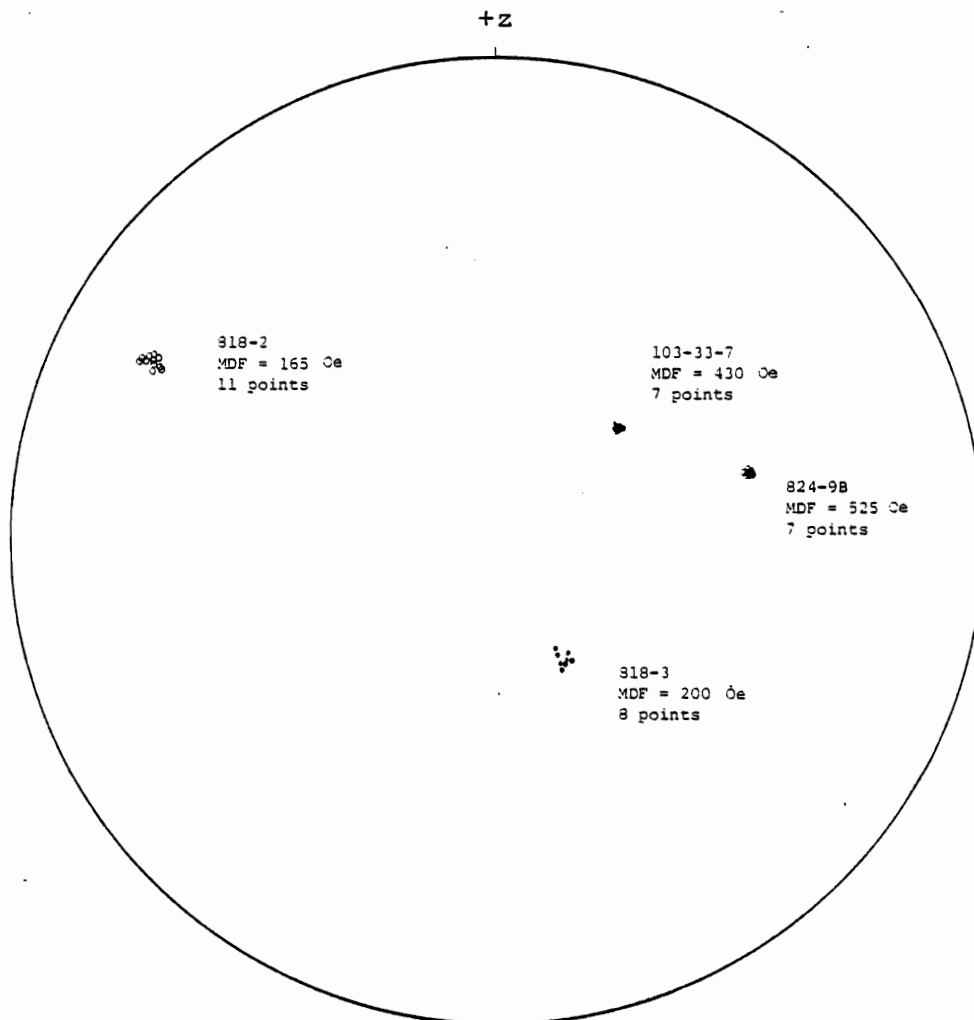
Figure 13. Wulff stereonet plots (southern hemisphere projection) of the measured magnetic directions with successive steps of af demagnetization from 25 to 500 Oe of 5 samples collected during the AMAR expedition. The number of points indicates the number of demagnetization steps. Also noted is the sample number and MDF of each sample. Declination is arbitrary.

remanence are not a large component of the NRM. The remaining samples were therefore routinely demagnetized at steps of 50 oe to only 200 oe. All samples remained stable through this demagnetization sequence and further demagnetization was not necessary to remove soft components of remanence.

The stable NRM was taken as the vector average of the three closest sequentially measured directions. Some of the stable NRMs were determined by H.P. Johnson at the University of Washington, following similar procedures to those described here.

Measuring Segregation Vesicle Inclinations

In order to determine the orientation of a rock given by segregation vesicles, these vesicles must be examined in at least two thin sections from the same rock sample which are cut at a known orientation to each other. These sets of segregation vesicle inclinations, measured in each thin section, represent projections of the horizontal plane, defined by the crescent-shaped linings or lunes of residue in segregation vesicles, in the plane of the thin section. These measurements are equivalent to apparent dips. In the same way that two apparent dips can be used to determine the true dip of a planar feature (Billings, 1972; and Ragan, 1973), sets of segregation vesicle inclinations measured in a pair of thin sections from the same rock sample can be manipulated to give an indication of the three dimensional or true segregation vesicle orientation of the rock.

As previously described, the meniscus of aphanitic residue generally appears as a crescent-shaped lining in segregation vesicles. Assuming that the orientation of the meniscus is controlled by gravity (Bideau and others, 1977), a line connecting the points of the lune represents a projection or apparent dip of the horizontal plane at the time the residual melt in segregation vesicles solidified, in the plane of the thin section. Symmetrical crescents give the most reliable indication of this apparent dip.

In this study, thin section chips were routinely cut along two mutually perpendicular planes containing the reference vertical axis, the xy and the xz planes (Figure 10). For rocks which are oriented by megascopic features, these thin sections are vertically oriented with respect to the cooling position of the rock. For unoriented rocks these sections are only oriented relative to the arbitrarily assigned axes of the minicore.

The segregation vesicle inclination or apparent dip is measured as the angle between the reference horizontal (y or z axis) and the line connecting the points of the crescent of the meniscus. To measure this angle a standard petrographic microscope, equipped with an ocular with cross hairs and a mechanical stage set on a rotating stage divided in degrees is used. The thin section is set in the mechanical stage so that, when viewed through the ocular, the +x axis appears at the top, the +z or +y axis appears to the right of the observer, the rotating stage reads zero with respect to the vernier scale

on the stationary stage clamp, and the cross hairs are parallel

to the x and y or z axes. Beginning at one corner of the thin

section, the mechanical stage is used to systematically tra-

verse the entire slide. Each segregation vesicle encountered

is measured. The segregation vesicle inclination can range

from 0° to 360° and is given by the amount of counter clock-

wise rotation required to orient each segregation vesicle so

that a line connecting the points of the crescent is parallel

to the E-W cross hair, the meniscus appears concave upward

(toward the top of the field of view) and the N-S cross hair

forms the axis of symmetry of the meniscus (Figure 14).

MATHEMATICAL MANIPULATION OF SEGREGATION VESICLE INCLINATION DATA SETS: STATISTICAL TECHNIQUES AND COMPUTATION OF STRUCTURAL AND PALEOMAGNETIC PARAMETERS

Introduction

The segregation technique involves making observations

which are recorded as the measurement of segregation vesicle

inclinations. Associated with these directional data are

errors. Small systematic errors may result from inaccuracies

in the orientation of thin sections. For samples recovered

in DSDP cores,deviations of the drill core (from which mini-

core samples are later taken) may result in thin section

orientation errors up to 5°. Small errors (less than 3° and

usually less than 1°) may also be introduced by inaccurate

minicore sampling, inaccuracies in thin section cutting, grin-

ding or alignment of the thin section chip on the glass slide, or

improper alignment of the thin section on the microscope stage.
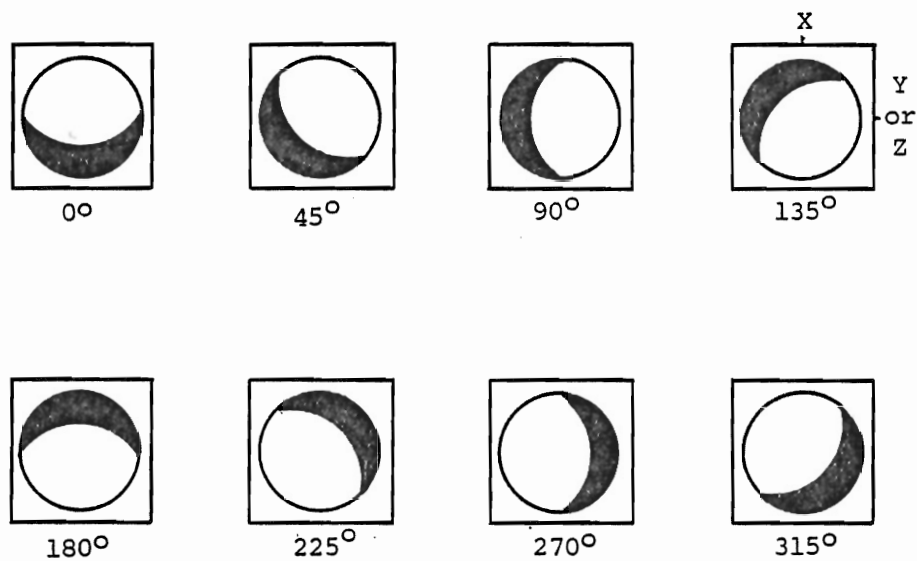
Figure 14. Schematic illustration of conventions used for measuring segregation vesicle inclinations. Notice they are measured from 0° to 360° as the amount of counter clockwise rotation required to align the points of the crescent parallel to the reference horizontal axis with the curvature of the crescent concave upward.

In most cases these errors can be determined by using a gonio-
meter to measure the angle between pairs of thin section chips
and by marking the chips so that the orientation of the thin
section on the microscope stage can be measured with respect
to the cross hairs. If necessary, data can be corrected for
such errors.

Even after removal of systematic errors, data are scat-
tered. The amount of scatter inherent in the data is partly
controlled by the orientation of the thin section plane with
respect to the original vertical axis of the rock. Sections
cut parallel to the original vertical axis will minimize scat-
ter, whereas sections nearly perpendicular to this axis will
maximize scatter because these sections are cut along a plane
which is close to the horizontal plane defined by the residue
in segregation vesicles. Small variations in the orientation
of the residues, therefore, result in a large variation in
the apparent dips observed in thin section, and data from
such sections may be expected to show scatter about 360°.

No satisfactory explanation has been given for the inherent
scatter of segregation vesicle inclinations, although some sug-
gestions have been made (Bideau and others, 1977). Consequent-
ly, it is unkown if there is any process which controls the
distribution of the scatter in a way which can be predicted.
This scatter in the data is, therefore, assumed to be randomly
distributed. The specific distribution assumed depends upon
the desired property of the distribution, as will be discussed.
However, all are variations of a normal distribution. That is,

small errors are more likely than large errors, negative and positive errors have the same probability, and the best estimate of the mean is the least squares value.

Inspection of equal area rose diagrams showing the frequency distribution of segregation vesicle inclinations indicates that the assumption of the random distribution of errors is probably valid. These diagrams illustrate that the distribution of inclinations approximates a bell-shaped curve on a circle (Figure 10).

Because the reliability of the interpretation of the data depends upon the "goodness" of the data, proper statistical treatment is essential. It is imperative that meaningful measures of dispersion be recorded with each estimate of the mean.

The following discussion is of the statistical and geometrical manipulations that are applied to segregation vesicle inclination data sets. This discussion is necessary here in order to understand the tests of the segregation vesicle technique which follow. The discussion is presented assuming, as is shown later, that the technique works.

Statistical Techniques of Two-Dimensional Directional Data

Introduction

The segregation vesicle inclinations measured in each thin section plane can range 0° to 360° (Figure 14). These are, therefore, measurements of direction which are distributed about a circle.

Previously, methods of linear statistics were used to analyze problems of directional data (Bideau and others, 1977). There are problems, however, with using conventional linear statistical techniques for this purpose. The analysis of linear directions depends heavily upon the choice of the zero direction. For example, if zero degrees is taken to indicate a linear value, and the average of 350° and 20° is desired, linear techniques give a value of 185°. Obviously, the appropriate mean is 5°. This answer is obtainable by adjusting the zero direction so that the problem reduces to an average of 260° and 290°. Such adjustment, however, requires individual investigation of every data set. Arc distances also bring points closer together than line distances. Measures of standard deviation must, therefore, be transformed to account for data distributed on a circle rather than on a line. The natural periodicity of a circle requires the points cannot be infinitely far away and, therefore, different measures of scatter and tests of uniformity from those used for linear data must be applied (Mardia, 1972; and Batschelet, 1965).

Circular statistical techniques are used here to circumvent these problems. All computations assume either a circular normal distribution as described by Von Mises (1918, in Mardia, 1972), or a wrapped normal distribution.

A variable is said to have a Von Mises distribution if the probability density function of a variable, Θ, is described by,

$$f(\alpha) = Ce^{k(\alpha-\Theta)} \tag{1}$$

where, Θ is the mean angle, k is the concentration parameter, α is an angle of the population, and C is a constant which is a function of k (Batschelet, 1972).

The wrapped normal distribution is generated by wrapping a linear normal distribution around a circle. The probability density function for this distribution with a mean angle of zero and standard deviation = σ, is given by,

$$f(\alpha) = \frac{1}{\sigma\sqrt{2\pi}} \sum_{k=-\infty}^{+\infty} \exp\left(-\frac{1}{2}\frac{(\alpha+2\pi k)^2}{\sigma^2}\right) \tag{2}$$

where, α is any angle of the population (Mardia, 1972).

The shapes of the wrapped normal and Von Mises distribution are similar (Figure 15). The most obvious differences between the two distributions are the points of inflection, which are located at one standard deviation from the mean. Inspection indicates that the assumption of a wrapped normal distribution results in a larger estimate of the standard deviation of the data set than the assumption of a Von Mises distribution. In the limiting cases, when the concentration parameter, k, approaches zero or infinity, the two distributions tend to the same point distribution. A satisfactory agreement of the two distributions for intermediate values of k was verified by Stephen (1963, in Mardia, 1972).

The important statistical parameters of the circular normal distribution to the segregation vesicle problem are described here. The computations which must be applied routinely are
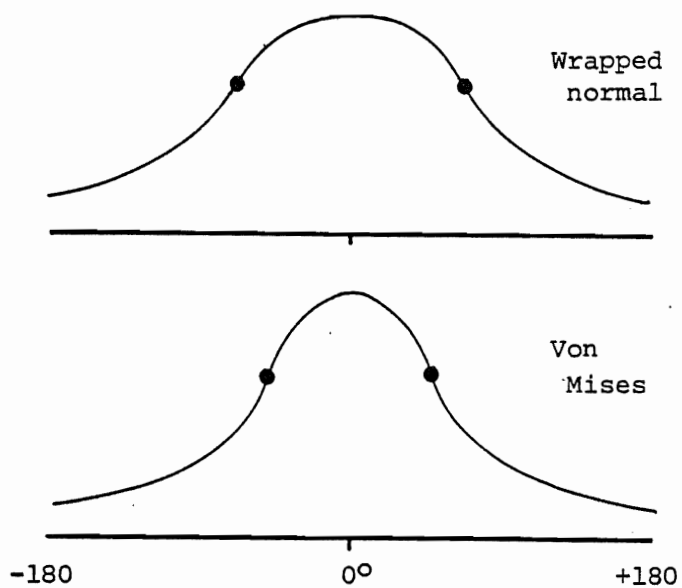
Figure 15. A graphical comparison of the wrapped normal and Von Mises distribution with a mean vector θ=0, a length of the mean vector an 0.4464, and K=1. Dots are located at the points of inflection (after Batschelet, 1965).

accomplished by computer program CIRST (Appendix II).

Average Segregation Vesicle Inclination (Circular Mean)

Each segregation vesicle inclination measured, ad_i, is considered to be a vector of unit length on a circle. To determine the average inclination of these vectors, measured in a single thin section, each one is resolved into its X (horizontal) and Y (vertical) components. So that,

for ad_i, i=1,n

$$X_i = \cos (ad_i) \tag{3}$$

$$Y_i = \sin (ad_i). \tag{4}$$

The average of the X and Y components is given by,

$$C = \sum_{i=1}^{n} X_i/n \tag{5}$$

$$S = \sum_{i=1}^{n} Y_i/n \tag{6}$$

where n is the number of measurements in each data set. The average vector, then, is given by,

$$AD = \arctan (S/C) \tag{7}$$

(Mardia, 1972 and Batschelet, 1972).

AD is computed for each thin section of a pair of thin sections from the same rock sample. This results in an AD1 and AD2. AD1 is the average segregation vesicle inclination of the x̄z thin section, and AD2 is the average segregation vesicle inclination of the xy thin section. AD1 and AD2 then are the apparent dips which represent the average projection

of the true dip, or orientation, of the rock given by segregation vesicles onto each of the thin sections.

Values for AD1 and AD2 can range from 0° to 360°. A value of 0° to 90° or 270° to 360° indicates that the apparent dip is upright with respect to the orientation axes of the minicore. Values between 90° and 270° indicate that the apparent dip is overturned. Values near 90° or 270° indicate that the apparent dip is vertical and parallel or subparallel to the x axis of the minicore.

Length of the Mean Vector

The vector AD has both magnitude and direction on the unit circle. The magnitude, or length of this vector is given by,

$$R = (C^2 + S^2)^{1/2} \tag{8}$$

So that, $0 \leq R \leq 1$.

The value of R depends upon how well the data are clustered. An R value close to unity signifies well clustered data with a well defined preferred orientation. Whereas, for a perfectly uniform distribution of the data R will equal zero (Mardia, 1972; and Batschelet, 1972).

Rayleigh Test of Uniformity

The segregation vesicle technique assumes that the meniscus of aphanitic residue in segregation vesicles is preferentially oriented with respect to the earth's gravity field. It is, therefore, desirable to determine if in fact there is a pre-

ferred orientation to a given data set.

The Rayleigh test of uniformity is used to check for pre-ferred orientation of circular directional data. The null hypothesis of this test is that the distribution is uniform, or, there is no preferred orientation. To reject this hypothe-sis, R must exceed a critical value. Critical values of R for a given sample size, assuming a Von Mises distribution, have been computed (Stephens, 1969, in Mardia, 1972) (Appendix III).

For computation here, values for R at the 10 percent level of significance were taken from Appendix III, with interpola-tions where necessary, so that, for every whole number from n=2...50, there is a corresponding R value. These values are stored as an array in CIRST (Appendix II). The computed R value is compared to the appropriate value in the array. If the computed R value exceeds the value in the array, the data are said to be preferentially oriented. If the opposite is the case, then the uniform hypothesis is accepted.

Acceptance of the uniform hypothesis does not indicate that the three-dimensional distribution of the orientation of resi-dual melt is uniform. It only means that the projection of this distribution onto the plane of the thin section is uni-form. Recall that this can result if the thin section chip is cut nearly parallel to the original horizontal surface. To check for this possibility, a thin section should be made at a different orientation to the one with a uniformly distributed data set.

V-Test

The V-test is a modification of the Rayleigh test. It leads to significance only if there is a clustering of data around a known direction. The test is important only when rocks can be oriented by a megascopic orientation feature. If this is the case, it can be used to test for clustering of the measured segregation vesicle inclinations about the orientation given by megascopic criteria. This test may be used to indicate such clustering even if there is a bimodal distribution (perhaps caused by a complex cooling history) to the measured segregation vesicle inclinations. The test is not included in CIRST because it is not generally applicable and computations are easily executed.

The null hypothesis is that there is no evidence that the measured directions are clustered about a predicted direction. To test this hypothesis, the component, V', of r, (where r = Rn) in the known direction, Θ, is calculated by,

$$V' = r \cos AD(\cos \Theta) + r \sin AD(\sin \Theta). \tag{9}$$

If Θ and AD are opposing vectors, V' will equal zero. Large values of V' indicate a large component of R in the known direction, signifying that, it is more likely that the null hypothesis can be rejected.

Batschelet prepared a table (after Keeton, 1969 in Batschelet, 1972) of critical values for the statistic, u, where,

$$u = (2/n)^{1/2}V', \tag{10}$$

for various values of n and P (level of significance). If the

calculated u value exceeds the critical value listed in the table (Appendix IV), then the null hypothesis can be rejected at the specified level of significance. There is indication, then, that the data are clustered about the known direction.

Significantly, a data set may fail the Rayleigh test of uniformity, but pass the V-test, if a large enough component of the measured directions is in the known direction. The V-test is, therefore, a more useful test if there is a predicted direction since it can be used to test for clustering on a specific part of the circle. Whereas, the Rayleigh test can only test for clustering on any part of the circle (Batschelet, 1972).

Concentration Parameter

The concentration parameter, K, ranges from 0 to infinity. As indicated by the probability density function of the Von Mises distribution (eq. 1), high values of K signify well clustered data about the mean direction.

An estimate of K is important here for calculation of the 95 percent confidence interval of the mean. Maximum likelihood estimates of K, $\hat{K}$, based on the length of the mean vector, R, were derived by Batschelet (1965, in Mardia, 1972, Appendix 2.3). These values are stored as an array in CIRST and the appropriate value is retrieved after R is computed.

Confidence Intervals for the Mean Direction

The confidence interval for the mean direction is an estimate of the interval about the true mean within which the estimated, or calculated, mean lies with a given probability. This is the most important measure of dispersion calculated. It is this measure of dispersion which is propagated onto other quantities derived from AD1 and AD2.

Graphical methods, based on the Von Mises, distribution are available for determining the 95 and 99 percent confidence intervals for the mean once n and R are known (Batschelet, 1972). The 95 percent confidence interval can also be computed by an approximation from Mardia (1972). According to this approximation,

$$k' = nR\hat{K} \tag{11}$$

The 95 percent confidence interval ESAD, is then given by,

$$ESAD = 1.96/\sqrt{K'}, \text{ in radians.} \tag{12}$$

The approximation by Mardia is included in CIRST. ESAD1 and ESAD2 are the 95 percent confidence intervals of AD1 and AD2, respectively.

Other measures of dispersion calculated by CIRST but not critical to the segregation vesicle problem are described in Appendix II.

Rose Diagrams

Program CIRST is also used to plot frequency distributions of the data for each sample. To eliminate distortion these distributions are plotted on equal area Rose diagrams (Figure 10). The radius of the equal area Rose diagram is incremented as the square root of the frequency, thus conserving area. The class width is 20°.

Calculation of Structural and Paleomagnetic Parameters and the Propagation of Errors Onto These Quantities

Introduction

By the preceding calculations four quantities are determined. These are the two average segregation vesicle inclinations (or apparent dips) AD1 and AD2, along with their associated errors, ESAD1 and ESAD2, (the 95 percent confidence interval for AD1 and AD2, respectively). From these measured quantities two more quantities are derived. These quantities are the true dip, D, and the dip direction or trend, T, with respect to the orientation axes of the minicore sample. It is necessary to formulate a mathematical model which describes the relationship between the measured parameters, AD1 and AD2, and the derived parameters, T and D. That is

$$T = f_1 \ (AD1, \ AD2), \ and \tag{13}$$

$$D = f_2 \ (AD1, \ AD2). \tag{14}$$

But, because there are statistical errors associated with AD1 and AD2, there is no unique solution for T and D.

A theory of errors, therefore, is needed to determine how ESAD1 and ESAD2 propagate onto T and D. This relationship is given by the law of propagation of the variance-covariance matrix, or simply, the covariance law (Vaníček, 1973).

By this law

$$E_X = BE_L B^T \tag{15}$$

where, E_X is the error matrix for the derived quantities, and E_L is the error matrix for the known, or measured quantities. B is an X by L matrix, where X and L are the number of derived and measured variables, respectively, which expresses the relationship between the known and unknown variables. B^T is the transposed B matrix. It is a transfer function which shows how the errors in the derived quantities relate to the errors in the measured quantities.

For some samples a stable magnetic direction consisting of a declination, DEC1, and inclination, ENC1, with respect to the orientation axes of the minicore is also measured (Figure 12). For these samples two other quantities are derived, the corrected stable magnetic inclination, ENC2, and, AZI, which is the horizontal angle between T and the projection of the corrected magnetic direction onto the horizontal plane, DEC2. ENC2 and AZI are given by the orientation of ENC1 and DEC1 when the plane defined by T and D was in the horizontal position. This determination requires a simultaneous rotation of ENC1 and DEC1 as T and D are rotated to a reference horizontal position.

A mathematical model which describes the relationship between the calculated parameters, T and D, the measured parameters,

in ENC1 and DEC1, and the desired derived parameters ENC2, and AZI, is necessary. So that,

$$ENC2 = f_3 \text{ (ENC1, DEC1, T, D) and} \qquad (16)$$

$$AZI = f_4 \text{ (ENC1, DEC1, T, D).} \qquad (17)$$

But, there are errors associated with T and D, as well as a covariance between these errors. There is, therefore, no unique solution for ENC2 and DEC2. Again, by the covariance law (Vaníček, 1973) (eq. 15), the manner in which the errors in T and D are propagated onto ENC2 and AZI can be computed.

The derivations necessary for application of the covariance law to the segregation vesicle problem are after R. Boutilier (per. com., 1980). Complete derivations are in Appendices V-VIII. The calculation of T, D, ENC2, AZI, and their associated errors (95 percent confidence intervals) is accomplished by computer program ROTSTAT (Appendix IX).

Calculation of Dip and Trend

As previously mentioned, the average segregation vesicle inclination measured in each of a pair of thin sections from one rock sample, AD1 and AD2, is analogous to a structural apparent dip. There are several graphical and mathematical techniques for computing a true dip and trend (dip direction), or structural attitude, from two apparent dips (for example see Ragan, 1973; Billings, 1972; or Phillips, 1971). The formalism here is after R. Boutilier (per. com., 1980) (Appendix V).

According to the coordinate system shown on Figure 16, the
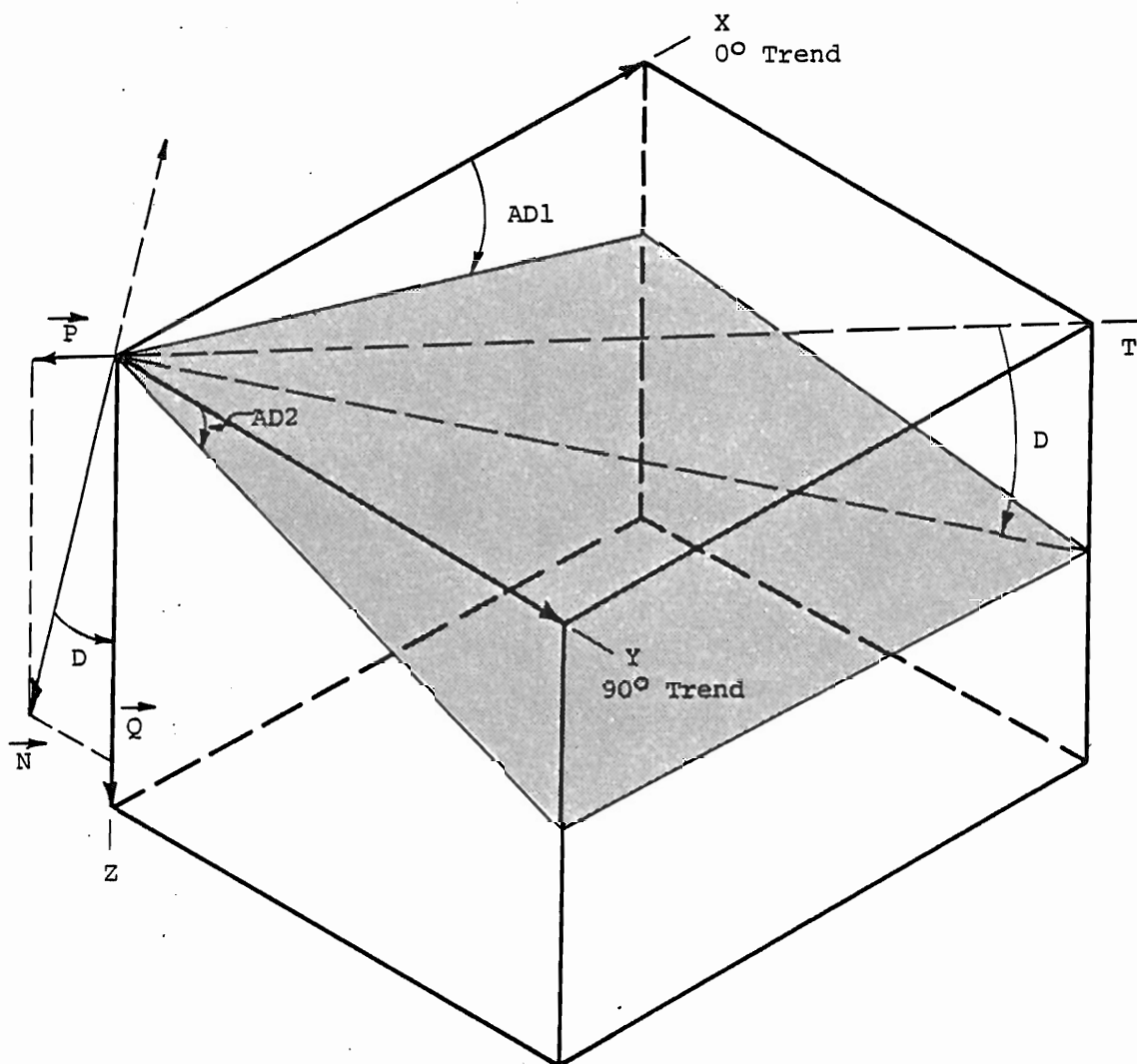
Figure 16. Block diagram showing the coordinate system
used to calculate the dip = D and trend = T from two appar-
ent dips (average segregation vesicle inclinations), AD1
and AD2. N is the normal to the (AD1, AD2) plane. Q is
the projection of N onto Z. P is the projection of N onto
the horizontal (X, Y) plane. +Z, +X, and +Y are equivalent
to the -x, +z, and +y axes, respectively, which are
ascribed to minicore samples.

apparent dips, AD1 and AD2, define two unit vectors with the coordinates,

$$\hat{AD1} = (\cos AD1,\ 0,\ \sin AD1),\ \text{and} \tag{18}$$

$$\hat{AD2} = (0,\ \cos AD2,\ \sin AD2).$$

These two vectors define a plane. The vector defining the normal, or pole to the plane, $\vec{N}$, is given by the cross product or AD1 and AD2, so that

$$\vec{N} = \hat{AD1} \times \hat{AD2} =$$

$$(-\cos AD2 \sin AD1,\ -\cos AD1 \sin AD2,\ \cos AD1 \cos AD2) \tag{19}$$

The magnitude of this vector is given by,

$$|\vec{N}| = \sqrt{(\cos^2 AD2 \sin^2 AD1) + (\cos^2 AD1 \sin^2 AD2) + (\cos^2 AD1 \cos^2 AD2)} \tag{20}$$

The unit vector defining the pole to the (AD1, AD2) plane is therefore,

$$\hat{N} = \vec{N}/|\vec{N}|.$$

The true dip of the (AD1, AD2) plane, D, is the maximum angle this plane makes with the horizontal (X, Y) plane. This is calculated as the angle $\hat{N}$ makes with the Z axis (Figure 16). By the dot product rule,

$$\vec{N} \cdot \hat{z} = |\vec{N}|\ |\hat{z}| \cos D \tag{21}$$

Since, $\quad \hat{z} = (0,\ 0,\ 1),$ \hfill (22)

$$\cos D = \frac{1}{|\vec{N}|} (\cos AD1 \cos AD2). \tag{23}$$

Values for D range from $+90^\circ$ to -90°. 0° dip indicates that the plane is horizontal. Upright dips have

positive angles. A vertical plane will have a dip of $90°$.
If the plane is overturned, the dip angle will be negative.

The trend, T, is given by the angle $-\vec{N}$ makes with the X
axis after being projected onto the horizontal (X, Y) plane.
If $\vec{P}$ is the projection of $\vec{N}$ onto the (X, Y) plane and $\vec{Q}$ is the
projection of $\vec{N}$ onto the Z axis, then,

$$\vec{N} = \vec{P} + \vec{Q} \text{ and,} \tag{24}$$

$$\vec{P} = \vec{N} - \vec{Q}. \tag{25}$$

It can then be shown that (Appendix V)

$$\vec{Q} = (\vec{N} \cdot \hat{Z})\hat{Z}. \tag{26}$$

By substitution of (eq. 26) into (eq. 25),

$$\vec{P} = \vec{N} - (\vec{N} \cdot \hat{Z})\hat{Z}. \tag{27}$$

-P is taken because the trend of the dip direction will be in
the opposite quadrant of the trend of the vector defining the
pole to the plane (Figure 16). From (eqs. 21, 22 and 23),
$(\vec{N} \cdot \hat{Z}) = \cos AD1 \cos AD2$. Therefore, from (eq. 9)

$$\vec{P} = (-\cos AD2 \sin AD1, -\cos AD1 \sin AD2, 0). \tag{28}$$

The magnitude of the vector is given by,

$$|\vec{P}| = \sqrt{\cos^2 AD2 \sin^2 AD1 + \cos^2 AD1 \sin^2 AD2}. \tag{29}$$

By the dot product rule, the angle, T, that -P makes with the X
axis is given by

$$-\vec{P} \cdot \hat{X} = |-\vec{P}| \; |\hat{X}| \cos T. \tag{30}$$

Since, $\hat{X} = (1, 0, 0)$, and $|-\vec{P}| = |\vec{P}|$,   (30)

$$\cos T = \frac{\cos AD2 \sin AD1}{|\vec{P}|} \qquad (31)$$

T can range from 0° to 360°. It is measured from the +X toward the +Y axis (Figure 16). Its value has no significance with respect to geographic meridians. If D is less than zero, then $\vec{N}$ will be in the same quadrant as T. In this case a correction is applied, so T = T + 180°.

If the plane given by T and D is nearly vertical, then one or both of the average apparent dips may be close to 90° or 270°. In this case, small errors in the apparent dip may move the average value from the upright into the overturned field. This problem may create a pair of apparent dips in which one is upright while the other is overturned. It is physically impossible to resolve such a data set into a single plane which can be defined by a T and D. An arbitrary correction of the average dips must, therefore, be made when both dips are not either upright or overturned.

According to the correction, the apparent dip with the smaller 95 percent confidence interval is taken as being the correct value. If this apparent dip is upright, then the plane is assumed to be upright, and if it is overturned, the plane is assumed to be overturned. The apparent dip with the larger 95 percent confidence interval is then moved the smallest distance possible which will make it compatible with the other apparent dip. This correction is automatically performed by ROTSTAT (Appendix IX) if necessary, and a message is printed to

indicate that such a correction has been made. The program then proceeds as usual.

The Error in Dip and Trend

According to the covariance law, the manner in which the errors in AD1 and AD2 propagate onto T and D is given by,

$$E_{T, D} = B E_{ESAD1, ESAD2} B^T \tag{32}$$

More simply stated, $E_{T, D}$, the errors in T and D, are related to the errors in AD1 and AD2, $E_{ESAD1, ESAD2}$, weighted by function, B, which describes how T and D vary with AD1 and AD2 at the point of evaluation. Mathematically,

$$\begin{vmatrix} S_T^2 & S_{TD} \\ S_{DT} & S_D^2 \end{vmatrix} = \begin{vmatrix} \frac{\partial T}{\partial AD1} & \frac{\partial T}{\partial AD2} \\ \frac{\partial D}{\partial AD1} & \frac{\partial D}{\partial AD2} \end{vmatrix} \begin{vmatrix} ESAD1^2 & ESAD12 \\ ESAD21 & ESAD2^2 \end{vmatrix} \begin{vmatrix} \frac{\partial D}{\partial AD1} & \frac{\partial D}{\partial AD2} \\ \frac{\partial T}{\partial AD2} & \frac{\partial D}{\partial AD2} \end{vmatrix} \tag{33}$$

where, ESAD12 and ESAD21 are the correlations between the errors in AD1 and AD2, and because there is no correlation between AD1 and AD2 (or the xz and xy thin sections), ESAD12 = ESAD21 = 0.

By multiplication of the above matrices,

$$S_T^2 = \left(\frac{\partial T}{\partial AD1}\right)^2 ESAD1^2 + \left(\frac{\partial T}{\partial AD2}\right)^2 ESAD2^2, \tag{34}$$

$$S_D^2 = \left(\frac{\partial D}{\partial AD1}\right)^2 ESAD1^2 + \left(\frac{\partial D}{\partial AD2}\right)^2 ESAD2^2, \text{ and} \tag{35}$$

$$S_{TD} = S_{DT} = \left(\frac{\partial T}{\partial AD1}\right)\left(\frac{\partial D}{\partial AD1}\right) ESAD1^2 + \left(\frac{\partial T}{\partial AD2}\right)\left(\frac{\partial D}{\partial AD2}\right) ESAD2^2. \tag{36}$$

Equation (34) states that the error in the trend, S_T, is a function of the error in the average apparent dips, ESAD1 and ESAD2, weighted by the rate of change of the trend with each average apparent dip, $\partial T/\partial AD1$ and $\partial T/\partial AD2$. Similarly, (from eq. 35), the error in the dip, S_D, is a function of the error in the average apparent dips, ESAD1 and ESAD2, weighted by the rate of change of the dip with each average apparent dip, $\partial D/\partial AD1$ and $\partial D/\partial AD2$.

It can be shown (Appendix VI), using equations (23) and (31),

$$\frac{\partial T}{\partial AD1} = \frac{-\tan AD2 \cos^2 T}{\sin^2 AD1}, \tag{37}$$

$$\frac{\partial T}{\partial AD2} = \frac{\cos^2 T}{\tan AD1 \cos^2 AD2}, \tag{38}$$

$$\frac{\partial D}{\partial AD1} = \frac{\cos^2 D}{\cos^2 T} \left\{ \frac{\cos T}{\cos^2 AD1} - \frac{\tan AD1 \sin T \tan AD2 \cos^2 T}{\sin^2 AD1} \right\}, \tag{39}$$

and $$\frac{\partial D}{\partial AD2} = \frac{\sin T \cos^2 D}{\cos^2 AD2}. \tag{40}$$

By the above derivations, all variables necessary to calculate S_T and S_D are known. The result of equations (34) and (35) will be the 95 percent confidence interval for T and D, respectively. Because the equations assume a wrapped normal distribution, values for S_T and S_D can range from zero to infinity. It may seem as though S_T and S_D should not be able to exceed 180°, but because by the wrapped assumption periodic errors are not superimposed and added to the same area, there are no limits to the maximum value for the error. Although the wrapped assumption will give a slightly larger estimate of the

error than the Von Mises distribution, for intermediate values

of k agreement is satisfactory (Stephens, 1963). Values for

S_T and S_D larger than 180° can simply be interpreted as errors

of 180°. In other words, the data are so bad that is is not

known where, within 95 percent confidence, the vector lies.

Any measure of dispersion of AD1 and AD2 can be entered

into the error matrix. The result of S_T and S_D will be that

statistical property which is input into the error matrix.

Equation (36) describes the covariance of T and D. This

is an important parameter since T and D are not statistically

independent. Any change in either quantity will affect the

other quantity.

Calculation of the Corrected Magnetic Direction and Azimuth of the Trend

For some samples a stable magnetic direction, M1, is mea-

sured relative to the orientation axes of the minicore. However,

the segregation vesicle orientation of the rock, defined by D,

T, S_T and S_D, was not known when this direction was measured.

To correct for the dip of the rock, M1 must be rotated about an

axis perpendicular to T as the plane defined by T and D is

rotated back to the reference horizontal (Figure 17).

There are several graphical and mathematical methods for

the simultaneous rotation of a vector and plane (e.g. Billings,

1972; Ragan, 1973; Phillips, 1971; and Johnson, 1939). The

mathematical method used here is after R. Boutilier (per. com.,

1980). According to this formalism, the coordinate system
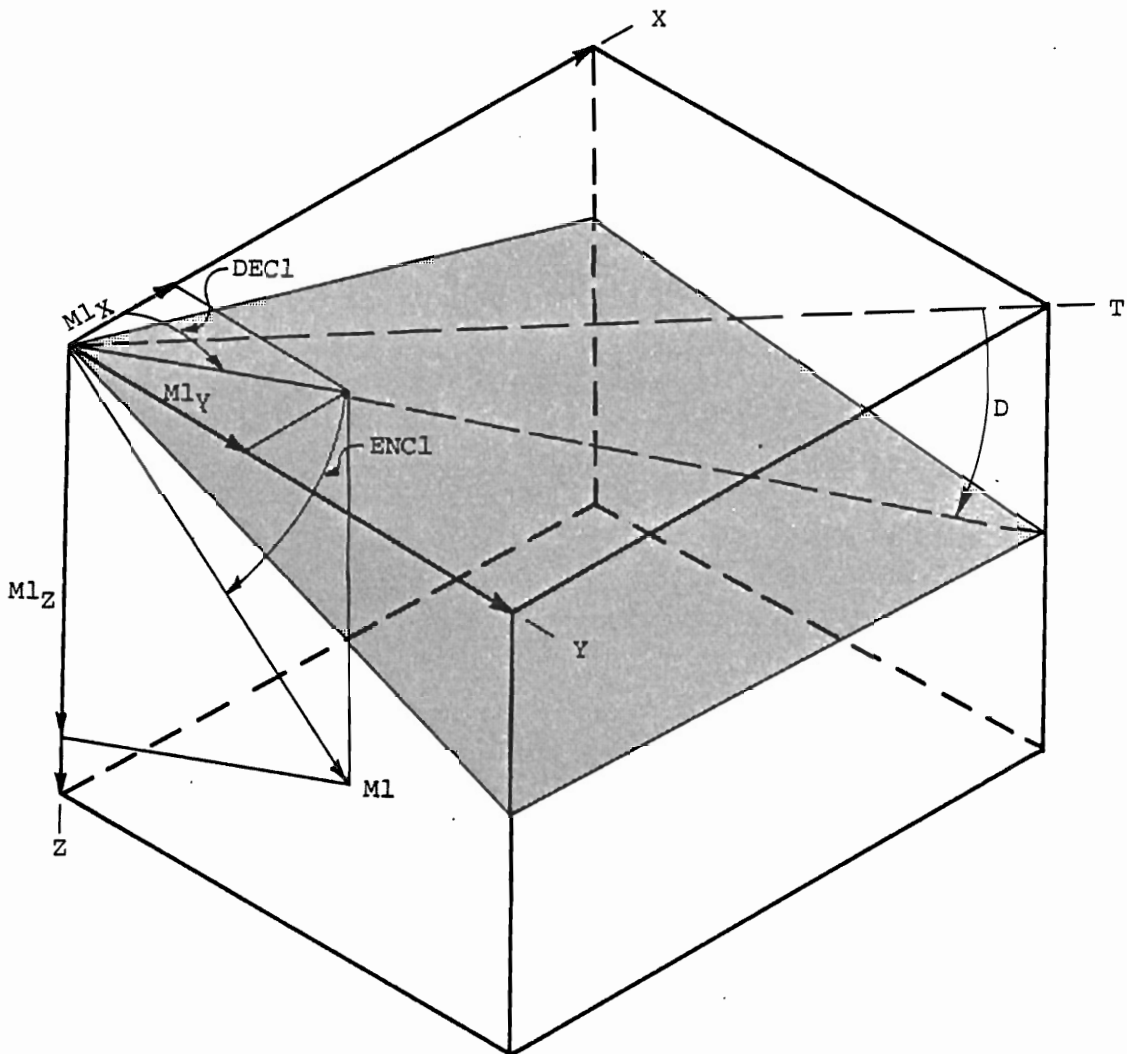
Figure 17. Block diagram showing the coordinate system within which the measured magnetic inclination (Ml) is defined. D and T are the dip and trend of the shaded plane, respectively. Ml_X, Ml_Y, and Ml_Z are the projection of Ml onto the X, Y, and Z axes respectively. DECl is the declination and ENCl is the inclination of Ml with respect to the X, Y, and Z coordinate system. +X, +Y, and +Z are equivalent to minicore axes z, y, and -x, respectively.

(Figure 17) is rotated until it is in the plane given by T and D, with X in the direction of T. M2 is then calculated as the components of the Ml vector in the rotated coordinate system.

The computations necessary are accomplished by computer program ROTSTAT (Appendix IX). The complete derivation is in Appendix VII.

Ml is given by a declination, DEC1, and inclination, ENC1, measured with respect to the orientation axes of the minicore. According to the coordinate system on Figure 17, Ml defines a unit vector given by the components,

$$Ml_Z = \sin ENC1 \tag{41}$$
$$Ml_X = \cos ENC1 \cos DEC1$$
$$Ml_Y = \cos ENC1 \sin DEC1.$$

The coordinate system is first rotated about the Z axis by the angle T. So that, X' points in the direction of D (Figure 18). Following this rotation

$$Ml_X' = Ml_X \cos T + Ml_Y \sin T \tag{42}$$
$$Ml_Y' = -Ml_X \sin T + Ml_Y \cos T$$
$$Ml_Z' = Ml_Z.$$

For the final rotation of the coordinate system, the (X', Z') plane is rotated about the Y' axis by the angle D. So that, X' is in the direction of D (Figure 19). Following this rotation,
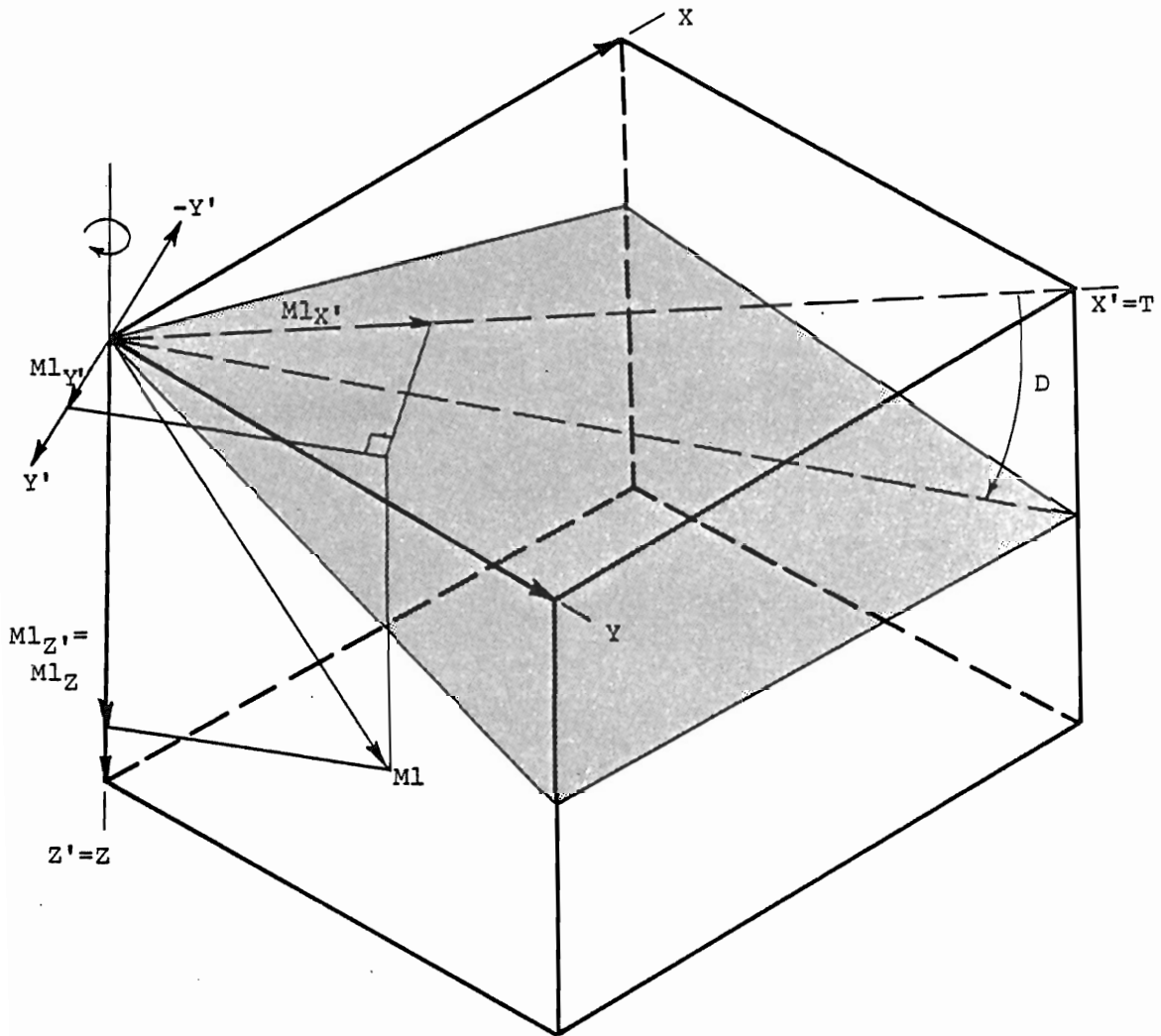
Figure 18. Block diagram illustrating the orientation of
the coordinate system (X', Y', Z') following rotation of
the X, Y, and Z system about the Z axis until X'=T. $M1_{X'}$,
$M1_{Y'}$, and $M1_{Z'}$ are the projections of M1 onto the X', Y',
and Z' axes, respectively.

Figure 19. Block diagram illustrating rotation of the X', Y', and Z' axes about the Y' axis by the angle D. $Ml_{X''}$, $Ml_{Y''}$, and $Ml_{Z''}$ are projections of Ml onto the X", Y", and Z" axes, respectively. X" and Y" lie in the shaded plane. Z" is normal to the plane. DEC2 and ENC2 are the declination and inclination, respectively, of the Ml vector to the X", Y", and Z" axes.

$$Ml_X" = Ml_X'\cos D + Ml_Z'\sin D \qquad (43)$$

$$Ml_Y" = Ml_Y' \qquad .$$

$$Ml_Z" = -Ml_X'\sin D + Ml_Z'\cos D$$

The components of Ml in the new rotated coordinate system then, are

$$\hat{M2} = (Ml_X", Ml_Y", Ml_Z") \qquad (44)$$

The corresponding inclination, ENC2, and declination, DEC2, are given by,

$$\sin ENC2 = Ml_Z", \text{ and} \qquad (45)$$

$$\cos DEC2 = Ml_X"/\cos ENC2, \qquad (46)$$

where, DEC2 is the horizontal angle between T = 0 degrees and the projection of M2 onto the (X", Y") plane. It is not the deviation of magnetic declination from true north. For most samples the in-place magnetic declination cannot be determined because they either rotate about a vertical axis during sampling (drill core samples), are not sampled in place (dredge and submersible samples) or, if sampled in place are not properly oriented (submersible samples).

The azimuth of the trend is calculated assuming that DEC2 points toward magnetic north or south, for normally, or reversely, magnetized rocks, respectively. If the rocks are reversely magnetized then DEC2 = DEC2 + 180. The azimuth of the trend, AZI, is then given by,

$$AZI = 360 - DEC2. \qquad (47)$$

The Error in the Corrected Magnetic Direction and Azimuth of the Trend

By the preceding calculation, ENC2 and AZI are given as function of T and D. However, there are errors associated with T and D, S_T, S_D and S_{TD} (eqs. 34, 35 and 36). Hence, there is no real unique solution for ENC2 and AZI. By the covariance law the manner in which the errors in T and D propagate onto ENC2 and AZI is given by,

$$E_{ENC2,\ AZI} = BE_{S_T,S_D,S_{TD}},B^T \tag{48}$$

More simply stated, the error in ENC2, S_E, and AZI, S_A, is related to the error in T and D (S_T and S_D, respectively), and the covariance between the errors in T and D (S_{TD}), weighted by a function, B, which describes the relationship between ENC2 and AZI, and, T and D. Therefore,

$$\begin{vmatrix} S_A^2 & S_{AE} \\ S_{EA} & S_E^2 \end{vmatrix} = \begin{vmatrix} \frac{\partial AZI}{\partial T} & \frac{\partial AZI}{\partial D} \\ \frac{\partial ENC2}{\partial T} & \frac{\partial ENC2}{\partial D} \end{vmatrix} \begin{vmatrix} S_T^2 & S_{DT} \\ S_{DT} & S_D^2 \end{vmatrix} \begin{vmatrix} \frac{\partial AZI}{\partial T} & \frac{\partial ENC2}{\partial T} \\ \frac{\partial AZI}{\partial D} & \frac{\partial ENC2}{\partial D} \end{vmatrix} \tag{49}$$

By multiplication of the above matrices,

$$S_A^2 = (\frac{\partial AZI}{\partial T})^2\ S_T^2 + 2(\frac{\partial AZI}{\partial T}\ \frac{\partial AZI}{\partial D}\ S_{TD}) + (\frac{\partial AZI}{\partial D})^2\ S_D^2 \tag{50}$$

and

$$S_E^2 = (\frac{\partial ENC2}{\partial T})^2\ S_T^2 + S(\frac{\partial ENC2}{\partial T}\ \frac{\partial ENC2}{\partial D}\ S_{TD}) + (\frac{\partial ENC2}{\partial D})\ S^2 D \tag{51}$$

Equation 50 states that the error in AZI is equal to the error in T, D and the covariance between these errors, weighted by the rates of change of AZI with T, $\partial AZI/\partial T$, and D, $\partial AZI/\partial D$.

Similarly, (by eq. 51) the error in ENC2 is equal to the error in T, D, and the covariance between these errors, weighted by the rate of change of ENC2 with both T and D (∂ENC2/∂T, and ∂ENC2/∂D, respectively). The quantity S_{TD} is important here because the error in AZI and ENC2 is a function of the rate of change of these variables with both T and D. Since there is correlation between the errors in T and D, the covariance between these errors, S_{TD}, must be considered in the calculation.

It can be shown that (Appendix VIII),

$$\frac{\partial ENC2}{\partial T} = \frac{\sin D(Ml_X \sin T - Ml_Y \cos T)}{\cos ENC2} \tag{52}$$

$$\frac{\partial ENC2}{\partial D} = \frac{-(Ml_Z' \sin D + Ml_X' \cos D)}{\cos ENC2} \tag{53}$$

$$\frac{\partial AZI}{\partial T} = \frac{1}{\sin AZI \cos^2 ENC2}\{\cos ENC2 \cos D(Ml_X \sin T -$$
$$Ml_Y \cos T) - Ml_X'' \sin ENC2(\frac{\partial ENC2}{\partial T})\}$$

$$\frac{\partial AZI}{\partial D} = \frac{1}{\sin AZI \cos^2 ENC2}\{\cos ENC2(Ml_X' \sin D - \tag{55}$$
$$Ml_Z' \cos D) - Ml_X'' \sin ENC2(\frac{ENC2}{\partial D})\}$$

Solutions for Ml_X, Ml_Y, Ml_Z', Ml_X' and Ml_X'', were given by equations (41), (42) and (43).

By the above derivations all variables necessary to calculate S_A and S_E are known. The result of equations (50) and (51) is the 95 percent confidence interval for the azimuth of the trend and the corrected magnetic inclination, respectively. As with the values of S_T and S_D, the error can range from

zero to infinity because periodic errors are not added. Any
error greater than 180° can be taken to equal 180°. Compu-
tation of an error greater than or equal to 180° indicates
that it is now known, within 95 percent confidence, where
the vector lies in space.

Again, any measure of dispersion can be used as input
quantities. The statistical property of the calculated error
will be the same as the input error.

Finally, S_A and S_E are calculated for $S_T = 0.0$. The re-
sults of this calculation may be important when the plane given
by D and T is horizontal. When this is the case T is undefined.
It may, therefore, be desirable to know the error in AZI and
ENC2 only due to the dip.

Acceptability of Statistical Techniques and Test Cases

In the preceding calculations a previously established,
theoretically acceptable statistical procedure for the propa-
gation of errors, the covariance law, is adhered to. Any
other justification of the theoretical acceptability of this
law is beyond the scope of this thesis. The method is accept-
able providing the mathematical models describing the relation-
ship between the known and derived parameters are correct, and
the derivations of the covariance law applicable to the se-
gregation vesicle problem are correct.

To help test the validity of this approach several hypo-
thetical cases were investigated in which, due to the geo-

metrical arrangement of AD1, AD2, T, D, and M1, certain confidence intervals for T, D, ENC2, and AZI, were intuitively expected. A qualitative judgement of the reasonableness of errors calculated by the covariance law could, therefore, be made. Six of these cases are described.

    Test Case 1

The xz thin section plane is almost perpendicular to T. The xy thin section plane is cut almost parallel to the plane containing T and D. There are no magnetic data for this hypothetical sample so 999.999 is recorded for DEC. In ROTSTAT outputs, INC is printed in place of ENC. ROTSTAT produces the following output:

    Processing Test Case 1

    Input Data: AD1 =   1.00000

                    SAD1 =   5.00000

                     AD2 =   35.00000

                    SAD2 =   20.00000

                     DEC =   999.99900

                     INC =   0.00000

    Calculated Dip = 35.00836

           Trend = 88.57193

    Calculated Errors S(DIP) = 19.98982

                    S(TREND) = 7.21836

    No magnetic data for this sample.

    The results of the computation are that the error for the dip is similar to the value for the error in AD2, and the

value for the error in the trend is similar to the value for the error in AD1. These calculated errors are reasonable because AD2 is the apparent dip most "controlling" the dip and AD1 is the apparent dip most "controlling" the trend.

Test Case 2

The attitude of the plane by AD1 and AD2 is almost perfectly horizontal. The trend direction should, therefore, be undefined with an error greater than or equal to 180°. ROTSTAT produces the following output,

Processing Test Case 2

Input Date: AD1 =   .10000

               SAD1 =   5.00000

                AD2 =   .10000

               SAD2 =   5.00000

                DEC = 999.99900

                INC =   0.00000

Calculated Dip =   .14142

       Trend = 44.99989

Calculated Errors S(DIP)   =   4.99997

               S(TREND) = 2025.72829

No magnetic data for this sample.

The error in the trend is 2025.73°. This value is consistent with the expected error. The error in the dip is similar to the errors in AD1 and AD2. This value should be expected because AD1 = AD2 and T is at the midpoint between

AD1 and AD2. Therefore, neither apparent dip will have more influence on the error in the true dip.

Test Case 3

In this case the dip is almost vertical and the T direction bisects the angle between AD1 and AD2. Small changes in the dip should cause large changes in the trend. The expected error in T is again greater than or equal to 180°. As shown below, the results of the calculation are consistent with the expected value.

```
Processing Test Case 3
Input Data          AD1 =      89.00000
                   SAD1 =       5.00000
                    AD2 =      89.00000
                   SAD2 =      10.00000
                    DEC =     999.99900
                    INC =       0.00000
Calculated Dip =   89.29288
        Trend =   44.99989
Calculated Errors S(DIP)  =      3.95344
                 S(TREND) =    320.33583
```

No magnetic data for this sample.

The value for the error in D may seem smaller than expected. However, when the dip direction is nearly vertical, small changes in either apparent dip will not affect the value of the true dip.

Test Case 4

In this case the attitude is nearly horizontal, as in test case 2. However a magnetic direction is added. The expected result is that the error in AZI should be equal to or greater than 180°. The error in ENC2 is expected to be similar to the error in D. Finally, when ST = 0, the error in AZI should be small. The following printout from ROTSTAT shows that the results of the calculation are consistent with the expected values.

```
    Processing Test Case 4

    Input Data        AD1 =      .10000

                     SAD1 =     5.00000

                      AD2 =      .10000

                     SAD2 =     5.00000

                      DEC =    60.00000

                      INC =    40.00000

    Calculated Dip =    .14142

           Trend = 44.99989

    Calculated errors S(DIP)   =     4.99997

                     S(TREND)  = 2025.72829

    Calculated corrected magnetic inclination  =    39.86339

    Calculated azimuth of trend                 =   345.03049

    Calculated errors in inclination and azimuth:

        S(AZI)  =   2021.64873

        S(INC)  =      4.99998

    Calculated errors in inclination and azimuth:

        S(AZI)  =      1.07845

        S(INC)  =      4.83029
```

Note that the last calculation is for trend error = 0.0.

Test Case 5

This example is the same as test case 1 with the addition
of magnetic data. DEC1 is almost parallel to T. According to
this geometry the magnetic vector rotates almost in the plane
given by T and D. The expected results are that the error in
ENC2 will be similar to the error in D and the error in AZI will
be similar to the error in T. This is, in fact, the case shown
by the results of the calculation below. The error in AZI may
be somewhat smaller than expected indicating a small value for
S_{TD}.

Processing Test Case 5

Input Data: AD1 =   1.00000

                   SAD1 =   5.00000

                    AD2 =   35.00000

                   SAD2 =   20.00000

                    DEC =   88.60000

                    INC =   60.00000

Calculated Dip =   35.00836

        Trend =   88.57193

Calculated Errors S(DIP)   =   19.98982

                  S(TREND)   =   7.21836

Calculated corrected magnetic inclination =   24.99164

Calculated azimuth of trend   =   359.98451

Calculated errors in inclination and azimuth:

```
S(AZI)  =    3.90570

S(INC)  =   19.98998
```

Calculated errors in inclination and azimuth:

```
S(AZI)  =     .00247

S(INC)  =   19.98982
```

Note that the last calculation is for trend error = 0.0.

Test Case 6

This test case is identical to test case 3 with the addi-
tion of magnetic data. According to test case 3, T was unde-
fined within 95 percent confidence. The magnetic vector added
has a declination almost parallel to T and ENC1 less than D.
Because the axis of rotation (the perpendicular to T) is not
constrained, ENC2 will vary rapidly with T. Based on this
geometry, rotated values for ENC2 can be either positive or
negative. The error in ENC2 should, therefore, be equal to
or greater than 180°. As shown below, the calculated errors
are consistent with the expected results.

Processing Test Case 6

```
Input Data:      AD1  =    89.00000

                SAD1  =     5.00000

                 AD2  =    89.00000

                SAD2  =    10.00000

                 DEC  =    75.00000

                 INC  =    20.00000
```

Calculated Dip = 89.29288

Trend = 44.99989

Calculated errors S(DIP) =   3.95344

S(TREND) = 320.33583

Calculated corrected magnetic inclination = -54.04849

Calculated azimuth of trend   = 126.84272

Calculated errors in inclination and azimuth:

S(AZI) = 266.18465

S(INC) = 257.76944

Calculated errors in inclination and azimuth:

S(AZI) =   4.36244

S(INC) =   2.37057

Note that the last calculation is for trend error = 0.0.

Summary of Statistical Method

The segregation vesicle inclinations measured in each pair
of thin sections from a minicore sample are entered into compu-
ter program CIRST (Appendix II). This program is designed to
use circular statistical techniques (Batschelat, 1972; and
Mardia, 1972) to compute the average segregation vesicle in-
clination of each thin section of the pair, AD1 and AD2 (eq.
7) and the 95 percent confidence interval of each mean, ESAD1
and ESAD2 (eq. 12). CIRST also plots equal area rose diagrams
which show the frequency distribution of the segregation vesi-
cle inclinations measured in each thin section and executes
the Rayleigh test of uniformity to check for preferential

orientation of these inclinations. If a megascopic orientation of the rock sample is known, the V-test can be used to test for clustering of the measured segregation vesicle inclinations about the orientation of the rock given by megascopic criteria.

AD1, AD2, ESAD1, and ESAD2, are then entered into computer program ROTSTAT. This program is designed to compute the true dip, D, and its associated error, S_D, and the dip direction, T, along with its associated error, S_T, with respect to the orientation axes of the minicore sample (eqs. 18-31). The errors, S_D and S_T, are due to the errors in ESAD1 and ESAD2 and are determined by application of the covariance law (Vaniček, 1973) (eqs. 32-40).

If a stable magnetic direction with respect to the orientation axes of the minicore was measured for a sample, the declination, DEC1, and inclination, ENC1, are entered into computer program ROTSTAT along with the other parameters. ROTSTAT computes the corrected magnetic inclination, ENC2, and, AZI, the horizontal angle between T and the corrected magnetic declination, DEC2. These values are determined by a series of mathematical manipulations included in ROTSTAT which accomplish the simultaneous rotation of ENC1 and DEC1 as the plane defined by T and D is rotated back to the reference horizontal position (eqs. 41-47). The program also computes, according to the covariance law (Vaniček, 1973) (eqs. 48-55), the errors associated with ENC2, S_E, and AZI, S_A, because of the errors, S_T and S_D.

RESULTS OF TESTS OF THE SEGREGATION VESICLE TECHNIQUE

Test for Preferred Orientation

The segregation vesicle technique assumes that the cup-shaped lining of aphanitic residue is preferentially oriented with respect to the earth's gravity field. Equal area histograms (Figure 10) show an apparent preferred orientation of segregation vesicle inclinations measured in a given thin section. As a quantitative test of preferred orientation, the Rayleigh test of uniformity was applied to the segregation vesicle inclination data sets from the 17 samples which were oriented by megascopic criteria.

Calculated R values (eq. 8) for these samples are listed on Table 3. Recall that this value can range from 0 to 1, with values close to 1 signifying well clustered data. The rejection of an R value for the Rayleigh test, however, is strongly weighted by the number of measurements. If there are a large number of measurements small R values can still signify preferentially oriented data.

In 94 percent of the cases (data from 47 thin sections) randomness of segregation vesicle inclinations can be rejected at the 1 percent level of significance (Table 3) indicating that the assumption of preferential orientation generally is correct. For 6 percent of the cases (data from 3 thin sections) randomness cannot be rejected (Table 3). In these cases, samples are from rocks oriented by MC-3. Because the megascopic orientation is of poor quality, the chance of increasing

Table 3. Segregation vesicle orientation and paleomagnetic data for samples which can be oriented by megascopic orientation features. Abreviations are from the text.

Sample number	MC	Nxz	AD1	ESAD1	Rxz	Uxz	Nxy	AD2	ESAD2	Rxy	Uxy	D	S_D	ENC1	ENC2	S_E
818-2	2		351	5			3	0.4	25	0.93	2.28	9	5	-10.8	-14	23
818-3	1	2	6	11	0.99	1.97	2	341	11	0.99	1.88	20	11	58.9	68	11
821-4	2	3	2	18	0.97	2.37	3	3	13	0.99	2.41	4	15	81.6	81	15
821-6-A2	1	32	355	11	0.85	5.55	18	6	10	0.93	6.81	8	10	62.5	63	11
-C1	1	8	358	22	0.87	3.47	11	353	27	0.73	3.42	7	26	62.5	68	22
821-9-A3	1	19	10	19	0.76	3.51	10	347	21	0.85	3.70	16	19	57.0	46	20
-B1	1	12	2	18	0.86	4.20	44	353	11	0.79	7.40	7	12	57.4	58	18
822-6-A1	2	10	347	14	0.92	4.04	19	7	19	0.76	4.67	14	15	42.4	47	17
-A4	2	26	7	14	0.83	5.93	17	348	13	0.89	5.11	13	13	3.41	36	13
823-8-A3	2	9	4	9	0.98	4.17	4	341	21	0.94	2.50	19	21	-53.6	-35	19
-B1	2	11	2	15	0.91	4.29	4	17	20	0.95	2.56	17	20	-52.5	-62	15
824-9-A1	2	39	1	17	0.64	5.68	17	9	10	0.95	5.43	10	10	-32.4	-40	12
-A2	2	47	8	21	0.51	5.01	24	23	32	0.47	3.00	24	31	-31.7	-56	31
-B	2	14	341	31	0.61	3.19	18	17	14	0.88	5.05	25	23	-32.4	-39	21
828-5	2	9	356	9	0.98	4.14	2	333	11	0.99	1.76	28	11	42.9	36	9
831-1	3	5	338	31	0.83	2.56	4	6	45	0.72	2.04	23	31	56.0	58	42
831-3	1	54	2	7	0.91	9.49	25	1	11	0.90	6.36	2	8	52.4	51	10
831-6	1	9	7	13	0.94	3.96	6	353	26	0.86	2.96	10	20	36.6	43	26
831-14	3	4	5	8	0.99	2.80	2	340	11	1.00	0.94	20	11	31.7	25	8
832-2	1	6	6	34	0.75	2.59	4	356	11	0.99	2.82	7	30	28.6	21	26
103-5-1	3	19	29	71	0.24	1.31	10	1	54	0.45	1.99	30	70	51.6	67	47
103-33-6B	1	19	8	14	0.87	5.30	5	7	10	0.98	3.09	10	12	5.81	65	10
-6WHOI	1	12	359	17	0.88	4.29	10	357	27	0.75	3.55	3	26	56.0	56	17
-7A	1	22	350	19	0.72	4.71	12	348	19	0.85	4.07	15	18	52.0	43	19
103-33-41	2	5	22	18	0.95	2.79	7	5	23	0.87	3.24	22	18	75.4	57	18

apparent scatter of the data due to the orientation of the
plane of observation is increased. For this reason results
of application of the Rayleigh test to unoriented samples have
no significance as a test of the assumption of preferred orien-
tation, and are not considered.

The V-test

Showing that segregation vesicle inclinations have a pre-
ferred orientation is insufficient without also showing that
the preferential orientation is related to the earth's gravity
field. This direction is taken as the normal to subhorizontal
megascopic cooling features. Equal area histograms (Figure
10) show a clustering of segregation vesicle inclinations a-
round this direction, indicated as 0°. A quantitative measure
of clustering about a known direction, the V-test, was applied
to the segregation vesicle inclination data from the 17 mega-
scopically oriented rock samples. Recall that according to
this test, to reject random clustering a computed u value (eq.
10) must exceed a critical value and the number of measurements
must equal or exceed 5 (Appendix IV).

Computed u values are listed on Table 3. Random clustering
can be rejected in 71 percent of the cases at P >.0001, in 13
percent of the cases at P = .001 to .0001, in 8 percent of the
cases at P = .005 to .001, and in the remaining 8 percent of the
cases at P >0.1. Data from the 3 cases that passed the Ray-
leigh test, also passed the V-test. This result indicates
that although data are randomly distributed in these cases,

there is a significant component of the measured inclinations around the earth's gravity field.

Comparison of the Segregation Vesicle Orientation With the Megascopic Orientation

The most obvious test of the technique is for agreement between the segregation vesicle orientation of the rock and that given by megascopic orientation features. The average segregation vesicle inclination, AD, $\pm$ one 95 percent confidence interval of the mean, ESAD, computed from each data set, should be within the limits of reliability of the orientation given by megascopic features. The calculated dip, D, $\pm$ one 95 percent confidence limit of this dip, S_D, given by a combination of the average segregation vesicle inclination in each pair of thin sections from a rock sample, should also fall within the limits of reliability of the horizontal surface given by the megascopic orientation feature. Comparison of the values for AD1 and ESAD1, AD2 and ESAD2, and D and S_D, with the reliability of the megascopic orientation (Table 3), indicate that these conditions are met in all cases. There is no case where the orientation of the rock given by segregation vesicles does not agree with that given by the megascopic orientation feature.

To test for reproducibility, multiple samples were taken from 6 of the rocks. In all cases there is good reproducibility of the orientation given by segregation vesicles, and good agreement between the segregation vesicle and megascopic

orientation (Table 3).

Reliability of the Segregation Vesicle Technique as a Structural Tool

As previously mentioned, in order to use the technique to determine the structural dip of sea floor basalts recovered by drill core, two criteria must be satisfied. It must be shown that the segregation vesicle orientation of the rock agrees with that given by megascopic criterion. This condition is satisfied (Table 3). Secondly, the error margin of the segregation vesicle orientation must be reasonably small.

Bideau and others (1977) estimated that by the segregation vesicle technique they could be sure of the orientation of a rock within about 15°. However, they only tested the technique on two rock samples oriented by megascopic geopetal features. They also did not take into consideration that the segregation vesicle technique only gives an estimate of some average orientation of the rock, with which is associated a certain error. A more rigorous approach is necessary to establish the limits of reliability of the segregation vesicle technique as a structural tool.

The sample set for this test includes 17 rock samples which were oriented by segregation vesicles and megascopic criterion (Table 3) and the additional 17 samples were oriented by segregation vesicles only (Table 4). The average dip (D) and 95 percent confidence interval of the dip, S_D, was calculated for these samples.

Table 4. Segregation vesicle orientation and paleomagnetic data for samples which can not be oriented by megascopic orientation features. Abbreviations are from the text.

Sample number	AD1	ESAD1	AD2	ESAD2	D	S_D	ENC1	ENC2	S_E
818-8	6	51	32	34	32	39	51.9	84	47
820-3	179	19	181	26	-1	23	-37.7	38	26
-P1	190	10	153	24	-29	23	-67.2	66	25
822-3-A1	169	21	201	7	-24	10	30.1	-53	7
824-3-CB-P1	134	21	138	30	-54	17	-20.8	36	29
829-4-STL	344	16	304	28	56	27	38.5	81	25
829-12	359	17	339	26	21	26	44.8	64	24
832-3-P3	122	46	117	46	-69	27	-7.7	-55	40
103-4-4-P2	267	15	196	55	-87	15	-57.7	24	15
103-4-5	358	35	31	36	31	36	-81.9	-51	36
103-9-33	326	50	322	25	46	28	44.5	52	46
103-21-2-A3	80	23	71	44	81	17	-60.6	20	16
103-23-9	1	65	65	21	65	21	18.8	67	27
103-24-1	142	37	331	61	-89	61	29.2	56	35
103-33-2	9	15	18	16	19	15	64.1	48	15
103-33-39-A1	3	22	325	29	35	29	50.3	36	21
103-33-40	204	36	173	24	-24	35	72.5	-78	26
103-46-3	51	39	246	53	90	53	21.1	59	11

Cumulative frequency curves of S_D (Figure 20) show that previously oriented samples generally have smaller errors than unoriented samples. This is because thin sections cut from previously unoriented rocks are more likely to be cut at a large angle to the original vertical axis than those which are oriented, resulting in a larger apparent scatter due to the direction of observation.

The central curve (Figure 20) can be used to determine the limits of reliability of the segregation vesicle technique as a structural tool, assuming that some of the time rocks recovered by drill core will have a subhorizontal dip. It shows that 50 percent of the samples have errors less than 19°, and 90 percent of the samples have errors less than 36°. Although smaller errors are desireable, these errors are not too large to preclude some structural interpretation.

Because two lines can be used to define a plane of any orientation, a further test of the validity of the technique as a structural tool was undertaken in which 3 thin sections were cut at different orientations to each other from an unoriented rock sample. When plotted on a stereonet, the average segregation vesicle inclination determined for each of the thin sections all fit essentially the same plane (Figure 21). This test indicates that two thin sections are adequate to define the horizontal plane given by segregation vesicles. Measuring inclinations in a third section will not add significant information.
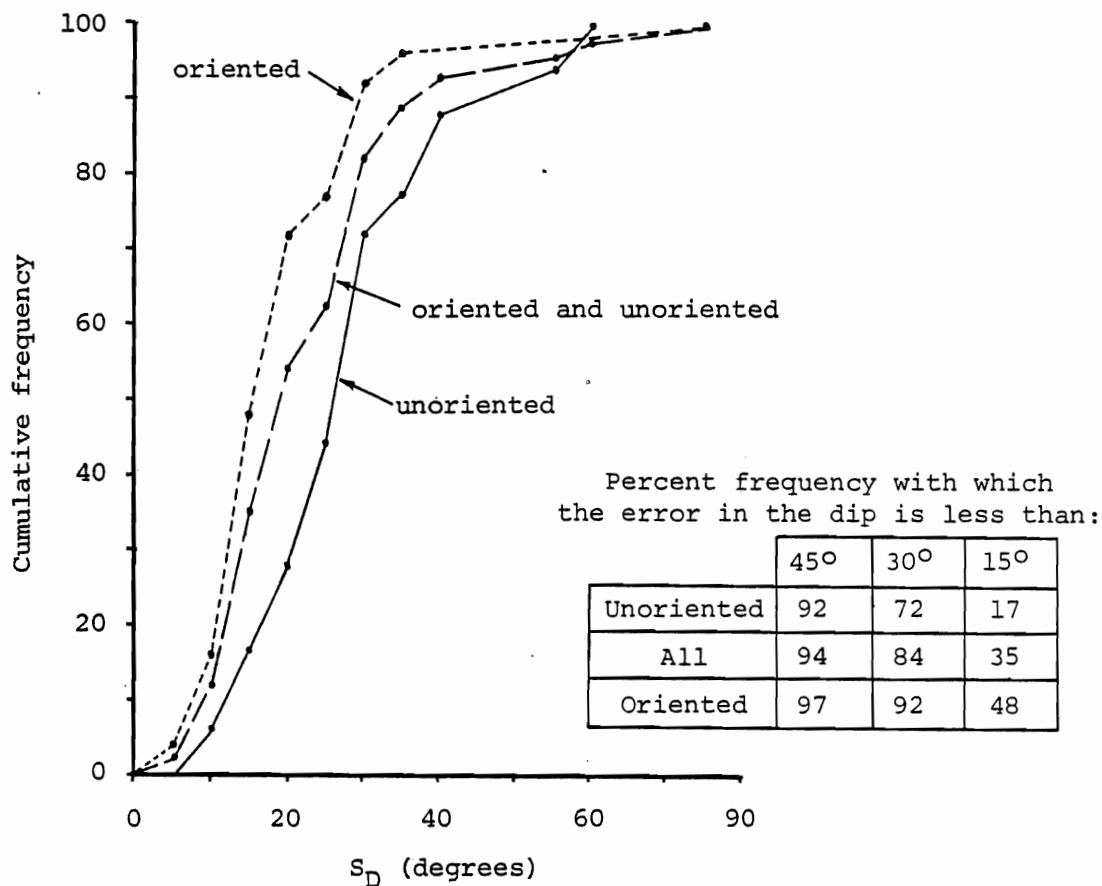
Figure 20. Cumulative frequency curve of the 95 percent confidence interval of the calculated dip (original horizontal surface), S_D. Class width is 5°. Data are from Tables 3 and 4. The graphs show that, considering all of the test samples, in 90 percent of the cases the error is less than 36°. The table lists the frequency of other errors.

Sample 332A
29.1 33-36
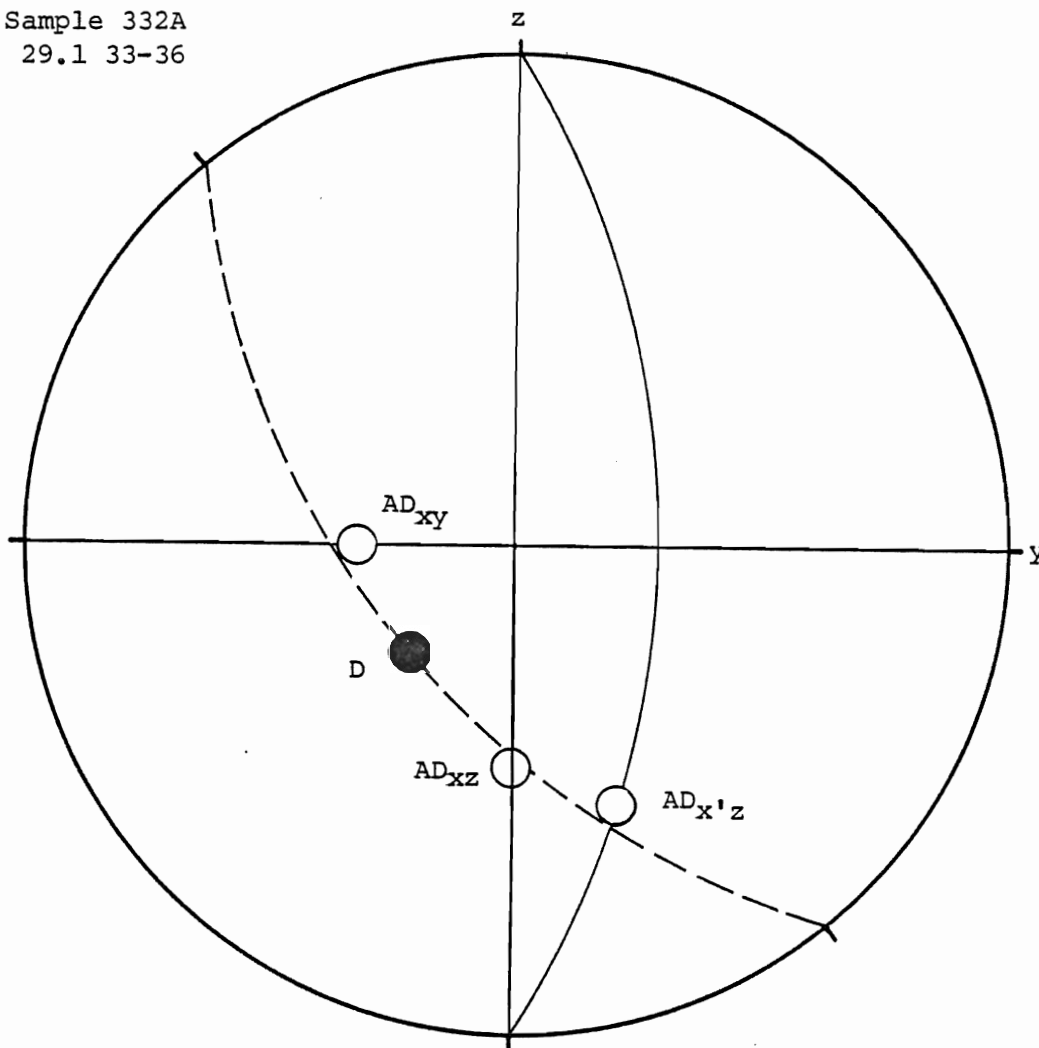
Figure 21. Stereonet plot of three average apparent dips
(AD_{xy}, AD_{xz}, and $AD_{x'z}$) determined from segregation vesicle
studies of 3 thin sections from the same rock sample. All
apparent dips fit essentially the same plane.

Reliability of the Segregation Vesicle Technique as a Paleo-
magnetic Tool

Bideau and others (1977) suggested that the main application
of the segregation vesicle technique might be to orient dredge
haul basalt samples for paleomagnetic purposes. They indicated
that by using the technique the magnetic polarity of a sea-floor
basalt could be determined outside a band of 20° latitude cen-
tered around the paleoequator. This estimate was based on
what they believed to be the degree of certainty of the orien-
tation technique.

By a more rigorous treatment of the segregation vesicle
data (eqs. 48-55), the manner in which errors in the orientation
of the rock given by segregation vesicles propagates onto the
rotated magnetic vector can be determined. By considering
these errors, a more reasonable assessment of how well the mag-
netic polarity of rocks oriented by segregation vesicles agrees
with the polarity of rocks of the same age and geographic loca-
tion oriented by the accepted megascopic criteria can then be
made. Calculation of these errors is also necessary to deter-
mine the geographic limits of the application of the technique
for paleomagnetic purposes.

The magnetic inclinations of 17 unoriented rock samples
was measured (Table 4). Because these rocks are not oriented
there is a large variation of these measured inclinations
(Figure 22A). To determine the magnetic inclination acquired
by these rocks upon cooling, they were oriented by the segre-
gation vesicle technique, and the measured magnetic vectors were
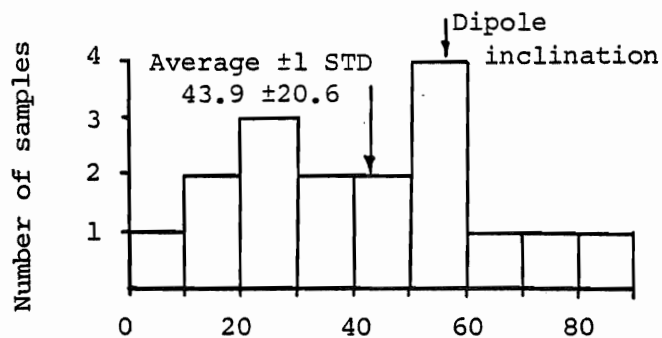
Figure 22A . Frequency distribution of the absolute value of measured magnetic inclination of unoriented samples. The average value of multiple samples from the same rock is used here. Data are from Table 4.
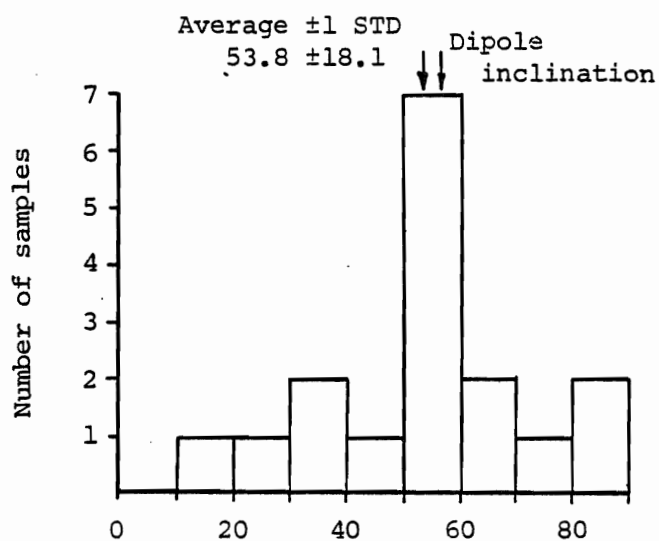
Figure 22B . Frequency distribution of the absolute value of magnetic inclinations rotated according to the segregation vesicle orientation of the rock. The average inclination of multiple measurements from different cores of the same rock is used here. Data are from Table 4.
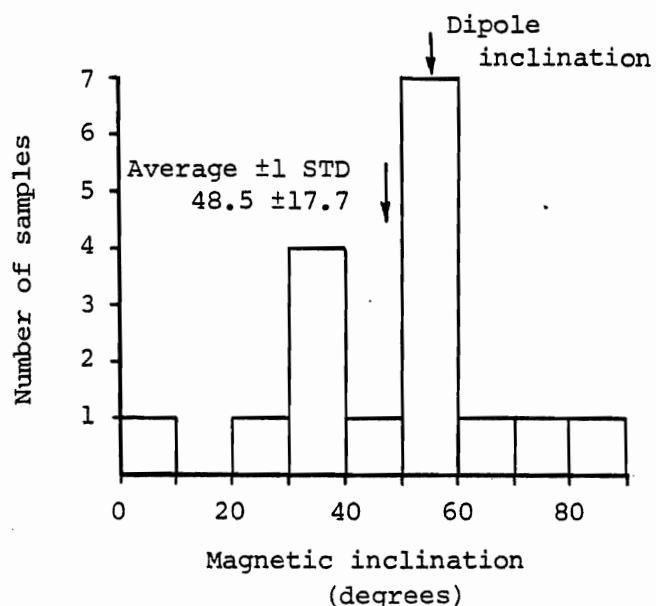
Figure 22C . Frequency distribution of the absolute value of measured magnetic inclination of samples oriented by megascopic features. The average inclination of multiple measurements from different cores of the same rock is used here. Data are from Table 3.

rotated according to these orientations. These corrected magnetic inclinations are more tightly clustered about the expected dipole value (56°) with an average inclination of 54° and a standard deviation of 18° (Figure 22B).

This distribution compares well with the measured magnetic inclination of rocks oriented by megascopic criteria (Figure 22C). The similarity of these distributions indicates that the segregation vesicle technique is at least as good a tool for orienting rocks for paleomagnetic purposes as the accepted megascopic criteria. In fact, in all but 2 cases, or 89 percent of the time, the average rotated magnetic inclination, $\pm$ one 95 percent confidence interval (S_E) of this average, contains the dipole inclination (Figure 23).

There is a large variation in the S_E from sample to sample (Figure 23). These values limit the latitude at which it is possible to determine the magnetic polarity of a rock sample. If the error in the rotated inclination exceeds the mean inclination then the polarity of the rock cannot be determined within 95 percent confidence. For 95 percent of the cases S_E is less than 44.5° (Figure 24). By the tangent rule for an axially centered dipolar magnetic field (Irving, 1964), 44.5° of inclination occurs at $\pm 26^\circ$ of the paleoequator. Outside this latitude the technique probably can be used to determine the polarity of samples which have segregation vesicles 95 percent of the time. The technique has the accuracy Bideau and others (1977) suggested only 50 percent of the time.
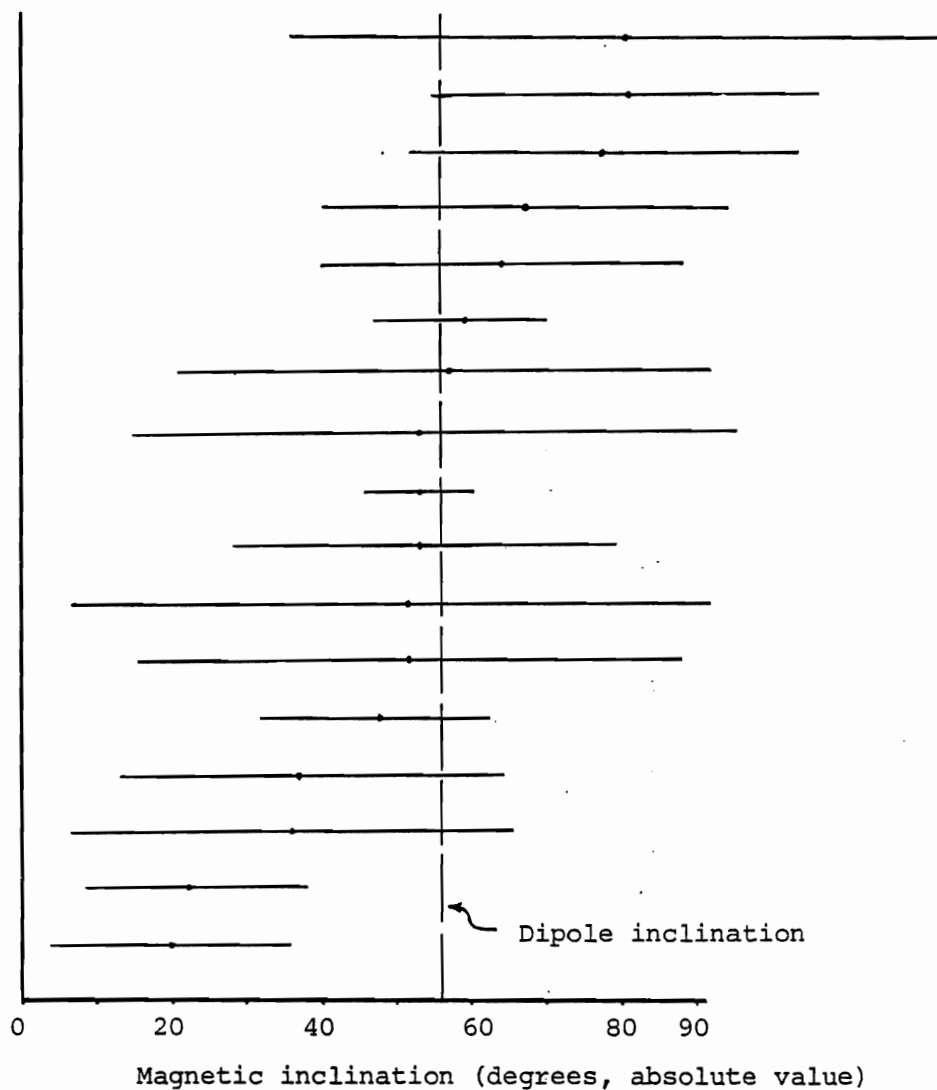
Figure 23. Graphic display of the corrected magnetic in-
clination, determined by the segregation vesicle technique,
plus or minus one 95 percent confidence interval of this
value. The figure shows that in 89 percent of the cases
the calculated inclination includes the expected dipole
inclination. Data are from Table 4. Average values of the
two samples from 820-3 are plotted.
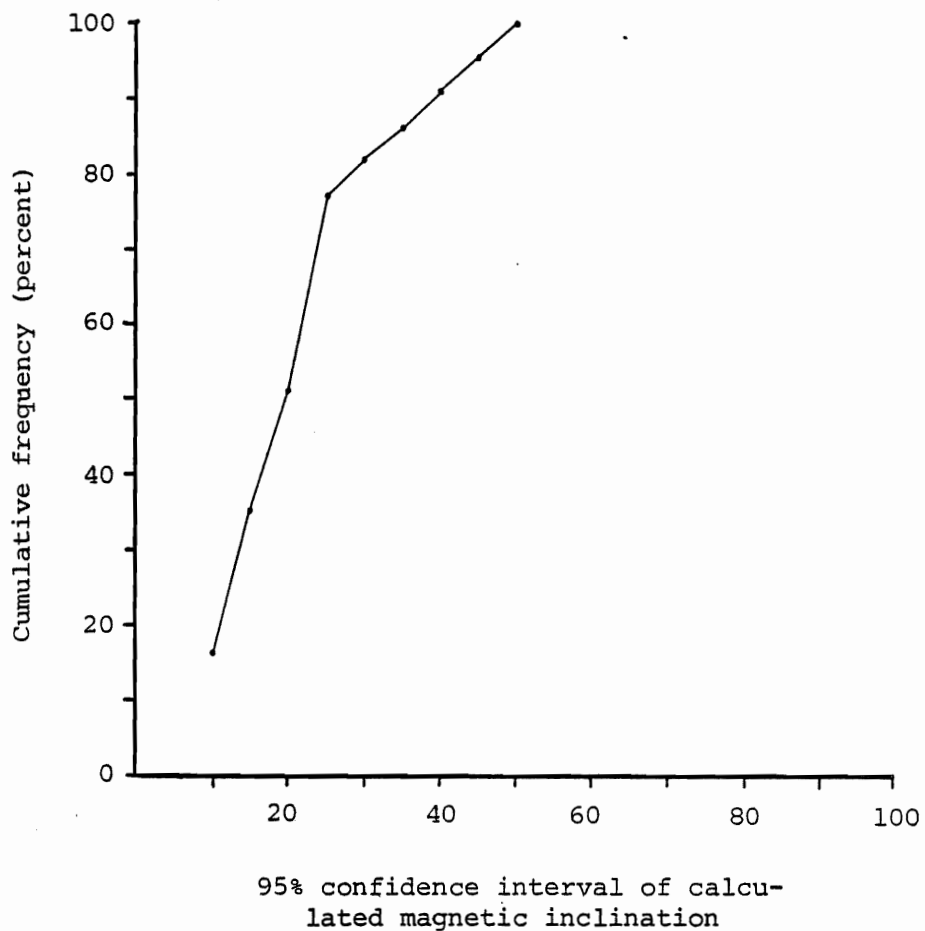
Figure 24. Cumulative frequency curve showing that in 95 percent of the cases (n = 43) the error in the calculated magnetic inclination based on the segregation vesicle technique is less than 44.5°. Data are from Tables 3 and 4.

Practicality and Usefulness of the Technique

The segregation vesicle technique is a time consuming method of rock orientation. It is only useful if segregation vesicles occur frequently enough to make them worth looking for. It is only worth pursuing if the structural and/or paleomagnetic information gained adds significantly to the solution of a problem.

Three hundred-sixteen thin sections from 158 rock samples collected during the AMAR cruise were examined for segregation vesicles. Only 34 of the rock samples or 22 percent have sufficient segregation vesicles to orient the rocks. Thirty-eight of the rock samples collected during the cruise were oriented by megascopic criteria. Seventeen of these were also oriented by the segregation vesicle technique. An additional 17 of these samples were oriented only by the segregation vesicle technique. These 17 samples increased paleomagnetic coverage of the study area by about 45 percent. This increase in data added significantly to the reconstruction of the magnetic evolution of the area. The cost, however, was 316 thin sections, a minimum of 150 hours of microscope work, and another 300 hours for paleomagnetic data processing, rock orientation and thin section chip preparation.

As a tool for determining the structural dip and corrected magnetic polarity profile of sea floor basalt samples recovered by drill core, the segregation vesicle technique is unsurpassed. Basalts examined from the DSDP holes studied (Figure 2) all

contain segregation vesicles with some frequency of occurrence. On average, about 30 percent of the rock samples taken from these holes have segregation vesicles which can be used to determine the dip of the rocks, providing more structural information than has ever been available for these holes. Once the dip of the rock is known the corrected magnetic polarity can be determined giving some insight into the pre-deformational stratigraphic and paleomagnetic characteristics of the rocks recovered.

Problems with Application of the Technique

Several problems can complicate the application of this technique to structural and paleomagnetic studies. There may be a very broad range to the measured segregation vesicle angles that cannot be minimized significantly by changing the direction of observation. This scatter may be caused by a complex cooling history resulting in more than one generation of vesicles and fillings, rotation or deformation of the rock during or shortly after intrusion of residual melt into vesicles, or removal or deformation of some of the segregation vesicle during thin sectioning, or as a result of secondary alteration of the rock. Additionally, it may be possible for the rock to rotate between the time it acquires its segregation vesicle and megascopic orientation (around the solidus temperature of the rock, 800 to 1200°C) and the time it acquires its magnetic direction (around the Curie temperature of the rock, 150°C).

A complex cooling history may be indicated by chemical studies of the aphanitic residue. In this case residue in the vesicles may be expected to exhibit differing stages of chemical evolution.

The fact that rotated magnetic inclinations cluster about the expected dipole value (Figure 22) suggests that subsolidus rotation prior to magnetization is not generally a problem. If it were, these inclinations would be randomly distributed. Careful sampling may help avoid complications of rotation or deformation during or shortly after intrusion of the magma residue. Samples taken from the more massive parts of pillows and flows are the last to cool and, therefore, are likely to solidify and pass through the Curie temperature after the flow or pillow stops moving.

Some destruction of the original shape of the magma residue in some segregation vesicles during thin sectioning or by alteration is inevitable. Such vesicles are obvious when viewed in thin section and can be avoided by only measuring vesicles with very distinct and fairly symmetrical linings of residual melt in fairly spherical vesicles.

If there is any doubt about the quality of the data, if tests for preferred orientation are not satisfied, or if the errors in the derived parameters are unreasonably large, the information should not be used for paleomagnetic or structural interpretations.

APPLICATION OF THE SEGREGATION VESICLE TECHNIQUE TO THE
AMAR MAGNETIC POLARITY PROBLEM

INTRODUCTION

Three previous magnetic investigations of the Famous Rift

Valley (Figure 1) revealed reversely magnetized rocks within

the limits of the Brunhes positive central anomaly. Several

reversely magnetized zones appeared in the inversion solution

of a deep-tow magnetometer line which crossed the Narrowgate

study area in the vicinity of line A-A' (MacDonald, 1977) (Fig-

ures 25 and 26). These reversals correspond to surface magne-

tics which show a low in the central anomaly just south of the

deep-tow line (Atwater and others, 1978; and Phillips and others,

1975). Additionally, 22 percent of the rocks recovered from the

Famous Rift Valley floor during the Famous expedition which

could be oriented, have reversed magnetic polarities (Johnson

and Atwater, 1977). Segregation vesicle studies of one of these

reversed rocks (sample number KNR 42-114) suggests, however,

that it may have been oriented upside down with respect to its

cooling position during measurement of its magnetic polarity.

Suggested explanations for these reversals were: 1) rever-

sal due to a self reversing magnetic mineral, 2) sampling of

a young magnetic field reversal within the Brunhes normal mag-

netic epoch, 3) accelerated hydrothermal alteration of titano-

magnetite to titanomaghemite resulting in reverse polarization,

and 4) older crust (>0.69 m.y.) left in the median valley due to

random shifts in the axis of spreading. None of these explana-
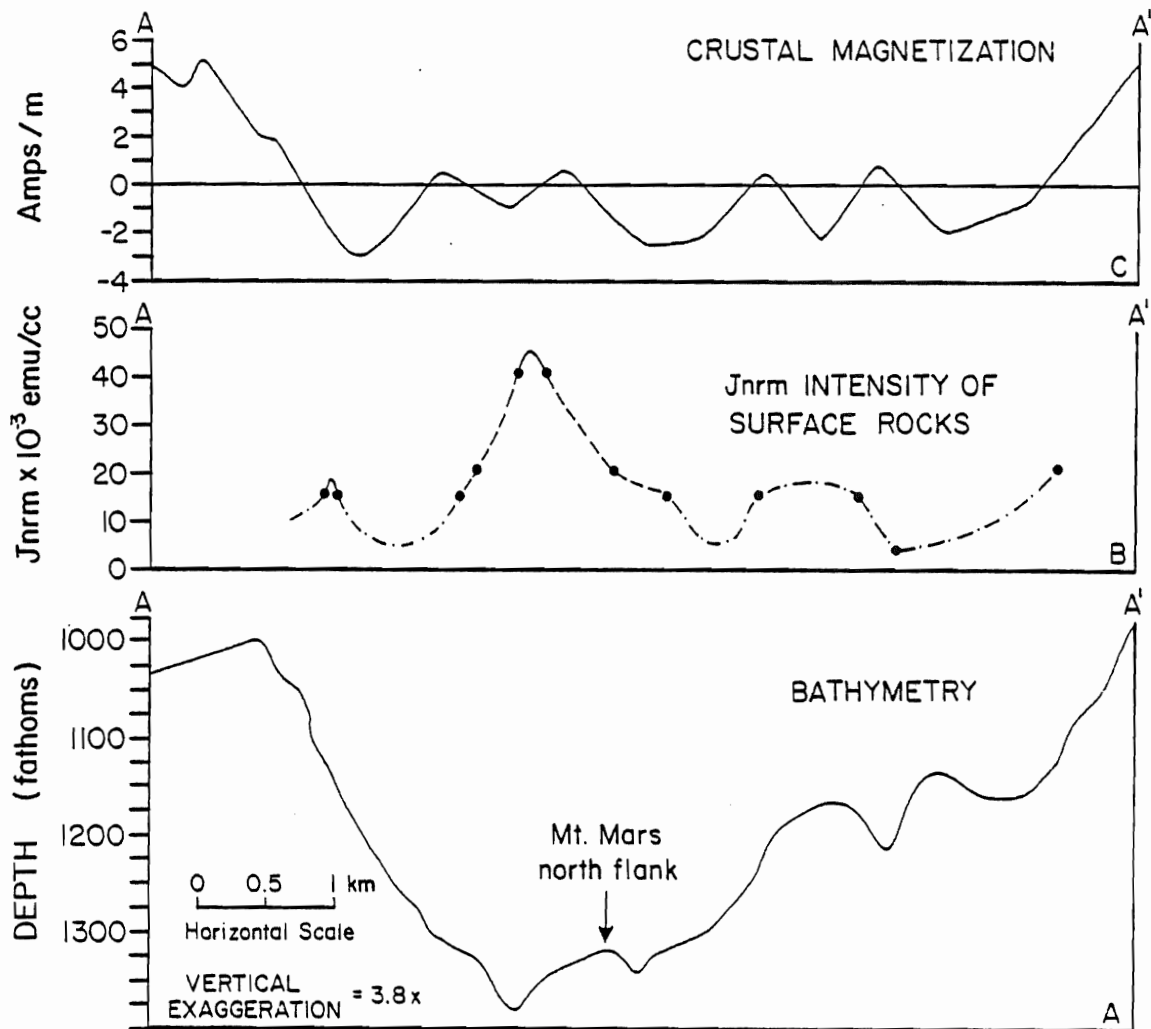
Figure 25. Graphs showing bathymetric (A) and magnetic intensity (B and C) profiles along line A-A' (Figure 25). Profile C shows crustal magnetization based on the solution of deep-tow magnetometer data (after Macdonald, 1977). It shows reversely magnetized zones occurring within the walls of the rift valley. Shown for comparison is a profile of remanent intensity of surface rocks (Figure 27). Solid lines indicated well located data; dashed lines indicate approximately located data; dash-dot lines indicate contours or data points projected onto A-A'.
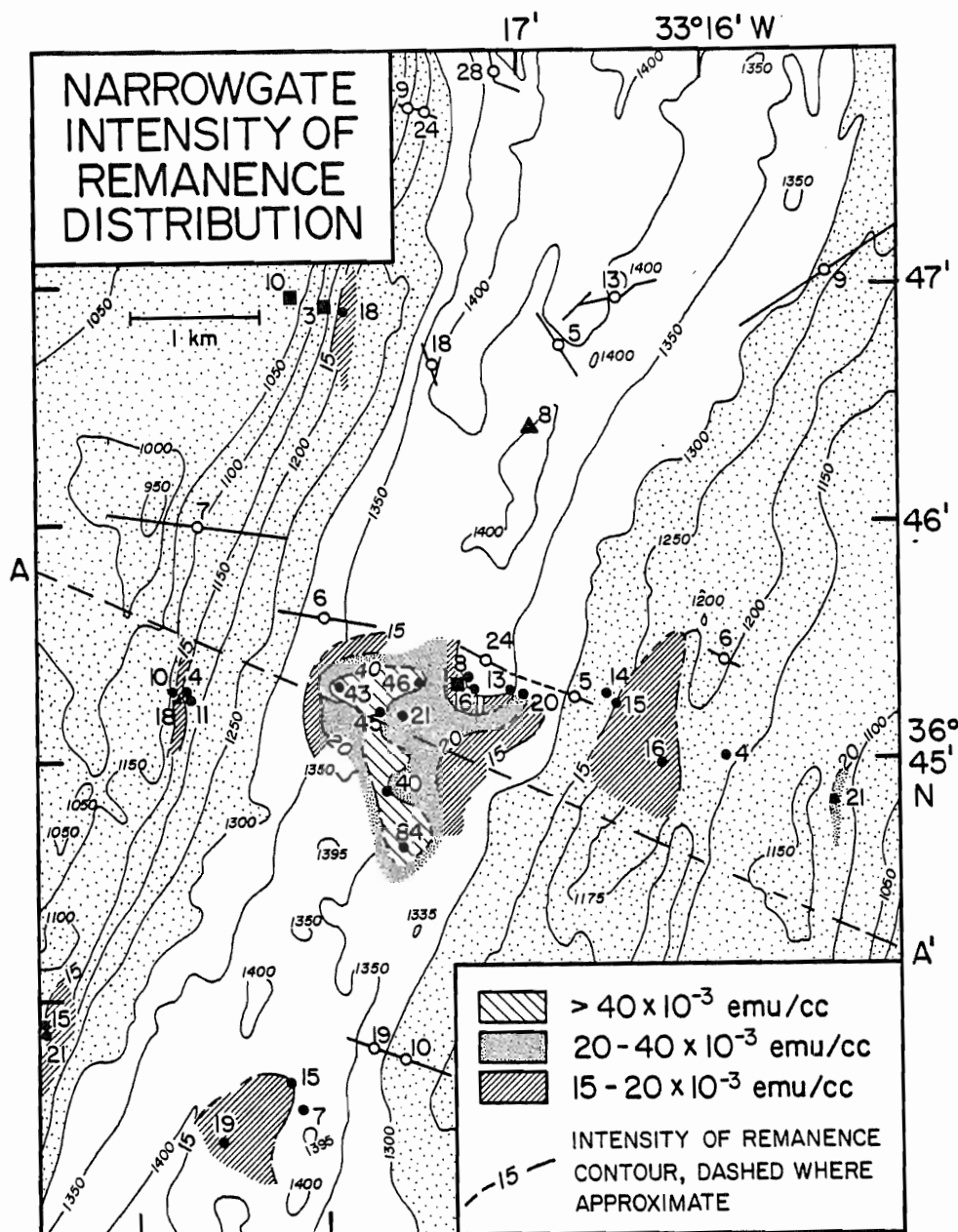
Figure 26. Map showing distribution of remanent intensity (Jnrm) of rocks collected during the AMAR cruise.

tions were considered conclusive (MacDonald, 1977; and Johnson and Atwater, 1977).

The main impetus of the AMAR 1978 Expedition was to examine the origin and extent of this apparently reversely magnetized crust within the Brunhes normal epoch. This investigation was accomplished by a detailed study of the magnetic properties of rocks recovered from the Narrowgate and Amar study areas (Figure 1). Sampling methods and procedures were previously discussed in the introductory chapter.

MAGNETIC POLARITY

The rocks collected during the AMAR cruise were recovered by submersible and dredge. In order to determine their magnetic polarity they had to be reoriented with respect to their cooling position on the sea floor. As previously mentioned, 38 of the samples collected were oriented according to MC-1, 2,or 3 (Figure 11). The segregation vesicle technique was also used to orient 17 of these 38 samples as well as an additional 17 samples which were not oriented by any other criteria. The measured magnetic direction of the latter 17 samples was then rotated with respect to the segregation vesicle orientation according to the procedure described (Figures 16-19).

The locations and magnetic polarities of the oriented samples collected from the study areas are shown on Figures 27 and 28. The bulk, but not all of the samples are normally magnetized. Within the Narrowgate study area 6 of the 36
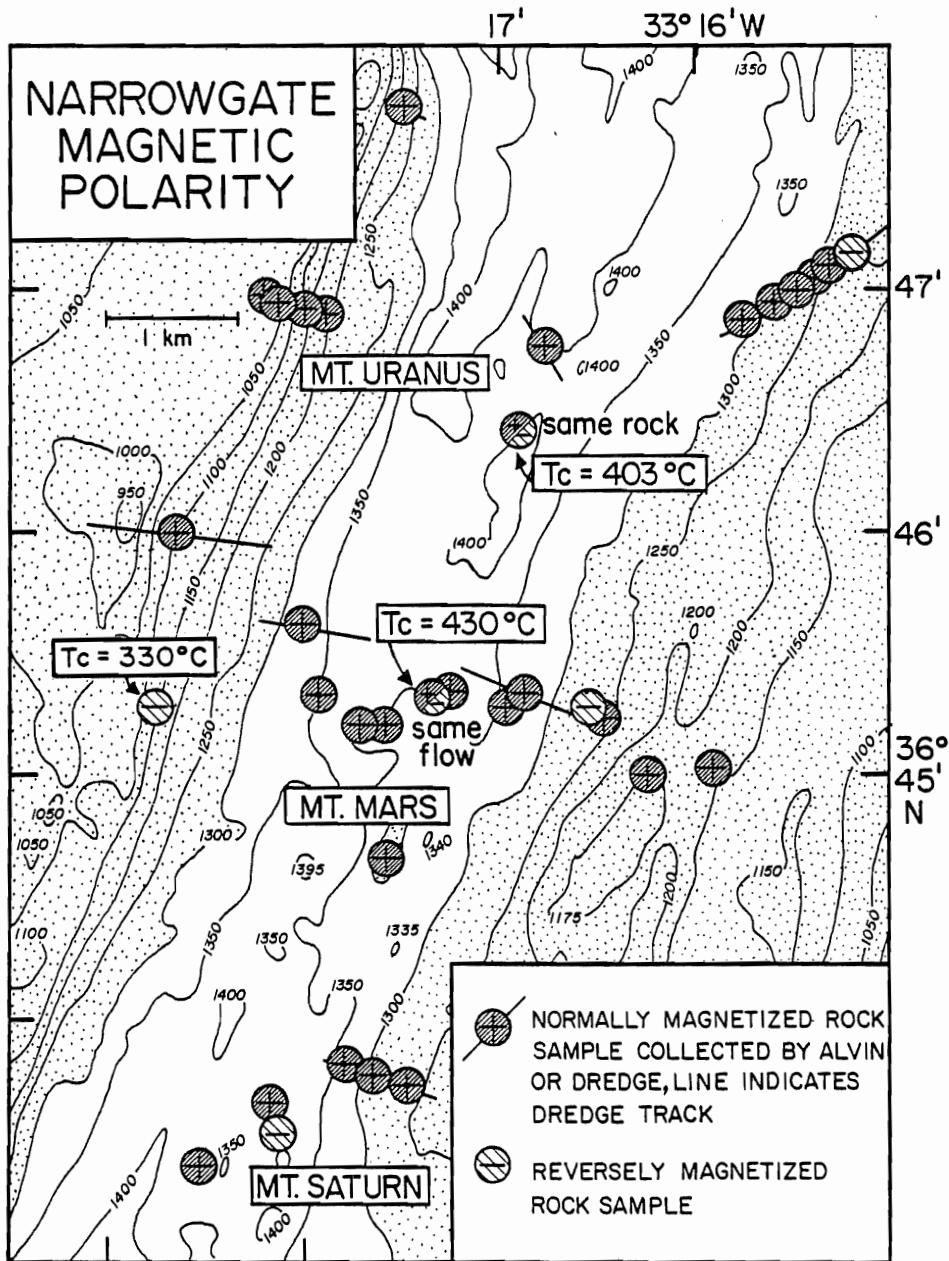
Figure 27. Map showing magnetic polarity of rocks re-
covered from the Narrowgate study area during the AMAR
cruise. In two cases both reversely and normally magne-
tized rocks were recovered from the same pillow of flow.
In these two cases the reversely magnetized rock has the
high Curie temperature indicated. Location of the study
area is shown on Figure 1.
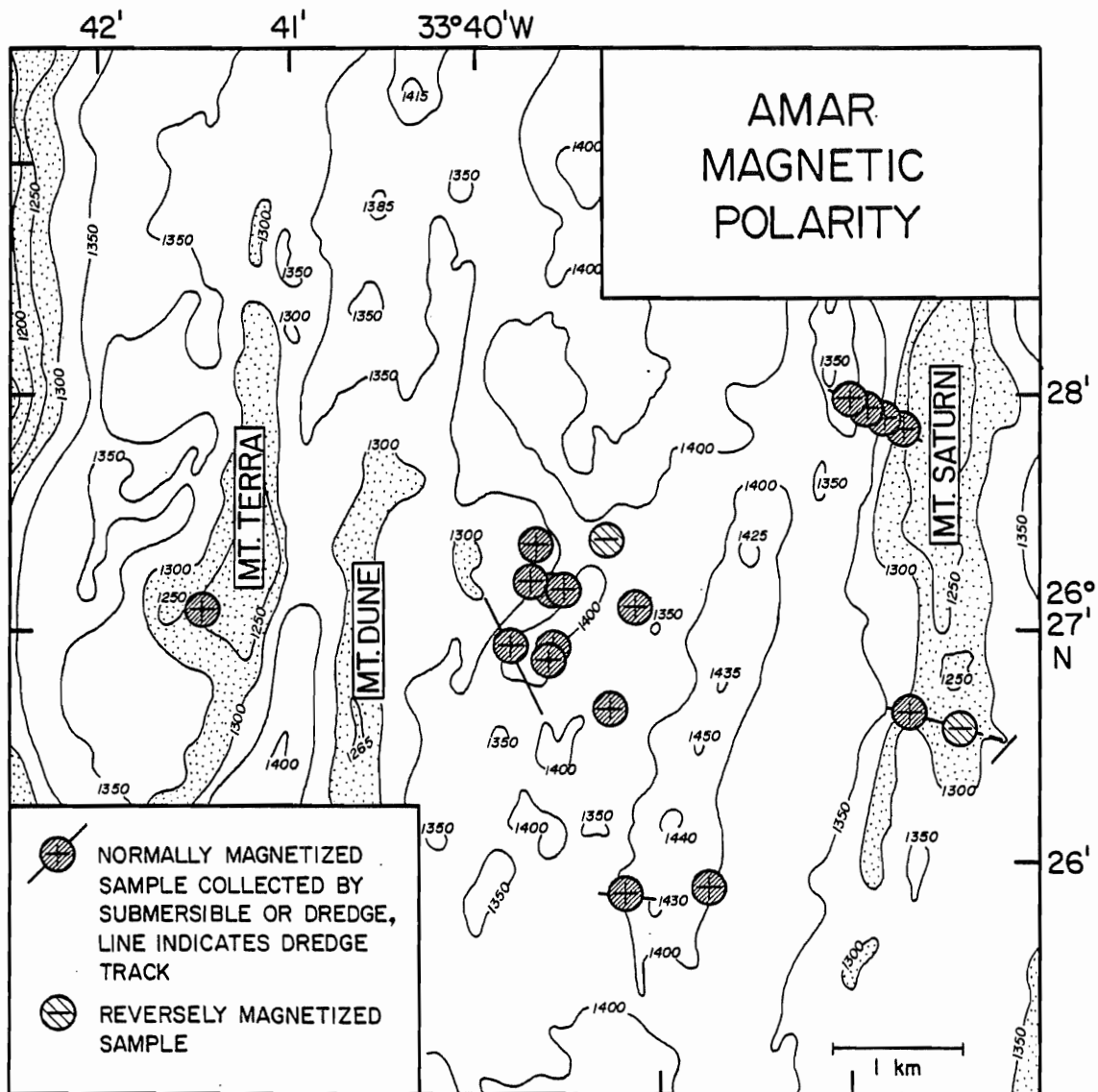
Figure 28. Magnetic polarity of rocks recovered from the Amar study area during the AMAR cruise. Location of study area is shown on Figure 1.

samples, or about 17 percent, are reversely magnetized. Three
are from the valley floor and 3 are from the valley walls.
Within the Amar study area 2 of the 19 oriented samples, or
about 10.5 percent, are reversely magnetized.

Three of the reversely magnetized samples from the Narrow-
gate area have Curie temperatures in excess of 300° C. These
samples are fragments of thin (1-2 cm thick) cooling levels or
sheet flows. The samples from the Mt. Uranus and Mt. Mars
areas (Figure 27) are parts of a pillow or flow from which other,
normally magnetized samples were collected.

The high Curie temperature of these reversed samples indi-
cates oxidation of the original titanomagnetite to titanomaghe-
mite (Ozima and others, 1974; Honnorez and others, 1978; and
Peterson and others, 1979), a process which can lead to self-
reversal of the original direction of magnetization (Verhoogan,
1962; O'Reilly and Banerjee, 1966; Johnson and Merrill, 1973;
and Ryall and Ade-Hall, 1975). If self-reversal occurred, it
must have been very localized, at least in the case of the Mt.
Uranus and Mt. Mars rocks. Although self-reversed rocks are
rarely found (Hall and Ryall, 1977) a similar occurrence of
within-flow opposed magnetic polarities possibly caused by self-
reversal, was recognized in two subaerial flows by Heller (1980)
and Heller and Peterson (1981).

The 5 remaining reversely magnetized rocks have properties
of remanent intensity, Curie temperature, and inclination which
are similar to the normally magnetized rocks (Table 5). Of the

Table 5. The magnetic properties (±1 standard deviation) of normally and reversely magnetized rocks recovered from the Narrowgate and Amar study areas.

	NARROWGATE		AMAR	
	Normal	Reversed	Normal	Reversed
Number of samples	36	3	19	2
Inclination (°)	50.5 ± 17.6	61.6 ± 13.9	43.9 ± 19.4	56.3 ± 6.9
Jnrm (x10^{-3}emu/cc)	14.8 ± 11.5	9.8 ± 3.6	14.3 ± 6.4	16.0 ± 3.5
Tc (°C)	211 ± 37	198 ± 6	228 ± 54	243 ± 9

possible explanations for reversely magnetized rocks previously mentioned, the only explanation compatible with this similarity of magnetic properties is eruption of the reversed rocks during a short reversed event within the Brunhes normal epoch. Twelve different polarity excursions within the Bruhnes epoch, during the last 40,000 years, have been documented, including the Laschamp event which occurred 8,000 to 20,000 years ago (Barendregt, 1981; and Bohommet and Babkine, 1967). Because the rocks within the median valley probably are less than several tens of thousand years old (Bryan and Moore, 1977) any of these recent excursions may have been sampled.

CONCLUSION

The segregation vesicle technique can be used to orient sea floor basalts recovered by dredge or submersible for magnetic polarity studies. This technique was successfully applied to rocks collected during the AMAR expedition and increased the magnetic polarity information available by almost 50 percent.

Although most of the rocks recovered from the study areas are normally magnetized, there are two sets of reversely magnetized rocks. One set is characterized by relatively high Curie temperatures and the rocks were sampled from pillows or flows from which other normally magnetized rocks were also recovered (Figure 27). These characteristics suggest that the reversed magnetizations are the result of self-reversal.

The second set (Table 5) is characterized by magnetic properties equivalent to the normally magnetized rocks. These rocks may have been erupted during a short reversed event within the Brunhes epoch.

APPLICATION OF THE SEGREGATION VESICLE TECHNIQUE TO STRUCTURAL
AND PALEOMAGNETIC STUDIES OF SEA-FLOOR BASALTS RECOVERED BY
DRILL CORES

INTRODUCTION

Probably the most significant application of the segrega-
tion vesicle technique is as a tool for determining the struc-
tural state and pre-deformational magnetic polarity profile of
oceanic basaltic basement rocks recovered in cores. The DSDP
has penetrated a vertical thickness of nearly 600 m into oceanic
basement. Although the petrological, geochemical, geophysical,
and magnetic properties of these cores have been described in
the Initial Reports of the DSDP, without application of the
segregation vesicle technique there has been no way of directly
determining the structural dip of the rocks recovered in these
holes. It has also been impossible to determine how post-de-
positional structural complexities may have altered the original
volcanic stratigraphy or magnetic polarity profile of the rock
units recovered in these holes.

A method of using the segregation vesicle technique to de-
fine dip units, corrected magnetic units, and to construct re-
stored (pre-deformational) profiles is described. The manner
in which lithologic units may be used to help define, or may
relate to dip and magnetic units is also discussed.

For the purpose of demonstrating the general applicability
of the technique, and exemplifying how the technique may be
applied to basement rocks recovered in cores, the technique
is applied to several DSDP cores from the North Atlantic.

Application of the technique for rigorous structural and paleomagnetic studies requires a much closer sample spacing than was possible for this study. However, based on the results presented, some preliminary interpretations are made.

PROCEDURE

The DSDP drill recovers a cored section of rock approximately 6 cm in diameter. These sections vary in length depending upon the cohesive properties of rocks recovered.

Upon recovery the core is split along its length so that one of the split sections may be preserved intact while the other section is sampled for study. Cored pieces that are long enough to preclude the possibility that the piece tumbled about an axis other than the vertical during drilling (that is, greater than 6 cm in length) are marked with orientation arrows indicating the in-place vertical and "up" direction of the drilled piece (Figure 29).

It is crucial that any section of core chosen for application of the segregation vesicle technique be greater than 6 cm in length and unambiguously labeled with such orientation marks. If there is any doubt about the orientation of a sample in the main core barrel or any indication that a section may have been inverted during handling that section of core should not be used for structural studies.

For application of the segregation vesicle technique, 2.5 cm diameter minicore samples are drilled perpendicular to the
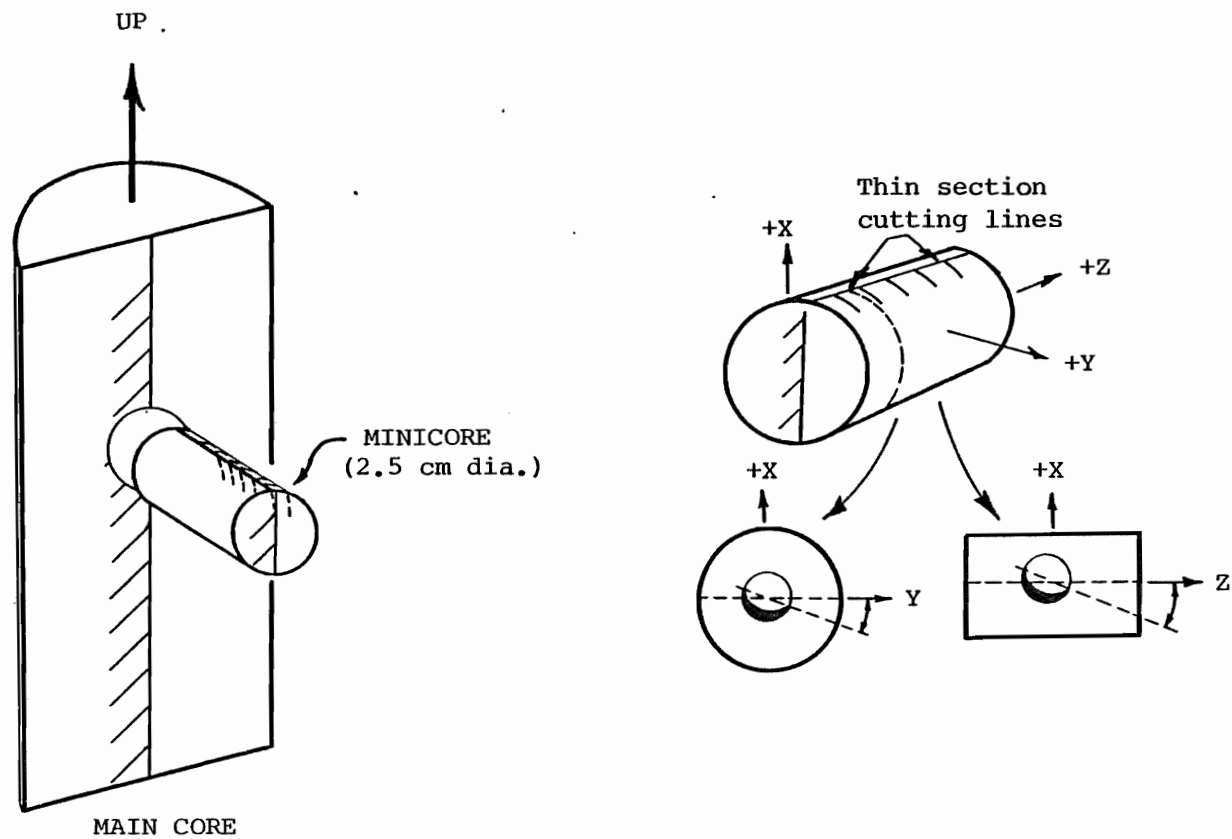
Figure 29. Illustration showing the conventions used for sampling of rocks recovered in DSDP cores and for thin sections used for the segregation vesicle technique.

vertical axis of oriented pieces in the main core. In order to preserve the orientation of the minicores these samples are marked with a line indicating the top of the core and hatchures which extend to the right of this line (Figure 29). The minicore is then labeled with respect to its location in the main core following DSDP conventions (Melson, Rabinowitz and others, 1978a).

In order to standardize the direction in which segregation vesicle and magnetic inclinations are measured (Figures 12 and 14) orientation axes are assigned to each minicore so that +x marks the up direction of the minicore and +y and +z mark the in-place horizontal plane. +y points in the direction of the hatchures at the top of the core and +z points down the core (Figure 29).

Prior to cutting the minicores for thin sectioning, the stable magnetic direction is measured according to the conventions described for horizontally drilled samples (Figure 12) and using the magnetometer and demagnetization unit previously described. The procedure followed for determining the stable magnetic inclination and declination is after Bleil and Smith (1979). This magnetic inclination and declination are referred to as ENC1 and DEC1, respectively. Because drill core samples rotate about a vertical axis during sampling, declination has no geographic significance and is relative only to the orientation axes of the sample. If samples were received from paleomagnetists who previously determined the paleomagnetism of the sample, these samples were rechecked using the

Dalhousie spinner magnetometer to be sure that the reported stable magnetic direction conformed to the conventions used here. Corrections were applied when necessary.

After determining ENC1 and DEC1, two thin sections are made of each rock sample from rock chips cut along two mutually perpendicular planes one containing the xy and the other containing the xz axes (Figure 29). The segregation vesicle inclinations in each thin section are measured according to the conventions illustrated on Figure 14. These measurements are entered into computer program CIRST (Appendix II). The results of CIRST output, along with values of ENC1 and DEC1 for each sample, are then entered in computer program ROTSTAT (Appendix IX) as previously discussed in the section on statistical techniques. The significant outputs of the computations performed by these programs are the dip (D) of the sample, the magnetic inclination. (ENC2) corrected for the dip, and the direction of the dip (AZI) assuming that the horizontal component of ENC2 points toward magnetic north if the rock is normally magnetized, or south if the rock is reversely magnetized, in the northern hemisphere.

By variations of this approach the technique may be applied to basalt samples collected by any drill core regardless of the width of the core barrel. The only requirement is that sections of rock are recovered which preserve the in-place rock sequence and orientation. The technique cannot be applied to drilling projects in which chips are recovered.

DEFINITION OF DIP UNITS

Dip units may be defined by using this technique. In this study these structural units consist of consecutive rock samples which have a similar dip as indicated by segregation vesicles or megascopic geopetal features. Boundaries between dip units are placed where the dips of consecutive samples differ. Because sample spacing usually is great and core recovery is low the division between dip units is somewhat arbitrary. However, structures such as breccia zones or zones of rock containing slickensided surfaces, abrupt changes in lithology such as sediment layers or changes in phenocrysts abundance or composition, or the boundaries of chemical units are used as boundaries for dip units if they occur between two samples having differing dips. If dip changes occur within rock units that apparently are otherwise homogeneous, the contact between dip units is placed at the midpoint between samples of differing dip.

Although this technique may be capable of providing much structural information about the ocean floor, there are several problems to be aware of when interpreting results. It is almost always impossible to know the dip of the rocks between samples. Although dip units can be defined, this problem makes it difficult to distinguish between local structures, such as flow surface rubble, and major structures, such as the dip of a series of rock layers, with certainty. Furthermore, drill cores represent only a narrow window into the vertical structure

of oceanic crust. The lateral extent of any unit defined is unknown. Observations are made only at the outcrop scale, and without the control provided by a series of adjacent holes or detailed surficial mapping, any regional interpretations based on drill core data are speculative.

CORRECTED MAGNETIC UNITS

Corrected magnetic units are defined by consecutive rock samples which have a similar corrected magnetic inclination (ENC2) as determined by the segregation vesicle technique. Magnetic units are divided between samples of differing ENC2. The same problems encountered in defining and interpreting dip units are encountered here. The method for determining the position of a contact between magnetic units is the same as that used for defining dip units.

RESTORED PROFILES

Restored lithologic profiles are constructed by reorienting tilted beds to a horizontal attitude. The true thickness (Tm) measured perpendicular to the dip of each unit is observed in this orientation. The true thickness of lithologic units is given by

$$Tm = (\cos(D))t$$

where t is the maximum vertical or downhole thickness of a lithologic unit and D is the dip of the unit. The value of D used to calculate Tm of a lithologic unit is either the D of a sample

from that unit, the average D of more than one sample from
that unit if the dips are similar, the average D of the rocks
of the structural unit containing the lithologic unit, or the
D of a rock from a nearby unit. If the dips of more than one
sample from the same lithologic unit are different, then the
unit is subdivided and the D included in each subdivision is
used to calculate the Tm of that subdivision.

Because there is an error associated with D, S_D, there is
also an error associated with Tm. To determine this error, Tm
is also calculated using $D = D + S_D$ and $D = D - S_D$. The Tm
calculated using the shallower of the resulting dips will give
the maximum value for Tm and is referred to as Tmax. The Tm
calculated using the steeper of the resulting dips will give a
minimum value and is referred to as Tmin. If D is nearly ver-
tical, addition of S_D may not result in a steeper dip. In
this case the Tmin value recorded is the same as the Tm value.

The total Tm, Tmin, Tmax of the lithologic rock units re-
covered is calculated by a summation of these values for each
unit. Restored magnetic polarity profiles are constructed by
repositioning magnetic units so that they correspond to the re-
stored position of the lithologic units which they contain.
The true thickness of corrected magnetic units is computed
by a summation of the Tm of each lithologic unit contained in
the magnetic unit.

These profiles restore only the dip. They are not neces-
sarily representative of the original lithologic and magnetic

section prior to deformation. Such an interpretation excludes the possibility of repetition or deletion of units due to faulting or other deformation.

THE DIRECTION OF DIP (AZI)

As previously described the azimuth of the trend is computed assuming that DEC2 points toward magnetic north if the sample is normally magnetized and south if the sample is reversely magnetized (eqs. 46 and 47). There are, however, several problems with this assumption.

During deformation, rocks may rotate about a vertical axis, inclined axis or be subjected to multiple phases of deformation resulting in rotation about multiply oriented axes. Reorientation of the rocks, according to the method used here, however, assumes that dips are the result of simple, single-stage rotation about a horizontal axis. Reorientation of the rocks, according to this method will restore the magnetic inclination back to the angular value it had prior to tilting. But, if rotation occurred about a non-horizontal axis, the restored declination cannot be used as an indicator of the direction of magnetic north with respect to the dip of the rock. This problem is thoroughly discussed by MacDonald (1980).

As an example of this problem, consider the case where a horizontal layer of rock which is magnetized according to an axially centered geomagnetic dipole, is deformed in two stages. The first rotation is a 15° counter-clockwise rotation about

a vertical axis and the second stage is a 45° tilt to the west about a horizontal axis. The in-place dip direction of the rocks is 290°. Reorientation of the rocks according to the method used here, however, will give a dip direction (AZI) of 315°.

Additionally, paleosecular variation has resulted in angular dispersions of the virtual geomagnetic dipole ranging from about 13° to 0° latitude to 20° at 90° latitude over the past 5 m.y. (McElhinny and Merrill, 1975). Thus, even if the assumption of single-stage rotation about a horizontal axis is correct, there is a question about how good a single magnetic measurement is as an indicator of magnetic north. Due to secular variation alone the in-place declination of any sample may not only deviate from the average position of the present day magnetic north, but the measured declinations between samples may also be expected to vary. According to the method of determining AZI used here such deviations would result in a small apparent change in the direction of dip. This problem of determining absolute dip direction may be compounded if there has been a significant northward component of motion of the crust during formation of the volcanic pile.

Finally, the statistical error associated with AZI (S_A) commonly is large for several reasons. Obviously, S_A will be expected to be large if there is a large amount of scatter to the measured segregation vesicle inclinations. If the restored inclination (ENC2) is steep then small errors in the

segregation vesicle orientation of the rock will result in large errors in the restored declination which is used to calculate AZI. S_A may also be large if the dip of the rock is shallow because as the dip approaches $0°$ the direction of the dip becomes more poorly defined.

Due to these problems, it is difficult to make definite interpretations regarding the direction of the dip of rock units. Consistency of AZI values of rock units, however, may indicate that the units were deformed together about the same axis of rotation.

THE GEOLOGIC STRUCTURE AND PALEOMAGNETISM OF EXTRUSIVE BASALTIC ROCKS RECOVERED DURING LEGS 37, 45, AND 46 OF THE DEEP SEA DRILLING PROJECT

Geological and Geophysical Setting of Leg 37

The segregation vesicle technique was applied to some rocks recovered from Holes 332A, 332B, and 334 which were drilled during Leg 37 of the DSDP. These holes were drilled about 30 and 100 km to the west of the Mid-Atlantic Ridge (332 and 334, respectively) at about $37°$ N latitude (Aumento, Melson and others, 1977a and c)(Figure 2).

The interpretation of sea-surface magnetic anomaly profiles across site 332 indicated that this hole was drilled into the eastern side of a negative anomaly which is part of the Gilbert reverse polarity epoch between positive anomalies 2' and 3 (Ade-Hall, Aumento and others, 1976). The age assigned to this

anomaly is about 3.2 to 3.8 m.y. (Talwani and others, 1971).

Assuming a uniform spreading rate the estimated age of the crust responsible for this anomaly at site 332 was calculated to be 3.5 $\pm$ 0.1 m.y. (Aumento, Melson and others, 1977a). A near bottom geophysical survey using a deeply towed instrument package, however, indicated that the sea surface anomaly pattern is misleading because it fails to account for an eastward phase shift of the observed anomaly, with respect to the source, due to the strike of the ridge. Solutions of deep tow magnetometer data indicated that Hole 332 penetrated the broad (4 km wide) transition zone between the Gauss and Gilbert epochs (MacDonald, 1976). The age assigned to this transition zone is about 3.2 m.y. (Talwani and others, 1971). Interpretations of an additional near-bottom magnetometer survey (Greenewalt and Taylor, 1978) indicated that the hole was situated in a transition zone in the Gibert reversed epoch following the Cochiti normal event, giving a slightly older age (+0.38 m.y.) to the crust at this site, according to McElhinny (1973).

Based on these data, and assuming that a uniformly magnetized layer located within the upper oceanic basement crust is the source of the surface magnetic anomaly (Vine and Matthews, 1963; Atwater and Mudie, 1973; and Talwani and others, 1971), the basement rocks recovered were expected to either be reversely magnetized with inclinations consistent with the dipole field inclination (56°) (Ade-Hall, Aumento and others, 1976) or have unpredictable inclinations since the behaviour

of the earth's magnetic field during a reversal is unknown
(MacDonald, 1976).

Paleontological age dating indicates that the oldest sediment cored at site 332 is 3.2 $\pm$ 0.6 m.y. (Miles and Howe, 1977). This age is consistent with the basement age given by fission track dating of 3.6 $\pm$ 0.4 m.y. (Mitchell and Aumento, 1977) and the paleomagnetic age assuming either the interpretation of Ade-Hall and others, (1975); MacDonald, (1976), Aumento, Melson and others, (1977), or Greenwalt and Taylor, (1978).

The sea-surface magnetic anomaly profile in the vicinity of site 334 indicated that the hole penetrated crust magnetized during positive anomaly 5. Talwani and others (1971) assigned an age interval from 8.71 to 9.94 m.y. to this anomaly. Blakely (1974) however, proposed that the anomaly 5 interval began earlier, at 10.21 m.y. Assuming a uniform spreading rate the age for the magnetic source at Hole 334 was calculated to be 8.9 m.y. (Aumento, Melson and others, 1977c). The basement rocks recovered were therefore, expected to have magnetic inclinations around $+56^{\circ}$ (the normal dipole field inclination).

Paleontological age dating indicates that the oldest sediment cored at site 334 is 9.8 + 2.0/-1.8 m.y. (Miles and Howe, 1977). This age is older than both the calculated age at this site assuming a uniform spreading rate (Aumento, Melson and others, 1977c) and the age interval assigned to anomaly 5 by Talwani and others (1971). It is, however, within the age

bounds of anomaly 5 proposed by Blakely (1974).

Hole 332A

Introduction

Hole 332A penetrated 330.5 m of basaltic basement rocks with an average recovery of ten percent. The rocks recovered were divided into 7 major lithologic units and 48 subunits identified on the basis of phenocryst composition and the presence of glassy rinds, or changes in grain size, respectively. Because of the poor recovery the boundaries of rock units are somewhat arbitrary. The hole was interpreted as consisting primarily of pillow basalts interlayered with basalt breccia, rubble, and sedimentary rocks (Figure 30). The pillows primarily are aphyric to moderately plagioclase - and sparsely olivine - phyric basalts. Massive flows, sheet flows, and intrusive rocks may also have been recovered (Aumento, Melson and others 1977a).

The basaltic rocks were divided into magma groups on the basis of major element geochemistry. Magma groups 1 and 2 are interlayered with group 6 and group 3 is interlayered with group 4 (Figure 30). This relationship was interpreted to suggest coeval eruption from separate magma chambers (Flower and others, 1977).

Seven magnetic superunits were defined on the basis of the in-place magnetic inclination of the basement rocks. These measured in-place inclinations indicate that the upper part of

Figure 30 (following pages). DSDP Hole 332A core log.
A) Shows the lithologic units, subunits, and lithology of
each subunit as identified by Aumento and others (1977b).
An explanation of symbols is on Figure 31. The dip of the
rocks of each subunit interpreted from segregation vesicle
studies is schematically represented. B) Illustrates the
distribution of magma groups. Data are from Flower and
others (1977). C) Illustrates the in-place magnetic units
and superunits. Open boxes and solid lines are centered
over the average magnetic inclination of the rocks included
in each unit with the width of the box indicating the stan-
dard deviation. The average inclination of superunits is
indicated by dashed lines with horizontal bars indicating
the standard deviation. Circles with numbers indicate the
in-place inclination and sample number of the samples
studied. Dashed vertical line indicates the dipole inclin-
ation. Data are from Hall and Ryall (1977) and Table 6.
D) Shows the dip and 95 percent confidence interval of the
dip of each sample, the dip of the dip units defined, and
the dip of the megascopic geopetal features. Data are
from Table 6. E) Shows the corrected magnetic units.
Dashed vertical line indicates the dipole inclination.
Horizontal bars in D and E indicate the 95 percent confi-
dence interval of each determination.

148
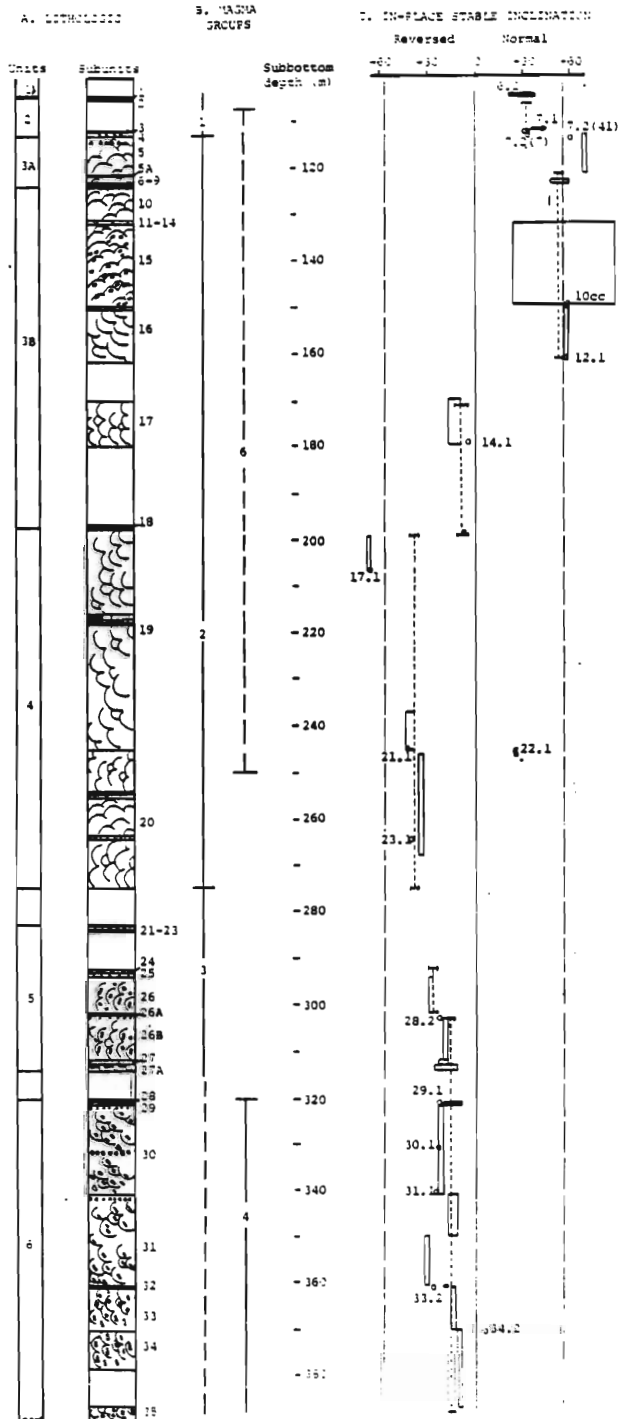
332A CORE LOG

332A CORE LOG

Figure 30. Continued.

Aphyric basalt

Possible intrusive
unit

Plagioclase-phyric
basalt

Gabbro

Olivine-phyric
basalt

Serpentinized
peridotite

Pyroxene-phyric
basalt

Intrusive breccia
clast

Massive or sheet
flow basalt

Breccia

Pillow basalts,
convex upward

Rubble

Diabase

Basaltic sand
and gravel

Limestone, chalk
or ooze
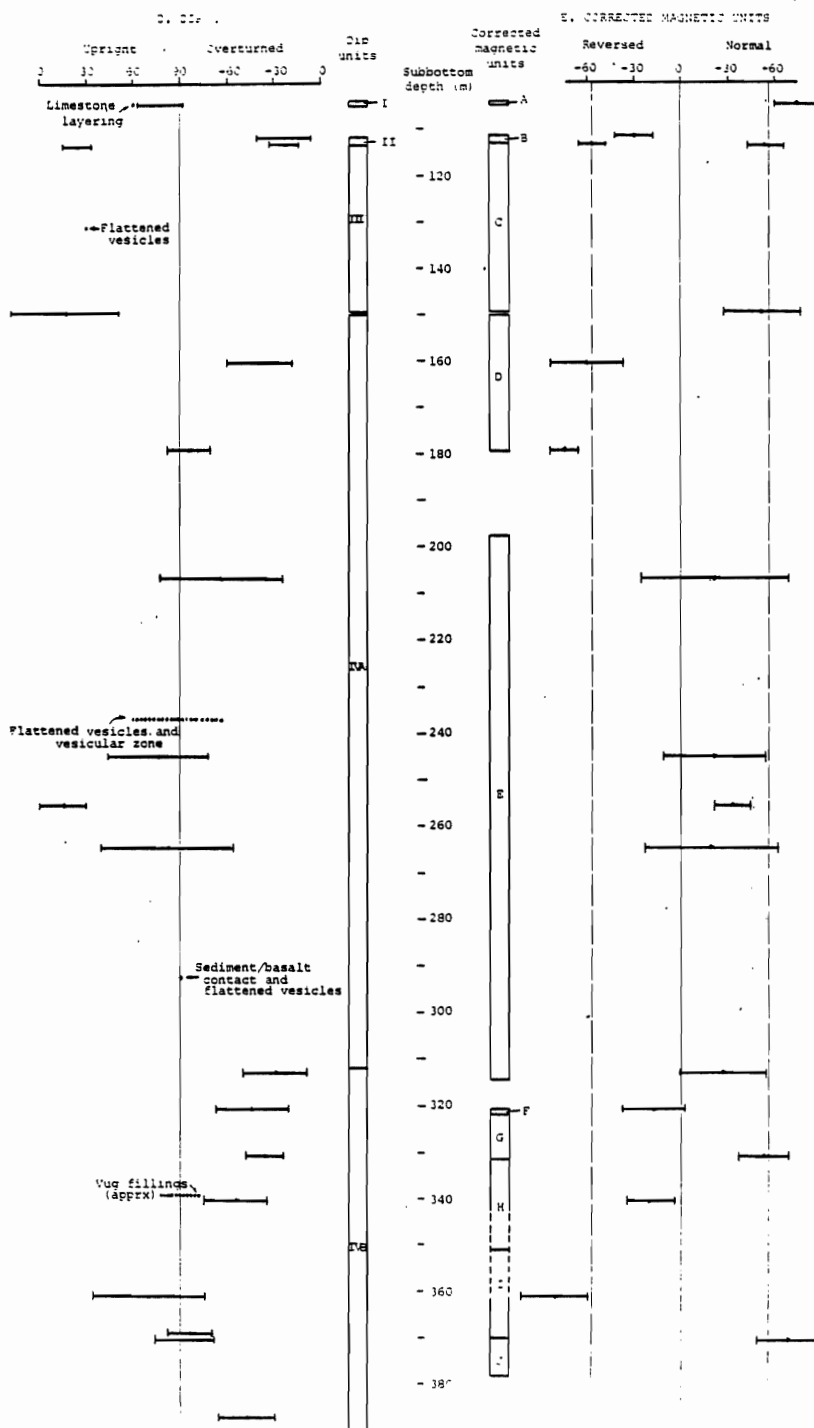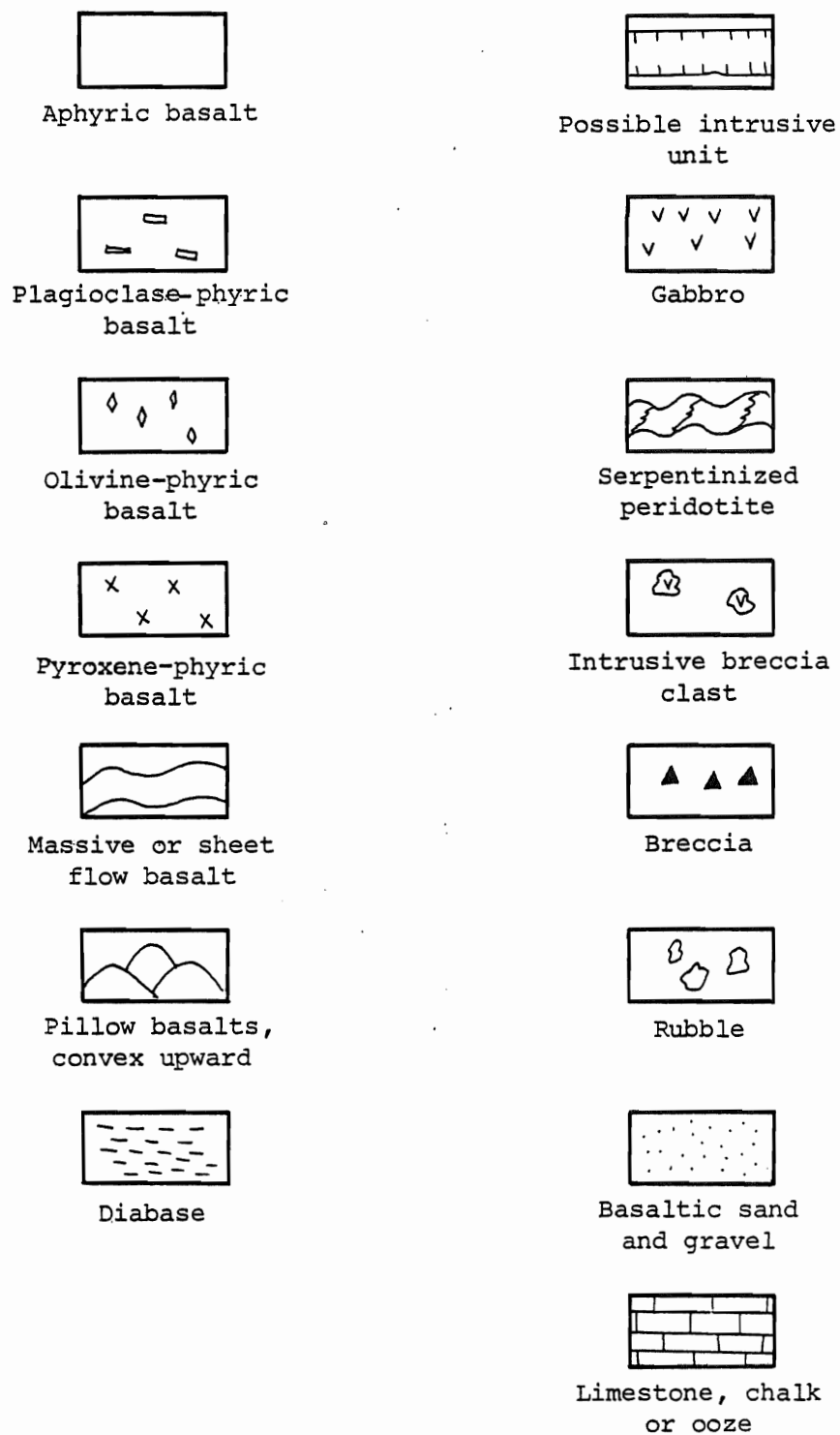
Figure 31. Explanation of symbols used on Figures 30, 33,
35, 37, and 40.

the hole is normally magnetized with shallow to dipolar inclinations. This is followed by a reversely magnetized section with shallow inclinations (Figure 30) (Hall and Ryall, 1977).

Segregation Vesicle Studies

Nineteen of the 46 samples collected from Hole 332A have segregation vesicles of sufficient quality and abundance to orient the rocks. These 19 samples represent the cored interval from about 104 m subbottom, at the sediment/basalt interface, to 390 m subbottom. The lithologic units, magma groups and in-place magnetic units included in this section of core are illustrated on Figure 30. The sample location and measured in-place magnetic inclination of each sample is on Figure 30 and Table 6.

Dip Units

Studies of segregation vesicle inclinations of these 19 samples indicate that Hole 332A penetrated a structurally complex section of basement rocks. The dip (D) and 95 percent confidence interval of the dip (S_D) of each sample is listed on Table 6 and illustrated on Figure 30.

Megascopic geopetal features clearly indicative of the cooling position of the rocks are rare in the core. Where they occur they usually are slightly ambiguous in their interpretation, but are used to help define dip units. The

Table 6. Structural and paleomagnetic data resulting from segregation vesicle studies of basalts from DSDP hole 332A. Abbreviations are from the text. ENC1 values are from Aumento and others (1977a).

Sample number	Subbottom depth (m)	$D(°)$	$S_D(°)$	ENC1 (°)	ENC2 (°)	$S_E(°)$	$AZI(°)$	$S_A(°)$
6.2 (92-94)	104.42	+77	14	+29.7	+74	14	1	17
7.1 (8-11)	111.58	-23	18	+43.3	-30	13	49	29
7.2 (7-10)	113.07	-23	9	+34.9	-57	9	10	35
7.2 (41-44)	113.41	+24	10	+61.5	+55	11	56	19
10cc (78-81)	149.48	+17	34	+59.3	+52	25	54	69
12.1 (122-125)	160.22	-39	21	+58.3	-61	23	56	32
14.1 (123-126)	179.23	-84	14	-5.2	-75	10	138	35
17.1 (14-17)	206.64	-64	40	-67.3	+21	49	24	13
21.1 (57-60)	245.07	+76	33	-43.9	+21	32	149	3
22.1 (141-144)	255.41	+15	15	+24.9	+33	13	122	48
23.1 (106-109)	264.56	+82	42	-41.1	+19	43	221	50
28.2 (61-64)	313.11	-29	20	-22.8	+27	28	268	61
29.1 (33-36)	320.83	-44	23	-22.8	-18	20	156	35
30.1 (104-107)	331.04	-36	13	-24.2	+53	16	131	38
31.1 (95-98)	340.45	-55	20	-24.9	-20	16	143	26
33.2 (128-131)	361.28	+69	37	-27.3	-82	22	35	360
34.1 (113-116)	369.13	-84	17					
34.2 (136-139)	370.54	-88	19	+6.0	+68	22	248	29
36.1 (67-70)	387.67	-48	18					

locations and descriptions of these features are shown on
Figure 30.

Based on these data, the interval of core studied is
divided into dip units for the purpose of constructing re-
stored profiles. The boundaries of these units along with a
schematic representation of the dip of each lithologic unit
is shown on Figure 30.

Dip unit I is defined by both segregation vesicle data
and megascopic geopetal features. Segregation vesicles from
sample 6.2 indicate a dip of 77° upright. Laminae in an
overlying limestone indicate a dip of about 60°. Dip unit
I is defined as containing lithologic subunits 1 and 2.
Segregation vesicles and megascopic orientation features
are from subunit 2. Subunit 1 is also included in this dip
unit because of its proximity to the oriented samples. The
upper contact of this structural unit is placed at the sedi-
ment/basaltic basement interface at the top of lithologic
subunit 1. The lower contact is placed at the base of litho-
logic subunit 2. Below this unit no rocks were recovered for
an approximately 6.5 m interval. The rocks below this inter-
val differ in dip.

Dip unit II is defined by samples 7.1 (8-11) and 7.2
(7-10) which are shallowly dipping and overturned. These sam-
ples are from lithologic subunits 3 and 5, respectively. Dip
unit II is interpreted as including all of subunit 3, the
intervening subunit 4 which is lithogically similar to 3,

and the upper part of subunit 5. The lower limit of this unit is placed at 103.4 m where a calcite cemented basalt breccia occurs. Rocks below this breccia differ in dip.

Dip unit III is defined by samples 7.2 (41-44) and 10cc (78-81) which have similar, shallow and upright dips. Between these two samples, at about 131 m, flattened vesicles suggest a similar dip of about 30°. The flow units of this interval are separated by glassy margins. Vesicle size decreases from about 2 to 0.5 mm downward away from these margins, suggesting along with the segregation vesicle data, that the units are upright.

This dip unit is interpreted to contain lithologic subunit 5, beginning at the base of the welded breccia, and lithologic subunit 15 from which the minicores were sampled as well as the intervening lithologic units. Segregation vesicles indicate that the underlying rock unit has a differing dip.

Below dip unit III segregation vesicles indicate that the rocks are gently to steeply dipping and primarily overturned. Dip unit IV, characterized by this variable assortment of dips, is defined by samples 12.1 (122-125) to 36.1 (67-70) (Table 6). This unit is divided into subunits IVA and IVB. With the exception of samples 22.1 (141-144) and 36.1 (67-70), these subunits are characterized by an increasing dip with increasing depth.

Subunit IVA is defined by samples 12.1 (122-125) to
23.1 (106-109) which were taken from lithologic subunits
16, 17, 19,and 20. The orientation of flattened vesicles
and a basalt/sediment contact within subunit 24 indicate
a nearly vertical dip similar to that of sample 23.1 (106-
109). Subunit IVA is,therefore, interpreted as containing
lithologic subunits 16, 17, 19,and 24 as well as the inter-
vening lithologic subunits. Although no samples from litho-
logic subunits 25 to 26B were available they are included
with this dip unit because they are lithologically similar
to subunit 24. Segregation vesicles of a sample from subunit
27A indicate a differing dip. The lower limit of IVA is,
therefore, interpreted to be at the base of lithologic sub-
unit 26B, where a change in lithology occurs.

Subunit IVB is defined by samples 28.2 (61-64) to 36.1
(67-70) which were taken from lithologic subunits 27A, 29,
30, 33, 34,and 35. The orientation of secondary material
which partly fills vugs at 340.05 m (Figure 30) substan-
tiates the dip given by segregation vesicles. Unit IVB
is interpreted as containing the lithologic subunits from
which the samples were taken as well as the intervening
rocks.

Corrected Magnetic Units

Segregation vesicle studies indicate that the rocks re-
covered in Hole 332A are dipping, resulting in a reorientation

of the magnetic direction acquired by the rocks upon cooling.
By correcting for the dip of the rocks according to the ro-
tation method described (Figures 17, 18,and 19) the corrected
magnetic direction (ENC2) of the rock samples studied was
determined (Table 6). The core interval studied is divided
into 10 corrected magnetic polarity units (Figure 30 and Table
7) on the basis of these corrected magnetic directions which
are different from the in-place record.

Magnetic unit A is defined by sample 6.2 (92-94). The
corrected inclination indicates that this sample originally
was normally magnetized with an inclination close to the
dipole value. Unit A is interpreted as containing lithologic
subunits 1 and 2 which are lithologically similar and also
correspond to dip unit I.

Magnetic unit B is defined by samples 7.1 (8-11) and
7.2 (7-10). Corrected inclinations indicate that both of
these samples originally had reversed polarities with inclin-
ations close to the dipole value. This magnetic unit is in-
terpreted to contain lithologic subunits 3, 4,and the upper
part of 5. The lower limit is placed at the breccia zone
of subunit 5. The sample taken below this zone has an op-
posing corrected polarity. This boundary corresponds to the
lower boundary of dip unit II.

Magnetic unit C is defined by samples 7.2 (41-44) and
10cc (78-81). Corrected inclinations indicate that both these
samples originally were normally magnetized with inclinations

Table 7. Corrected magnetic units of DSDP hole 332A. Sample numbers and dips are from Table 6. Lithologic units are from Figure 30. Abbreviations are from the text.

Corrected magnetic unit	Samples included	Lithologic subunits included	Average ENC2 ($^\circ$)	Average S_E ($^\circ$)	t (m)	Tm (m)
A	6.2	1, 2	+74	14	3.80	0.85
B	7.2, 7.2(7)	3, 4, 5U	−44	11	5.60	5.15
C	7.2(41), 10cc	5L−15	+54	18	36.10	33.93
D	12.1, 14.1	16, 17	−68	16	38.57	14.79
E	17.1, 21.1, 22.1 23.1, 28.2	18−27A	+24	33	129.53	49.42
F	29.1	28, 29	−18	20	3.92	2.82
G	30.1	30U	+53	16	10.00	7.93
H	31.1	30L−32	−20	16	29.53	19.32
I	33.2	33	−82	22	9.35	2.26
J	34.2	34	+68	22	12.60	0.44

close to the dipole value. Unit C is interpreted to include lithologic subunits 5 and 15, from which the samples were taken, as well as the intervening subunits. This magnetic unit corresponds to dip unit III.

Magnetic unit D is defined by samples 12.1 (122-125) and 14.1 (123-126) both of which have corrected inclinations that are reversed and near the dipolar value. Unit D is interpreted to contain lithologic subunits 16 and 17 from which these samples were taken.

Magnetic unit E is defined by samples 17.1 (14-17) to 28.2 (61-64). Corrected magnetic inclinations indicate that all these rocks were normally magnetized with shallow inclinations. The unit is interpreted to contain lithologic subunits 19, 20, and 27A from which the samples were taken as well as the intervening subunits. Subunit 18 is also included in Unit E because of its lithologic similarity to subunit 19 and because of its proximity to sample 17.1 which was taken from subunit 19.

Magnetic unit F is defined by sample 29.1 (33-36) which has a corrected inclination that is reversed and shallow. This unit is interpreted to contain lithologic subunit 29, from which the sample was taken down to the top of the basalt breccia zone at the top of subunit 30, as well as subunit 28. Subunit 28 is also included because of its proximity to sample 29.1 and its lithologic similarity to subunit 29.

Magnetic unit G is defined by sample 30.1 (104-107) which,

when the dip correction is applied, is normally magnetized with a dipolar inclination. This unit is interpreted to include the upper part of lithologic subunit 30 from which the sample was taken. It extends to the base of a zone of basalt rubble. The sample below this zone has an opposing polarity.

Magnetic unit H is defined by sample 31.1 (95-95) which has a reversely magnetized and shallow corrected inclination. This magnetic unit is interpreted to contain the lower part of lithologic subunit 30 from which the sample was taken as well as subunits 31 and 32, which are also included with unit H because they are lithologically similar to 30. A sample from subunit 33, which is lithologically distinct from the above units, has a differing corrected inclination.

Magnetic unit I is defined by sample 33.2 (128-131) which has a reversed and dipolar corrected inclination. This magnetic unit is interpreted to contain lithologic subunit 33 from which the sample was taken.

Magnetic unit J is defined by sample 36.1 (67-70) which is normally magnetized with a dipolar inclination according to the corrected value. Unit J is interpreted to include lithologic subunit 34 from which the sample was taken.

Restored Profiles

The 19 samples studied represent a vertical thickness of about 286 m. Segregation vesicle studies, however, suggest

that these rocks are tilted. Therefore, the vertical thick-
ness of rock units penetrated may be greater than the true
thickness (Tm) of each rock unit. The Tm, Tmin, and Tmax of
each lithologic subunit along with the dip used to calculate
each thickness is listed on Table 8. The Tm of lithologic
units, subunits and magma groups is shown on Figure 32. These
data suggest that a true thickness of only about 142 m of rock
units was penetrated. As in the vertical section, the thick-
ness of aphyric rock units exceeds that of phyric units.

The true thickness of magnetic units, based on the true
thickness of corresponding lithologic units is listed on
Table 7 and illustrated on Figure 32. These data suggest
that normally magnetized units have a true thickness greater
than twice that of reversely magnetized units.

Hole 332B

Introduction

Hole 332B penetrated 583 m into basaltic basement with an
average recovery of 21 percent. The rocks recovered were divided
into 11 major lithologic units and 45 subunits on the basis of
phenocryst composition and the presence of glassy rinds, or
changes in grain size, respectively. The core was described
as consisting primarily of layers of pillow basalt with minor
intercalations of brecciated basalt, sedimentary, and possibly
intrusive rock units. Subunit 7 consists almost entirely of
diabasic rocks of probable intrusive origin. Such rocks are

Table 8. The vertical thickness and true thickness of lithologic subunits of DSDP hole 332A. Sample numbers and dips are from Table 6. Lithologic subunits and lithologic thicknesses are from Figure 30. Abbreviations are from the text.

Lithologic subunit	Vertical t(m)	D(°)	Dmin (°)	Dmax (°)	Tm (m)	Tmin (m)	Tmax (m)	Source of D sample number(s)
1	0.20	77	63	89	0.04	0.003	0.09	6.2
2	3.60	"	"	"	0.81	0.063	1.63	"
3	3.81	23	9	36	3.51	3.08	3.76	7.1, 7.2(7)
4	0.97	"	"	"	0.89	0.78	0.96	"
5U	0.82	"	"	"	0.75	0.66	0.81	"
5L	7.67	20	14	42	7.21	5.70	7.44	7.2(41), 10cc
5A	0.18	"	"	"	0.17	0.13	0.17	"
6	1.46	"	"	"	1.37	1.08	1.42	"
7	0.40	"	"	"	0.38	0.30	0.39	"
8	0.39	"	"	"	0.37	0.29	0.38	"
9	0.19	"	"	"	0.18	0.14	0.18	"
10	7.09	"	"	"	6.66	5.27	6.87	"
11	0.16	"	"	"	0.15	0.12	0.15	"
12	0.21	"	"	"	0.20	0.16	0.20	"
13	0.14	"	"	"	0.13	0.10	0.14	"
14	0.16	"	"	"	0.15	0.12	0.16	"
15	18.05	"	"	"	16.96	13.41	17.51	"
16	16.00	39	18	61	12.43	7.76	15.27	12.1
17	22.57	84	70	--	2.36	2.36	7.72	14.1
18	9.08	64	44	"	3.98	3.98	6.53	17.1
19	47.52	"	"	"	20.83	20.83	34.18	"
20U,L	20.63	79	43	--	3.94	3.94	15.09	21.1, 23.1
20M	9.00	15	0	30	8.69	7.79	9.00	22.1
21	8.98	79	43	--	1.71	1.71	6.57	21.1, 23.1
22	0.29	"	"	"	0.06	0.06	0.21	"
23	4.43	"	"	"	0.84	0.84	3.24	"
24	4.77	"	"	"	0.91	0.91	3.24	"
25	0.96	"	"	"	0.18	0.18	0.70	"
26A,B	18.41	"	"	"	3.51	3.51	13.46	"
27,A	5.46	29	9	49	4.77	3.58	5.39	28.2
28	3.13	44	21	77	2.25	0.70	2.92	29.1
29	0.79	"	"	"	0.57	0.18	0.74	"
30	19.60	36	23	49	15.86	12.86	18.04	30.1
31	19.78	55	35	75	11.35	5.12	16.20	31.1
32	0.15	76	49	--	0.04	0.04	0.53	33.2, 34.1
33	9.35	"	"	"	2.26	2.26	6.13	"
34	12.6	88	69	--	0.44	0.44	4.52	34.2
35	7.00*	48	30	66	4.68	2.85	6.06	36.1

　　　　TOTAL t = 286　　　　　　　TOTAL Tm= 141.59

*To 390 m
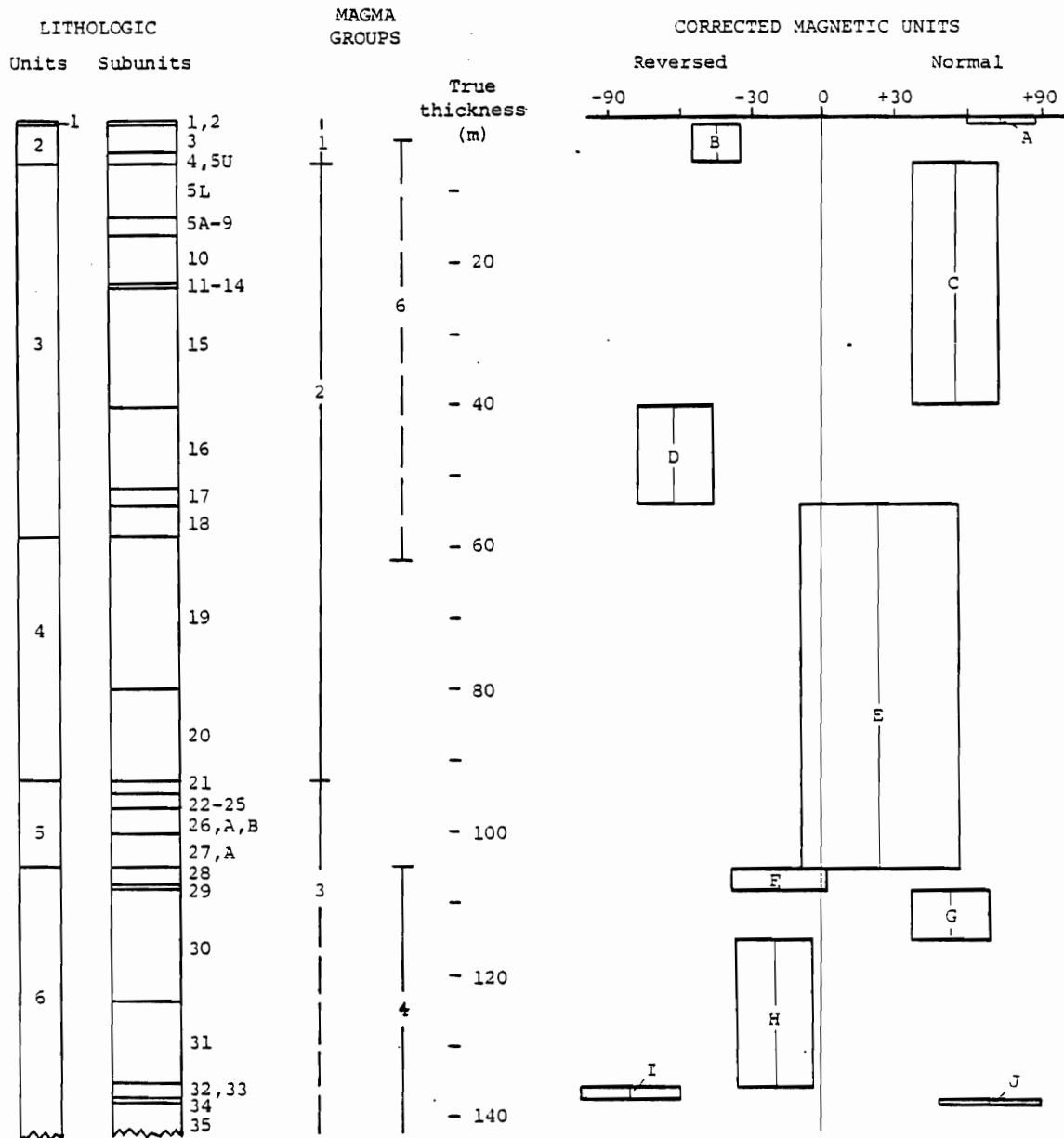
Figure 32. Restored profiles showing the true thickness of lithologic units and subunits, magma groups, and corrected magnetic units shown on Figure 30. Data are from Tables 7 and 8. Open boxes, A-J, are centered over the corrected magnetic inclination of the rocks contained in each unit. The average 95 percent confidence interval of these samples is indicated by the width of the box.

also common in subunits 9, 10, and 11. Breccia increases in abundance toward the bottom of the hole and is especially common in unit 9 (610.1-721.5 m subbottom). The lowermost unit, unit 11 (712.0-721.5 m subbottom) consists entirely of basaltic rubble of mixed lithologies. The recovered rock fragments are fractured and contain slickensided surfaces (Figure 33) (Aumento, Melson, and others, 1977a).

The recovered basaltic rocks were divided into 7 magma groups on the basis of major element geochemistry. The most distinctive chemical break, characterized by an abrupt change in the ratio of Mg to Mg + Fe, occurs at 400 m subbottom depth (Flower and others, 1977).

The basement rocks were divided into 9 magnetic super units on the basis of in-place magnetic inclinations. These units are reversely magnetized as might be expected on the basis of the surface magnetic anomaly pattern. The inclinations are shallow, however, with respect to the expected dipole value ($\pm 56°$) (Hall and Ryall, 1977) (Figure 33).

Segregation Vesicle Studies

Of the 9 minicore samples collected from this hole 5 have segregation vesicles of sufficient abundance and quality to orient the rocks. These 5 samples represent the cored interval from about 322.5 to 450.0 m subbottom, which consists of lithologic units 3A, 3B, and a portion of 4, litho-

332B CORE LOG

A. LITHOLOGIC   B. MAGMA GROUPS   C. IN-PLACE STABLE INCLINATION
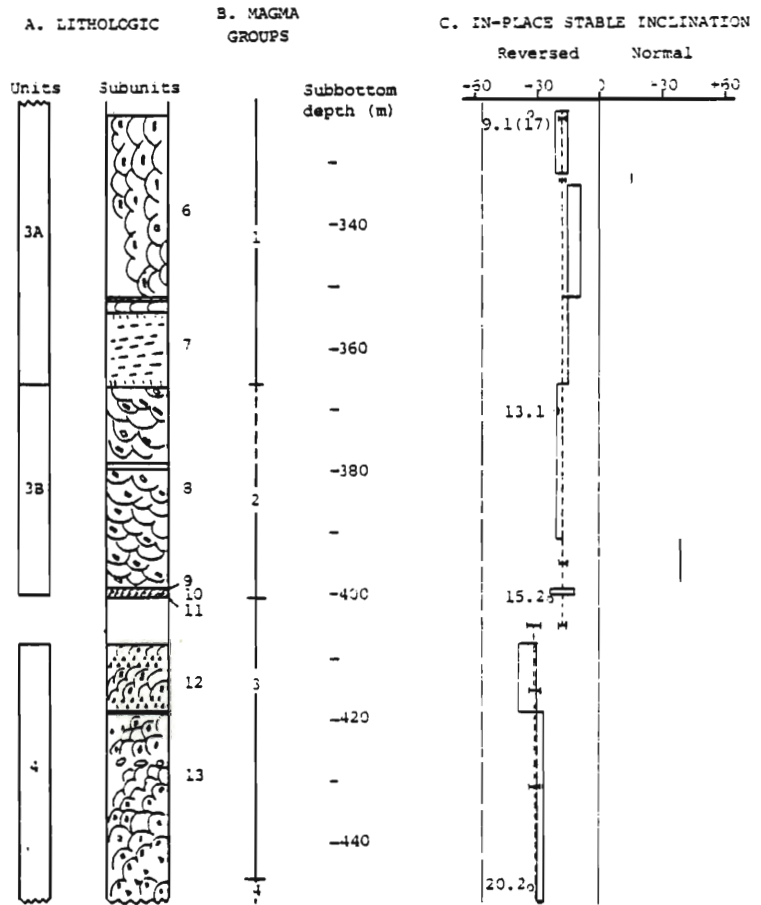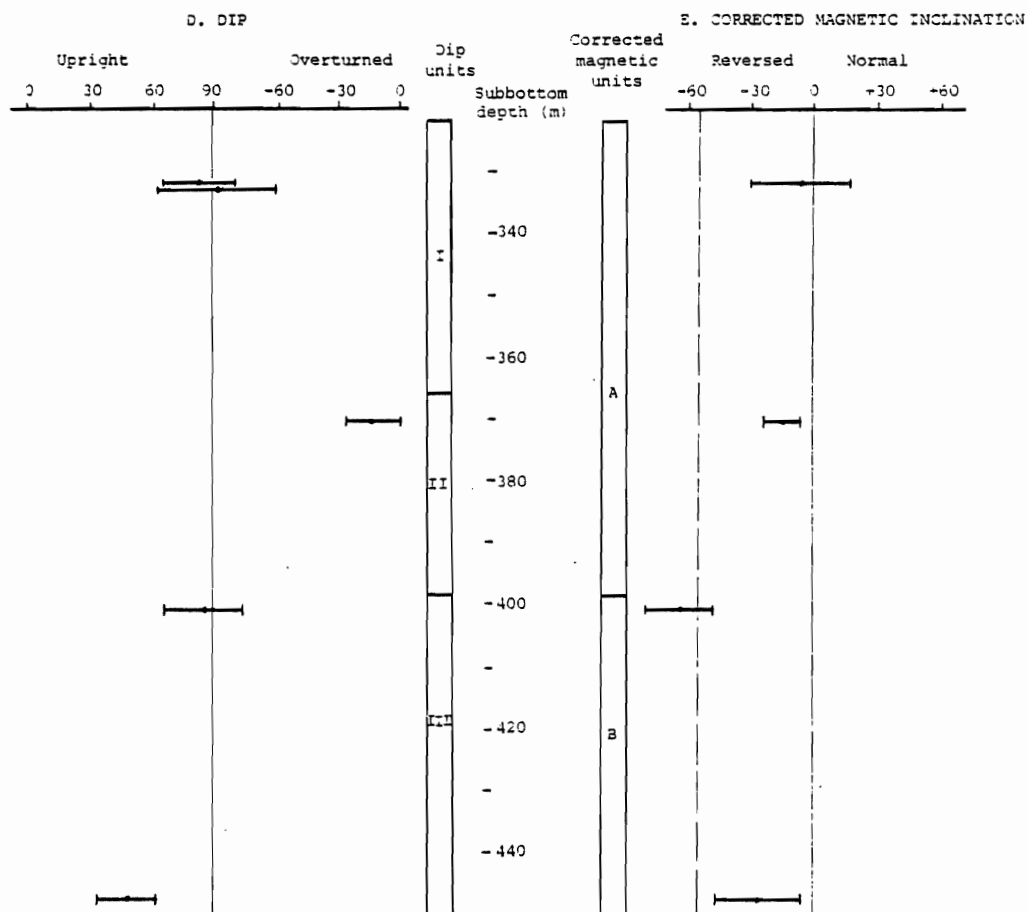
332B CORE LOG

Figure 33. DSDP hole 332B core log. Explanation is the same as Figure 30 except in C) in-place magnetic polarity data for individual samples are from Table 9; in D) Data are from Table 9; and in E) data are from Tables 9 and 10.

logic subunits 6 to 12 and a portion of 13, magma groups
1 to 4, and shallow, reversely magnetized rocks (Figure
33 and Table 9).

Dip Units

Studies of segregation vesicle inclinations of these
5 samples indicate that at least some of the rock units are
steeply dipping and even overturned. The dip (D) and 95 per-
cent confidence interval of the dip (S_D) of each sample is
listed on Table 9 and illustrated on Figure 33. Based on
these dips, and for the purpose of constructing restored
profiles, the interval of core studied is divided into dip
units.

Dip unit I is defined by samples 9.1 (17-20) and 9.1
(112-113) which have similar, nearly vertical dips. Both
of these samples are from lithologic subunit 6. Unit I is
interpreted as including all of lithologic subunits 6 and 7.
Although no samples from subunit 7 were studied for segrega-
tion vesicles, is is included with unit I because it is part
of the same lithologic unit and magma group.

Dip unit II is defined by sample 13.1 (72-74) which has
a shallow, overturned dip. This sample is from lithologic
subunit 8. Although no other samples from this subunit were
available, all of the rocks of subunit 8 are included in dip
unit II.

Table 9. Structural and paleomagnetic data resulting from segregation vesicle studies of basalts from DSDP hole 332B. Abbreviations are from the text. ENC1 values are from Aumento and others (1977a).

Sample number	Subbottom depth (m)	D(°)	S_D(°)	ENC1 (°)	ENC2 (°)	S_E(°)	AZI(°)	S_A(°)
9.1 (17-20)	332.18	+83	18	-33.3	-6	24	303	3
9.1 (112-113)	333.12	-88	29					
13.1 (72-74)	370.60	-14	13	-20.9	-15	10	259	47
15.2 (83-85)	400.83	+86	20	-23.4	-64	16	227	26
20.2 (6-8)	447.56	+49	15	-33.5	-27	21	333	16

Two samples 15.2 (83-85) and 20.2 (6-8), from the lower portion of the core interval studied have moderately steep to steep, upright dips. Sample 15.2 (83-85) is from lithologic subunit 10 and sample 20.2 (6-8) is from subunit 13. This dip unit is defined as containing subunits 10 and 13 from which samples 15.2 and 20.2 were taken as well as the intervening subunits, 11 and 12. Subunit 9 is also included with dip unit III on the basis of its proximity and lithologic similarity to subunit 10. The bottom of the unit is placed at 450 m subbottom just below the depth from which sample 20.2 was taken.

Corrected Magnetic Units

Reorientation of the rocks back to the horizontal position with simultaneous rotation of the measured magnetic direction indicates that the paleomagnetic polarity profile probably was different from the present in-place record. On the basis of the corrected magnetic inclinations (ENC2) of the samples (Table 9) the core interval studied is divided into two corrected magnetic polarity units (Figure 33 and Table 10).

Magnetic unit A is defined by samples 9.1 (17-20) and 9.1 (112-113). Corrected magnetic inclinations indicate that both of these samples originally had shallow reversed polarities. Unit A is interpreted as containing lithologic subunits 6 and 8 from which the samples were taken as well as the intervening subunit 7. The average ENC2 of the samples contained

Table 10. Corrected magnetic units of DSDP hole 332B. Sample numbers and dips are from Table 9. Lithologic subunits are from Figure 33. Abbreviations are from the text.

Corrected magnetic unit	Samples included	Lithologic subunits included	Average ENC2 (°)	Average (°)	t (m)	Tm (m)
A	9.1, 13.1	6, 7, 8	−10.5	17.0	76.25	35.02
B	15.2, 20.2	9, 10, 11 12, 13	−45.5	18.5	50.89	29.93

in unit A is -10.5° with an average S_E of 17.0°.

Magnetic unit B contains samples 15.2 (83-85) and 20.2 (6-8). Corrected magnetic inclinations indicate that both of these samples originally had reversed polarities with steeper inclinations than those of Unit A. This magnetic unit is interpreted as containing lithologic subunits 10 and 13 from which the samples were taken as well as the intervening subunit 12. Subunit 9 is also included in this magnetic unit because of its proximity and lithologic similarity to subunit 10 from which sample 15.2 (83-85) was taken. The average ENC2 of samples contained in B is -45.5° with an average S_E of 18.5°.

Restored Profiles

Because segregation vesicle studies suggest that the rock units recovered from Hole 332B are tilted, the vertical thickness of rock units penetrated may be greater than the true thickness (Tm). The Tm, Tmin, and Tmax of each lithologic subunit along with the dip used to calculate each thickness is listed on Table 11. The Tm of each lithologic unit, subunit and magma group is shown on Figure 34.

The 5 samples studied represent a vertical thickness of 127.50 m of rock. The true thickness of these rock units, however, may be only about 65 m. These data suggest that subunits consisting of or containing probable intrusive rocks

Table 11. The vertical thickness and true thickness of lithologic subunits of DSDP hole 332B. Sample numbers and dips are from Table 9. Lithologic subunits are from Figure 33. Abbreviations are from the text.

Lithologic subunit	Vertical t(m)	D(°)	Dmin (°)	Dmax (°)	Tm (m)	Tmin (m)	Tmax (m)	Source of D sample number(s)
6	29.22	85.5	61.0	--	2.29	2.29	14.17	9.1(17), 9.1(112)
7	14.46	"	"	--	1.13	1.13	7.01	"
8	32.57	14	1	27	31.60	29.02	32.56	13.1
9	0.4	86	66	--	0.003	0.003	0.16	15.2
10	2.03	"	"	--	0.14	0.14	0.83	"
11	3.82	"	"	--	0.27	0.27	1.55	"
12	13.98	49	34	64	9.17	6.13	11.59	20.02
13	31.02	"	"	"	20.35	13.60	25.72	"
TOTAL t = 127.50				TOTAL Tm= 64.95				
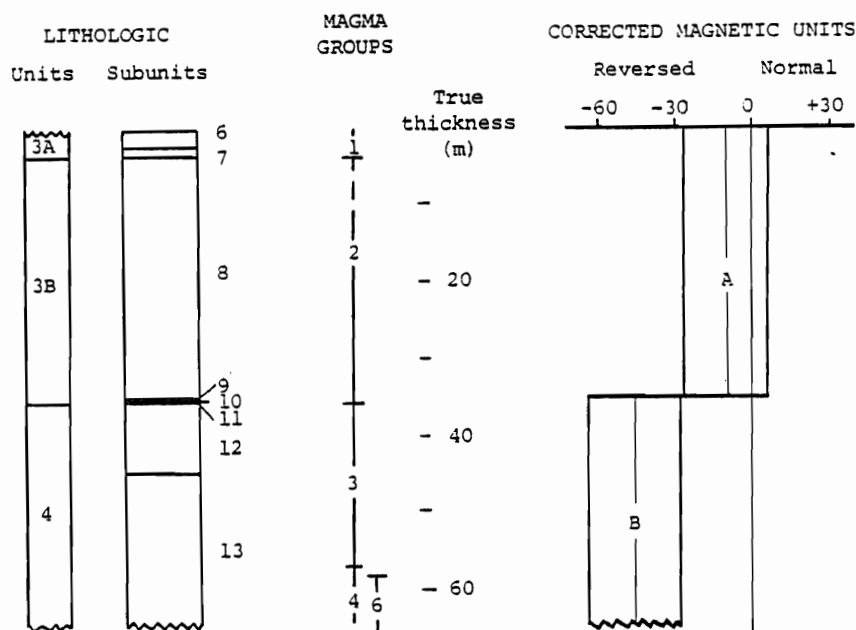
Figure 34. Restored profiles showing the true thickness of lithologic units and subunits, magma groups, and corrected magnetic units shown on Figure 33. Data are from Tables 10 and 11. Open boxes A and B are centered over the average corrected magnetic inclination of rocks contained in each unit. The average 95 percent confidence interval of the inclination of the samples is indicated by the width of the box.

(subunits 7, 9, 10, and 11) are over-represented in the vertical section. These subunits actually are only about 1 m in thickness. A possibility, however, is that the diabasic units were vertically intruded prior to tilting and because the rocks were later tilted by about 85°, the vertical thickness of intrusive units penetrated is the true thickness of the units. If this is the case, calculation of the true thickness according to the method described gives an erroneous result. This is a problem to be aware of when doing segregation vesicle studies, but it is impossible to resolve.

Subunit 8, consisting of plagioclase-phyric basalt, may be the thickest unit followed by the highly olivine-phyric basalt of subunit 13. Magma group 2, characterized by a high content of FeO and TiO_2 may represent the thickest sequence of eruptive units.

The true thickness of corrected magnetic units based upon the Tm of the lithologic unit with which they correspond suggests that unit A is only slightly thicker than unit B (Table 10 and Figure 34).

Hole 334

Introduction

Hole 334 penetrated 117 m of oceanic basement rocks with 20 percent recovery. Basement was encountered at 259.5 m subbottom. The rocks recovered were divided into 3 lithologic units. Unit 1 consists of 12 m of sparsely plagioclase-,

augite-and olivine-phyric basalt. Unit 2 consists of 45 m of
aphyric basalt with interbeds of glassy rinds and sedimentary
layers. Fourteen cooling units were recognized in units 1
and 2 but the type of flow unit was not defined. Unit 3 con-
sists of 65.5 m of interlayered gabbro and serpentinized peri-
dotite and breccia. The breccias contain plutonic clasts in
a chalk matrix. These breccias were tentatively interpreted
as indicating cold extrusion or uplift of the plutonic com-
plex prior to eruption of the overlying extrusive rocks (Aumen-
to and Melson and others, 1977c). The two extrusive lithologic
units correspond to two separate magma groups (Flower and
others, 1977).

The basement rocks were divided into two magnetic super-
units on the basis of in-place stable magnetic inclinations.
The upper unit corresponds to the extrusive rock sequence and
is normally magnetized with a dipolar inclination as might be
predicted on the basis of the surface magnetic anomaly. The
lower unit corresponds to the plutonic rock complex. These
rocks have scattered inclinations but primarily are reversely
magnetized (Hall and Ryall, 1977).

Segregation Vesicle Studies

Segregation vesicles could be used to orient three of the
five samples examined from Hole 334. These three samples re-
present the cored interval from about 265 to 295 m subbottom.

This interval consists of lithologic unit 2, magma group 2, and the normally magnetized magnetic super unit (Figure 35 and Table 12).

Dip Units

Studies of segregation vesicle inclinations of these three samples indicate that the rock units have uniformly shallow and upright dips. Only 1 dip unit is identified (Figure 35 and Table 12).

Corrected Magnetic Units

Reorientation of the rocks to their original horizontal position with simultaneous rotation of the measured magnetic direction indicates that the corrected magnetic polarity profile is similar to the in-place profile. A single, normally magnetized magnetic unit is recognized. In all cases reorientation of the rocks moves the measured magnetic direction closer to the expected dipole value. The average corrected inclination of the rocks contained in this unit is equivalent to the dipole value (Figure 35 and Tables 12 and 13).

Restored Profiles

Segregation vesicle studies suggest that the rock units penetrated by Hole 334 are only gently dipping, and hence the
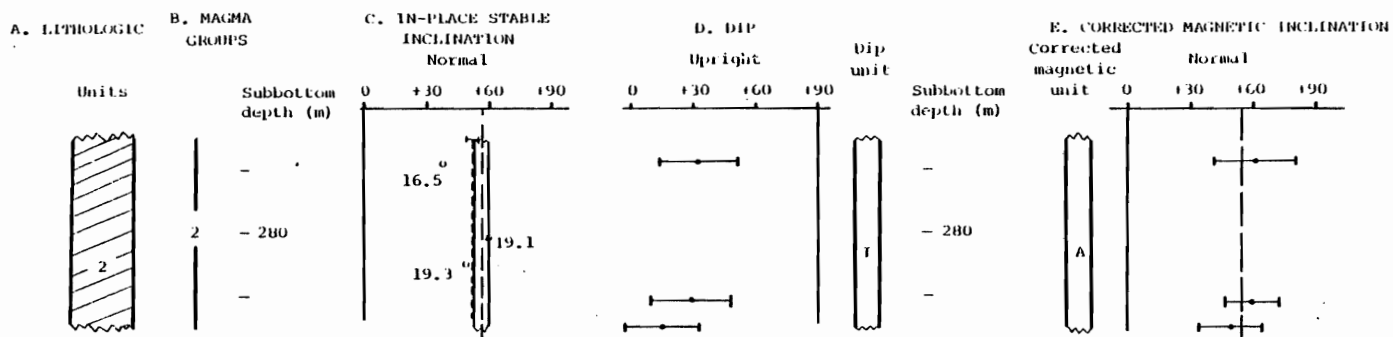
Figure 35. DSDP hole 334 core log. Explanation is the same as Figure 30 except in A) slanted lines indicate average dip only and do not represent rock type and data are from Aumento and others (1977c); in C) in-place magnetic polarity data for individual samples are from Table 12; in D) data are from Table 12; and in E) data are from Tables 12 and 13.

Table 12. Structural and paleomagnetic data resulting from segregation vesicle studies of basalts from DSDP hole 334. Abbreviations are from the text. ENC1 values are from Aumento and others (1977c).

Sample number	Subbottom depth (m)	$D(°)$	$S_D(°)$	ENC1 (°)	ENC2 (°)	$S_E(°)$	AZI(°)	$S_A(°)$
16.5 (19-21)	268.69	+32	19	+38.4	+61	20	240	65
19.1 (6-9)	291.06	+29	20	+60.0	+59	13	298	31
19.3 (93-95)	294.93	+15	18	+48.2	+49	15	265	59

Table 13. Corrected magnetic unit of DSDP hole 334. Sample numbers and dips are from Table 12. Lithologic unit is from Figure 35. Abbreviations are from the text.

Corrected magnetic unit	Samples included	Lithologic subunits included	Average ENC2 ($^{\circ}$)	Average S_E ($^{\circ}$)	t (m)	Tm (m)
A	16.5, 19.1 19.3	2	56	16	35.00	31.72

true thickness of rock units (32 m) may be similar to the vertical thickness (35 m). The vertical thickness of the magnetic unit also may be representative of the true thickness of this unit (Figure 36, and Tables 13 and 14).

Geological and Geophysical Setting of Legs 45 and 46

The segregation vesicle technique was applied to some rocks recovered from Holes 395, 395A, and 396B which were drilled during Legs 45 and 46 of the Deep Sea Drilling Project. Holes 395 and 395A were drilled at the same site, about 50 km to the west of the Mid-Atlantic Ridge south of the Kane Fracture Zone at 225° N latitude. Hole 396B was drilled at about the same latitude, but 150 km to the east of the Mid-Atlantic Ridge (Melson, Rabinowitz and others, 1978b; and Dmitriev, Heirtzler and others, 1978b) (Figure 2).

Magnetic anomaly patterns indicated that Holes 395 and 395A were drilled into crust magnetized during positive anomaly 4' and Hole 396B penetrated crust magnetized during anomaly 5. The rocks recovered were, therefore, expected to be normally magnetized with inclinations consistent with the dipole of value ($\sim 40^{\circ}$). Assuming a variable spreading rate, the crustal ages at Sites 395 and 396 were calculated to be 6.5 and 8.8 m.y., respectively (Purdy and others, 1978).

The oldest sediment penetrated at Site 396B is 13.6 $\pm$ 1.6 m.y. old based on coccolith assemblages (Burky, 1978).

334, RESTORED

LITHOLOGIC   CORRECTED MAGNETIC UNIT

   Unit   Normal
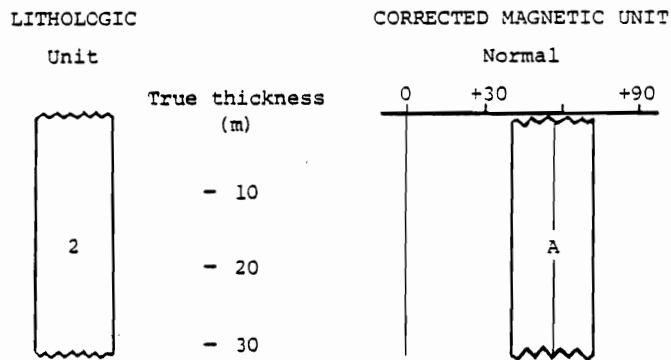
Figure 36. Restored profiles showing the true thickness of the lithologic unit and corrected magnetic unit shown on Figure 35. Data are from Tables 13 and 14. Box A is centered over the average corrected inclination of the rocks contained in that unit. The average 95 percent confidence interval of the inclination of these samples is indicated by the width of the box.

Table 14. The vertical thickness and true thickness of the lithologic unit of DSDP hole 334. Sample numbers and dips are from Table 12. The lithologic unit is from Figure 35. Abbreviations are from the text.

Lithologic unit	Vertical t(m)	D(°)	Dmin (°)	Dmax (°)	Tm (m)	Tmin (m)	Tmax (m)	Source of D sample number(s)
Part of 2	35	25	6	44	31.72	25.18	34.81	16.5, 19.1, 19.3

This age is clearly older than the maximum age of anomaly 5 (Blakely, 1974) which the hole penetrated and also older than the calculated age of the crust based on sea floor spreading rates (Purdy and others, 1978).

Holes 395 and 395A

Introduction

Hole 395 and 395A penetrated a total of 571 m into igneous basement crust with 58 and 18 percent recovery, respectively. The rocks recovered were divided into lithologic units on the basis of phenocryst composition and abundance, extent of brecciation or fracturing, and abundance of secondary minerals. Hole 395 was divided into 4 lithologic units and Hole 395A was divided into 23 units. The top 4 units are the same in each hole.

The basement section recovered consists primarily of aphyric (58 percent) and phyric (31 percent) pillow basalts with interlayers of breccia (7 percent) and plutonic sequences (4 percent). The aphyric and phyric basalts are chemically distinct and each was divided into 4 chemical groups designated as A_1-A_4 and P_1-P_4, respectively. The breccias generally consist of carbonate-cemented basalt fragments. The uppermost breccia layer and plutonic complex (interpreted as talus) contain fragments or layers of gabbro and serpentinized peridotite. Thick sequences of breccia occur near the bottom of the section

(Figure 37) (Melson, Rabinowitz and others, 1978b).

The in-place magnetic inclination of the rocks included in each chemical group generally is uniform (Figure 37). Inclinations generally are close to the dipole value for the site's latitude. Three polarity intervals were recognized with reversals occurring at about 255 and 570 m subbottom (Johnson, 1978).

Segregation Vesicle Studies

Eight of the 31 samples collected from these holes could be oriented by the segregation vesicle technique. These 8 samples represent the cored interval from about 96 to 581 m subbottom. The lithologic, chemical, and in-place magnetic units included in this section of core as well as sample locations and the measured magnetic inclination of each sample are shown on Figure 37 and listed on Table 15.

Dip Units

Studies of segregation vesicles of these samples indicate that the rocks sampled generally are gently dipping and upright. Exceptions to this are samples 33.2 and 58.1 which were recovered adjacent to breccia zones and are steeply dipping (Figure 37).

395 and 395A CORE LOG
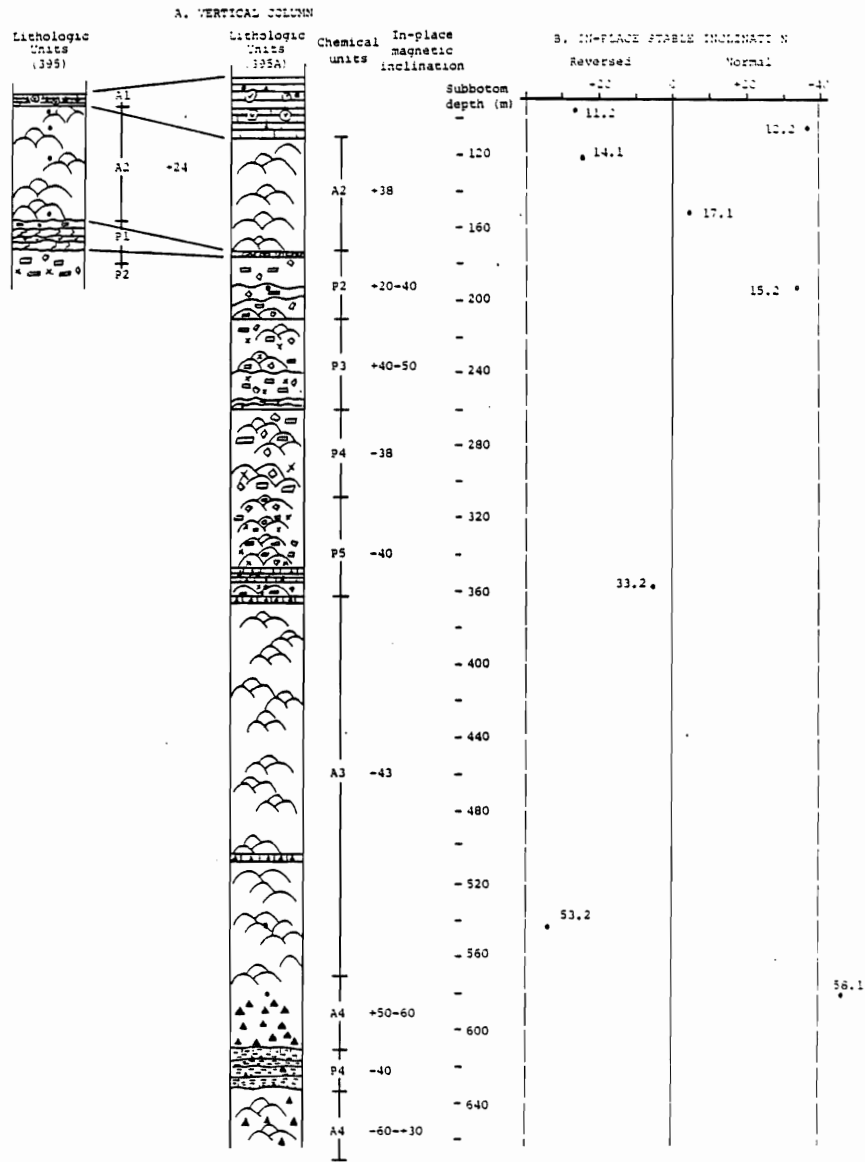
395 and 395A CORE LOG
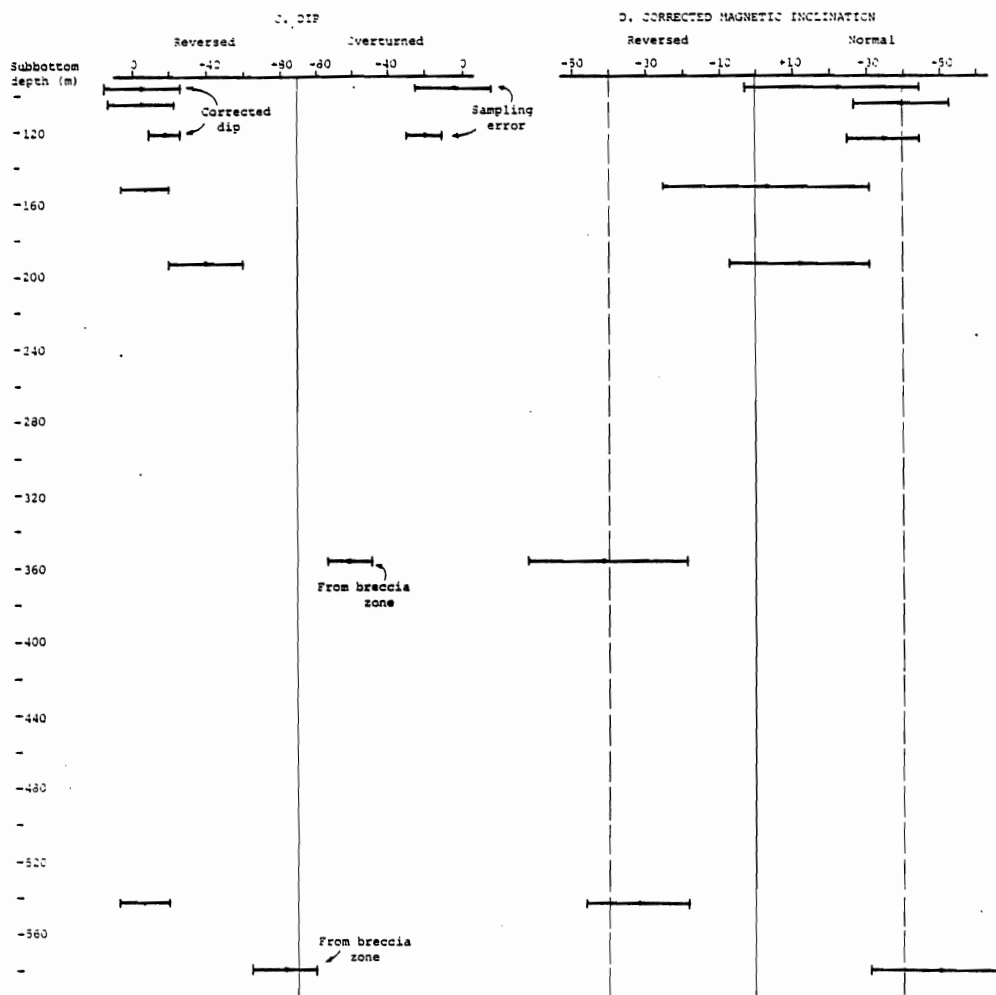
Figure 37. DSDP Holes 395 and 395A core log. A) A strat-
igraphic column modified after Melson and others (1978b).
An explanation of symbols used is on Figure 31. The dip
is schematically represented. Dots indicate sample locations
from Table 15. B) The in-place magnetic inclination of the
samples studied and the sample numbers. C) The dip.
D) The corrected magnetic inclination of the samples. Bars
indicate the 95 percent confidence interval of each deter-
mination. Data for B, C, and D are from Table 15. The
dashed vertical lines indicate the dipole inclination.

Table 15. Structural and paleomagnetic data resulting from segregation vesicle studies of basalts from DSDP holes 395 and 395A. Abbreviations are from the text.

DSDP HOLE 395

Sample number	Subbottom depth (m)	$D(°)$	$S_D(°)$	ENC1 $(°)$	ENC2 $(°)$	$S_E(°)$	$AZI(°)$	$S_A(°)$
11.2 (114-116)	96.2	-4*	21	-26.0	+22	25	19	342
12.2 (140-142)	105.7	+5	18	+37.3	+40	13	240	175
14.1 (95-97)	122.7	-19*	10	-24.5	+35	10	240	38
17.1 (19-21)	150.3	+7	13	+4.8	+3	28	74	239

DSDP HOLE 395A

Sample number	Subbottom depth (m)	$D(°)$	$S_D(°)$	ENC1 $(°)$	ENC2 $(°)$	$S_E(°)$	$AZI(°)$	$S_A(°)$
15.2 (78-81)	198.3	+40	20	+33.6	+12	19	51	15
33.2 (77-79)	356.3	-61	12	-4.5	-41	23	223	34
53.2 (6-8)	543.1	+6	14	-36.4	-32	14	316	138
58.1 (134-136)	580.8	+83	18	+46.3	+50	19	356	27

*Sampling error , correct values are D = +4° AZI = 195° for 11.2 (114-116)

D = +19° AZI = 60° for 14.1 (95-97)

Corrected Magnetic Units

Restoration of the rocks back to their horizontal position with simultaneous rotation of the measured magnetic direction does not remove the occurrence of polarity reversals in the vertical section. But because dips are gentle the corrected polarity profile is similar to the in-place record (Figure 37 and Table 15).

Restored Profile

The rocks recovered are nearly flat lying, except for the local steep dips associated with brecciated zones. The true thickness of rock and magnetic units recovered, therefore, probably is similar to the vertical thickness of units penetrated.

Hole 396B

Introduction

Two hundred fifty five m of basaltic basement crust were penetrated during drilling of Hole 396B with about 30 percent recovery. The rocks recovered were divided into 8 lithologic units. The section consists primarily of sparsely to moderately plagioclase-and olivine-phyric pillow basalts (Units 1, 2, 4, and 7) with a shallow sill or flow of similar composition (Unit 3), and interlayers of carbonate cemented basaltic breccia, and sand and gravel (Units 5, 6, and 8). These litho-

logic units were divided into 3 major chemical units (A,
B and C) and 6 subunits (Dmitriev, Heirtzler and others,
1978b) (Figure 38).

The possible origins of the basaltic sand and gravel
layers have been discussed by several authors (Dmitriev,
Heirtzler and others, 1978b; Dick and others, 1978; and Sch-
mincke and others, 1978). They interpreted the sand and
gravel to be hyaloclastite formed by selective splintering
of glassy margins due to thermal shock which were later con-
centrated as talus at the base of a volcanic edifice or fault
scarp, or by bottom current activity. The freshness of the
glass shards indicates isolation from alteration activity
possibly due to burial by subsequent flows or slumping of
pillow mounds.

Four magnetic units were defined on the basis of the
measured in-place stable magnetic inclination. The magnetic
inclination generally is quite uniform within each unit.
None of the units, however, have inclinations consistent with
the expected dipole value ($\pm 40.3^{o}$). I and IV are normally
magnetized with shallow inclinations, whereas II and III are
reversely magnetized with steep and shallow inclinations,
respectively (Peterson, 1978) (Figure 38).

Segregation Vesicle Studies

Nine of the 22 samples collected from Hole 396B have

396B CORE LOG

A. VERTICAL COLUMN

Lithologic Units | Chemical units | In-place magnetic inclination | Subbottom depth (m)

B. IN-PLACE STABLE INCLINATION
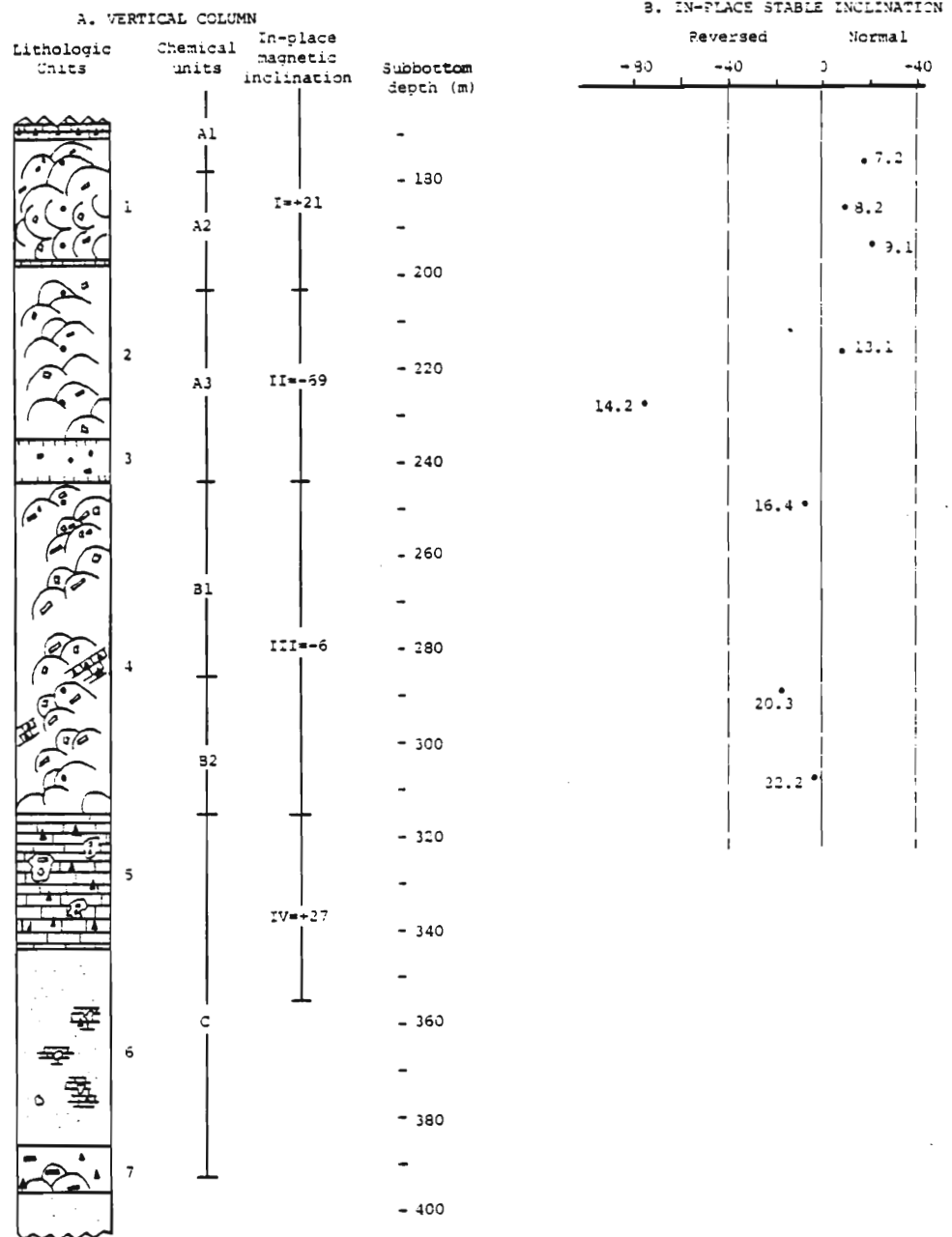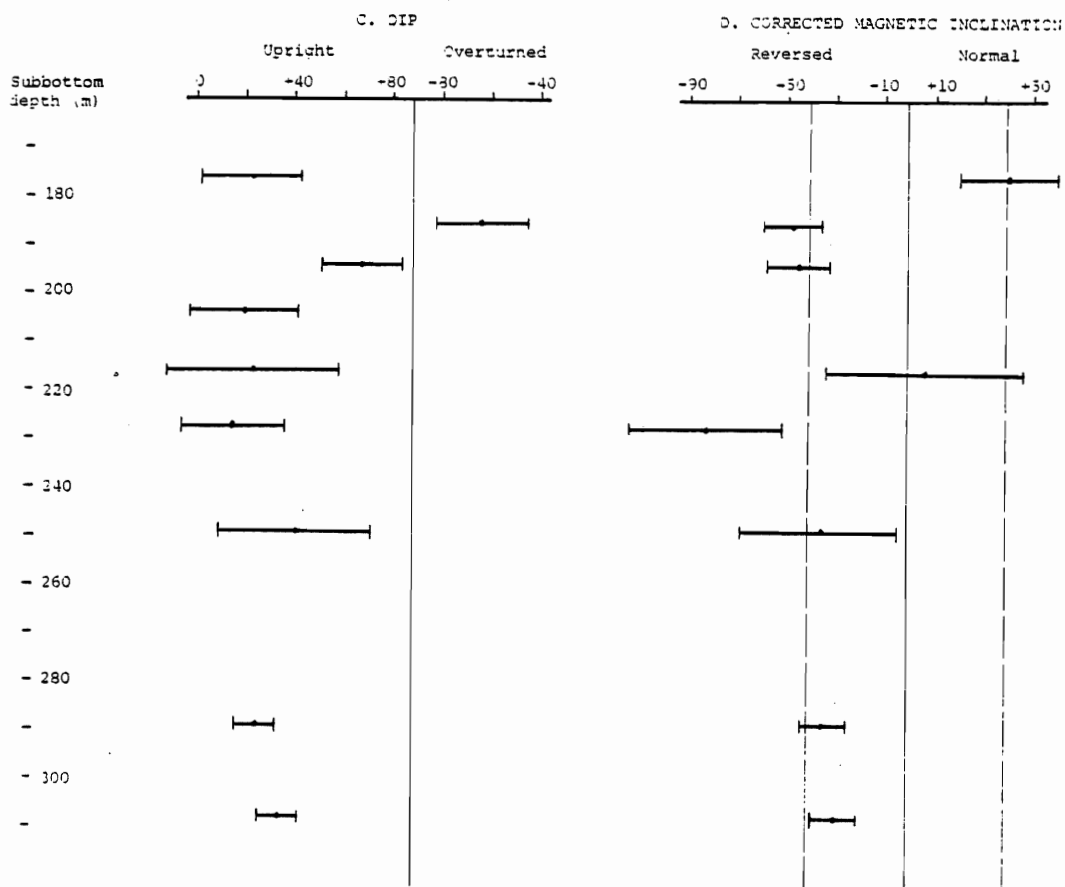
396B CORE LOG

Figure 38. DSDP hole 396B core log. A) A stratigraphic column modified after Dmitriev and others (1978b). Dots indicate sample locations from Table 16. The dip of each unit is schematically represented. An explanation of symbols is on Figure 31. B) The in-place magnetic inclination of samples studied and the sample numbers. C) The dip. D) The magnetic inclination of the samples. Bars indicate the 95 percent confidence interval. Data for B, C, and D are from Table 16. The dashed vertical lines indicate the dipole inclination.

segregation vesicles of sufficient quality and abundance to orient the rocks. These 9 samples represent the cored interval from about 165 to 325 m subbottom. The lithologic and in-place magnetic units included in this section of core as well as sample locations and the measured magnetic inclination of each sample are shown on Figure 38 and Table 16.

Dip Units

Studies of segregation vesicle inclinations of these 9 samples indicate that the rock units sampled generally are gently dipping and upright. Segregation vesicles from two samples of lithologic unit 1 indicate, however, that these rocks are steeply dipping (Table 16 and Figure 38). This isolated occurrence of steeply dipping rocks may be the result of penetration of a local rubble zone or disruption of the rock units during drilling. These samples are from the basalt overlying the sedimentary layer which separates lithologic unit 1 from 2. These rocks may have been rotated into the softer sediments below during drilling.

Corrected Magnetic Units

Reorientation of the rocks back to their original horizontal position with simultaneous rotation of the measured magnetic direction indicates that the corrected magnetic polarity profile is different from the in-place record. The rocks have corrected magnetic inclinations similar to the

Table 16. Structural and paleomagnetic data resulting from segregation vesicle studies of basalts from DSDP hole 396B. Abreviations are from the text.

Sample number	Subbottom depth (m)	$D(°)$	$S_D(°)$	ENC1 $(°)$	ENC2 $(°)$	$S_E(°)$	AZI$(°)$	$S_A(°)$
7.2 (96-99)	176.46	+23	20	+18.0	+40	20	202	69
8.2 (69-71)	185.69	-63	19	+9.9	-47	12	105	20
9.1 (70-72)	193.70	+68	17	+21.0	-45	13	200	25
10.2 (21-23)	204.21	+20	22					
13.1 (62-64)	216.62	+24	35	+8.5	+7	41	84	91
14.2 (68-70)	227.68	+16	21	-75.5	-82	32	295	129
16.4 (37-39)	249.37	+41	31	-7.0	-36	32	233	70
20.3 (8-11)	289.58	+25	8	-16.6	-34	9	130	23
22.2 (94-96)	307.94	+35	8	-2.7	-29	9	134	20

dipole value and are divided into two corrected magnetic units (Table 16 and Figure 38). The upper unit (A) is defined by sample 7.2 (96-99), which is normally magnetized. The unit is interpreted as extending from the bottom of the upper breccia of lithologic unit 1 to the base of chemical unit A_1 (165-178 m subbottom). Magnetic unit B (178-325 m subbottom) includes the remaining reversely magnetized samples.

Sample 13.1 has an anomalously shallow inclination and a large error associated with this inclination. Because of the large error and the fact that this sample is from a highly altered portion of the core, it is difficult to attach any significance to the inclination.

Restored Profiles

The 9 samples studied represent a vertical thickness of 160 m of basement. Assuming that the bulk of the rock layers are gently dipping, with an average dip of 26° (calculated from Table 16, excluding samples 8.2 and 9.1), the true thickness of rock units penetrated is 144 m. Assuming this same average dip, the true thickness of magnetic units A and B is 12 and 132 m, respectively.

RESULTS OF DIP DIRECTION CALCULATIONS

The problems of estimating the direction of dip of drill core basalt samples oriented by the segregation vesicle technique have been discussed in the introductory section of this chapter. The dip direction (AZI), calculated according to the method described in the chapter on statistical techniques, and the 95 percent confidence interval of this direction (S_A) are listed for each sample in Tables 6, 9, 12, 15, and 16 and illustrated in Figure 39. The results of AZI calculations discussed here assume single stage rotation about a horizontal axis. As previously discussed, in order to interpret these results rigourously, additional sampling is required.

With two exceptions the rock samples studied from Hole 332A apparently dip to the east. Most, but not all of the samples from the top of the hole dip to the NE, whereas rocks toward the bottom of the hole dip toward the SE or SW (Figure 39). This discrepancy in the preferred orientation of AZI values raises the possibility that the lower units were rotated prior to emplacement of the upper units.

Most of the samples from Hole 332B apparently dip toward the west. The average dip direction of one of the samples is to the east, but the error associated with this AZI is large (Figure 39).

The samples studied from Hole 334 have the most uniform dip directions. All AZI values suggest that the rocks dip toward
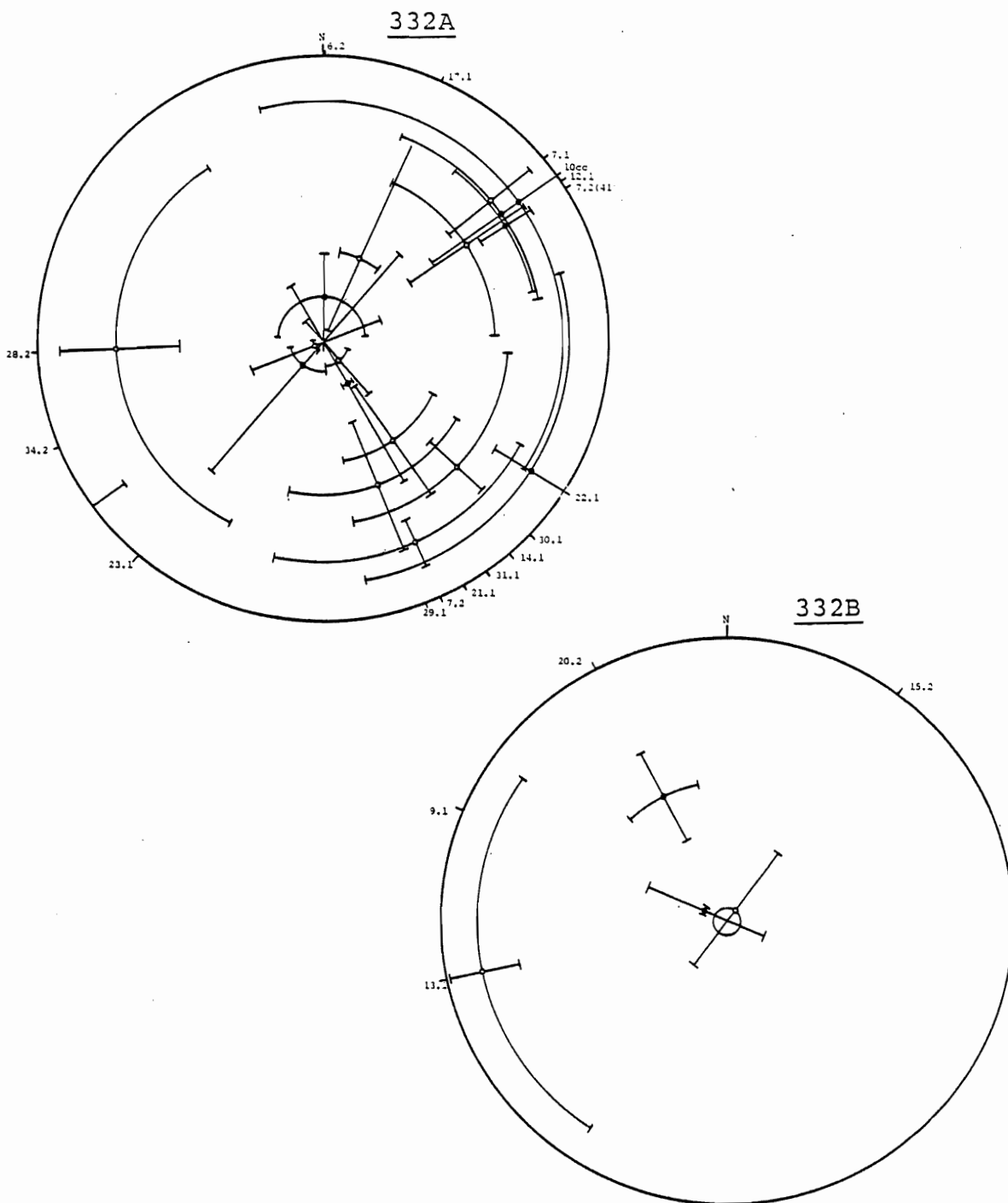
Figure 39. Lambert equal area projection plots of the dips and dip directions of rock samples studied. Dips range from 0° at the perimeter of the circle to 90° at the center of the circle. Upright dips are indicated by solid circles and overturned dips are indicated by open circles. Radial bars indicate the error in the dip and arcuate bars indicate the error in the dip direction. Data are from Tables 6, 9, 12, 15, and 16. In most cases only AZI values with errors less than 175° are plotted.

334

395, 395A

396B
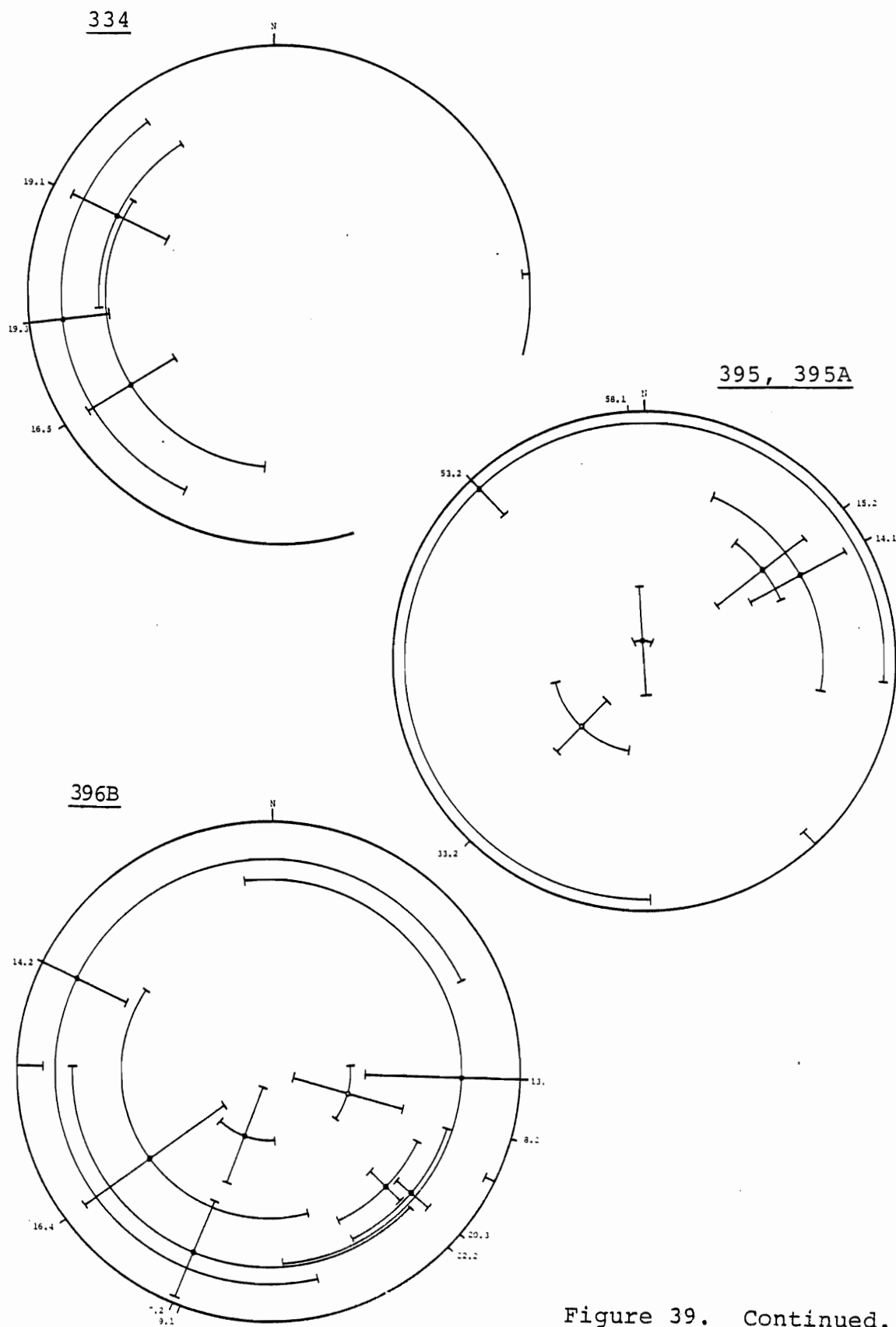
Figure 39. Continued.

the west, dipping away from the rift valley axis.

Few data from Holes 395 and 395A are available for dip direction interpretations. Most samples from these holes have AZI values with extreme errors (greater than 175°) because of the sub-horizontal dip of the rocks. Additionally, samples 33.2 and 58.1 are from the vicinity of breccia zones so the structural data from these samples may not be generally relevant. Sample 53.2 has an AZI value suggesting a dip direction to the NW, however, the error for this value is 138°. Samples 14.1 and 15.2 have AZI values suggesting dips to the NE with reasonably small errors (38° and 15°, respectively).

With two exceptions, most of the samples studied from Hole 396B apparently are dipping to the SW and SE. However, the errors associated with most of these AZI values are large due to the sub-horizontal dip of the rocks. Exceptions to this are the steeply dipping rocks which have dips toward the SE and SW, and the two samples near the bottom of the hole which apparently dip toward the SE.

SUMMARY OF SEGREGATION VESICLE STUDIES

Segregation vesicles occur in 26 to 60 percent of the rock samples collected from the five DSDP holes studied. They can be used to determine the structural dip of the rocks and the corrected magnetic inclinations, although there are errors associated with these determinations. Based on these data,

restored profiles can be constructed. The differences between the dips of the rocks and corrected magnetic polarity profiles of the different DSDP holes studied suggest that the upper Atlantic oceanic crust is structurally and magnetically hetero-geneous.

The cores studied exhibit varying degrees of structural complexity (Figure 40). Hole 332A is the most complex. Al-though dips in the upper 50 m of core primarily are sub-hori-zontal or gently dipping and upright, a small section is al-most completely overturned. Below 150 m subbottom most of the rocks are moderately to steeply dipping and several of the units are overturned. Steeply dipping and overturned rocks also characterize most of the section of DSDP Hole 332B stu-died. In contrast, the rocks recovered from Holes 334, 395, 395A, and 396B generally are gently dipping and upright with the exception of rocks recovered near breccia zones or sedi-ment layers.

Although dip directions are poorly constrained, some pre-liminary observations can be made (Figure 39). Dip directions from the Leg 37 samples studied suggest that the rocks located along one side of a rift valley are not uniformly dipping in the same direction. Rocks from the most structurally complex hole, 332A, primarily dip toward the NE at the top of the hole, changing to a SE direction toward the bottom of the hole. In contrast, the rocks studied from Hole 332B, drilled only 100
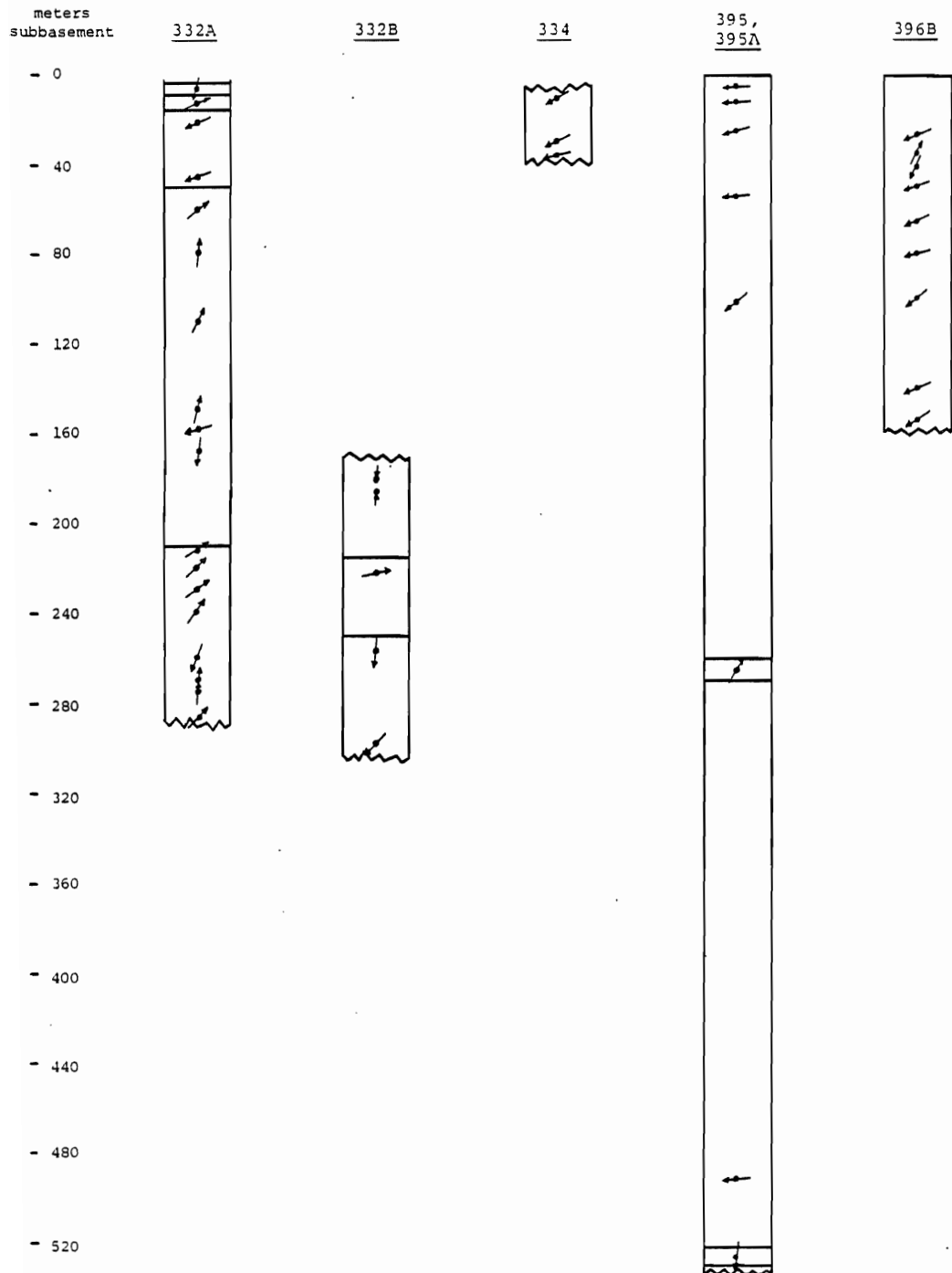
Figure 40. Possible distribution of dip units of the cores studied. Arrows indicate sample locations and the dip of each sample. Arrows pointing up indicate upright dips, whereas arrows pointing down indicate overturned dips. Dip units, previously defined, are divided by horizontal lines.

m from 332A, primarily dip toward the west, as do the rocks studied from Hole 334. Results of AZI calculations for Hole 396B may suggest that these rocks, which were located on the west side of a rift valley, dip toward the SE. Two samples from Holes 395 and 395A suggest that these samples, which are from the east side of a rift valley, dip toward the NE.

The corrected magnetic inclinations of the rock samples studied are always somewhat different than the in-place inclination. In most cases reorientation of the rocks brings the measured magnetic inclination closer to the dipole value (Figures 30, 33, 35, 37, and 38). If rocks are moderately to steeply dipping as in Holes 332A and 332B, reorientation may result in a corrected magnetic polarity profile which is very different from the in-place profile.

Reorientation of the rocks does not remove the occurrence of polarity reversals in the vertical section (Figure 41). The most complex sequence of these reversals occurs in Hole 332A. The corrected magnetic profile for this hole reveals eight polarity changes in the vertical section. This is the only hole where the corrected magnetic profile is more complex than the in-place record. In Holes 395 and 395A two polarity changes occur in the corrected profile, as in the in-place record (Figure 37). Only 1 reversal probably occurs in both the in-place and corrected magnetic profiles of 396B. This reversal in the corrected profile, however, occurs near the top of the section at the base of chemical unit A_1 rather
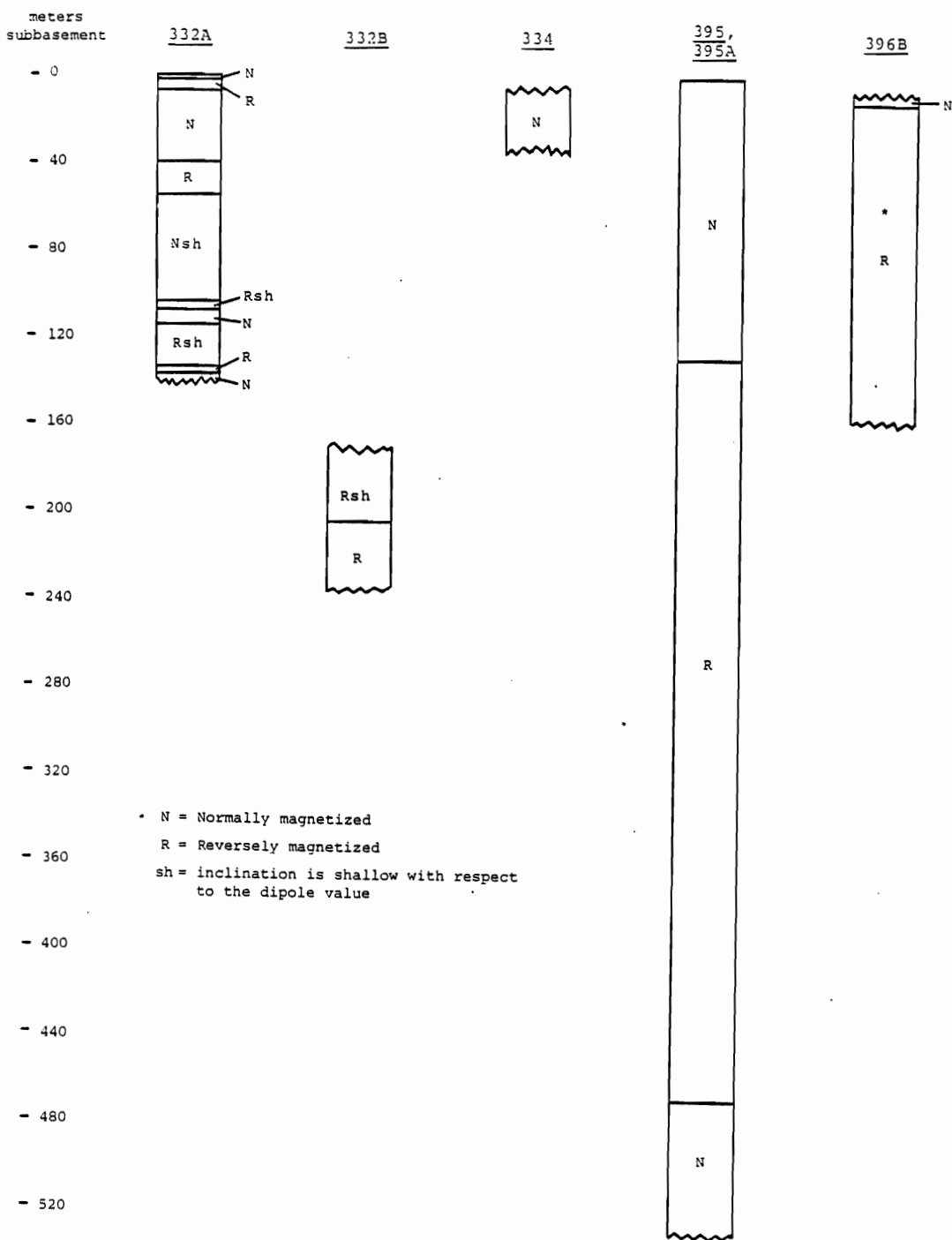
Figure 41. Possible distribution of corrected magnetic polarity units. True thicknesses are indicated. Depth subbottom is indicated assuming the rocks above the interval of core studied are undeformed. (*) indicates normally magnetized rock with shallow inclination sampled here but is apparently an isolated occurrence from a very altered portion of the core.

than at the base of chemical unit A_2, as it does in the in-place profile. Holes 332B and 334 exhibit no polarity reversals in the section of core studied, however, the rock samples studied from Hole 332B have corrected magnetic inclinations which are not uniformly dipolar.

With the possible exception of Holes 395 and 395A, the true thickness of rock units is less than the vertical thickness of rock units penetrated. In Holes 332A and 332B the true thickness of rock units may only be 49 and 51 percent, respectively, of the vertical thickness penetrated. In contrast, at Sites 334 and 396B the true thickness of rock units may be about 90 percent of the vertical thickness penetrated.

Because of tilting, the relative abundance of different rock or magnetic units in the stratigraphic section may be incorrectly determined if such estimates are based upon the vertical thickness of rock units. For example, segregation vesicle studies of rocks from Hole 332A suggest that the thickness of aphyric rocks exceeds that of phyric rocks in both the vertical in-place as well as the restored profiles. However, such studies of rocks from Hole 332B suggest that lithologic subunits consisting of or containing probable intrusive rocks have a true thickness which is less than 5 percent of their vertical thickness. Additionally, although the in-place magnetic units from Hole 332A indicate that the bulk of the rocks are reversely magnetized, segregation vesicle studies suggest

that the normally magnetized units actually have a true
thickness greater than twice that of reversely magnetized
units.

Due to the limited number of samples the segregation
vesicle studies presented cannot be used to give a precise
indication of the geologic structures, or predeformational
profiles of the holes studied. The results presented, how-
ever, do indicate that segregation vesicles commonly occur
in seafloor rocks and that, given enough samples, they probably
can be used to determine the geologic structure of oceanic
basaltic basement rocks recovered in drill cores. The studies
presented also indicate that segregation vesicle studies may
help determine the original volcanic and magnetic stratigraphy
of such rocks.

POSSIBLE CAUSES OF OBSERVED DIPS

A detailed analysis of ocean floor structure and tectonics
is beyond the scope of this thesis and is not possible based
upon the data presented here. It must be re-emphasized that
drill cores represent only a narrow window into oceanic crust
and that the lateral and exact vertical extent of any dip or
magnetic unit cannot be determined.

Nevertheless, drill cores provide one of the best methods
of directly observing a vertical section of oceanic crust, and
the segregation vesicle technique presently is the only way
of directly determining the dip of rocks recovered. Based on

the segregation vesicle studies presented, some preliminary interpretations about oceanic crustal structure of the North Atlantic can be made.

The most interesting results of these segregation vesicle studies are the apparent differences in structural style between the cores studied. Rocks studied from Hole 332A have a random assortment of dips which include steeply dipping and overturned rocks. Whereas, Holes 334, 395 and 395A, and 396B are characterized by predominantly gently dipping rocks Figure 40). The complex sequence of polarity reversals in the corrected magnetic polarity profile of Hole 332A along with the interfingering chemical units (Figure 30) also suggests the repetition of rock units.

Steeply dipping rock units, overturned rock units, and the repetition of these units in the vertical section may be caused by a variety of structural features including thrust faults and overturned folds (for example, see Billings, 1972). However, first motion seismic studies (Sykes, 1967), and field observations (Needham and Francheteau, 1974; Ballard and others, 1975; and Ballard and van Andel, 1977) indicate that spreading ocean basins are dominated by an extensional stress regime. Structures observed in these cores must, therefore, be explained by processes which may result from the response of brittle oceanic crust to a tectonic regime in which the maximum compressive stress is vertical and the minimum compressive stress

is horizontal (Anderson, 1951). This simple stress regime may be modified by the isostatic response of the crust to thinning in the axial region resulting from extension, loading in the axial region due to accumulation of the volcanic pile and, as the crust ages, cooling, contraction, and loading of the crust with sediment (Sleep, 1969; Lachenbruch, 1973; Osmaston, 1971; Sleep and Rosendahl, 1979; and Tapponnier and Francheteau, 1978).

Within this sort of tensional regime there are several possible processes which could cause the structures observed in the cores. These are discussed below. The terminology used to refer to different morphologic regions of the rift valley is from Ballard and Moore (1977).

Formation of the Volcanic Stratigraphy and Syn-depositional Deformation

The original volcanic stratigraphy is likely to be complex. Within the central volcanic province volcanic edifices are built and, in the depressions between these edifices, accumulation of lavas from neighboring central volcanoes and off-axis volcanism are superimposed on, and interfinger with, older volcanics. These flows also fill in the depressions between older flow ridges and previously formed fissures. This sequence may then be overlain by much younger tumuli lava cones or haystacks (Ballard and van Andel, 1977; and Atwater and others, 1978). Furthermore, due to random shifts in the axis

of volcanism, significantly older rocks (possibly as much
as 0.7 m.y. older) may be exposed at the surface, juxtaposed
against very young rocks, or occur at shallow depths (MacDonald,
1977; Johnson and Atwater, 1977; and Atwater and MacDonald,
1978). As a result of this extrusion and spreading sequence,
a complex volcanic pile may accumulate which consists of an
interfingering and locally unconformable arrangement of flows
which originated from several different sources during episodes
of volcanism that occurred over a long period of time (Needham
and others, 1976).

Flow top breccia and flow front talus may be interlayered
with these flows and may partially mantle the tops and toes of
steep flow fronts (covering 9 to 20 percent of the surface)
(Luyendyk and MacDonald, 1977; Ballard and van Andel, 1977;
and Ballard and Moore, 1978). This rubble may form shortly
after extrusion as a result of pillow flow collapse or instan-
taneously at the base of an advancing flow. Fragments appear
to be small (less than 30 cm) and are at least smaller than
the size of the pillows from which they originated (Luyendyk
and MacDonald, 1977). Although such rubble layers are likely
to be thin because they will either be buried by subsequent
flows, or by the flow from which they form (Atwater, 1979),
such consolidated talus apparently is exposed in fault scarps
at the base of the rift valley north of the Oceanographer
Fracture Zone, forming layers tens of meters thick (P.J.
Fox, per. com., 1981).

Because layers of such breccia or talus may be thin
and consist of small randomly oriented fragments, they can-
not explain the apparently thick sequence of steeply dipping
and overturned rocks observed in Holes 332A and 332B. The
rubble will also originate from a common parent and cannot
explain the sequence of corrected magnetic units observed
in Hole 332A. It may explain, however, the local occurrence
of steeply dipping rocks in Holes 395, 395A, and 396B.

Deformation Associated With Subsidence of the Volcanic Edifice
Within the Central Valley

Volcanic edifices are reduced in height by approximately
100 m shortly after their formation (Ballard and van Andel,
1977). Ballard and van Andel (1977) suggested that the re-
duction in height is caused by vertical collapse. The effect
of this collapse on the structure of the rocks is unknown and
may not be observable in outcrop due to burial by subsequent
flows. The rare observation of some tilted pillowed units in
surface exposures of the central volcanic province (Ballard
and van Andel, 1977) suggests that collapse may be accompanied
by tilting.

Hall (1979) and Hall and Robinson (1979) suggested that
as a volcanic edifice is transported away from the volcanic
zone it begins to subside resulting in tilting of the entire
edifice toward the axial zone. If such subsidence occurs it
probably results in uniformly tilted blocks or tilted blocks

which increase in dip with depth (Figure 42) and, although
it cannot explain the variety of dips observed in Holes 332A
and 332B, it may explain the more uniform dips and dip direc-
tions of the other holes studied.

Although the effect of subsidence-related tilting of
large blocks within the central valley or marginal tectonic
province is speculative, surface observations do indicate
that the volcanic carapace is significantly disrupted before
it leaves the valley floor. Flows are broken and offset by
numerous closely spaced faults and fissures (Ballard and van
Andel, 1977; Crane and Ballard, 1981; and Ballard and Moore,
1977), most delicate extrusive features of flows are destroyed
(Ballard and others, 1975) and in some areas it is impossible
to trace individual flow units laterally (Atwater and others,
1978).

Deformation Associated With the Formation of the Valley Walls

After formation of the extrusive layer, deformation oc-
curs as a consequence of uplift of incremental parcels of the
crust to form the valley walls and the incorporation of new
crust onto the passive plate margin. Four processes may oc-
cur at this area and during this time that could cause rota-
tion of rock units. These are: rotation of rock units along
curved or tilted normal faults, the formation of fault breccia,
rotation of the extrusive sequence due to diapiric rise or
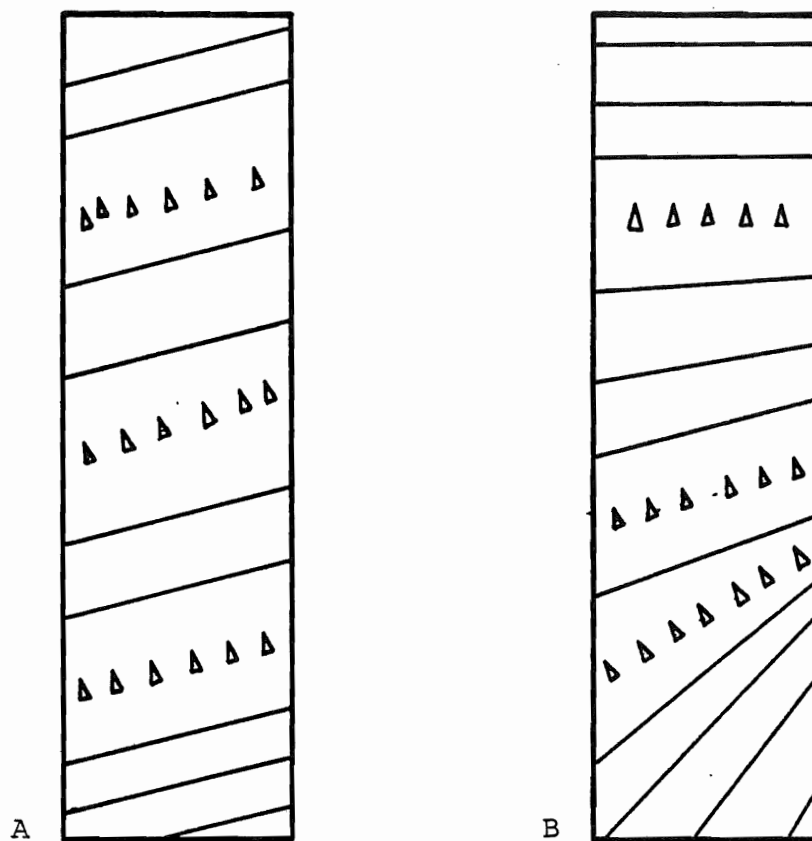
Figure 42. Schematic cross sections of uniformly dipping rocks (A) and rocks which increase in dip with depth (B). Section A may be expected if subsidence-related tilting occurs after formation of the volcanic carapace, whereas, B may develop if such tilting occurs during formation of the volcanic carapace. Triangles indicate possible layers of flow top breccia.

tectonic emplacement of gabbros and serpentinized perido-
tites, and mass wasting due to local gravitational instabil-
ity of rock masses.

Observations during submersible dives (Ballard and van
Andel, 1977; Atwater and others, 1978; and Stroup and Fox,
1981) indicate that the topography of the valley walls is
formed by a stair-step arrangement of normal faults dividing
blocks with widths of 10 to a couple hundred meters. Such
faults may be conjugate but the fault surfaces most commonly
exposed dip toward the rift axis at angles ranging from 45°
to 75° (MacDonald and Luyendyk, 1977; Atwater, 1979; and
Laughton and Searle, 1979). Although such faults are expected
to dip at 60°, as a consequence of the orientation of the
principal stress axes (Anderson, 1951), the faults may be-
come listric with depth due to increased confining pressure
(Anderson, 1971; and Hafner, 1951). Because of the occurrence
of talus at the base of these fault scarps the amount of ver-
tical displacement is poorly known but may range from 100 m
to 400 m (Ballard and van Andel, 1977; and Ramberg and van
Andel, 1977), to possibly as much as 650 m (Stroup and Fox,
1981) along faults located at the boundary between the valley
floor and the rift valley walls. These faults are discontin-
uous along strike, being disrupted (at intervals of 50 to a
few hundred meters on the Caymen rift valley walls) by faults
trending perpendicular to ridge axis, by removal of part of

the scarp by mass wasting, or by rotational movement of a fault block (MacDonald and Luyendyk, 1977; and Stroup and Fox, 1981). Movement along these faults of the valley walls as well as along associated antithetic or drag faults, (Hamblin, 1965; and Crane and Ballard, 1978) may result in substantial tilting of crustal blocks.

These closely spaced faults may be superimposed upon listric faults of a regional scale. As reviewed by Verosub and Moores (1981), listric faults have been repeatedly described in the Basin and Range province of the SW United States (Moores and others, 1969; Anderson, 1971; and Proffett, 1977) but only recently have been recognized as possibly being important structural features of oceanic crust (Verosub and Moores, 1981; and Laughton and Searle, 1979). According to the model presented by Verosub and Moores, (1981) major listric faults are likely to be separated by about 1 km horizontally and extend to depths of about 2 km. As a consequence of movement along such faults, rock units, which intersect the fault plane at a high angle (60° to 90°) (Anderson, 1951), may be nearly vertically dipping and overturned at depth where the fault plane flattens (Anderson, 1971; Moores and others, 1969; and Proffett, 1977).

These faulting mechanisms of both the local and regional scale, may explain the occurrence of the gently dipping rock units of Holes 334, 395, and 396, and may even lead to the formation of steeply dipping rocks as in Holes 332A and 332B.

If a fault plane is intersected, then changes in the dip of the rocks may be expected to occur across the fault plane (Figure 43). Such faulting, however, cannot explain the variability of dips and the complex assemblage of polarity reversals observed in Hole 332A. Furthermore, vertically dipping rocks are only likely to occur at depth where the fault planes flatten and may not be expected at the depths penetrated during drilling.

Fault breccia may occur along these fault planes or within fault zones. Fault zones may be 50 to 100 m wide and consist of a series of fault slivers separated by zones of cemented breccia, 20 to 50 cm thick, in tabular sheets which parallel fault planes (Ballard and van Andel, 1977). The rocks observed in such breccia zones consist of angular clasts (Ballard and van Andel, 1977; and Atwater, 1979) and it seems reasonable to expect clasts to be a chaotic assemblage of rocks of mixed age and lithology which have been randomly rotated. Such breccias may explain some of the complexities observed in the holes studied, especially the anomalously dipping rocks of Holes 395, 395A, and 396B, but generally lack the dimensions apparently necessary to account for most of the observed dips (Figure 44).

Diapiric rise or tectonic emplacement of gabbros or serpentinized peridotites may disrupt surrounding extrusive rocks. There is some evidence to suggest that there is cold
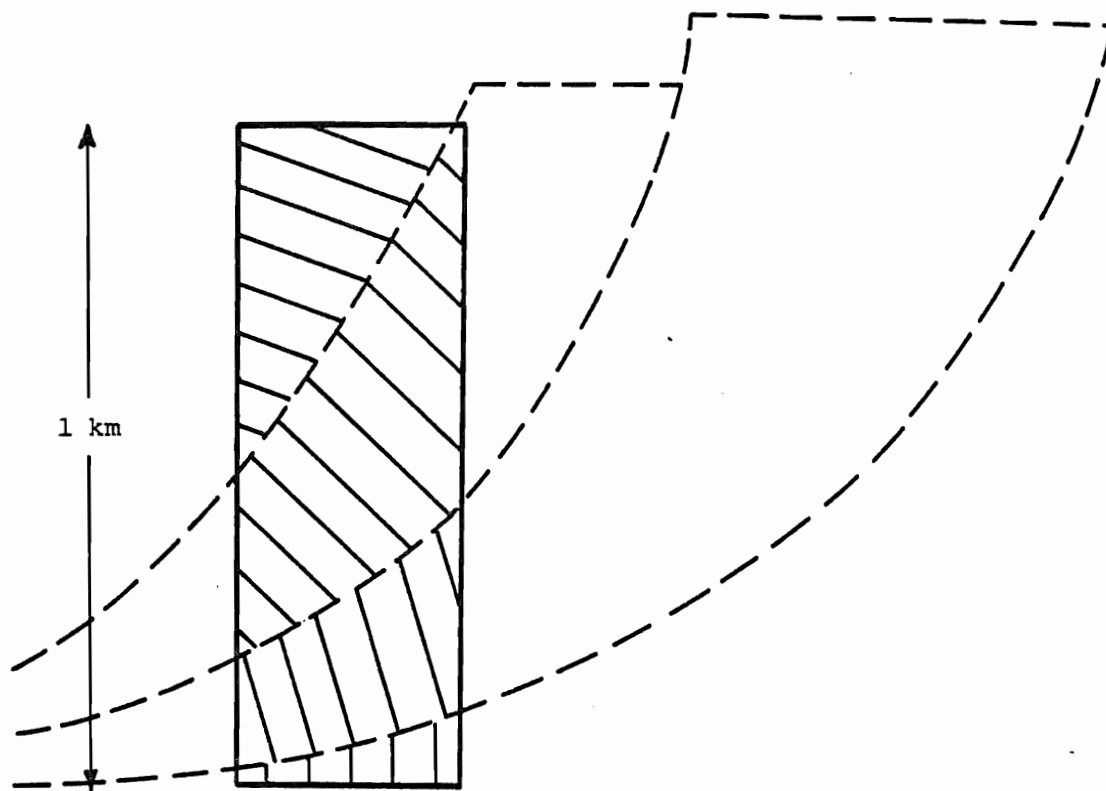
Figure 43. Schematic cross section showing possible distribution of dips in a vertical section through a series of tilted and listric faults. Dashed lines indicate fault planes. Dip may change abruptly across fault planes as well as increase with depth. Breccia may occur along fault plane.
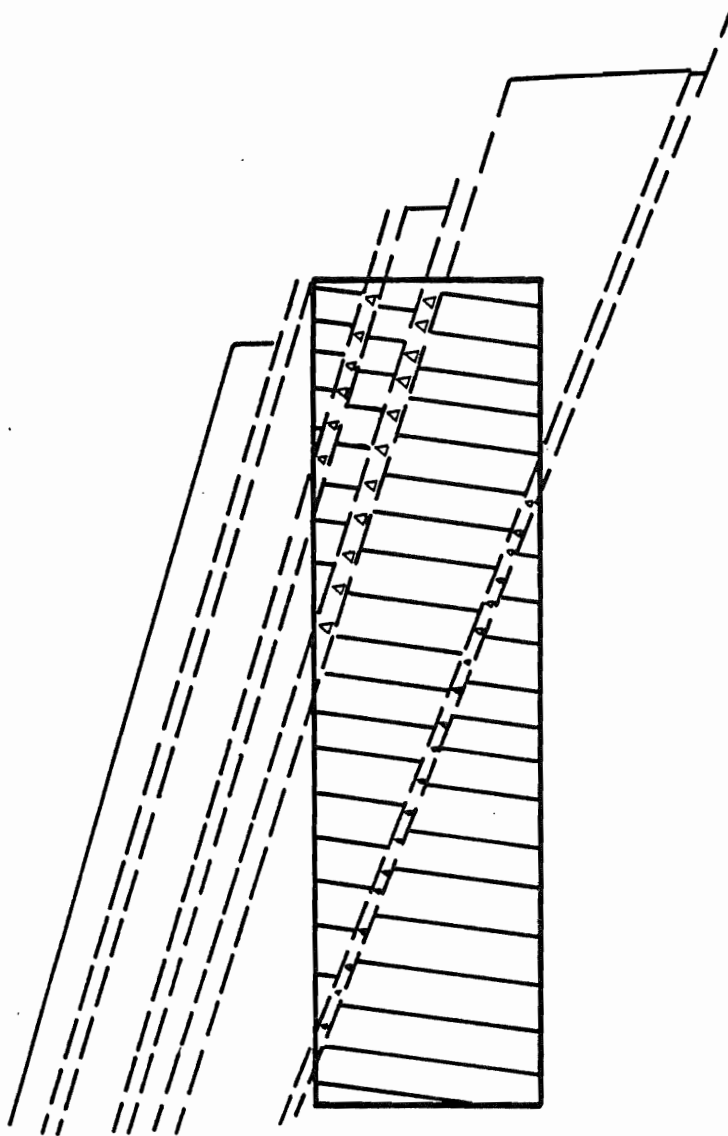
Figure 44. Schematic cross section showing possible distribution of coherently dipping and brecciated (triangles) layers in a vertical section through a fault zone.

emplacement of such rocks at shallow depths within the upper oceanic crustal layers (Helmstaedt, 1977; Arai and Fujaii, 1978; and Perfit, 1977). Studies of diapirism on land indicate that deformation resulting from diapirism can range from simple tilting of the surrounding rock layers away from the rising plug (Billings, 1972) to more complex faulting and tilting of faulted blocks (Atwater and Forman, 1959). In the Diablo Range, California, steeply dipping and overturned strata were observed in brecciated fault contact with "piercement" plugs of serpentine of the Franciscan complex (Oakeshott, 1968), although it is not clear how much of this deformation occurred prior to piercement. In the Paradox Basin in the central part of Upheaval dome, the complex of intensely deformed folded, faulted, steeply dipping and overturned strata may have formed as a result of diapiric flowage of salt at depth (Mattox, 1969). Country rock may even be incorporated into diapirically rising masses and emplaced at a shallower level (Bailey, 1926 in Freeman, 1968).

As of yet, however, there is no evidence to indicate that diapirism substantially disrupts the extrusive sequence on the sea floor. The basalts associated with serpentized rocks examined during this study are not significantly deformed (Holes 334, 395 and 395A).

Submarine mass wasting can also cause tilting of rocks.

In the mid-ocean environment mass wasting may result in the formation of talus ramps or slump blocks consisting of megabreccias, which may significantly modify the morphology of the rift valley and rift valley walls (Stroup and Fox, 1981).

Talus ramps were observed forming wedges, with horizontal and vertical dimensions of 100 m in the Famous area at the base of fault scarps along the valley walls. The talus consists of clasts 1 to 2 m in size and is expected to contain a chaotic assortment of rock fragments. Slump scars of undescribed dimensions were also observed along some of the fault faces (Ballard and van Andel, 1977).

Talus ramps are ubiquitous features of the rift valley walls of the Mid-Caymen Rise and may almost completely fill in the area between inward facing step-like fault scarps, forming gently sloping terraces. Talus fragments are gravel sized to greater than a meter in diameter (Stroup and Fox, 1981).

Large masses of megabreccia which can result from mass wasting have not been observed in the rift valley. However, because of the restricted field of view of a submersible diver, large slump blocks which have the same surficial characteristics as in-place rocks, may also appear to be in-place (P.J. Fox, per. com., 1981).

Mass wasting can occur any time the gravitational forces

acting to move material downslope exceed the cohesive and frictional forces acting to keep material from sliding. In the rifting environment, rocks exposed due to uplift along the valley walls are likely to lack cohesive strength because, as previously discussed, the volcanic carapace is significantly disrupted by faults and fissures produced on the valley floor. Drilling indicates the occurrence of poorly cemented brecciated layers or soft sediment layers between flows. Furthermore, the rocks exposed along fault scarps are observed in places to be jointed, fractured, and even foliated (Stroup and Fox, 1981). All of these features may act as planes of weakness along which downslope movement may occur. Additionally, earthquakes, which are a common phenomenon of accreting plate margins, may initiate mass wasting (Ericksen, 1974).

Subaerial examples of mass wasting by gravity sliding indicate that large masses of rock can be transported several km during sliding and are broken during transport resulting in the deposition of a megabreccia (Burchfiel, 1966). The megabreccia of the Black Mountain slide at the Nevada, Arizona border is at least 10 km long and a few hundred meters thick. It consists of a poorly sorted chaotic mixture of Black Mountain rocks with clasts as long as 100 m (Lowell, 1951).

This sort of mass wasting (Figure 45) could explain the apparently chaotic distribution of dip units, the variable size of these units, and the apparent repetition of
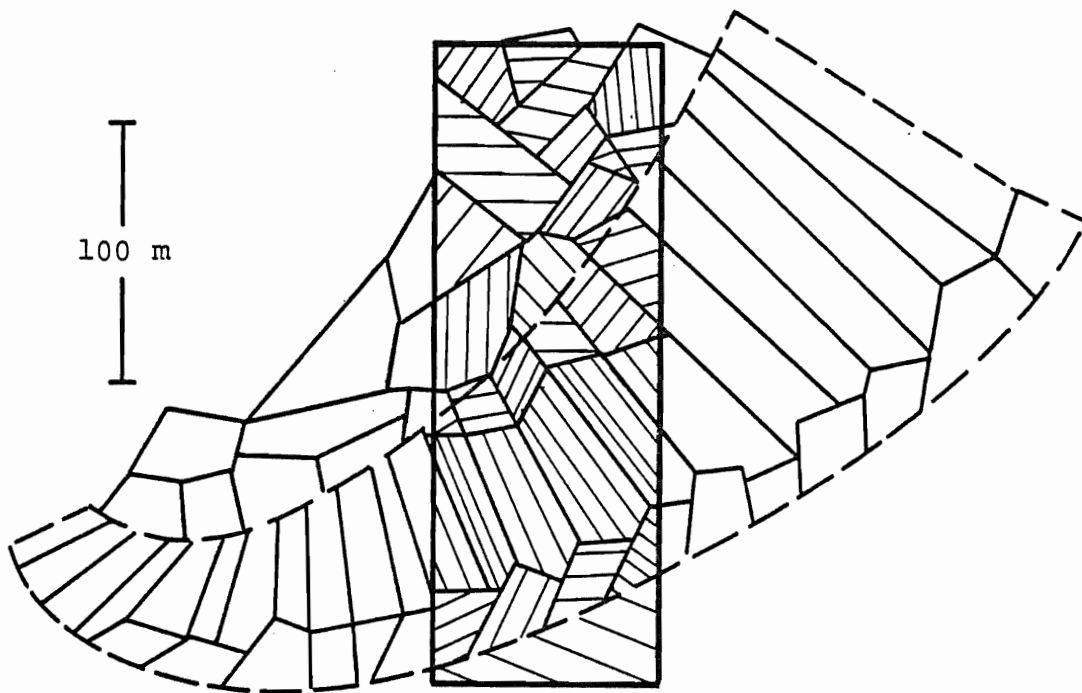
Figure 45. Schematic cross section showing possible random distribution of dips resulting from mass wasting of a fault scarp. The large slump block is disrupted at the base and overlain by blocks of talus.

corrected magnetic units in Hole 332A. Mass wasting may also be responsible for the steeply, but non-uniformly dipping rocks observed in the portion of the Hole 332B studied. Such a style of deformation also allows for the possibility that some areas of the sea floor rocks may resemble megabreccias, as Holes 332A and 332B, whereas, other areas may be only moderately deformed as Holes 334, 395 and 395A, and 396B, thus explaining the heterogeneity of dip unit complexity observed between the drill cores studied. Although it may seem unlikely for tilts resulting from mass wasting to have a uniform dip direction, blocks deposited by debris slides (Barnes, 1958, in Ericksen, 1974) and slump slides (Savage, 1968) may have consistent dip directions. The apparent change in dip direction with depth in Hole 332B (Figure 39) may suggest two episodes of sliding. If the boundary between slides is placed between samples 17.1 and 21.1, then the upper slide may be about 126 m thick and the observed thickness of the lower slide may be 156 m.

Conclusion

Results of the segregation vesicle studies presented suggest that the upper 500 m of oceanic crust in the North Atlantic is structurally heterogeneous. Although samples studied from Holes 334, 395 and 395A, and 396B, seem to be only gently dipping with the rare occurrence of steeply

dipping or overturned rocks, Holes 332A and 332B seem to be highly deformed, consisting of a random distribution of dips in the vertical section. Any explanation of the observed structures must account for this heterogeneity and also be consistent with the results of previous structural studies of mid-ocean ridges, where ocean crust probably acquires most of its structural complexities.

The deformational process suggested here is one in which coherent fault blocks located along the valley walls are separated by ramps of talus or megabreccia which resulted from mass wasting of uplifted fault blocks (Figure 46). Rocks within coherent fault blocks may be gently dipping due to preservation of tilts associated with subsidence of rocks in the median valley or due to rotation of fault blocks along the valley walls. Although the rocks within these blocks probably have uniformly shallow dips and uniform dip directions, there may be rare occurrences of steeply dipping rocks due to flow top brecciation, minor deformation associated with formation of the volcanic carapace, or small scale fault brecciation (Figures 42, 44 and 44). Holes 334, 395 and 395A, and 396B may have been recovered from crust which once formed such coherent fault blocks.

Uplifted fault blocks may be modified by mass wasting which results in the formation of piles of megabreccia consisting of a chaotic assortment of large blocks of randomly
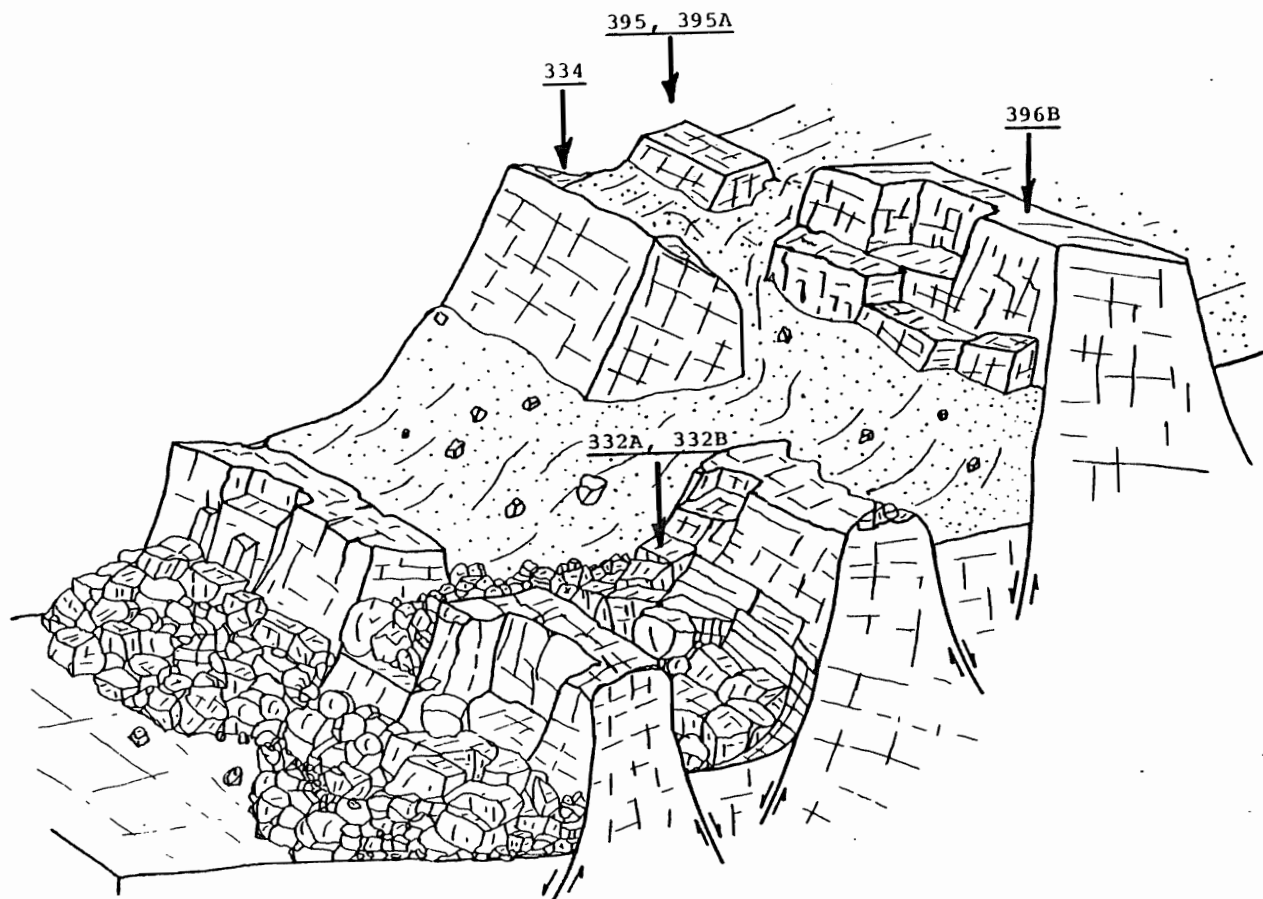
Figure 46. Schematic diagram showing possible structure of rift valley walls and indicating the type of deformation which may have caused the structures observed in the DSDP holes studied. Distribution of talus and configuration of faults is after Stroup and Fox (1981).

dipping rocks (Figure 45). Holes 332A and 332B may have pene-
trated rocks deposited by such mass wasting. Mass wasting
seems to be the simplest explanation for the apparently
complex assemblage of dip units observed in these holes and
the complex sequence of polarity reversals observed in Hole
332A.

As ocean crust ages it is subjected to much deformation
beginning with some sort of collapse of the volcanic edifice
followed by, fracturing, faulting, and fissuring of the crust
in the central valley region, uplift and faulting onto the
valley walls, and finally readjustment of the crust due to
cooling, contraction, and load of sediments. Because of this
history of structural evolution, the heterogeneity and com-
plexity of dips observed in these cores should be expected to
be typical of upper oceanic crustal layers in the North At-
lantic.

CONSEQUENCES FOR THE MAGNETIC SOURCE LAYER PROBLEM

Although sea floor magnetic lineations are used to de-
termine plate motions and spreading rates, the source of
this anomaly pattern is unclear. One of the most contro-
versial issues is whether or not the "source layer" is re-
stricted to the upper 500 to 700 m of oceanic basement or
extends to depths of several kms (Harrison, 1976; Johnson,
1979; and Blakely and Cande, 1979).

Results of the segregation vesicle studies presented

here suggest that rock units in the North Atlantic may commonly be tilted and that thick megabreccias of upper crustal rocks may form on the sea floor. This study, then, suggests that at least some of the time the magnetic source layer cannot be in the upper 500 m of oceanic crust because the rocks are structurally disturbed.

If deformation occurs by mass wasting and results in the formation of megabreccias, then it is possible that less deformed, more uniformly magnetized rocks occur at depth. However, if listric faults are common features of the mid-ocean ridge environment, then rocks are likely to be more steeply dipping and highly deformed at depth than at the surface.

If the source layer is within the upper 500 m of oceanic crust, then these segregation vesicle studies suggest that at least some of the time the surface magnetic anomaly may not be indicative of the earth's magnetic field at the time that portion of crust formed, but may record the results of a complex interaction between original magnetization and structural deformation. This possibility seems unlikely, however, because, with the exception of Hole 396B, the age of the rocks interpreted from the surface magnetic anomaly agrees with the paleontological age of the oldest sediment overlying basement rocks in the holes studied, suggesting that the anomaly reflects the original magnetization of the

crust.

Hole 396B presumably penetrated anomaly 5 age rocks. The age of the oldest sediment, however, is clearly older than the maximum age of this anomaly and corrected magnetic inclinations indicate that the bulk of the rocks recovered are reversely magnetized. Although the explanation of the anomalously old paleontological age is uncertain, the sediments show considerable re-working (Burky, 1978) possibly suggesting they were tectonically transported to their position above the older basement rocks (Johnson, 1978). The reversely magnetized basement rocks may have been extruded during one of the reversed events of anomaly 5.

Because the rocks studied in Holes 334, and 395 and 395A, are gently dipping, the in-place and corrected magnetic inclinations of the rocks studied are similar. In Hole 334 these inclinations agree with the surface magnetic anomaly. The corrected inclinations, however, are closer to the dipole value. Holes 395 and 395A, however, penetrated positive anomaly 4, and yet there are two polarity reversals in the vertical section. In fact, the in-place record indicates that only one third of the column is normally magnetized. These holes, however, may have penetrated one of the many reversed events of anomaly 4 (Melson, Rabinowitz and others, 1978b).

Although the interpretation of the magnetic anomaly observed above the crust in the vicinity of Holes 332A and 332B is controversial, all investigators agree that the crust

was formed during a polarity transition occurring between about 3.2 and 3.8 m.y. ago. This age is consistent with the paleontological age of the oldest sediments recovered. However, the rock units recovered in these holes may have been shuffled by mass wasting resulting in a repetition of rock and magnetic units. Prior to mass wasting the corrected magnetic units of Hole 332A may have had a depositional magnetic stratigraphy which might characterize a polarity transition. Normal and reversely magnetized units with dipolar inclinations may have been separated by a transition zone of rocks with non-dipolar inclinations.

Alternatively, the upper 500 m can be the magnetic source layer if the dips described in the cores studied do not occur on a regional scale, so that the magnetic signal of coherent blocks of rocks is much more important to the formation of the surface anomaly pattern than that produced by locally deformed rocks. The non-dipolar in-place inclinations and conflicting polarity relative to the surface anomaly, of many of the other rocks recovered from the North Atlantic by deep sea drilling (Yeats, Hart and others, 1976; Luyendyk, Cann and others, 1978a, b and c; and Donnelly, Francheteau and others, 1979b and c), however, suggests that tilted rocks are to be expected.

SUMMARY OF MAIN CONCLUSIONS

The main conclusions of this thesis are:

1) Segregation vesicles can be used to orient sea-floor basalts collected by dredge or submersible for paleomagnetic polarity studies, and can be used to determine the dip and corrected magnetic inclination of rocks recovered in drill cores which preserve the in-situ orientation of the rock.

2) The segregation vesicle technique of sea-floor basalt orientation is reliable, but because there is scatter to the individual segregation vesicle orientations in a rock sample, the error associated with dip determinations will usually be 36° or less, whereas the error associated with corrected magnetic inclination determinations will usually be $\pm 44.5^O$ or less.

3) Routine application of the technique will greatly increase the number of sea-floor basalt samples available for paleomagnetic polarity studies.

4) As a tool for determining the structural dip and corrected magnetic polarity of rocks recovered in drill cores, the segregation vesicle technique is unsurpassed. Routine application of this technique to basalts recovered in DSDP cores will provide more structural information than has ever been available from these holes.

5) Application of this technique to rocks recovered in DSDP Holes 332A, 332B, 334, 395 and 395A, and 396B, which pene-

trated North Atlantic oceanic crust, suggest that this crust is structurally heterogeneous. Rock samples studied in Holes 334, 395 and 395A, and 396B, suggest that the crustal layers penetrated are gently dipping and upright, whereas, rock samples studied in Holes 332A and 332B suggest that the crustal section penetrated is highly deformed and consists of steeply dipping and overturned rock units.

6) The deformational process suggested to explain the observed heterogeneity is one in which fault blocks, located along the valley walls, which are internally undeformed, or only moderately tilted, are separated by ramps of talus or megabreccia which resulted from mass wasting of the uplifted fault blocks.

7) Because of tilting, the true thickness (measured perpendicular to the dip) of rock units penetrated is going to be less than the vertical thickness. Where rocks are steeply dipping, as in Holes 332A and 332B, the true thickness may be 50 percent less than the vertical thickness. This indicates that the dip of rock units must be considered when trying to characterize the abundance of different lithologic units in a stratigraphic section of oceanic crust.

8) Tilting also causes reorientation of the magnetic direction acquired by the rock upon cooling, so that the in-place magnetic inclinations of rocks recovered in a drill core may be different from their original inclinations. This indicates

that segregation vesicles must be used to orient rocks recovered in drill cores before interpretations can be made about the depositional magnetic stratigraphy of the section of crust recovered. This tilting implies that if the source layer of marine magnetic lineations is in the upper 500 m of ocean basement crust then, at least some of the time, these lineations may not record the earth's magnetic field at the time that portion of crust formed, but instead may record the results of a complex interaction between initial magnetization and structural deformation. Alternatively this may be evidence for a deeper magnetic source layer.

REFERENCES

Ade-Hall, J., Aumento, F., and others, 1976, Sources of
    magnetic anomalies on the Mid-Atlantic Ridge: Na-
    ture, v. 255, p. 389-390.

Ade-Hall, J.M., Fink, L.K., and Johnson, H.P., 1976, Pe-
    trography of opaque minerals, Leg 34, in Hart, S.R.,
    and Yeats, R.S., eds., Initial Reports of the Deep
    Sea Drilling Project, v. 34: Washington (U.S.
    Government Printing Office) p. 349-362.

Anderson, E.M., 1951, The dynamics of faulting, Second
    edition: Edinburgh, Oliver and Boyd, 206 p.

Anderson, R.E., 1971, Thin skinned distension in Tertiary
    rocks of southeastern Nevada: Geological Society of
    America Bulletin, v. 82, p. 43-58.

Arai, S., and Fujii, T., 1978, Petrology of ultramafic rocks
    from site 395, in Melson, W.G., Rabinowitz, P.D., and
    others, Initial Reports of the Deep Sea Drilling Pro-
    ject, v. 45: Washington (U.S. Government Printing
    Office) p. 587-594.

ARCYANA, 1975, Transform fault and rift valley from bathy-
    scaph and diving saucer: Science, v. 190, p. 108-116.

Atwater, G.I. and Forman, M.J., 1959, Nature and growth
    of southern Louisiana salt domes and its effect on
    petroleum accumulation: American Association of Pe-
    troleum Geologists Bulletin, v. 43, p. 2592-2622.

Atwater, T.M., 1979, Constraints from the Famous area con-
    cerning the structure of the oceanic section, in
    Talwani, M., Harrison, C., and Hayes, E., eds., Deep Drilling
    Results in the Atlantic Ocean: Ocean Crust: Maurice
    Ewing Series 2, Ammerican Geophysical Union, Washington,
    D.C., p. 33-42.

Atwater, T.M., Ballard, R., and others, 1978, Expedition
    cruise report, AMAR 1978 - A coordinated submersible,
    photographic mapping and dredging program in the Mid-
    Atlantic Rift valleys near 37.5°N: Massachusetts In-
    stitute of Technology Internal Report, 203 p.

Atwater, T.M., and MacDonald, K.C., 1978, AMAR 78 preliminary
    results II: Gradiometer results in the Narrowgate
    magnetic anomaly region (abs.): EOS Transactions of
    the American Geophysical Union, v. 59, p. 1198.

Atwater, T.m., and Mudie, J.D., 1973, Detailed near bottom geophysical study of the Gorda rise: Journal of Geophysical Research, v. 78, p. 8665-8686.

Aumento, F., Melson, W.G., and others, 1977a, site 332, in Aumento, F., Melson, W.F., and others, Initial Reports of the Deep Sea Drilling Project, v. 37: Washington (U.S. Government Printing Office) p. 15-199.

_____, 1977b, site 333, in Aumento, F., Melson, W.G., and others, Initial Reports of the Deep Sea Drilling Project, v. 37: Washington (U.S. Government Printing Office) p. 201-238.

_____, 1977c, site 334, in Aumento, F., Melson, W.G., and others, Initial Reports of the Deep Sea Drilling Project v. 37: Washington (U.S. Government Printing Office) p. 239-287.

Bailey, E.B., Clough, C.T., and others, 1924, Tertiary and post-Tertiary geology of Mull, Loch Aline, and Oban: Memoirs of the Geological Survey, Scotland, 445 p.

Bailey, T.L., 1926, The Gueydan, a new middle Tertiary formation from the southwestern Coastal Plain of Texas: Texas University Bulletin 2645, 187 p.

Ballard, R.D., Bryan, W.B., Heirtzler, J.R., Keller, G., Moore, J.G., and van Andel, Tj., 1975, Manned submersible observations in the FAMOUS area: Mid-Atlantic Ridge: Science, v. 190, p. 103-108.

Ballard, R.D., and Moore, J.G., 1977, Photographic atlas of the Mid-Atlantic Ridge rift valley: Springer-Verlag, New York, 114 p.

Ballard, R.D., and van Andel, Tj.H., 1977, Project FAMOUS: Operational techiques and American submersible operations: Geological Society of America Bulletin, v. 88, p. 495-506.

Baragar, W.R.A., Plant, G.A., Pringle, G.J., and Schan, M., 1977, Petrology and alteration of selected units of Mid-Atlantic Ridge basalts sampled from sites 332 and 335, DSDP: Canadian Journal of Earth Sciences, v. 14, p. 837-874.

Barendregt, R.W., 1981, Dating methods of Pleistocene deposits and their problems: VI. Paleomagnetism: Geoscience Canada, v. 8, p. 56-64.

Batschelet, E., 1965, Statistical methods for the analysis of problems in animal orientation and certain biological rhythyms: American Institute of Biological Sciences, Washington, D.C., 57 p.

_____, 1972, Recent statistical methods for orientation data, in Galler, S.R., Schmidt-Koenig, K., Jacobs, G., and Belleville, R., eds., Animal Orientation and Navigation: National Aeronautics and Space Administration, Washington, D.C., p. 61-91.

Bellaiche, G., Cheminée, J.L., and others, 1974, Inner floor of the rift valley: First submersible study: Nature, v. 250, p. 558-560.

Bernoulli, D., Garrison, R.E., and McKenzie, J., 1978, Petrology, isotope geochemistry, and origin of dolomite and limestone associated with basaltic breccia, Hole 373A, Tyrrhenian Basin, in Hsu, K.J., Montadert, L., and others, Initial Reports of the Deep Sea Drilling Project, Part I: Washington (U.S. Government Printing Office) p. 541-558.

Bideau, D., Hekinian, R., and Francheteau, J., 1977, Orientation of ocean floor basaltic rocks at the time of cooling: A general method: Contributions to Mineralogy and Petrology, v. 65, p. 19-28.

Billings, M.P., 1972, Structural geology: Prentice-Hall Inc., Englewood Cliffs, New Jersey, 606 p.

Blakely, R.J., 1974, Geomagnetic reversals and crustal spreading rates during the Miocene: Journal of Geophysical Research, v. 79, p. 2979-2985.

Blakely, R.J., and Cande, S.C., 1979, Marine magnetic anomalies: Reviews of Geophysics and Space Physics, v. 17, p. 204-214.

Bleil, U., and Smith, B., 1979, Paleomagnetism of basalts, Leg 51, in Donnelly, T., Francheteau, J., Bryan, W., Robinson, P., Flower, M., Salisbury, M., and others, Initial Reports of the Deep Sea Drilling Project, v. 51, 52, and 53, Part 2: Washington (U.S. Government Printing Office) p. 1351-1361.

Bonhommet, N., and Babkine, J., 1967, Sur la presence d'aimantations inversees dan la chaines des puy: Compte-rendu hebdomadaire des seances de l'Academic des Sciences, Paris, v. 264, p. 92-94.

Bottinga, Y., and Weill, D.F., 1970, Densities of liquid silicate systems calculated from partial molar volumes of oxide components: American Journal of Science, v. 269, p. 169-182.

Bryan, W.B., 1972, Morphology of quench crystals in submarine basalts: Journal of Geophysical Research, v. 77, p. 5812-5819.

Bryan, W.B., and Moore, J.G., 1977, Compositional variations of young basalts in the Mid-Atlantic Ridge rift valley near 36°49'N: Geological Society of America Bulletin, v. 88, p. 566-570.

Burchfiel, B.C., 1966, Tin Mountain landslide, southeastern California, and the origin of megabreccia: Geological Society of America Bulletin, v. 77, p. 95-100.

Burky, D., 1978, Neogene coccolith stratigraphy, Mid-Atlantic Ridge, Deep Sea Drilling Project Leg 45, in Melson, W.G., Rabinowitz, P.D., and others, 1978, Initial Reports of the Deep Sea Drilling Project, v. 45: Washington (U.S. Government Printing Office), p. 307-317.

Carmichael, J.S.E., Turner, F.J., and Verhoogan, J., 1974, Igneous petrography: McGraw-Hill Book Company, San Francisco, California, 739 p.

Choukroune, P., 1979, Structural study of basaltic rocks showing brittle deformation (Deep Sea Drilling Project Legs 51, 52 and 53, sites 417 and 418), in Donnelly, T., Francheteau, J., Bryan, W., Robinson, P., Flower, M., Salisbury, M., and others, Initial Reports of the Deep Sea Drilling Project, v. 51, 52, and 53, Part II: Washington (U.S. Government Printing Office), p. 1491-1498.

Clark, M.J., Hall, J.M., and Peirce, J.W., 1978, Rock and paleomagnetic evidence for the existence and nature of a Cayman Trough spreading center: Canadian Journal of Earth Science, v. 15, p. 1930-1940.

Crane, K., and Ballard, R.D., 1978, AMAR 78, preliminary results: Narrowgate tectonics and structure (ANGUS results) (abs.): EOS Transactions of the American Geophysical Union, v. 59, p. 1198.

_____, 1981, Volcanics and structure of the Famous-Narrowgate Rift: evidence for cyclic evolution: Journal of Geophysical Research, v. 86, p. 5112-5124.

Delaney, J.R., Muenow, D.W., and Graham, D.G., 1978, Abundance and distribution of water, carbon and sulfur in glassy rims of submarine pillow basalts: Geochimica et Cosmochimica Acta., v. 42, p. 581-594.

Dick, H.J.B., Honnorez, J., and Kirst, P.W., 1978, Origin
of the abyssal basaltic sand, sandstone and gravel
from DSDP Hole 396B, Leg 46, in Dmitriev, L., Heritz-
ler, J., and others, Initial Reports of the Deep Sea
Drilling Project, v. 46: Washington (U.S. Govern-
ment Printing Office) p. 331-339.

Dietz, R.S., and Holden, J.C., 1970, Reconstruction of Pan-
gaea: Breakup and dispersion of Continents, Permian
to Present: Journal of Geophysical Research, v. 75,
p. 4939-4956.

Dmitriev, L., Heirtzler, J., and others, 1978a, Introduction
and explanatory notes, in Dmitriev, L., Heirtzler, J.,
and others, Initial Reports of the Deep Sea Drilling
Project, v. 46: Washington (U.S. Government Printing
Office) p. 3-13.

_____, 1978b, Holes 396A and 396B, in Dmitriev, L., Heirtz-
ler, J., and others, 1978, Initial Reports of the Deep
Sea Drilling Project, v. 46: Washington (U.S. Govern-
ment Printing Office) p. 15-86.

Donnelly, T.W., 1972, Deep-Water, shallow-water, and subaerial
island-arc volcanism: An example from the Virgin Islands:
Geological Society of America, Memoir 132, p. 401-414.

Donnelly, T.W., Francheteau, J., and others, 1979a, Intro-
duction and explanatory notes, in Donnelly, T., Fran-
cheteau, J., Bryan, W., Robinson, P., Flower, M.,
Salisbury, M., and others, Initial Reports of the
Deep Sea Drilling Project, v. 51, 52, and 53, Part I:
Washington (U.S. Government Printing Office) p. 5-22.

_____, 1979b, Site 417, in Donnelly, T., Francheteau, J.,
Bryan, W., Robinson, J., Flower, M., Salisbury, M.,
Initial Reports of the Deep Sea Drilling Project, v.
51, 52, and 53, Part 1: Washington (U.S. Government
Printing Office) p. 23-350.

_____, 1979c, Site 418, in Donnelly, T., Francheteau, J.,
Bryan, W., Robinson, P., Flower, M., Salisbury, M.,
and others, Initial Reports of the Deep Sea Drilling
Project, v. 51, 52, and 53, Part 1: Washington (U.S.
Government Printing Office) p. 351-626.

Duffield, A., 1978, Significance of contrasting vesicularity
in basalt from DSDP Sites 407, 408, and 409 on the west
flank of the Reykjanes Ridge, in Luyendyk, B.P., Cann,
J.R., and others, 1978, Initial Reports of the Deep
Sea Drilling Project, v. 49: Washington (U.S. Govern-
ment Printing Office) p. 715-719.

Elliott, R.B., 1956, The Eskdalemuir tholeiite and its contribution to an understanding of tholeiite genesis: Mineralogical Magazine, v. 31, p. 245-254.

Ericksen, G.E., 1974, Landslide incidence and mechanisms during earthquakes: Project Report, (IR) NC-37, U.S. Geological Survey, Reston, Virginia, 29 p.

Fisher, J.C., 1948, The fracture of liquids: Journal of Applied Physics, v. 19, p. 1062-1067.

Flower, M.F.J., Robinson, P.T., and Schmincke, H.-U., 1977, Petrology and geochemistry of igneous rocks, DSDP Leg 37, in Aumento, F., Melson, W.F., and others, Initial Reports of the Deep Sea Drilling Project, v. 37: Washington (U.S. Government Printing Office), p. 653-679.

Fox, P.J., and Opdyke, N.D., 1973, Geology of the oceanic crust: Magnetic properties of oceanic rocks: Journal of Geophysical Research, v. 78, p. 5139-5154.

Freeman, P.S., 1968, Exposed middle Tertiary mud diapirs and related features in south Texas, in Braunstein, J., and O'Brien, G.D., eds., Diapirs and Diapirism, A Symposium: American Association of Petroleum Geologists, Tulsa, Oklahoma, p. 162-182.

Greenwalt, D., and Taylor, P.T., 1978, Near-bottom magnetic measurements between the FAMOUS area and DSDP sites 332 and 333: Geological Society of America Bulletin, v. 89, p. 571-576.

Gross, M.G., 1972, Oceanography a view of the earth: Prentice-Hall, Inc., Englewood Cliffs, New Jersey, 581 p.

Hafner, W., 1951, Stress distribution and faulting: Geological Society of America Bulletin: v. 62, p. 373-391.

Hall, J.M., 1979, A model for the structure state of the upper half kilometer of North Atlantic Ocean layer 2, in Talwani, Harrison, C., and Hayes, D.E., eds., Deep Drilling Results in the Atlantic Ocean: Ocean Crust: Maurice Ewing Series 2, American Geophysical Union, Washington, D.C., p. 166-168.

Hall, J.M., and Robinson, P.T., 1979, Deep crustal drilling in the North Atlantic Ocean: Science, v. 204, p. 573-586.

Hall, J.M., and Ryall, P.J.C., 1977, Paleomagnetism of base-
    ment rocks, Leg 37, in Aumento, F., Melson, W.G., and
    others, Initial Reports of the Deep Sea Drilling Pro-
    ject, v. 37: Washington (U.S. Government Printing
    Office) p. 425-448.

Hamblin, W.K., 1965, Origin of "reverse drag" on the down-
    thrown side of normal faults: Geological Society of
    America Bulletin, v. 76, p. 1145-1164.

Hamilton, D.L., Burnham, C.W., and Osborne, E.F., 1964, The
    soluability of water and effects of oxygen fugacity
    and water content on crystallization in mafic magmas:
    Journal of Petrology, v. 5, p. 21-39.

Harker, A., 1904, The Tertiary igneous rocks of Skye: Memoirs
    of the Geological Society of the United Kingdom, 481 p.

Harrison, C.G.A., 1976, Magnetization of the oceanic crust:
    Geophysical Journal of the Royal Astronomical Society,
    v. 47, p. 257-283.

Heirtzler, J.R., 1975, Project FAMOUS, first voyages down to
    the Mid-Atlantic Ridge, where the earth turns inside out:
    National Geographic Magazine, v. 147, p. 586-603.

Heller, F., 1980, Self-reversal of natural remnant magnetiza-
    tion in the Olby-Laschamp lavas: Nature, v. 284, p. 334-
    335.

Heller, F., and Peterson, N., 1981, A self-reversal explanation
    for the Laschamp-Olby geomagnetic polarity event (abs.):
    EOS Transactions, American Geophysical Union, v. 62, no.
    17, p. 232.

Helmstaedt, H., 1977, Post magmatic textures and fabrics
    of gabbros and peridotites from DSDP Site 334, in Au-
    mento, F., and Melson, W., and others, Initial Reports
    of the Deep Sea Drilling Project, v. 37: Washington
    (U.S. Government Printing Office) p. 757-762.

Honnorez, J., Böhlke, J.K., and Honnorez-Guerstein, B.M.,
    1978, Petrographical and geochemical study of the low-
    temperature submarine alteration of basalt from Hole
    396B, in Dmitriev, L., Heirtzler, J., and others, Ini-
    tial Reports of the Deep Sea Drilling Project, v. 46:
    Washington (U.S. Government Printing Office), p. 299-330.

Irving, E., 1964, Paleomagnetism and its application to geo-
    logical and geophysical problems: John Wiley and Sons,
    Inc., New York, 399 p.

Johnson, C.H., 1939, New mathematical and "stereographic net" solutions to problem of two tilts - with applications to core orientation: Bulletin of the American Association of Petroleum Geologists, v. 23, p. 663-685.

Johnson, H.P., 1978, Paleomagnetism of igneous rock samples - DSDP Leg 45, in Melson, W.G., Rabinowitz, P.D., and others, Initial Reports of the Deep Sea Driling Project, v. 45: Washington (U.S. Government Printing Office), p. 387-406.

_____, 1979, Magnetization of the oceanic crust: Reviews of Geophysics and Space Physics, v. 17, p. 215-226.

Johnson, H.P., and Atwater, T.M., 1977, Magnetic study of basalts from the Mid-Atlantic Ridge, lat. 37°N: Geological Society of America Bulletin, v. 88, p. 637-647.

Johnson, H.P., and Merrill, R.T., 1973, Low-temperature oxidation of a titanomagnetite and the implications for paleomagnetism: Journal of Geophysical Research, v. 78, p. 4938-4949.

Johnson, J.R., 1979a, Transitional basalts and tholeiites from the East Pacific Rise, 9°N: Journal of Geophysical Research, v. 84, p. 1635-1651.

Judd, J.W., 1890, The porphylites of the Western Isles of Scotland, and their relation to the andesites and diorites of the district: Quarterly Journal of the Geological Society of London, v. 46, p. 340-385.

Juteau, T., Noack, Y., Whitechurch, H., and Courtois, C., 1979, Mineralogy and geochemistry of alteration products in Holes 417A and 417D basement samples (Deep Sea Drilling Project Leg 51), in Donnelly, T.W., Francheteau, J., Bryan, W., Robinson, P., Flower, M., Salisbury, M., and others, Initial Reports of the Deep Sea Drilling Project, v. 51, 52, and 53, Part 2: Washington (U.S. Government Printing Office) p. 1273-1297.

Keeton, W.T., 1969, Orientation by pigeons: is the sun necessary? Science, v. 165, p. 922-928.

Khitarov, N.I., and Kadik, A.A., 1973, Water and carbon dioxide in magmatic melts and pecularities of the melting process: Contributions to Mineralogy and Petrology, v. 41, p. 205-215.

Kuno, H., 1965, Fractionation trends of basaltic magmas in lava flows: Journal of Petrology, v. 6, p. 302-321.

Kuno, H., Yamasaki, K., Iida, C., and Nagashima, K., 1957, Differentiation of Hawaiian magmas: Japaneese Journal of Geology and Geography, v. 28, p. 179-218.

Kusznir, N.J., and Bott, M.H.P., 1976, A thermal study of the formation of oceanic crust: Geophysical Journal of the Royal Astronomical Society, v. 47, p. 83-85.

Lachenbruch, A.H., 1973, A simple mechanical model for ocean spreading centers: Journal of Geophysical Research, v. 78, p. 3395-3417.

Laughton, A.S., and Searle, R.C., 1979, Tectonic processes at slow spreading ridges, in Talwani, M., Harrison, C.G., and Hayes, D.E., Deep Drilling Results in the Atlantic Ocean: Ocean Crust: Maurice Ewing Series 2: American Geophysical Union, Washington D.C., p. 15-32.

Levine, H.S., 1972, Formation of vapor nuclei in high temperature melts: Journal of Physical Chemistry, v. 76, p. 2609-2614.

_____, 1973, Homogeneous nucleation of CO bubbles in Fe-C-O melts: Metallurgical Transactions, v. 4, p. 777-782.

Lowell, C.R., 1951, Megabreccia developed downslope from large faults: American Journal of Science, v. 249, p. 343-353.

Luyendyk, B.P., Cann, J.R., and others, 1978a, Site 407, in Luyendyke, B.P., Cann, J.R., and others, Initial Reports of the Deep Sea Drilling Project, v. 49: Washington (U.S. Government Printing Office) p. 21-100.

_____, 1978b, Site 410, in Luyendyk, B.P., Cann, J.R., and others, Initial Reports of the Deep Sea Drilling Project, v. 49: Washington (U.S. Government Printing Office) p. 227-313.

_____, 1978c, Site 411, in Luyendyk, B.P., Cann, J.R., and others, Initial Reports of the Deep Sea Drilling Project, v. 49: Washington (U.S. Government Printing Office) p. 315-338.

Luyendyk, B.P., and MacDonald, K.C. 1977, Physiography and structure of the inner floor of the FAMOUS rift valley: Observations with a deep-towed instrument package: Geological Society of America Bulletin, v. 88, p. 648-663.

MacDonald, K.C., 1976, Geomagnetic reversals and the deep drill hole at DSDP site 332: Journal of Geophysical Research, v. 81, p. 4163-4165.

_____, 1977, Near-bottom magnetic anomalies, asymmetric spreading, oblique spreading, and tectonics of the Mid-Atlantic Ridge near 37°N: Geological Society of America Bulletin, v. 88, p. 541-555.

MacDonald, K.C., and Atwater, T.M., 1978, AMAR 78 preliminary results: I. Evolution of the median rift (abs.): EOS Transactions of the American Geophysical Union, v. 59, p. 1198.

MacDonald, K.C., and Luyendyk, 1977, Deep-two studies of the structure of the Mid-Atlantic Ridge crest near lat 37°N: Geological Society of America Bulletin, v. 88, p. 621-636.

MacDonald, W.D., 1980, Net tectonic rotation, apparent tectonic rotation, and structural tilt correction in paleomagnetic studies: Journal of Geophysical Research, v. 85, p. 3659-3669.

Mardia, K.V., 1972, Statistics of directional data: Academic press, London, England, 357 p.

Mattox, R.B., 1968, Upheaval dome, a possible salt dome in Paradox Basin, Utah, in Braunstein, J., and O'Brien, G.D., eds., Diapirs and Diapirism, a symposium: American Association of Petroleum Geologists, Tulsa, Oklahoma, p. 215-227.

McElhinny, M.W., 1973, Palaeomagnetism and plate tectonics: Cambridge, Cambridge University Press, 358 p.

McElhinny, M.W. and Merrill, R.T., 1975, Geomagnetic secular variation over the past 5 m.y.: Reviews of Geophysics and Space Physics, v. 13, p. 687-708.

Melson, W.G., Rabinowitz, P.D., Natland, J.H., Bougault, H., and Johnson, H.P., 1978a, Cruise objectives and major results, analytical procedures, and explanatory notes, in Melson, W.G., Rabinowitz, P.D., and others, Initial Reports of the Deep Sea Drilling Project, v. 45: Washington (U.S. Government Printing Office) p. 5-20).

_____, 1978b, Site 395: 23°N, Mid-Atlantic Ridge, in Melson, W.G., Rabinowitz, P.D., and others, Initial Reports of the Deep Sea Drilling Project, v. 45: Washington (U.S. Government Printing Office) p. 131-264.

Miles, G.C., and Howe, R.C., 1977, Biostratigraphy summary, Leg 37, Deep Sea Drilling Project, in Aumento, F., Melson, W., and others, Initial Reports of the Deep Sea Drilling Project, v. 37: Washington (U.S. Government Printing Office) ·p. 977-983.

Mitchell, W.S., and Aumento, F., 1977, Fission track chronology of basaltic glasses, in Aumento, F., Melson, W., and others, Initial Reports of the Deep Sea Drilling Project, v. 37: Washington (U.S. Government Printing Office) p. 625-628.

Moore, J.G., 1965, Petrology of deep-sea basalt near Hawaii: American Journal of Sciences, v. 263, p. 40-52.

_____, 1970, Water content of basalt erupted on the ocean floor: Contributions to Mineralogy and Petrology, v. 28, p. 272-279.

Moore, J.G., Batchelder, J.N., and Cunningham, C.G., 1977, CO_2-filled vesicles in mid-ocean basalts: Journal of Volcanology and Geothermal Research, v. 2, p. 309-327.

Moore, J.G., and Calk, L., 1971, Sulfide spherules in vesicles of dredged pillow basalt: American Mineralogist, v. 56, p. 476-488.

Moores, E.M., Scott, R.B., and Lumsden, W.W., 1969, Tertiary tectonics of the White Pine - Grant Range region, east central Nevada, and some regional implications: Geological Society of America Bulletin, v. 79, p. 1703-1726.

Murase, T., and McBirney, A.R., 1973, Properties of some common igneous rocks and their melts at high temperatures: Geological Society of America Bulletin, v. 84, p. 3563-3592.

Natland, J.H., 1978, Chemical and magnetic stratigraphy of Holes 396 and 396B, in Dmitriev, L., Heirtzler, J., and others, 1978, Initial Reports of the Deep Sea Drilling Project, v. 46: Washington (U.S. Government Printing Office) p. 425-430.

Needham, H.D., Choukrone, P., Cheminée, J.L., Le Pichon, X., Francheteau, J., and Tapponnier, J., 1977, The accreting plate boundary: Ardoukoba Rift (northeast Africa) and the oceanic rift valley: Earth and Planetary Science Letters, v. 28, p. 439-453.

Needham, H.D., and Francheteau, J., 1974, Some characteristics of the rift valley in the Atlantic Ocean near 36°48' north: Earth and Planetary Science Letters, v. 22, p. 29-43.

Nicholls, G.D., 1958, Autometasomatism in the Lower Spilites of the Builth Volcanic Series: Quaterly Journal of the Geological Society of London, v. 114, p. 137-162.

Oakeshott, G.B., 1968, Diapiric structures in Diablo Range, California, in Braunstein, J., and O'Brien, G.D., eds., Diapirs and Diapirism, A Symposium: American Association of Petroleum Geologists, Tulsa Okalahoma, p. 228-243.

O'Reilly, W., and Banerjee, S.K., 1966, Oxidation of titanomagnetites and self-reversal: Nature, v. 211, p. 26.

Osann, 1889, in Neues. Jahrb. für Min. & c., v. I, p. 304.

Osmaston, M.F., 1971, Genesis of ocean ridge median valleys and continental rift valleys: Tectonophysics, v. 11, p. 387-405.

Ozima, M., Joshima, M., and Kinoshita, H., 1974, Magnetic properties of submarine basalts and the implications on the structure of oceanic crust: Journal of Geomagnetism and Geoelectricity, v. 26, p. 335-354.

Peck, D.L., Moore, J.G., Kojima, G., 1965, Crystallization of Alae lava lake, short note: U.S. Geological Survey Professional Paper 525-A, p. A160.

Peck, D.L., Wright, T.L., and Moore, J.G., 1966, Crystallization of tholeiitic basalt in Alae Lava Lake, Hawaii: Bulletin Volcanologique, v. 29, p. 629-656.

Perfit, M.R., 1977, Petrology and geochemistry of mafic rocks from the Cayman Trench: Evidence for spreading: Geology, v. 5, p. 105-110.

Peterson, N., 1978, Rock and paleomagnetism of basalts from site 396B, Leg 46, in Dmitriev, L., Heirtzler, J., and others, 1978, Initial Reports of the Deep Sea Drilling Project, v. 46: Washington (U.S. Government Printing Office) p. 357-362.

Peterson, N., Eisenach, P., and Bleil, U., 1979, Low temperature alteration of the magnetic minerals in ocean floor basalts, in Talwani, M., Harrison, C.G., and Hayes, D.E., eds., Deep Drilling in the Atlantic Ocean: Ocean Crust: American Geophysical Union, Washington, D.C., p. 169-209.

Phillips, F.C., 1971, The use of stereographic projection in structural geology, third edition: Edward Arnold Publishers Ltd., London, England, 90 p.

Phillips, J.D., and Fleming, H.S., 1978, Multi-beam sonar study of the Mid-Atlantic Ridge rift valley, 36°-37°N: Geological Soceity of America Map Series, MC-19.

Phillips, J.D., Fleming, H.S., Feden, R., King, W.E., and Perry, R., 1975, Aeromagnetic study of the Mid-Atlantic Ridge near the Oceanographer Fracture Zone: Geological Society of America Bulletin, v. 86, p. 1348-1357.

Prevot, M., Lecaille, A., Francheteau, J., Hekinian, R., 1976, Magnetic inclination of basaltic lavas from the Mid-Atlantic Ridge near $37^{O}N$: Nature, v. 259, p. 649-653.

Proffett, J.M.,Jr., 1977, Cenozoic geology of the Yerington District, Nevada, and implications for the nature and origin of Basin and Range faulting: Geological Society of America Bulletin, v. 88, p. 247-266.

Purdy, G.M., Rabinowitz, P.D., and Schouten, H., 1978, The Mid-Atlantic Ridge at $23^{O}N$: Bathymety and magnetics, in Melson, W.G., Rabinowitz, P.D., and others, Initial Reports of the Deep Sea Drilling Project, v. 45: Washington (U.S. Government Printing Office) p. 119-128.

Ragan, D.M., 1973, Structural geology, an introduction to geometrical techniques, second edition: John Wiley and Sons, New York, 208 p.

Ramberg, I.B., and van Adnel, Tj.H., 1977, Morphology and tectonic evolution of the rift valley at lat $36^{O}36'N$, Mid-Atlantic Ridge: Geological Society of America Bulletin, v. 88, p. 577- 586.

Robinson, P.T., 1980, Thin section descriptions of rocks collected from DSDP Holes 483B and 484A: Unpublished report, 10 p.

Robinson, P.T., Flower, M.J.F., Swanson, D.A., and Staudigel, H., 1979, Lithology and eruptive stratigraphy of Cretaceous oceanic crust, western Atlantic Ocean, in Donnelly, T., Francheteau, J., Bryan, W., Robinson, P., Flower, M., Salisbury, M., and others, Initial Reports of the Deep Sea Drilling Project, v. 51, 52,and 53, Part II: Washington (U.S. Government Printing Office) p. 1535-1555.

Rosendahl, B.R., 1976, Evolution of oceanic crust 2. Constraints, implications and inferences: Journal of Geophysical Research, v. 81, p. 5305-5314.

Rosendahl, B.R., Raitt, R.W., Dorman, L.M., Bibee, L.D., Hussong, D.M., and Sutton, G.H., 1976, Evolution of oceanic crust 1. A physical model of the East Pacific rise crest derived from seismic refraction data: Journal of Geophysical Research, v. 81, p. 5294-5304.

Rosner, D.R., and Epstein, M., 1972, Effects of interface kinematics, capillary and solute diffusion on bubble growth rates in highly supersaturated liquids: Chemical Engineering Science, v. 27, p. 69-88.

Ryall, P.J.C., and Ade-Hall, J.M., 1975, Radial variation of magnetic properties in submarine pillow basalt: Canadian Journal of Earth Science, v. 12, p. 1959-1969.

Sato, H., 1978, Segregation vesicles and immiscible liquid droplets in ocean-floor basalt of Hole 396B, IPOD/DSDP Leg 46, in Dmitriev, L., Heirtzler, J., and others, Initial Reports of the Deep Sea Drilling Project, v. 46: Washington (U.S. Government Printing Office) p. 283-291.

Savage, C.N., 1968, Mass wasting, in Fairbridge, R.W., ed., The Encyclopedia of Geomorphology, Encyclopedia of Earth Science Series, v. III: Reinhold Book Corporation, New York, p. 696-700.

Scarfe, C.M., 1973, Viscosity of basic magmas at varying pressure: Nature Physical Science, v. 241, p. 101.

Schmincke, H.-U., Robinson, P.T., Ohnmacht, W., and Flower, M.F.J., 1978, Basaltic hyaloclastites from Hole 396B, DSDP Leg 47, in Dmitriev, L., Heirtzler, J., and others, Initial Reports of the Deep Sea Drilling Project, v. 46: Washington (U.S. Government Printing Office) p. 341-355.

Shaw, H.R., 1972, Viscosities of magmatic silicate liquids: An empirical method of prediction: American Journal of Science, v. 272, p. 870-893.

Shibata, T., DeLong, E., and Walker, D., 1979, Abyssal tholeiites from the Oceanographer Fracture Zone: Contributions to Mineralogy and Petrology, v. 70, p. 89-102.

Sleep, N.H., 1969, Sensitivity of heat flow and gravity to the mechanism of sea floor spreading: Journal of Geophysical Research, v. 74, p. 542-549.

Sleep, N.H., and Rosendahl, B.R., 1979, Topography and tectonics of mid-ocean ridge axes: Journal of Geophysical Research, v. 84, p. 6831-6839.

Smith, R.E., 1967, Segregation vesicles in basaltic lava: American Journal of Science, v. 265, p. 696-713.

Sollas, 1892, _in_ Sci. Proc. Roy. Dubl. Soc. (2), v. VIII, p. 93.

Sparks, R.S.J., 1978, The dynamics of bubble formation and growth in magmas: A review and analysis: Journal of Volcanology and Geothermal Research, v. 3, p. 1-37.

Sparks, R.S.J., Meyer, P., and Sigurdsson, H., 1980, Density variation amongst mid-ocean ridge basalts: Implications for magma mixing and the scarcity of primitive lavas: Earth and Planetary Science Letters, v. 46, p. 419-430.

Spera, F.J., and Bergman, S.C., 1980, Carbon dioxide in igneous petrogenesis I: Aspects of the dissolution of CO_2 in silicate liquids: Contributions to Mineralogy Petrology, v. 74, p. 55-66.

Stephens, M.A., 1963, Random walk on a circle: Biometrika, v. 50, p. 385-390.

_____, 1969, A goodness-of-fit-statistic for the circle, with some comparisons: Biometrika, v. 56, p. 161-168.

Stroup, J.B., and Fox, P.J., 1981, Geologic investigations in the Caymen Trough: Evidence for thin oceanic crust along the Mid-Caymen Rise: Journal of Geology, v. 85, p.

Sykes, L.R., 1967, Mechanism of earthquakes and the nature of faulting on the mid-ocean ridges: Journal of Geophysical Research, v. 72, p. 2131-2153.

Talwani, M., Windisch, C.C., and Langseth, M.G., 1971, Reykjanes Ridge Crest, a detailed geophysical study: Journal of Geophysical Research, v. 76, p. 473-517.

Tapponnier, P., and Francheteau, J., 1978, Necking of the lithosphere and the mechanics of slowly accreting plate boundaries: Journal of Geophysical Research, v. 83, p. 3955-3970.

Teall, J.J.H., 1889, On the amygdaloids of the Tynemouth Dyke: Geological Magazine, v. VI, p. 481-483.

_____, 1899, Petrography of the igneous rocks lower Silurian formation of the southern Uplands, _in_ Peach, B.N., Horne, J., and Teall, J.J.H., The Silurian Rocks of Britain: Memoirs of the Geological Survey of the United Kingdom, v. I Scotland, p. 84-91.

Thompson, G., Bryan, W.B., Frey, F.A., Dickey, J.S. and Suen, C.J., 1976, in Yeats, R.S., Hart, S.R., and others Initial Reports of the Deep Sea Drilling Project, v. 34: Washington (U.S. Government Printing Office) p. 215-226.

Upton, B.G.J., and Wadsworth, W.J., 1971, Rhyodacite glass in Réunion Basalt: Mineralogical Magazine, v. 38, p. 152-159.

Vaniček, P., 1973, Introduction to adjustment calculus: Department of Survey Engineering, University of New Brunswick, Fredericton, New Brunswick, 241 p.

Varnes, D.J., 1958, Landslide types and processes, in Eckel, E.D., ed., Landslides and engineering practice: National Research Council, Highway Research Board, Special Report 29, p. 20-47.

Verhoogan, J., 1962, Oxidation of iron-titanium oxides in igneous rocks: Journal of Geology, v. 70, p. 168-181.

Verosub, K.L., and Moores, E.M., 1981, Tectonic rotations in extensional regimes and their paleomagnetic consequences for oceanic basalts: Journal of Geophysical Research, v. 86, p. 6335-6350.

Vincent, E.A., 1950, The chemical composition and physical properties of the residual glass of the Kap Daussy tholeiitic dyke, east Greenland: Mineralogical Magazine, v. 29, p. 46-62.

Vine, F.J., and Matthews, D.H., 1963, Magnetic anomalies over oceanic ridges: Nature, v. 199, p. 947-949.

Von Mises, R., 1918, Über die "Ganzzahligkeit" der Atomgewicht und verwandte Fragen: Physikal. Z., v. 19, p. 490-500.

Walker, F., Vincent, H.G.C., and Mitchell, R.L., 1952, The chemistry and mineralogy of the Kinkell tholeiite, Stirlingshire: Mineralogical Magazine, v. 29, p. 895-908.

Wells, G., Bryan, W.B., and Pearce, T.H., 1979, Comparative morphology of ancient and modern pillow lavas: Journal of Geology, v. 87, p. 427-440.

Wilcox, W.R., and Kuo, V.H.S., 1973, Gas bubble nucleation during crystallization: Journal of Crystal Growth, v. 19, p. 221-228.

Yeats, R.S., Hart, S.R., and others, 1976, Site 319, in
      Yeats, R.S., Hart, R.S., and others, Initial Reports
      of the Deep Sea Drilling Project, v. 34: Washington
      (U.S. Government Printing Office) p. 19-80.

Yeats, R.S., and Mathez, E.A., 1976, Decorated vesicles in
      deep-sea basalt glass, eastern Pacific: Journal of
      Geophysical Research, v. 81, n. 23, p. 4277-4284.

APPENDIX I

CALCULATION OF THE PERCENT VOLUME DIFFERENCE BETWEEN THE
PRINCIPAL AND SUBSIDIARY SURFACE OF A SEGREGATION VESICLE

In thin section the diameter, D, of the segregation vesicle to the principal surface is measured and the percent fill of aphanitic residue in the vesicle, F, is estimated.

The area, A, of a circular vesicle to the principal surface is given by,

$$A = \pi D^2/4.$$

The area, a, of the vesicle to the subsidiary surface is given by,

$$a = A \left[1 - (F \times 10^{-2}) \right].$$

The diameter, d, of this inner sphere, then is,

$$d = \sqrt{a(4)/\pi}.$$

The volumes of the spherical vesicle, V_1 and V_2, to the principal and subsidiary surface, respectively, are,

$$V_1 = \pi D^3/6,$$
$$V_2 = \pi d^3/6.$$

The percent volume difference, ΔV, between the two spheres is given by,

$$\Delta V = (1 - V_2/V_1) 100.$$

APPENDIX II

COMPUTER PROGRAM, CIRST: THE CIRCULAR STATISTICAL PACKAGE

```
1       C       NANCY A. GRUVER
        C       GEOLOGY DEPARTMENT
        C       DALHOUSIE UNIVERSITY
        C       HALIFAX, NOVA SCOTIA
5               PROGRAM CIRST(TAPE1,INPUT,TAPE5=INPUT,OUTPUT,TAPE6=OUTPUT,
               5TAPE24=0)
                DIMENSION SAMPO(3), DATA(100), TRIGAT(100,3), T(100),
               6GROOP(18,4), CP(100), UNIFM(100)
                CALL INITQ(750)
10      C SAMPLE NUMBER CAN HAVE 25 CHARACTERS.  ENTER IN
        C COLUMNS 1 - 25.
        C ENTER NUMBER OF ANGLES IN COLUMNS 26-28.
              4 READ(5,5)SAMPO,N
              5 FORMAT(2A10,A5,I3)
15              IF(N.EQ.1)GO TO 800
                SUM1=0.0
                SUM2=0.0
                DO 15 I=1,N
        C ENTER DATA IN COLUMNS 1 TO 4, USE DECIMAL.
20      C DATA ARE ROUNDED TO THE NEAREST DEGREE.
        C DATA CAN VARY FROM 0 TO 360 DEGREES.
                READ(5,10)DATA(I)
             10 FORMAT(F4.0)
                TRIGAT(I,1)=DATA(I)
25              CALL DR(DATA(I))
        C THIS COMPUTES CIRCULAR MEASUREMENTS OF CENTRAL
        C TENDANCY.  FIRST EACH ANGLE IS READ AND THE
        C SINE AND COSINE IS COMPUTED.
                COSN=COS(DATA(I))
30              SUM1=SUM1+COSN
                SINE=SIN(DATA(I))
                SUM2=SUM2+SINE
                TRIGAT(I,2)=COSN
             15 TRIGAT(I,3)=SINE
35              WRITE(6,25)SAMPO,N
             25 FORMAT(1H8/1H1,2A10,A5,*    N=*,I3,//,2X,*ANGLE      COSINE      SINE*)
                DO 30 I=1,N
             30 WRITE(6,31)TRIGAT(I,1),TRIGAT(I,2),TRIGAT(I,3)
             31 FORMAT(3X,F4.0,3X,F6.3,3X,F6.3)
40      C C IS THE AVERAGE OF THE COSINES.
        C S IS THE AVERAGE OF THE SINES.
                C=SUM1/N
                S=SUM2/N
```

```
C R IS THE LENGTH OF THE MEAN VECTOR.  IT
C VARIES FROM 0 - 1 ON A UNIT CIRCLE.
C VALUES APPROACHING 1 SIGNIFY WELL CLUSTERED DATA.
      R=(C**2.+S**2.)**0.5
      A=S/C
C THE MEAN DIRECTION IS COMPUTED AND CORRECTIONS
C ARE MADE SO IT APPEARS IN THE RIGHT QUADRANT.
      PMEAN=ATAN(A)
      PMEAN=PMEAN*(45./ATAN(1.))
      IF(R.LT.1.)GO TO 45
   35 WRITE(6,40)
   40 FORMAT(* ERROR IN CALCULATION OF R > 1*)
      STOP
   45 IF(C)55,50,60
   50 WRITE(6,51)
   51 FORMAT(* ERROR C=0*)
      STOP
   55 FMEAN=PMEAN+180.
      GO TO 80
   60 IF(S)70,65,75
   65 WRITE(6,66)
   66 FORMAT(* ERROR S=0*)
      STOP
   70 FMEAN=PMEAN+360.
      GO TO 80
   75 FMEAN=PMEAN
C SV=CIRCULAR VARIANCE.  IT RANGES FROM 0 TO 1.
C FOR WELL CLUSTERED DATA, SV APPROACHES 0.
   80 SV=1.-R
C SD=CIRCULAR STANDARD DEVIATION.
      SD=((2.*SV)**0.5)*(360./6.28)
C THIS SORTS THE DATA, AND COMPUTES THE CIRCULAR RANGE.
      CALL VSRTA(DATA,N)
      DO 82 I=1,N
   82 CALL RD(DATA(I))
      M=N-1
      DO 85 I=1,M
      J=I+1
   85 T(I)=DATA(J)-DATA(I)
      T(N)=360.-DATA(N)+DATA(1)
      CALL VSRTA(T,N)
      RANGE=360.-T(N)
C CPK IS THE CONCENTRATION PARAMETER.
C IT IS READ FROM A TABLE STORED IN TAPE 1.  IT RANGES
C FROM 0 TO INFINITY.  HIGH VALUES INDICATE
C WELL CLUSTERED DATA.  THE 95% CONFIDENCE INTERVALS OF CPK ARE
C ALSO COMPUTED.
```

```
      READ(1,90)(CP(I),I=1,100)
   90 FORMAT(F6.2)
      IR=R*100.
      CPK=CP(IR)
      DF=N-1
      P=0.95
      D=(SUM1**2.+SUM2**2.)**0.5
      CALL MDCHI(P,DF,X,IER)
      WRITE(6,91)X
   91 FORMAT(1X,*X(95%)=*,F10.3)
      CPKUP=X/(2.*(N-D))
      P=0.05
      CALL MDCHI(P,DF,X,IER)
      WRITE(6,92)X
   92 FORMAT(1X,*X(0.5)=*,F10.3)
      CPKLOW=X/(2.*(N-D))
      B=N*R*CPK
C SIGMA = 95% CONFIDENCE INTERVAL OF THE MEAN.
      SIGMA=(1.96/(B**0.5))*(180./3.14)
C THIS READS THE CRITICAL VALUE FOR THE RALEIGH TEST OF UNIFORMITY.
      READ(1,100)(UNIFM(I),I=1,100)
  100 FORMAT(F4.2)
      I=N
      UNIHYP=UNIFM(I)
C   GROUP THE DATA
C CLASS WIDTH = 20 DEGREES.
  900 DO 910 J=1,18
      GROUP(J,2)=0.
      GROUP(J,3)=0.
  910 GROUP(J,4)=N
      E=0.0
      Z=0.
      X=0.
      W=20.
      DO 200 I=1,N
  110 IF(DATA(I).LE.W)120,140
  120 X=X+1
      IF(I.EQ.N)GO TO 140
      GO TO 200
  140 E=E+1
      GROUP(E,1)=W
      GROUP(E,2)=X
      GROUP(E,3)=X**0.5
      GROUP(E,4)=Z+GROUP(E,2)
      Z=GROUP(E,4)
      IF(DATA(I).GT.W)205,206
```

```
      205 W=W+20.
          X=0.
          GO TO 110
      206 W=W+20.
          X=0.
      200 CONTINUE
          IF(Z.EQ.N)220,210
      210 WRITE(6,215)
      215 FORMAT(* ERROR Z IS NOT EQUAL TO N*)
          STOP
      220 WRITE(6,300)SAMPO,N
      300 FORMAT(1HB/1H1,*SAMPLE NUMBER=*,2A10,A5,*N=*,I3,//,3X,*ANGLES*,
         78X,*UPPER CLASS LIMIT  FREQUENCY  FREQUENCY(.5)  CUM.FREQ.*)
          E=0.
          I=0
      310 E=E+1
          I=I+1
          WRITE(6,320)DATA(I),GROUP(E,1),GROUP(E,2),GROUP(E,3),GROUP(E,4)
      320 FORMAT(1H ,2X,F4.0,16X,F4.0,11X,F4.0,9X,F5.2,9X,F4.0)
          IF(I.EQ.N)390,400
      400 IF(E.EQ.18)500,310
      390 IF(E.EQ.18)GO TO 600
      370 E=E+1
          WRITE(6,330)GROUP(E,1),GROUP(E,2),GROUP(E,3),GROUP(E,4)
      330 FORMAT(1H ,22X,F4.0,11X,F4.0,9X,F5.2,9X,F4.0)
          IF(E.EQ.18)600,370
      500 I=I+1
          WRITE(6,340)DATA(I)
      340 FORMAT(1H ,2X,F4.0)
          IF(I.EQ.N)600,500
      600 WRITE(6,620)C,S,R
      620 FORMAT(1H ,*   C=*,F5.3,*   S=*,F5.3,*   R=*,F5.3)
          IF(R.LT.UNIHYP)602,604
      602 WRITE(6,603)UNIHYP
      603 FORMAT(1X,*  CRITICAL VALUE=*,F4.2,*  ACCEPT UNIFORM HYPOTHESIS,
         9  NO PREFERRED ORIENTATION*)
          GO TO 700
      604 WRITE(6,605)UNIHYP
      605 FORMAT(1X,*  CRITICAL VALUE=*,F4.2,*  REJECT UNIFORM HYPOTHESIS,
         8 DATA IS PREFERENTIALLY ORIENTED*)
      700 WRITE(6,705)RANGE,FMEAN,SIGMA
      705 FORMAT(1X,*RANGE=*,F6.2,*   MEAN=*,F6.2,* +/- SIGMA(95%)=*,F6.2)
      710 WRITE(6,711)SV,SD
      711 FORMAT(1H ,*CIRCULAR VARIANCE=*,F6.2,*   STANDARD DEVIATION=*,
         7F6.2)
      720 WRITE(6,721)CPKLOW,CPK,CPKUP
      721 FORMAT(1H ,*CONCENTRATION PARAMETER=*,F5.2,* < *,F5.2,* < *,F5.2
```

```
              7,*  AT 90% CONFIDENCE*)
185           REWIND 1
              CALL CIRCPLT (GROUP(1,3) , SAMPO , N , FMEAN , SIGMA , R , UNIHYP)
              GO TO 4
          800 STOP
              END
```

SUBROUTINE DR   73/172 OPT=0 TRACE   FTN 4.8+528   81/09.

```
1             SUBROUTINE DR(X)
              PI=4.*ATAN(1.)
              X=X*PI/180.
              RETURN
5             END
```

SUBROUTINE RD   73/172 OPT=0 TRACE   FTN 4.8+528   81/09

```
1             SUBROUTINE RD(X)
              X=X*45./ATAN(1.)
              RETURN
              END
```

```
 1          SUBROUTINE CIRCPLT (POINTS,SAMPO,N,FMEAN,SIGMA,R,UNIHYP)
            COMMON /LAVSA/ AAA(750) /LAVSB/ BBB(750)
            COMMON /LAVSC/ CCC(750) /LAVSD/ DDD(6,750)
            DIMENSION POINTS(18) , LABEL(2) , Q(6)
 5          DIMENSION SAMPO (3)
            INTEGER PLOT , PENUP , PENDOWN
            DATA PI/3.1415926/ , BLANK/1R / , PENUP/0/ , PENDOWN/1/
            DATA NPLOT /-1/

10          XC = 3.50        $       YC = 4.00          $       RMAX = 2.50
            DT = 0.05        $       DS = PI / 9.00     $       PLOT = 0
            NPLOT = NPLOT + 1
            XC = XC + (NPLOT * 12.0)

15    CC
      CC
      CC ****** FIRST PRINT THE PLOT HEADING IN THE SAMPO ARRAY. CENTER IT
      CC         UNDER THE CENTER OF THE CIRCLE PLOT.
      CC
            DO 10 K=1,25
20             LAST = 26 - K
               CHAR = (SHIFT(SAMPO((LAST-1)/10) , ((6*MOD((LAST-1),10)+6))
           #          .AND. 77B))
               PRINT9,CHAR , BLANK
 9             FORMAT(" CHAR= ",O20," (BLANK = ",O20,")")
25             IF (CHAR .NE. BLANK) GO TO 20
      10    CONTINUE
            GO TO 30

20    CALL XFSTQ (XC , YC-RMAX-0.8 , 0.25 , 0.25 , 0.0 , 0.0 , Q)
30          CALL LABLQ (SAMPO , -LAST , Q , PLOT)

      CC
      CC ****** FIND THE MAXIMUM DATA POINT AND SET THE SCALE FACTOR FOR
      CC         DRAWING THE CIRCLE PLOT.
35    CC
30    AMAX = POINTS(1)
            DO 40 K=2,18
               IF (POINTS(K) .GT. AMAX) AMAX = POINTS(K)
      40    CONTINUE
40          SCALE = RMAX / AMAX
```

```
CC
CC ****** DRAW THE OUTER LIMIT CIRCLE FOR THE PLOT. THEN DRAW IN THE
CC        X AND Y AXISES AND LABEL THE POSITIVE Y AXIS.
CC
CC
      T1 = PI / 2.0
      T2 = T1 + 2.0 * PI
      CALL ARCSQ (XC , YC , RMAX , T1 , T2 , DT , PLOT)

      Y = YC + (RMAX + 0.2)
      CALL ADPTQ (XC , Y , PENUP , PLOT)
      Y = YC - (RMAX + 0.2)
      CALL ADPTQ (XC , Y , PENDOWN , PLOT)

      X = XC - (RMAX + 0.2)
      CALL ADPTQ (X , YC , PENUP , PLOT)
      X = XC + (RMAX + 0.2)
      CALL ADPTQ (X , YC , PENDOWN , PLOT)
      ANGLE = 1H0
      Y = YC + (RMAX + 0.3)
      CALL XFSTQ (XC , Y , 0.15 , 0.15 , 0.0 , 0.0 , Q)
      CALL LABLQ (ANGLE , -1 , Q , PLOT)

      ANGLE = 2H90
      X = XC + (RMAX + 0.3)
      Y = YC - 0.07
      CALL XFSTQ (X , Y , 0.15 , 0.15 , 0.0 , 0.0 , Q)
      CALL LABLQ (ANGLE , 2 , Q , PLOT)

      ANGLE = 3H180
      Y = YC - (RMAX + 0.5)
      CALL XFSTQ (XC , Y , 0.15 , 0.15 , 0.0 , 0.0 , Q)
      CALL LABLQ (ANGLE , -3 , Q , PLOT)

      ANGLE = 3H270
      X = XC - (RMAX + 0.3 + 0.5)
      Y = YC - 0.07
      CALL XFSTQ (X , Y , 0.15 , 0.15 , 0.0 , 0.0 , Q)
      CALL LABLQ (ANGLE , 3 , Q , PLOT)

      MAXN = IFIX((AMAX ** 2) +0.1)
      DO 50 K=1,MAXN
         X = XC - 0.05
         Y = YC + SQRT(FLOAT(K)) * SCALE
         CALL ADPTQ (X , Y , PENUP , PLOT)
         X = XC + 0.05
         CALL ADPTQ (X , Y , PENDOWN , PLOT)
         CALL XFSTQ (X+0.01 , Y-0.07 , 0.15 , 0.15 , 0.0 , 0.0 , Q)
```

```
              CALL NMBRQ (FLOAT(K) , -1 , 1 , Q , PLOT)
 90        50 CONTINUE

     CC
     CC
     CC ****** NOW DRAW THE 18 PIE SEGMENTS THAT MAKE UP THE CIRCLE PLOT.
     CC        THE RADIUS OF EACH SEGMENT IS PROPORTIONAL TO THE
 95  CC        CORRESPONDING DATA POINT.
     CC
           T1 = PI / 2.0
           CALL ADPTQ (XC , YC , PENUP , PLOT)
           DO 60 K=1,18
100           T2 = T1
              T1 = T1 - DS
              IF (POINTS(K) .EQ. 0.0) GO TO 60
              SR = SCALE * POINTS(K)
              X = XC + SR * COS(T1)
105           Y = YC + SR * SIN(T1)
              CALL ADPTQ (X , Y , PENDOWN , PLOT)
           CALL ARCSQ (XC , YC , SR , T1 , T2 , DT , PLOT)
              CALL ADPTQ (XC , YC , PENDOWN , PLOT)
           60 CONTINUE
110
     CC
     CC
           LABEL(1) = 10H N =
           CALL XFSTQ(XC+3.00,YC+2.75,0.15,0.15,0.00,0.00,Q)
115        CALL LABLQ(LABEL,4,Q,PLOT)
           CALL XFSTQ(XC+6.00,YC+2.75,0.15,0.15,0.00,0.00,Q)
           CALL NMBRQ(FLOAT(N),-1,1,Q,PLOT)

           LABEL(1) = 10HMEAN =
120        CALL XFSTQ(XC+3.00,YC+2.50,0.15,0.15,0.00,0.00,Q)
           CALL LABLQ(LABEL, 7,Q,PLOT)
           CALL XFSTQ(XC+6.00,YC+2.50,0.15,0.15,0.00,0.00,Q)
           CALL NMBRQ(FMEAN,2,1,Q,PLOT)

125        LABEL(1) = 10H95 PCT. SI
           LABEL(2) = 10HGMA =
           CALL XFSTQ(XC+3.00,YC+2.25,0.15,0.15,0.00,0.00,Q)
           CALL LABLQ(LABEL,15,Q,PLOT)
           CALL XFSTQ(XC+6.00,YC+2.25,0.15,0.15,0.00,0.00,Q)
130        CALL NMBRQ(SIGMA,3,1,Q,PLOT)
```

```
      LABEL(1) = 10HR =
      CALL XFSTQ(XC+3.00,YC+2.00,0.15,0.15,0.00,0.00,Q)
      CALL LABLQ(LABEL,10,Q,PLOT)
135   CALL XFSTQ(XC+6.00,YC+2.00,0.15,0.15,0.00,0.00,Q)
      CALL NMBRQ(R,2,1,Q,PLOT)
       LABEL(1) = 10HUNIHYP =
      CALL XFSTQ(XC+3.00,YC+1.75,0.15,0.15,0.00,0.00,Q)
      CALL LABLQ(LABEL,10,Q,PLOT)
140   CALL XFSTQ(XC+6.00,YC+1.75,0.15,0.15,0.00,0.00,Q)
      CALL NMBRQ(UNIHYP,3,1,Q,PLOT)

      CALL DISPQ(PLOT,100.0)
      CALL ADPTQ (XC , YC , 0 , PLOT)  $  CALL WEREQ (XD , YO)
145   CALL REMVQ(PLOT)

      RETURN
      END
```

Some measures of dispersion are computed by CIRST which are not critical to the segregation vesicle problem. These are described below.

Circular Range

Circular range is a measure of the smallest arc that includes all the measured angles. To calculate the range, the data are first sorted so that in the data set

$$\{ad_1 \ldots ad_n\}$$

ad_1 is the minimum value, and ad_n is the maximum value. The arc length between each angle is measured by

$$T_i = ad_{i+1} - ad_i, \quad i = 1, n - 1$$

$$T_n = 2\pi - ad_n - ad_1$$

T values are then sorted so that T_1 is the minimum value and T_n is the maximum arc length without any points in between. The circular range is then given by,

$$CR = 2\pi - T_n$$

(Mardia, 1972).

Circular Variance

Circular variance, CV, is a measure of the average difference between the mean direction and the smallest angle it makes with all the measured directions. It is given by

$$CV = 1 - \frac{1}{n} \sum_{i=1}^{n} \cos(ad_i - AD)$$

By manipulation of equations 3, 4, 5, 6, 7 and 8, it can be shown that

$$C = R \cos AD = \frac{1}{n} \sum_{i=1}^{n} \cos(ad_i) \text{ and,}$$

$$S = R \sin AD = \frac{1}{n} \sum_{i=1}^{n} \sin(ad_i)$$

and therefore,

$$CV = 1 - R.$$

Circular variance, therefore, ranges from 0 to 1. For well clustered data R approaches 1, so CV approaches 0 (Mardia, 1972, p. 22).

Circular Standard Deviation

Assuming a wrapped normal distribution, circular variance (CV) can be related to standard deviation (SD) by:

$$1 - CV = e^{-1/2 \, SD^2}.$$

The transformation of circular variance to standard deviation is, therefore, given by

$$SD = \{-2 \log (1 - CV)\}^{1/2}, \text{ in radians}$$

(Mardia, 1972, p. 74). Because the transformation is by the wrapped distribution, SD can range from 0 to infinity.

Confidence Intervals For the Concentration Parameter, $\hat{K}$

The 95 percent confidence interval for $\hat{K}$ is computed using a method described by Batschelet (1965). The upper and lower

values of X^2 (the test statistic of chi-square test) for P =
95 percent are read from a chi-square table for n - 1 degrees
of freedom. The upper and lower values for the confidence
interval of $\hat{K}$ ($\hat{K}u$ and $\hat{K}l$, respectively) are given by

$$Kl = \frac{X_l^2}{2(n-R)}, \qquad Ku = \frac{X_u^2}{2(n-R)}.$$

Graphs have been developed for determining confidence
intervals of $\hat{K}$ for $0 \leq \hat{K} \leq 5$. These are based on studies of
the theoretical distribution of R for a variety of circular
normal distributions by Stephens (1969, in Batschelet, 1972,
p. 78-80). Batschelet's (1965) method is included in CIRST
because it is more generally applicable. When $0 \leq \hat{K} \leq 5$, re-
sults can be compared to Stephen's graphs. The theoretical
acceptability of either method is not critical to the inter-
pretation of segregation vesicle data.

APPENDIX III

CRITICAL VALUES OF THE TEST STATISTIC R AT P=0.10 FOR THE RAYLEIGH TEST OF UNIFORMITY

Number of Measurements	R
5	.677
6	.618
7	.572
8	.535
9	.504
10	.478
11	.456
12	.437
13	.420
14	.405
15	.391
16	.379
17	.367
18	.357
19	.348
20	.339
21	.331
22	.323
24	.309
25	.303
30	.277
35	.256
40	.240
45	.226
50	.214
100	.150

Data are from Mardia (1972, Appendix 2.5)

APPENDIX IV

CRITICAL VALUES OF THE TEST STATISTIC u OF THE V-TEST

n	$P=0.10$	0.05	0.01	0.005	0.001	0.0001
5	$u=1.3051$	1.6524	2.2505	2.4459	2.7938	3.0825
6	1.3009	1.6509	2.2640	2.4695	2.8502	3.2114
7	1.2980	1.6499	2.2734	2.4858	2.8886	3.2970
8	1.2958	1.6492	2.2803	2.4978	2.9164	3.3578
9	1.2942	1.6486	2.2856	2.5070	2.9375	3.4034
10	1.2929	1.6482	2.2899	2.5143	2.9540	3.4387
11	1.2918	1.6479	2.2933	2.5201	2.9672	3.4669
12	1.2909	1.6476	2.2961	2.5250	2.9782	3.4899
13	1.2902	1.6474	2.2985	2.5290	2.9873	3.5091
14	1.2895	1.6472	2.3006	2.5325	2.9950	3.5253
15	1.2890	1.6470	2.3023	2.5355	3.0017	3.5392
16	1.2885	1.6469	2.3039	2.5381	3.0075	3.5512
17	1.2881	1.6467	2.3052	2.5404	3.0126	3.5617
18	1.2877	1.6466	2.3064	2.5424	3.0171	3.5710
19	1.2874	1.6465	2.3075	2.5442	3.0211	3.5792
20	1.2871	1.6464	2.3085	2.5458	3.0247	3.5866
21	1.2868	1.6464	2.3093	2.5473	3.0279	3.5932
22	1.2866	1.6463	2.3101	2.5486	3.0308	3.5992
23	1.2864	1.6462	2.3108	2.5498	3.0335	3.6047
24	1.2862	1.6462	2.3115	2.5509	3.0359	3.6096
25	1.2860	1.6461	2.3121	2.5519	3.0382	3.6142
26	1.2858	1.6461	2.3127	2.5529	3.0402	3.6184
27	1.2856	1.6460	2.3132	2.5538	3.0421	3.6223
28	1.2855	1.6460	2.3136	2.5546	3.0439	3.6258
29	1.2853	1.6459	2.3141	2.5553	3.0455	3.6292
30	1.2852	1.6459	2.3145	2.5560	3.0471	3.6323
40	1.2843	1.6456	2.3175	2.5610	3.0580	3.6545
50	1.2837	1.6455	2.3193	2.5640	3.0646	3.6677
60	1.2834	1.6454	2.3205	2.5660	3.0689	3.6764
70	1.2831	1.6453	2.3213	2.5674	3.0720	3.6826
100	1.2826	1.6452	2.3228	2.5699	3.0775	3.6936
500	1.2818	1.6449	2.3256	2.5747	3.0877	3.7140
1000	1.2817	1.6449	2.3260	2.5752	3.0890	3.7165

From Batschelet (1972)

APPENDIX V

DERIVATION OF THE FORMULAS FOR COMPUTING THE DIP AND TREND

The following derivation is after R. Boutilier, (per. com., 1980). This formalism is used because it is independent of arctangents. A mathematical model involving arctangents is not compatable with the error calculation because the derivation is undefined outside the field $-\pi/2 \leq atan(x) \leq +\pi/2$.

According to the coordinate system (Figure 16) the X, Y, and Z components of AD1 and AD2 are,

$$\hat{AD1} = (cosAD1, 0, sinAD1) \tag{1}$$

$$\hat{AD2} = (0, cosAD2, sinAD2) \tag{2}$$

$\vec{N}$, the normal to the (AD1, AD2) plane is given by the cross product of AD1 and AD2.

$$\vec{N} = \hat{AD1} \times \hat{AD2} - \begin{vmatrix} \hat{X} & \hat{Y} & \hat{Z} \\ cosAD1 & 0 & sinAD1 \\ 0 & cosAD2 & sinAD2 \end{vmatrix} \tag{3}$$

where X, Y, and Z are unit vectors.

The cross product of the two vectors is equivalent to the determinant of the vector matrix. The determinant of a matrix is given by,

$$\begin{vmatrix} a & b & c \\ d & e & f \\ g & h & i \end{vmatrix} = a(ei-hf) - b(di-gf) + c(dh-ge). \tag{4}$$

Therefore,

$$\vec{N} = A\hat{D}1 \text{ X } A\hat{D}2 = (-\cos AD2 \sin AD1, -\cos AD1 \sin AD2, \qquad (5)$$
$$\cos AD1 \cos AD2).$$

The magnitude of $\vec{N}$ is then given by,

$$|\vec{N}| = \sqrt{(\cos^2 AD2 \sin^2 AD1) + (\cos^2 AD1 \sin^2 AD2) + (\cos^2 AD1 \cos^2 AD2)}. \quad (6)$$

The unit vector, then, is,

$$\hat{N} = \vec{N}/|\vec{N}| \qquad (7)$$

The dip is calculated as the angle $\hat{N}$ makes with the Z axis (Figure 16). By the dot product rule, the dot product of two vectors is equal to the product of the two vectors times the angle between them. So that, given $\vec{A}$ and $\vec{B}$.

$$\vec{A} \cdot \vec{B} \quad A_X B_X + A_Y B_Y + A_Z B_Z$$
$$= |\vec{A}||\vec{B}|\cos\theta, \qquad (8)$$

where θ is the angle between the two vectors. Since $\hat{z} =$ (0, 0, 1),

$$\vec{N} \cdot \hat{z} = |\vec{N}||\hat{z}|\cos D, \qquad (9)$$

where D is the dip angle given by the angle between $\vec{N}$ and Z. Therefore, since $|\hat{z}| = 1$,

$$\{(\cos AD2 \sin AD1), (\cos AD1 \sin AD2), (\cos AD1 \cos AD2)\} \cdot (0,0,1) \quad (10)$$
$$= |\vec{N}|\cos D$$

The X and Y components drop out because they are multiplied by zero. Therefore,

$$\cos D = \frac{1}{|\vec{N}|}(\cos AD1 \cos AD2). \qquad (11)$$

The trend, T, will be the angle between the X axis and the projection of $-\vec{N}$ onto the (X, Y) plane. If $\vec{P}$ is the projection of $\vec{N}$ onto the (X, Y) plane, and $\vec{Q}$ is the projection of $\vec{N}$ onto the Z axis, then,

$$\vec{P} + \vec{Q} = \vec{N}, \quad \text{and} \tag{12}$$

$$\vec{P} = \vec{N} - \vec{Q}. \tag{13}$$

Because the projection of one vector onto another is given by the dot product of the two vectors times the vector onto which the other is being projected,

$$\vec{Q} = (\vec{N} \cdot \hat{Z})\hat{Z}. \tag{14}$$

By substitution of 14 into 13,

$$\vec{P} = \vec{N} - (\vec{N} \cdot \hat{Z})\hat{Z}. \tag{15}$$

$-\vec{P}$ is taken because, if the dip is upright, the trend of the dip direction will be in the opposite quadrant of the trend of the vector defining the pole to the plane. If the dip is overturned, both $\vec{P}$ and the dip direction will be in the same quadrant. In this case, 180° must be added to the resulting value for T.

$\vec{N}$ is known from (5). $(\vec{N} \cdot \hat{Z})$ is known from (9) and (11) and Z is known from (9). By substitution into (15),

$$\vec{P} = (-\cos AD2 \sin AD1, \; -\cos AD1 \sin AD2, \; +\cos AD1 \cos AD2) - \tag{16}$$
$$(0, \; 0, \; \cos AD1 \cos AD2).$$

Simplifying,

$$\vec{P} = (-\cos AD2 \sin AD1, \; -\cos AD1 \sin AD2, \; 0). \tag{17}$$

And,

$$|\vec{P}| = \sqrt{\cos^2 AD2 \sin^2 AD1 + \cos^2 AD1 \sin^2 AD2} \qquad (18)$$

T can now be determined as the angle $-\vec{P}$ makes with the X axis. By the dot product rule,

$$-\vec{P} \cdot \hat{X} = |-\vec{P}| \; |\hat{X}| \; \cos T. \qquad (19)$$

$\vec{P}$ and $|\vec{P}|$ are known from (17) and (18). $\hat{X} = (1,0,0)$.
Therefore, by substitution into (19),

$$\cos T = \frac{(+\cos AD2 \sin AD1 + \cos AD1 \sin AD2, \; 0) \cdot (1,0,0)}{|-\vec{P}|} \qquad (20)$$

Simplifying,

$$\cos T = \frac{\cos AD2 \; \sin AD1}{|\vec{P}|} \qquad (21)$$

APPENDIX VI

DERIVATION OF THE FORMULAS FOR COMPUTING THE ERROR IN THE
DIP AND TREND

The following derivations of the law of propagation

of the variance-covariance matrix (Vaníček, 1973) is after

R. Boutilier (per. com., 1980).

The following quantities are given:

AD1 and AD2,

ESAD1 and ESAD2, the 95 percent confidence interval of

AD1 and AD2, respectively, and

T and D.

The desired quantities are the error in $T = S_T$ and the

error in $D = S_D$. By the covariance law,

$$E_X = BE_L B^T. \tag{1}$$

E_X is the error matrix for the unknown variables. In this

case,

$$E_X = \begin{vmatrix} S_T{}^2 & S_{TD} \\ S_{DT} & S_D{}^2 \end{vmatrix}, \tag{2}$$

where $S_{DT} = S_{TD}$. E_L is the error matrix of the known quanti-

ties. In this case,

$$E_L = \begin{vmatrix} ESAD1^2 & ESAD12 \\ ESAD21 & ESAD2^2 \end{vmatrix} \tag{3}$$

Since there is no correlation between samples 1 and 2, ESAD12

ESAD21 = 0.

B is the matrix describing the relationship between the known and unknown variables. In this case,

$$B = \begin{vmatrix} \dfrac{\partial T}{\partial AD1} & \dfrac{\partial T}{\partial AD2} \\[2ex] \dfrac{\partial D}{\partial AD1} & \dfrac{\partial D}{\partial AD2} \end{vmatrix}. \tag{4}$$

B^T is the transposed B matrix which flips B about its diagonal, so that,

$$B^T = \begin{vmatrix} \dfrac{\partial T}{\partial AD1} & \dfrac{\partial D}{\partial AD1} \\[2ex] \dfrac{\partial T}{\partial AD2} & \dfrac{\partial D}{\partial AD2} \end{vmatrix}. \tag{5}$$

Therefore,

$$\begin{vmatrix} S_T^2 & S_{TD} \\[1ex] S_{DT} & S_D^2 \end{vmatrix} = \begin{vmatrix} \dfrac{\partial T}{\partial AD1} & \dfrac{\partial T}{\partial AD2} \\[2ex] \dfrac{\partial D}{\partial AD1} & \dfrac{\partial D}{\partial AD2} \end{vmatrix} \begin{vmatrix} ESAD1^2 & 0 \\[2ex] 0 & ESAD2^2 \end{vmatrix} \begin{vmatrix} \dfrac{\partial T}{\partial AD1} & \dfrac{\partial D}{\partial AD1} \\[2ex] \dfrac{\partial T}{\partial AD2} & \dfrac{\partial D}{\partial AD2} \end{vmatrix}. \tag{6}$$

By multiplication of the above matrices,

$$S_T^2 = \left(\frac{\partial T}{\partial AD1}\right)^2 ESAD1^2 + \left(\frac{\partial T}{\partial AD2}\right)^2 ESAD2^2, \tag{7}$$

$$S_D^2 = \left(\frac{\partial D}{\partial AD1}\right)^2 ESAD1^2 + \left(\frac{\partial D}{\partial AD2}\right)^2 ESAD2^2, \text{ and} \tag{8}$$

$$S_{TD} = S_{DT} = \left(\frac{\partial T}{\partial AD1} \cdot \frac{\partial D}{\partial AD2}\right) ESAD1^2 + \left(\frac{\partial T}{\partial AD2} \cdot \frac{\partial D}{\partial AD2}\right) ESAD2^2. \tag{9}$$

To solve equations (7), (8), and (9), the derivations of $\partial T/\partial AD1$, $\partial T/\partial AD2$, $\partial D/\partial AD1$ and $\partial D/\partial AD2$ are needed.

$\partial T/\partial AD1$ is given by:

$$\tan T = \tan AD2/\tan AD1 \tag{10}$$

$$\frac{\partial T}{\partial AD1} : \frac{\partial}{\partial AD1}(\tan T = \frac{\tan AD2}{\tan AD1}) \tag{11}$$

$$\therefore \sec^2 T \cdot \frac{\partial T}{\partial AD1} = \tan AD2(\frac{\tan AD1 \cdot 0 - 1 \cdot \sec^2 AD1}{\tan^2 AD1}) \tag{12}$$

$$\therefore \frac{\partial T}{\partial AD1} = \frac{-\tan AD2\cos^2 T}{\tan^2 AD1\cos^2 AD1} = \frac{-\tan AD2\cos^2 T}{\sin^2 AD1} \tag{13}$$

Similarly, $\partial T/\partial AD2$ is given by,

$$\sec^2 T \frac{\partial T}{\partial AD2} = \frac{1}{\tan AD1} \sec^2 AD2 \tag{14}$$

$$\therefore \frac{\partial T}{\partial AD2} = \frac{\cos^2 T}{\tan AD1\cos^2 AD1} \tag{15}$$

$\partial D/\partial AD1$ is given by,

$$\tan D = \tan AD1/\cos T \tag{16}$$

$$\frac{\partial D}{\partial AD1} : \frac{\partial}{\partial AD1}(\tan D = \frac{\tan AD1}{\cos T}) \tag{17}$$

$$\therefore \sec^2 D \frac{\partial D}{\partial AD1} = \frac{\cos T\sec^2 AD1 + \tan AD1^2\sin T}{(\cos T)^2} (\frac{\partial T}{\partial AD1}) \tag{18}$$

From equation (13),

$$\frac{\partial D}{\partial AD1} = \cos^2 D \{\frac{\cos T}{\cos^2 AD1} + \frac{\tan AD1\sin T(\frac{-\tan AD2\cos^2 T}{\sin^2 AD1})}{\cos^2 T}\} \tag{19}$$

Therefore,

$$\frac{\partial D}{\partial AD1} = \frac{\cos^2 D}{\cos^2 T} \{\frac{\cos T}{\cos^2 AD1} - \frac{\tan AD1\sin T\tan AD2\cos^2 T}{\sin^2 AD1}\} \tag{20}$$

Similarly,

$$\sec^2 D \, \frac{\partial D}{\partial AD2} = \frac{\tan AD1(\sin T \cdot \partial T/\partial AD2)}{\cos^2 T} \tag{21}$$

From equation (15)

$$\frac{\partial D}{\partial AD2} = \frac{\tan AD1 \sin T \cos^2 D}{\cos^2 T} \cdot \frac{\cos^2 T}{\tan AD1 \cos^2 AD2} \tag{22}$$

Simplifying,

$$\frac{\partial D}{\partial AD2} = \frac{\sin T \cos^2 D}{\cos^2 AD2} \tag{23}$$

It is possible, then, to solve equations (7), (8) and
(9), by substitution of equations (13), (15), (20), and
(23) as required.

APPENDIX VII

DERIVATION OF THE FORMULAS FOR COMPUTING THE CORRECTED MAGNETIC INCLINATION AND AZIMUTH OF THE TREND

The following derivation is after R. Boutilier, (per. com., 1980). This computation is used here because it is independent of arctangents. Arctangents are not compatable because they are undefined outside the field $-\pi/2 \leq atan(x) \leq +\pi/2$.

The following quantities are given:

$\hat{M}1$ = measured magnetic unit vector

$DEC1$ = declination of $\hat{M}1$

$ENC1$ = inclination of $\hat{M}1$

T = trend

D = dip

According to the coordinate system (Figure 17), the components of $\hat{M}1$ are,

$$M1_Z = sinENC1 \tag{1}$$

$$M1_X = cosENC1cosDEC1$$

$$M1_Y = cosENC1sinDEC1$$

After rotation of the XY plane about the Z axis until X' points in the direction of D,

$$M1_X' = M1_XcosT + M1_YsinT \tag{2}$$

$$M1_Y' = M1_YsinT + M1_YcosT$$

$$M1_Z' = M1_Z$$

The X'Z' plane is then rotated about the Y' axis by the angle D, so that X" is in the direction of D. Now the components of $\hat{M}1$ are,

$$Ml_X" = Ml_X'\cos D + Ml_Z'\sin D \tag{3}$$

$$Ml_Y" = Ml_Y'$$

$$Ml_Z" = -Ml_X'\sin D + Ml_Z'\cos D$$

The magnetic vector, then, has been rotated from,

$$\hat{M}1 = (Ml_X, Ml_Y, Ml_Z) \tag{4}$$

$$\text{to } \hat{M}1' = (Ml_X', Ml_Y', Ml_Z')$$

$$\text{to } \hat{M}1" = (Ml_X", Ml_Y", Ml_Z") = \hat{M}2.$$

The corresponding ENC2 of $\hat{M}2$ is,

$$\sin ENC2 = Ml_Z".$$

Therefore,

$$ENC2 = \sin^{-1}(Ml_Z") \tag{5}$$

The corresponding DEC2 of $\hat{M}2$ is,

$$\cos DEC2 = Ml_X"/\cos ENC2.$$

Therefore,

$$DEC2 = \cos^{-1}(Ml_X"/\cos ENC2). \tag{6}$$

DEC2 is the clockwise angle between T=0 degrees and DEC2. The azimuth of the trend, AZI, then is,

$$AZI = 360 - DEC2. \tag{7}$$

APPENDEX VIII

DERIVATION OF THE FORMULAS FOR COMPUTING THE ERROR IN
THE CORRECTED MAGNETIC INCLINATION AND THE AZIMUTH OF
THE TREND

The following quantities are given:

ENC2 and AZI,

T and D,

S_T, S_D and S_{TD}.

The desired quantity is the error in ENC2 = S_E and
the error in AZI = S_A. By the covariance law,

$$E_X = B \ E_L \ B^T \tag{1}$$

E_X is the error matrix for the unknown variables. In
this case,

$$E_X = \begin{vmatrix} S_A^2 & S_{AE} \\ S_{EA} & S_E^2 \end{vmatrix} \tag{2}$$

E_L is the error matrix of the known quantities. In this
case,

$$E_L = \begin{vmatrix} S_T^2 & S_{DT} \\ S_{TD} & S_D^2 \end{vmatrix} \tag{3}$$

B is the matrix which describes the relationship between
the known and unknown variables. In this case,

$$B = \begin{vmatrix} \dfrac{\partial AZI}{\partial T} & \dfrac{\partial AZI}{\partial D} \\ \dfrac{\partial ENC2}{\partial T} & \dfrac{\partial ENC2}{\partial D} \end{vmatrix} \tag{4}$$

B^T is the transposed B matrix, given by,

$$B^T = \begin{vmatrix} \dfrac{\partial AZI}{\partial T} & \dfrac{ENC2}{\partial T} \\[2em] \dfrac{\partial AZI}{\partial D} & \dfrac{ENC2}{\partial D} \end{vmatrix} \tag{5}$$

By multiplication of matrices (3), (4) and (5) according to the covariance law,

$$S_A^2 = \left(\frac{\partial AZI}{\partial T}\right)^2 S_T^2 + 2\left(\frac{\partial AZI}{\partial T} \frac{\partial AZI}{\partial D} (S_{TD})\right) + \left(\frac{\partial AZI}{\partial D}\right)^2 S_D^2, \tag{6}$$

and

$$S_E^2 = \left(\frac{\partial ENC2}{\partial T}\right)^2 S_T^2 + 2\left(\frac{\partial ENC2}{\partial T} \frac{\partial ENC2}{\partial D} (S_{TD})\right) + \left(\frac{\partial ENC2}{\partial D}\right)^2 S_D^2. \tag{7}$$

Derivations of $\partial AZI/\partial D$, $\partial AZI/\partial T$, $\partial ENC2/\partial D$ and $\partial ENC2/\partial T$ are required. Since,

$$sinENC2 = Ml_Z",$$

$$cosENC2(\frac{\partial ENC2}{\partial T}) = \frac{\partial Ml_Z"}{\partial T}. \tag{8}$$

Therefore,

$$\frac{\partial ENC2}{\partial T} = \frac{1}{cosENC2} \frac{\partial Ml_Z"}{\partial T} \tag{9}$$

Similarly,

$$\frac{\partial ENC2}{\partial D} = \frac{1}{cosENC2} \frac{\partial Ml_Z"}{\partial D}. \tag{10}$$

Since,

$$cosAZI = cosDEC2 = \frac{Ml_X"}{cosENC2}$$

$$-\sin AZI \frac{\partial AZI}{\partial T} = \frac{\cos ENC2 \, \partial Ml_X''/\partial T + Ml_X''\sin ENC2 \, \partial ENC2/\partial T}{(\cos(ENC2))^2} \qquad (11)$$

Therefore,

$$\frac{\partial AZI}{\partial T} = \frac{-1}{\sin AZI \cos^2 ENC2} \{ \cos ENC2 \frac{\partial Ml_X''}{\partial T} + Ml_X'' \cdot \qquad (12)$$

$$\sin ENC2 \frac{\partial ENC2}{\partial T} \}$$

Similarly,

$$\frac{\partial AZI}{\partial D} = \frac{-1}{\sin AZI \cos^2 ENC2} \{ \cos ENC2 \frac{\partial Ml_X''}{\partial D} + Ml_X''\sin ENC2 \cdot \qquad (13)$$

$$\cdot \qquad \frac{\partial ENC2}{\partial D}$$

Derivations of $\partial Ml_Z''/\partial T$, $\partial Ml_Z''/\partial D$, $\partial Ml_X''/\partial T$ and $\partial Ml_X''/\partial T$ are needed. Since,

$$Ml_Z'' = -Ml_X'\sin D + Ml_Z'\cos D, \qquad (14)$$

$$\frac{\partial Ml_Z''}{\partial T} = -\frac{\partial Ml_X'}{\partial T}\sin D + \frac{\partial Ml_Z'}{\partial T}\cos D. \qquad (15)$$

However,

$$\frac{\partial Ml_Z''}{\partial D} = Ml_X'\cos D - Ml_Z'\sin D \qquad (16)$$

Since,

$$Ml_X'' = Ml_X'\cos D + Ml_Z'\sin D \qquad (17)$$

$$\frac{\partial Ml_X''}{\partial T} = \frac{\partial Ml_X'}{\partial T}\cos D + \frac{\partial Ml_Z'}{\partial T}\sin D. $$

However,

$$\frac{\partial Ml_X''}{\partial D} = -Ml_X'\sin D + Ml_Z'\cos D. \qquad (19)$$

Derivations of $\partial Ml_X'/\partial T$ and $\partial Ml_Z'/\partial T$ are needed.
Since,

$$Ml_X' = Ml_X \cos T + Ml_Y \sin T \qquad (20)$$

$$\frac{\partial Ml_X'}{\partial T} = -Ml_X \sin T + Ml_Y \cos T. \qquad (21)$$

Since,

$$Ml_Z' = Ml_Z \qquad (22)$$

$$\frac{\partial Ml_Z'}{\partial T} = 0. \qquad (23)$$

By substitution of (21) and (23) into (18),

$$\frac{\partial Ml_X''}{\partial T} = \cos D(Ml_Y \cos T - Ml_X \sin T). \qquad (24)$$

By substitution of (21) and (23) into (15),

$$\frac{\partial Ml_Z''}{\partial T} = -\sin D(Ml_Y \cos T - Ml_X \sin T). \qquad (25)$$

Therefore, from (9) and (25)

$$\frac{\partial ENC2}{\partial T} = \sin D \frac{(Ml_X \sin T - Ml_Y \cos T)}{\cos ENC2} \qquad (26)$$

By substitution of (16) into (10),

$$\frac{\partial ENC2}{\partial D} = -\frac{(Ml_Z' \sin D + Ml_X' \cos D)}{\cos ENC2} \qquad (27)$$

By substituting (24) into (12),

$$\frac{\partial AZI}{\partial T} = \frac{-1}{\sin AZI \cos^2 ENC2} \{\cos ENC2 \cos D \cdot \qquad (28)$$

$$(Ml_Y \cos T - Ml_X \sin T) + Ml_X'' \sin ENC2 (\frac{\partial ENC2}{\partial T})\}$$

$\partial ENC2/\ T$ is given by (26).

By substituting (19) into (13),

$$\frac{\partial AZI}{\partial D} = \frac{-1}{sinAZIcos^2ENC2} \ \{-cosENC2(Ml_X'sinD - Ml_Z'cosD) \qquad (29)$$

$$+ \ Ml_X"sinENC2(\partial ENC2/\partial D)\}$$

$\partial ENC2/\partial D$ is given by (27).

S_A^2 can now be solved by substitution of (28) and (29) into (6). S_E^2 can be solved by substitution of (26) and (27) into (7).

APPENDIX IX

COMPUTER PROGRAM ROTSTAT

```
          PROGRAM ROTSTAT(INPUT,OUTPUT,TAPE1=INPUT,TAPE2=OUTPUT)
          DIMENSION TITLE(8)
          REAL MX,MY,MZ,MX1,MY1,MZ1,MX2,MY2,MZ2
          DATA PI/3.14159/
    C
    C        FIRST TRY AUGUST 7, 1980
    C
    C     THIS IS PROGRAM ROTSTAT.
    C     ---- -- ------- --------
    C     IT IS USED IN CONJUNCTION WITH
    C     THE SEGREGATION VESICLE TECH-
    C     NIQUE OF SEA FLOOR BASALT
    C     ORIENTATION
    C
    C     THE PURPOSE OF THIS PROGRAM
    C     IS TO:
    C       1.  COMPUTE THE TRUE DIP AND
    C           TREND (DIP DIRECTION) OF
    C           A BED USING THE TWO AVER-
    C           AGE APPARENT DIPS MEASURED
    C           IN EACH THIN SECTION OF A
    C           PAIR OF MUTUALLY PREPEN-
    C           DICULAR THIN SECTIONS FROM
    C           ONE ROCK SAMPLE.
    C
    C       2.  COMPUTE THE ERROR (95%
    C           CONFIDENCE INTERVAL) OF
    C           THE DIP AND TREND AS A
    C           FUNCTION OF THE ERROR
    C           ASSOCIATED WITH EACH
    C           APPARENT DIP.
    C
    C       3.  COMPUTE THE DIRECTION OF
    C           MAGNETIZATION AQUIRED BY
    C           THE ROCK UPON COOLING
    C           (PRESUMABLY IN A HORIZON-
    C           TAL POSITION) BY A SIMUL-
    C           TANEOUS ROTATION OF THE
    C           BED AND MEASURED MAGNETIC
    C           DIRECTION, AS THE BED IS
    C           ROTATED BACK TO THE HORI-
    C           ZONTAL POSITION.
```

```
43  C
44  C       4.    CALCULATE THE AZIMUTH OF
45  C             THE TREND ASSUMING THE
46  C             MAGNETIC DECLINATION
47  C             POINTS NORTH, IF NORMALLY
48  C             MAGNETIZED, OR SOUTH,
49  C             IF REVERSELY MAGNETIZED.
50  C
51  C       5.    COMPUTE THE ERROR (95%
52  C             CONFIDENCE INTERVAL) OF
53  C             THE CALCULATED MAGNETIC
54  C             INCLINATION AND AZIMUTH
55  C             OF THE TREND AS A FUNCTION
56  C             OF THE ERROR ASSOCIATED
57  C             WITH THE ORIENTATION OF
58  C             THE BED.
59  C
60  C       6.    CALCULATE THE ERROR (95%
61  C             CONFIDENCE INTERVAL) OF
62  C             THE CALCULATED INCLINATION
63  C             AND AZIMUTH OF THE TREND
64  C             ASSUMING THAT THE ERROR
65  C             ASSOCIATED WITH THE TREND
66  C             =0.
67  C
68  C
69  C
70  C    HOW TO SET UP DATA DECK.
71  C    --- -- --- -- ---- -----
72  C
73  C       -INPUT DATA ON CARDS-
74  C
75  C       CARD 1=TITLE CARD.
76  C       ------------------
77  C          TYPE THE SAMPLE NUMBER
78  C          ON THIS CARD IN COLUMNS
79  C          1-80.
80  C
81  C       CARD 2=SEGREGATION VESICLE
82  C       --------------------------
83  C              INCLINATION DATA.
84  C              -----------------
85  C          ENTER THE AVERAGE SEGRE-
86  C          GATION VESICLE INCLINATION
87  C          AND 95% CONFIDENCE INTER-
88  C          VAL OF THE MEAN DETERMINED
89  C          FOR EACH THIN SECTION CUT
```

```
90    C     FROM A SINGLE SAMPLE.
91    C     VALUES FOR THESE VARIABLES
92    C     CAN RANGE FROM 0-360 DEGREES.
93    C
94    C       ENTER, USNG DECIMAL---
95    C           MEAN(XZ)=AD1     IN   1-10
96    C       SIGMA95(XZ)=ESAD1 IN  11-20
97    C           MEAN(XY)=AD2     IN  21-30
98    C       SIGMA95(XY)=ESAD2 IN  31-40.
99    C       NOTE: AD1 CANNOT=0.0 OR 180.0
100   C
101   C     CARD 3=MAGNETIC DATA CARD.
102   C     --------------------------
103   C       ENTER THE MEASURED MAG-
104   C       NETIC DECLINATION AND
105   C       INCLINATION.  VALUES FOR
106   C       INCLINATION CAN RANGE
107   C       FROM +90 TO -90 DEGREES.
108   C       VALUES FOR DECLINATION
109   C       CAN RANGE FROM 0-360
110   C       DEGREES.
111   C
112   C       ENTER, USING DECIMAL--
113   C          DECLINATION=DEC IN  1-10
114   C          INCLINATION=ENC IN 11-20.
115   C       NOTE: ENTER 999.999 FOR DEC
116   C             IF NO MAGNETIC DATA.
117   C
118   C
119   C     READ AND PRINT THE DATA FOR
120   C       A SAMPLE
121   C     --------------------------
122   C
123         1    READ(1,4)TITLE
124         4    FORMAT(8A10)
125              IF(EOF(1))2,3,2
126         2    STOP ' JOB IS DONE '
127         3    READ(1,5)AD1,ESAD1,AD2,ESAD2
128         5    FORMAT(4F10.4)
129              READ(1,6)DEC,ENC
130              AFLAG=DEC
131         6    FORMAT(2F10.4)
132              WRITE(2,7)TITLE,AD1,ESAD1,AD2,ESAD2,DEC,ENC
133         7    FORMAT(1H1,///," PROCESSING ",8A10,/,
```

```
134                                 "  INPUT DATA : AD1 = ",F10.5,
135                      /,         "             SAD1 = ",F10.5,
136                      /,         "              AD2 = ",F10.5,
137                      /,         "             SAD2 = ",F10.5,
138                      /,         "              DEC = ",F10.5,
139                      /,         "              INC = ",F10.5)
140        C
141        C     CALCULATE D=DIP AND T=TREND
142        C     ---------------------------
143        C
144        C
145        C     COMPUTE THE TRUE DIP AND
146        C     TREND DIRECTION WIH RESPECT
147        C     TO THE ORIENTATION AXES OF
148        C     THE SAMPLE.   PROCEDURE IS
149        C     AFTER REGAN (1973) AND R.
150        C     BOUTILIER (PERS. COMM., 1980).
151        C         NOTE: ANGLE BETWEEN THIN
152        C               SECTION PLANES MUST
153        C               BE 90 DEGREES.  IF
154        C               THIS IS NOT THE CASE,
155        C               PROJECT THE MEASURED
156        C               APPARENT DIPS AND
157        C               CALCULATED ERRORS INTO
158        C               MUTUALLY PERPENDICULAR
159        C               PLANES.  ENTER PROJEC-
160        C               TED DATA.
161        C
162        C     BEFORE PROCESSING, CHECK TO SEE
163        C     IF ONE APPARENT DIP IS
164        C        UPRIGHT=270-360 OR 0-90
165        C     WHILE THE OTHER IS
166        C        OVERTURNED = 90-270 DEGREES.
167        C     AN ATTITUDE CANNOT BE CALCULATED
168        C     FROM SUCH A DATA SET.  MAKE THE
169        C     FOLLOWING ARBITRARY CORRECTION:
170        C     - FIND THE APPARENT DIP WITH
171        C         THE LARGER ERROR.
172        C     - MOVE IT THE SMALLEST DISTANCE
173        C         POSSIBLE TO MAKE IT COMPAT-
174        C         ABLE WITH THE OTHER APPARENT
175        C         DIP.
176        C     - NOTE THE CORRECTION.
177        C       PROCEED WITH THE CALCULATION.
178        C     ---------------------------
179        C
180        C
```

```
181          IF(AD1.GT.90.0.AND.AD1.LT.270.0.AND.AD2.GT.90.0.AND.AD2.LT.270.0)
182       .    GO TO 199
183          IF(AD1.GT.90.0.AND.AD1.LT.270.0)GO TO 198
184          IF(AD2.GT.90.0.AND.AD2.LT.270.0)GO TO 198
185          GO TO 199
186   198    IF(ESAD1.LT.ESAD2)THEN
187             IF(AD2.GT.90.0.AND.AD2.LT.270.0)THEN
188                IF(AD2.GT.180.0)THEN
189                   AD2=270.1
190                ELSE
191                   AD2=89.9
192                ENDIF
193             ELSE
194             IF(AD2.GE.0.0.AND.AD2.LE.90.0)THEN
195                AD2=90.1
196             ELSE
197                AD2=269.1
198             ENDIF
199             ENDIF
200          ELSE
201          IF(AD1.GT.90.0.AND.AD1.LT.270.0)THEN
202             IF(AD1.GT.180.0)THEN
203                AD1=270.1
204             ELSE
205                AD1=89.9
206             ENDIF
207          ELSEIF(AD1.GE.0.0.AND.AD1.LE.90.0)THEN
208                AD1=90.1
209             ELSE
210                AD1=269.1
211             ENDIF
212          ENDIF
213          WRITE(2,197)AD1,AD2
214   197    FORMAT(/," *********************** N O T E *********************** ",
215          /," ***** AD1 AND AD2 FORM AN IMPOSSIBLE SET - HAVE ***** ",
216       .  /," ***** TAKEN THE BEST CHOICE BASED ON LEAST      ***** ",
217       .  /," ***** ERROR AS SHOWN. MAY NOT BE CORRECT.       ***** ",
218       .  /," ****************************************************** ",
219          //," NEW AD1 = ",F10.5,", NEW AD2 = ", F10.5,//)
220   199    CONTINUE
221       C
222       C  CHANGE INPUT DATA TO RADIANS.
223       C  ----- ----- ---- -- --------
224          AD1=DR(AD1)
225          AD2=DR(AD2)
226          ESAD1=DR(ESAD1)**2
227          ESAD2=DR(ESAD2)**2
```

```
228       DEC=DR(DEC)
229       ENC=DR(ENC)
230   C
231   C   BEGIN COMPUTATION OF T AND D
232   C   ----- ----------- -- - --- -
233   C
234       SAD1=SIN(AD1)
235       CAD1=COS(AD1)
236       SAD2=SIN(AD2)
237       CAD2=COS(AD2)
238   C
239   C   THE VECTOR WHICH FORMS THE NORMAL
240   C   TO THE PLANE (XN) IS GIVEN BY
241   C   THE CROSS PRODUCT OF THE TWO
242   C   APPARENT DIPS  AD1 AND AD2.
243   C   --------------------------
244   C
245       XN1=-CAD2*SAD1
246       XN2=-CAD1*SAD2
247       XN3=CAD1*CAD2
248       P=SQRT(XN1*XN1+XN2*XN2)
249       XN=SQRT(P*P+XN3*XN3)
250   C
251   C   THE DIP (D) WILL BE THE ANGLE THIS
252   C   VECTOR (XN) MAKES WITH THE VERTICAL
253   C   AXIS.  THE DOT PRODUCT OF THE TWO
254   C   VECTORS IS EQUAL TO THE PRODUCT OF
255   C   THE TWO VECTORS TIMES THE ANGLE
256   C   BETWEEN THEM.  THEREFORE:
257   C   --------------------------
258   C
259       D=ACOS(XN3/XN)
260   C
261   C   TO DETERMINE THE TREND (T) THE
262   C   DIP VECTOR (D) IS PROJECTED ON
263   C   TO THE HORIZONTAL (ZY) PLANE.
264   C   THEN, USING THE DOT PRODUCT
265   C   RULE THE ANGLE THE PROJECTED
266   C   VECTOR MAKES WITH THE Z AXIS
267   C   IS DETERMINED.
268   C   --------------
269   C
270       T=ACOS(XN1/P)
```

```
271
272    C    THE BED IS OVERTURNED IS BOTH
273    C    AD1 AND AD2 ARE BETWEEN 90
274    C    AND 270 DEGREES.   AN OVERTURNED
275    C    BED IS INDICATED BY A NEGATIVE
276    C    SIGN OF DIP.
277    C    -------------
278    C
279         IF(AD1.GT.PI/2.0.AND.AD1.LT.3.0*PI/2.0.AND.AD2.GT.PI/2.0.AND.
280        .   AD2.LT.3.0*PI/2.0)D=-D
281         IF(XN2.LT.0.0)T=2.0*PI-T
282         IF(CAD1.GT.0.0.AND.CAD2.GT.0.0)GO TO 50
283         IF(CAD1.LE.0.0.AND.CAD2.LE.0.0)GO TO 50
284         T=T+PI
285    50    CONTINUE
286         T=T-PI
287         IF(T.LT.0)T=T+2.0*PI
288    C
289    C    CHANGE D AND T FROM RADIANS TO
290    C    DEGREES.   PRINT THE RESULTS.
291    C    ----------------------------
292    C
293
294         TDISP=RD(T)
295         DDISP=RD(D)
296         WRITE(2,11)DDISP,TDISP
297    11    FORMAT(/," CALCULATED DIP = ",F10.5,
298        .        /,"          TREND = ",F10.5)
299    C
300    C    CALCULATE ST, SD, STD
301    C    ---------------------
302    C
303    C    COMPUTATIONS ARE ACCORDING TO
304    C    THE LAW OF PROPAGATION OF VAR-
305    C    IANCE-COVARIANCE MATRIX (VANICEK,
306    C    P.,1973).   DERIVATIONS ARE BY
307    C    BOUTILIER, R., PERS. COMM., 1980).
308    C    ST=ERROR IN THE TREND =
309    C       F(DT/DAD1,ESAD1+DT/DAD2,ESAD2)
310
311    C    SD=ERROR IN THE DIP =
312    C       F(DD/DAD1,ESAD1+DD/DAD2,ESAD2).
313    C
314    C    STD=ERROR BETWEEN THE DIP
315    C       AND TREND =
316    C       F(DT/DAD1,DD/DAD1,ESAD1,
317    C       DT/DAD2,DD/DAD2.ESAD2).
318    C
```

```
319    C      ST AND SD ARE THE 95% CONFIDENCE
320    C      INTERVAL FOR THE TREND AND DIP,
321    C      RESPECTIVELY.
322    C      -------------
323    C
324           IF(D.LT.0.0)D=PI-D
325    C
326           CT=COS(T)
327           ST=SIN(T)
328           CD=COS(D)
329           SD=SIN(D)
330           AA=-SAD2*CT*CT/(CAD2*SAD1*SAD1)
331           BB=CT*CT*CAD1/(SAD1*CAD2*CAD2)
332           CC=(CD*CD/(CT*CT))*(CT/(CAD1*CAD1)-ST*SAD2*CT*CT/(CAD1*CAD2*SAD1))
333           DD=ST*CD*CD/(CAD2*CAD2)
334    C
335           EST2=AA*AA*ESAD1+BB*BB*ESAD2
336           ESD2=CC*CC*ESAD1+DD*DD*ESAD2
337           ESDT=AA*CC*ESAD1+BB*DD*ESAD2
338    C
339    C   CHANGE THE RESULT FROM RADIANS
340    C   TO DEGREES.   PRINT ST AND SD.
341    C   ------------------------------
342    C
343           ETDIS=RD(SQRT(EST2))
344           EDDIS=RD(SQRT(ESD2))
345           WRITE(2,8)EDDIS,ETDIS
346     8     FORMAT(/," CALCULATED ERRORS S(DIP) = ",F10.5,
347          .        /,"                     S(TREND) = ",F10.5)
348    C
349    C   IF DEC=999.999 NOTE THAT THERE
350    C   IS NO MAGNETIC DATA FOR THIS
351    C   SAMPLE.   GO TO THE NEXT SAMPLE.
352    C   ------------------------------
353    C
354           IF(AFLAG.EQ.999.999)THEN
355              WRITE(2,12)
356              GO TO 1
357           ENDIF
358     12    FORMAT(/,"  NO MAGNETIC DATA FOR THIS SAMPLE ")
359    C
360    C
361    C   CALCULATE ROTATED MAGNETIC
362    C      DECLINATION = DEC2
363    C      INCLINATION = ENC2
364    C   ------------------------------
```

```
365      C    THE FORMALISM IS AFTER BOUTILIER,
366      C    R. (PERS. COMM., 1980).
367      C
368           CDEC= COS(DEC)
369           SDEC=SIN(DEC)
370           CENC=COS(ENC)
371           SENC=SIN(ENC)
372      C
373      C    THE COORDINATE SYSTEM
374      C    ---------------------
375      C      CONVENTION EQUIVALENCES
376      C       HERE = SVT
377      C       -Z      +X = VERTICAL, UP
378      C       +X      +Z = HORIZONTAL, 0
379      C                    DEGREES DEC
380      C       +Y      +Y = HORIZONTAL, 90
381      C                    DEGREES DEC.
382      C
383      C    DEFINE THE MEASUED MAGNETIC
384      C    VECTOR, M, (UNIT VECTOR) BY
385      C    ITS X, Y AND Z COMPONENTS =
386      C    MX, MY AND MZ.
387      C
388           MX=CDEC*CENC
389           MY=SDEC*CENC
390           MZ=SENC
391      C
392      C    FIRST ROTATION
393      C    --------------
394      C     ROTATE THE XY PLANE UNTIL X' POINTS
395      C     IN THE DIRECTION OF THE DIP.
396      C     THAT IS, ROTATE BY ANGLE T = TREND.
397      C
398           MX1=MX*CT+MY*ST
399           MY1=-MX*ST+MY*CT
400           MZ1=MZ
401      C
402      C    SECOND ROTATION
403      C    ---------------
404      C     ROTATE THE X'Z' PLANE ABOUT
405      C     THE Y' AAXIS (WHICH IS NOW AT
406      C     90 DEGREES TO THE TREND) UNTIL
407      C     X'' IS IN THE DIRECTION OF THE
408      C     DIP.  THAT IS, ROTATE BY ANGLE
409      C     D = DIP.
```

```
410   C
411         MX2=MX1*CD+MZ1*SD
412         MY2=MY1
413         MZ2=-MX1*SD+MZ1*CD
414   C
415   C   THE CALCULATED MAGNETIC DIRECTION
416   C   ---------------------------------
417   C     THE DIPPING BED HAS NOW BEEN
418   C     ROTATED BACK TO THE REFERENCE
419   C     HORIZONTAL POSITION GIVEN BY THE
420   C     XY PLANE.
421   C     THE MAGNETIC VECTOR HAS ALSO
422   C     BEEN ROTATED
423   C       FROM M=(MX,MY,MZ)
424   C         TO M=(MX1,MY1,MZ1)
425   C         TO M=(MX2,MY2,MZ2).
426   C     THE CORRESPONDING INCLINATION
427   C     = ENC2 AND DECLINATION = DEC2
428   C     IS GIVEN BY:
429   C
430         ENC2=ASIN(MZ2)
431         SENC2=SIN(ENC2)
432         CENC2=COS(ENC2)
433         DEC2=ACOS(MX2/CENC2)
434         IF(MY2.LT.0.0)DEC2=2.0*PI-DEC2
435         IF(ENC2.LT.0.0)DEC2=DEC2+PI
436   C
437   C   WHERE DEC2 IS THE HORIZONTAL ANGLE
438   C   BETWEEN THE TREND = 0 DEGREES AND
439   C   THE PROJECTION OF M INTO THE
440   C   (MX2,MY2) PLANE.
441   C
442   C   CALCULATE AZI = AZIMUTH OF THE
443   C   TREND, ASSUMING M POINTS NORTH
444   C   FOR NORMALLY MAGNETIZED ROCKS,
445   C   OR SOUTH, FOR REVERSELY MAGNET-
446   C   IZED ROCKS.
447   C
448         AZI=2.0*PI-DEC2
449         SAZI=SIN(AZI)
450         CAZI=COS(AZI)
451   C
452   C   CHANGE THE RESULTS FROM RADIANS
453   C   TO DEGREES.   PRINT ENC2 AND AZI.
454   C
455         A2DIS=RD(AZI)
456         E2DIS=RD(ENC2)
```

```
457          WRITE(2,9)E2DIS,A2DIS
458      9   FORMAT(/," CALCULATED ORIGINAL MAGNETIC INCLINATION = ",F10,5,
459      .        /," CALCULATED AZIMUTH OF TREND         = ",F10.5)
460      C
461      C
462      C   CALCULATE THE ERRORS IN AZI
463      C          AND ENC2
464      C   ------------------------------
465      C
466      C COMPUTATIONS ARE ACCORDING TO
467      C THE LAW OF PROPAGATION OF
468      C VARIANCE-COVARIANCE MATRIX
469      C (VANICEK, P., 1973).  DERI-
470      C VATIONS ARE BY BOUTILIER, R.
471      C (PERS. COMM., 1980).
472      C
473      C   S(AZI)= 95% CONFIDENCE INTER-
474      C    VAL FOR THE AZIMUTH OF THE TREND
475      C    =F((DAZI/DT)ST)+((DAZI/DT)(DAZI/DD)
476      C        SDT)+((DAZI/DD)SD).
477      C
478      C   S(ENC)= 95% CONFIDENCE INTERVAL
479      C    FOR THE CALCULATED INCLINATION
480      C    =F((DENC2/DT)ST)+((DENC2/DT)(DENC2/
481      C        DD)STD)+((DENC2/DD)SD).
482      C
483      C
484          DEDT=SD*(MX*ST-MY*CT)/CENC2
485          DEDD=-(MZ1*SD+MX1*CD)/CENC2
486          DADD=(CENC2*(MX1*SD-MZ1*CD)-MX2*SENC2*DEDD)/(SAZI*CENC2*CENC2)
487          DADT=(-CENC2*CD*(MY*CT-MX*ST)-MX2*SENC2*DEDT)/(SAZI*CENC2*CENC2)
488      C
489      C 14    CONTINUE
490      C
491          SALFA2=DADT*DADT*EST2+2.0*DADT*DADD*ESDT+DADD*DADD*ESD2
492          SETA2= DEDT*DEDT*EST2+2.0*DEDT*DEDD*ESDT+DEDD*DEDD*ESD2
493      C
494      C CHANGE RADIANS TO DEGREES AND
495      C PRINT THE ERRORS.
496      C   ------------------------
```

```
497      C
498            ALFADIS=RD(SQRT(SALFA2))
499            ETADIS =RD(SQRT(SETA2))
500            WRITE(2,10)ALFADIS,ETADIS
501      10    FORMAT(/," CALCULATED ERRORS IN INCLINATION AND AZIMUTH : ",
502           .         /,"        S(AZI) = ",F10.5,
503           .         /,"        S(INC) = ",F10.5)
504      C
505      C   SET ST AND SDT TO 0.0 AND RE-
506      C   PEAT THE ERROR CALCULATION.
507      C   THE RESULT IS THE ERROR IN AZI
508      C   AND ENC2 ONLY DUE TO THE ERROR
509      C   IN THE DIP.  THIS VALUE MAY BE
510      C   SIGNIFICANT IF THE TREND IS
511      C   UNDEFINED, THAT IS THE BED IS
512      C   HORIZONTAL.
513      C
514            IF(EST2.NE.0.0)THEN
515                EST2=0.0
516                ESDT=0.0
517                GO TO 14
518            ENDIF
519            WRITE(2,51)
520      51    FORMAT("        NOTE THAT THE LAST CALCULATION IS FOR TREND ",
521           .        "ERROR = 0.0 ")
522            GO TO 1
523            END
```